PERMEABLE PAVEMENT SYSTEMS WITH LOW CARBON AND RECYCLED MATERIALS FOR CARIBBEAN SMALL ISLAND DEVELOPING STATES

JOHN MONROSE

A thesis submitted in partial fulfilment of the requirements of the University of the West of England, Bristol for the degree of Doctor of Philosophy

Faculty of Environment and Technology
Civil & Environmental Engineering Cluster
University of the West of England, Bristol (UWE Bristol)

January 2020

ABSTRACT

Permeable Pavement Systems (PPS) have traditionally been engineered as hybrid, source control pavements that accommodate light traffic and filter and temporarily detain stormwater. Over the last few decades, PPS have been shown to play a vital role in the management of stormwater. Although these pavements have been utilised across numerous municipalities in developed areas such as in Europe, Asia, United States of America (USA) and Australia, their utilisation across geologically confined nations, such as most Small Island Developing States (SIDS) is scarce. To this end, this research has presented PPS for adoption in SIDS with emphasis on Caribbean SIDS where urban stormwater management is a significant challenge. Unlike most larger states, the geographically and geologically confined nature of most SIDS present unique parameters for consideration when designing permeable pavements. Other SUDS such as detention/retention ponds and wetlands that provide vital stormwater storage, are often difficult to implement because of land/space restrictions. To further enhance the sustainability of permeable pavements, previous studies have identified recycled materials such as recycled aggregates, as having potential to replace some of the traditional natural materials (rocks, gravel, sand) used in the construction of permeable pavements. However, a research gap exists when considering the hydrological, pollutant removal, structural and long-term clogging and hydraulic conductivity performances of permeable pavements containing recycled and low-carbon materials. In this context, and as a second aim of this research project, were performance evaluations of tanked 0.2 m^2 pilot-scale permeable pavement rigs, adapted for use in a laboratory, that contained two recycled materials in the sub-base namely, Crushed Concrete Aggregates (CCA) and Cement-bounded Expanded Polystyrene beads (C-EPS). These rigs were evaluated and compared to other rigs of similar structure that contained natural aggregates of quartzite and basalt in the sub-base. A third recycled material referred to as Carbon-Negative Aggregates (CNA), was used in the production of novel Concrete Permeable Pavement Blocks (CPPB) for use in the surface layer of permeable pavements. Performance evaluations of the pilot - scale rigs demonstrated that CCA and C-EPS were suitable for use as alternative sub-base materials to natural aggregates in PPS. However, it was recommended that C-EPS only be used in permeable pavements with no traffic because of its low compressive strength. CNA was found unsuitable as an unbound sub-base material but was found suitable as replacement to natural aggregates in the production of CPPB. By using these low-carbon and recycled materials, opportunities are presented to significantly reduce the carbon footprint on the construction and implementation phase of pavements, conserve vital natural resources, reduce the ecological stress on landfills, preserve the environment and ultimately save capital. The proposed adoption of PPS across urban areas in Caribbean SIDS will most likely require policy shifts, aggressive education drives, cooperation and collaboration among stakeholders such as state agencies, universities, funding agencies and construction companies.

ACKNOWLEDGEMENT

This doctoral research project would not have been possible without the support and encouragement of many individuals who contributed their valuable time and assistance.

A gigantic thank you goes to my Director of Studies (first supervisor), Dr. Kiran Tota-Maharaj, for firstly providing me with the opportunity to engage in this exciting infrastructure project and for his guidance, support, professional advice and never-ending support throughout the tenure of my research.

Special thanks to my local supervisors Dr. Abrahams Mwasha and Dr. Denver Cheddie for the support and encouragement and for allowing various components of the research project to be conducted at the University of the West Indies, St. Augustine Campus, St. Augustine, Trinidad, W.I. (UWI) and at the University of Trinidad and Tobago, Point Lisas Campus, Trinidad W.I. (UTT).

I am grateful to Professor Colin Hills from the University of Greenwich, UK for providing me with the means of obtaining the Carbon-Negative Aggregates used in the research project. A special thank you is extended to Professor Chad Staddon and the International Securities Water Network for financial support at the University of the West of England, Bristol, UK (UWE Bristol).

I would like to express my sincerest appreciation to Mrs. Vitra Ramjattan-Harry, laboratory technician at the Process Engineering Unit of the UTT for her support, advice and guidance during the water quality testing phase of the research.

Many thanks to the technical staff at Department of Civil and Environmental Engineering of the UWI for their assistance and guidance throughout the numerous laboratory experiments conducted.

My sincerest appreciation to AECOM for supporting this research. The financial assistance provided was a true blessing. I wish to express many thanks and appreciation to Mr. Terry Buckley, (Senior Engineer, AECOM) for his support and permitting time off from work to facilitate my research.

Finally, to all my friends, family and well-wishers, I am grateful for all the support. I owe my deepest gratitude to my wife, Adafih for her love, patience, encouragement and support. To my 14-month old son, Jayden, you were an inspiration and a bundle of joy.

LIST OF PUBLICATIONS

Journal papers

Monrose, J. & Tota-Maharaj, K. (2018) Technological Review of Permeable Pavement Systems for Applications in Small Island Developing States. *CLEAN–Soil, Air, Water*. 46. (9), pp. 1700168.

Monrose, J., Tota-Maharaj, K., Mwasha, A. & Hills, C. (2019) Effect of carbon-negative aggregates on the strength properties of concrete for permeable pavements. *International Journal of Pavement Engineering*. pp. 1-9.

Monrose, J., Tota-Maharaj, K. & Mwasha, A. (2019) Assessment of the physical characteristics and stormwater effluent quality of permeable pavement systems consisting of recycled materials. *Road Materials and Pavement Design*. pp. 1-33

Monrose, J., Tota-Maharaj, K., Mwasha, A. & Staddon, C. (2019) Hydrologic performance of novel permeable pavements with recycled sub-base materials. *Journal of Hydrologic Engineering*. (under review)

Monrose, J., Tota-Maharaj K. & Mwasha, A. (2019) Diagnosis of low-carbon permeable pavements: bearing capacity and long-term clogging behaviour. *International Journal of Pavement Research and Technology*. (under review)

Conference papers

Monrose, J., Tota-Maharaj, K., Mwasha, A. & Hills, C. (2018) Utilisation of artificial carbon-negative aggregates in concrete for the production of permeable pavement blocks. APETT Technical Conference, 14 September 2018. Trinidad and Tobago, West Indies.

Monrose, J., & Tota-Maharaj, K. (2017). Hydrologic performance of permeable pavement systems utilising various sub-base materials for Caribbean applications. Proceedings of the 14th IWA/IAHR International Conference on Urban Drainage, 10–15 September 2017. Prague, Czech Republic.

Monrose, J., Tota-Maharaj, K., Cheddie, D. & Mwasha, A. (2017). A Permeable Pavement System Utilising Recycled Concrete Aggregate in the Sub-Base—Preliminary Laboratory

Performance Assessments. Proceedings of World Environmental and Water Resources Congress 2017, 22–25 May 2017. Sacramento, California.

Tota-Maharaj, K., **Monrose, J.** & Hills C. (2017). Novel permeable pavement systems utilising carbon-Negative Aggregate. Proceedings of NexGen Technologies for Mining and Fuel Industries, 15–17 February 2017. New Delhi, India.

Monrose, J., & Tota-Maharaj, K. (2016). Permeable Pavements as Low Impact Development Practices for Urban Runoff Mitigation and Sustainable Stormwater Management within the Built Environment for the Caribbean. 25th Silver Anniversary Annual Caribbean Water and Wastewater Association (CWWA) Conference & Exhibition, 24–28 October 2016. Trinidad and Tobago, West Indies.

Extended abstracts

Hills, C., **Monrose, J.**, Tota-Maharaj, K., & Carrey, P. (2018). Permeable Pavements with Low-Carbon Manufactured Carbonated Aggregates: Environmental and Economic Perspectives. SUDSnet International Conference, 30–31 August 2018. Coventry University, UK.

Monrose, J., Tota-Maharaj, K. & Mwasha, A. (2018). Pollutant removal efficacies of permeable pavements comprising recycled concrete aggregates. SUDSnet International Conference, 30–31 August 2018. Coventry University, UK.

Seminars and poster presentations

1. Postgraduate winter seminar, 15–16 January 2018. UWE-Arnolfini, UK.
2. Postgraduate winter seminar, 14–15 January 2019. UWE-Arnolfini, UK.
3. Postgraduate students' presentation, 8 May 2019. University of the West Indies, St. Augustine Campus, Department of Civil and Environmental Engineering, Trinidad and Tobago, West Indies (UWI).
4. Poster presentation, 29 May 2019. UWI Open Day.

TABLE OF CONTENTS

LIST OF FIGURES

LIST OF TABLES

LIST OF ABBREVIATIONS AND SYMBOLS

AAS	=	Atomic Absorption Spectrometry
AASHTO	=	American Association of State Highway and Transportation Officials
ACT	=	Accelerated Carbonation Technology
ADB	=	Asian Development Bank
ADT	=	Average Daily Traffic
AIMS	=	Atlantic Ocean, Indian Ocean, Mediterranean and South China Seas
APCr	=	Air Pollution Control residue
AS	=	Absolute Sensitivity
AST	=	Accelerated Simulation Techniques
ASTM	=	American Society for Testing and Materials
BMP	=	Best Management Practice
BPOA	=	Barbados Programme of Action
BS	=	British Standards
BSI	=	British Standards Institution
C_c	=	Coefficient of curvature
C_u	=	Coefficient of uniformity
Cu	=	Copper
CBP	=	Concrete Block Pavers
CBR	=	California Bearing Ratio
CCA	=	Crushed Concrete Aggregates
CDW	=	Construction and Demolition Waste
C-EPS	=	Cement-bound expanded polystyrene beads
CGP	=	Concrete Grid Pavers
CHI	=	Computational Hydraulics International
CMAA	=	Concrete Masonry Association of Australia
CNA	=	Carbon-Negative Aggregates
COD	=	Chemical Oxygen Demand
CHFS	=	Constant Head Full Scale
Cr	=	Chromium
CSO	=	Central Statistical Office
CPPB	=	Concrete Permeable Pavement Blocks
D_{10}	=	Particle diameter corresponding to 10% passing by weight
D_{30}	=	Particle diameter corresponding to 30% passing by weight
D_{60}	=	Particle diameter corresponding to 60% passing by weight

DS	=	Deviation Sensitivity
DO	=	Dissolved Oxygen
DRIT	=	Double Ring Infiltration Test
e	=	Voids ratio
E_0	=	Surface modulus
E. coli	=	Escherichia coli
EC	=	Electroconductivity
EMA	=	Trinidad and Tobago Environmental Management Authority
ENSO	=	El Niño Southern Oscillation
EPS	=	Expanded Polystyrene
ESALs	=	Equivalent Single Axle Loads
f_{cu}	=	Concrete compressive strength
f_{ct}	=	Concrete splitting tensile strength
Fe	=	Iron
FHFS	=	Falling Head Full Scale
FWD	=	Falling Weight Deflectometer
G_s	=	Specific gravity
GDP	=	Gross Domestic Product
GoRTT	=	Government of the Republic of Trinidad and Tobago
GoSL	=	Government of St. Lucia
HDI	=	Human Development Index
HSG	=	Hydrologic Soil Groups
ICPI	=	Interlocking Concrete Pavement Institute
IDB	=	Inter-American Development Bank
IPCC	=	Intergovernmental Panel on Climate Change
ITCZ	=	Intertropical Convergence Zone
ITZ	=	Interfacial Transition Zone
k	=	Hydraulic conductivity
LID	=	Low Impact Development
LIUDD	=	Low Impact Urban Design and Development
LWAA	=	Lightweight Artificial Aggregates
LWD	=	Lightweight Deflectometer
MARV	=	Minimum Average Roll Value
MDR	=	More Developed Regions
MDL	=	Minimum Detectable Levels

Mn	=	Manganese
MPL	=	Maximum Permissible Level
MSW	=	Municipal Solid Waste
n	=	Porosity
NCAT	=	National Centre for Asphalt Technology
NH_4-N	=	Ammonium-Nitrogen
NO_3-N	=	Nitrate-Nitrogen
NRMCA	=	National Ready Mixed Concrete Association
NSE	=	Nash-Sutcliffe Efficiency coefficient
NTU	=	Nephelometric Turbidity Units
OPC	=	Ordinary Portland Cement
Pb	=	Lead
PCSWMM	=	Personal Computer Stormwater Management Model
PFWD	=	Portable Falling Weight Deflectometer
PICP	=	Permeable Interlocking Concrete Pavers
PGP	=	Plastic Grid Pavers
PO_4^{3-}	=	Reactive Phosphorous
PPC	=	Premium Plus Cement
PPS	=	Permeable Pavement Systems
PSD	=	Particle Size Distribution
r	=	Pearson's coefficient
R^2	=	Coefficient of determination
RAP	=	Reclaimed Asphalt Pavement
RCA	=	Recycled Concrete Aggregates
RS	=	Relative Sensitivity
RMSE	=	Root-Mean-Square-Error
RSI	=	Rainfall Simulation Infiltrometer
RSIT	=	Rainfall Simulation Infiltrometer Test
SIDS	=	Small Island Developing States
SEM	=	Scanning Electron Microscope
SLSWMA	=	St. Lucia Solid Waste Management Authority
SO_4^{2-}	=	Sulphates
SPCZ	=	South Pacific Convergence Zone
SPSS	=	Statistical Package for the Social Sciences
SSD	=	Saturated Surface Dry

SWIFT	=	Stormwater Infiltration Field Test
SWMCOL	=	Trinidad and Tobago Solid Waste Management Company
SWMM	=	Stormwater Management Modelling
SUDS	=	Sustainable Urban Drainage Systems
TDR	=	Time Domain Reflectometer
TKN	=	Total Kjeldahl Nitrogen
TP	=	Total Phosphorous
TSS	=	Total Suspended Solids
UHI	=	Urban Heat Island
UN	=	United Nations
UN DESA	=	United Nations Department of Economic and Social Affairs
UNEP	=	United Nations Environment Programme
UNFCCC	=	United Nations Framework Convention on Climate Change
UN-OHRLLS	=	United Nations Office of the High Representative for the Least Developed Countries
US EPA	=	United States Environmental Protection Agency
VWC	=	Volumetric Water Content
WCR	=	Water Content Reflectometer
WG	=	Waste Glass
W.I.	=	West Indies
WSUD	=	Water Sensitive Urban Design
XRD	=	X-Ray Diffractometer
Zn	=	Zinc
γ	=	Bulk density (unit weight)
δ_w	=	density of water
$\overline{x}$	=	Mean
$\sigma_{\bar{x}}$	=	Standard error of the mean
σ	=	Standard deviation

CHAPTER 1. INTRODUCTION

1.1 Background and significance of the research

Sustainability has been recognised as an important concept for effective management of urban drainage (Goldenfum et al., 2007, Armitage, 2011, Butler and Davies, 2011). With accelerated urbanisation and global land alteration, the sustainability level of built and natural environments requires constant monitoring and assessment (Pakzad et al., 2017). Such sustainability assessment is challenged by the necessity to identify both science-based and policy-based indicators, which can justifiably differentiate what is and is not a contribution to sustainable development (Pakzad et al., 2017). The Brundtland Report (World Commission on Environment and Development, 1987) defines sustainable development as, that which addresses the issues and goals of the present age without bargaining the capacity of future generations to address their own needs. This definition has been employed in this research to question the sustainability of existing stormwater management methods in urban areas across Small Island Developing States (SIDS) with a focus on Caribbean SIDS and has been used to present Permeable Pavement Systems (PPS) as a suitable option for incorporation in urban areas as applicable.

For several decades, collection and conveyance of stormwater away from urban areas across SIDS have been managed via conventional drainage systems dominated by open channels and closed conduits (Geiger, 1990, Larsen and Gujer, 1997, UNEP, 2012). A conventional drainage system is mainly a single-objective design which focuses primarily on stormwater quantity control (Reed, 2004, Zhou, 2014). Conventional drainage systems considered runoff as a waste to be removed and disposed of quickly from developments (Pazwash, 2011). They do not focus on environmental concerns relating to water quality, visual amenity, biodiversity and ecological protection (Chocat et al., 2007, Zhou, 2014). In addition to these environmental fears, the limited capacity and flexibility of conventional drainage systems to adapt to future climatic variability and urbanisation has continuously been criticised (Henze et al., 1997b, Zhou et al., 2012).

Existing conventional urban drainage systems in SIDS are no longer sustainable due to the widely acknowledged impacts of climate change and urbanisation (Zhou et al., 2012, Huong and Pathirana, 2013). Numerous academics (Brabec et al., 2002, Cheng and Wang, 2002, Shuster et al., 2005, Dietz and Clausen, 2008, Pazwash, 2011, Guan et al., 2015) have reported that urbanisation increases stormwater runoff volume, flow rates and peak flows because of increases in impervious surface areas. High intensity rainfall events across SIDS

cause elevated flowrates because of increased impervious surface areas resulting in increased runoff volumes and peak flows and reduced infiltration and groundwater recharge (UN-DESA, 2015). This often leads to annual flooding and erosion problems downstream of the discharge area (Reed, 2004) because of the inadequate capacity of the existing drainage systems to handle these increased flows. Figure 1-1 illustrates one example, where a parking lot at a prominent shopping establishment in Trinidad and Tobago, West Indies (W.I.), became flooded and impassable to cars when flood waters backed up from a downstream detention pond. It must also be noted that some cities such as Port of Spain in Trinidad and Tobago and Castries in St. Lucia, W.I., are largely influenced by rising tides which further exacerbates the drainage problems faced. Further, urban drainage problems across numerous SIDS have often been exacerbated by poor land use practices, improper utilisation of drainage infrastructure (littering) and faulty designs. Moreover, subsequent operation and maintenance of existing drainage systems present major challenges to urban authorities (Parkinson, 2002, GoSL and World Bank, 2014).

Figure 1-1 Flooded parking lot, Trinidad, W.I. 2016

Sustainable Urban Drainage Systems (SUDS), Low Impact Development (LID), Water Sensitive Urban Design (WSUD) or Best Management Practices (BMPs) such as Permeable Pavement Systems (PPS), can most likely offer a viable solution to the stormwater management problems experienced within most SIDS (Parkinson, 2002). Other SUDS such as detention/retention ponds and wetlands that provide vital stormwater storage, are often difficult to implement because of land/space restrictions. PPS supersede conventional paving surfaces with an at-source (i.e. where rainfall makes landfall) control to prevent or significantly delay stormwater runoff generation (Fassman and Blackbourn, 2010).

Documented use of PPS dates to the early 1970s (Thelen et al., 1972). PPS have been engineered as hybrid pavements that are traditionally designed to accommodate light traffic such as pedestrian access, roadway shoulders, residential driveways and parking lots and to also serve as stormwater control infrastructure by providing infiltration through the surface and temporary detention of stormwater runoff within an aggregate reservoir (Scholz and Grabowiecki, 2007, Jato-Espino et al., 2016b, Rodríguez-Rojas et al., 2018). The stored water is eventually released into a receiving drainage channel or allowed to percolate underground. Utilisation of PPS can most likely be a viable option to bridge the gap between societal competing needs of urban development and stormwater management in SIDS through this hybrid function. The primary objectives of PPS are to reduce surface runoff quantities and peak flows; increase groundwater recharge; improve stormwater runoff quality and reduce pollution of natural watercourses (Rahman et al., 2015b, Weiss et al., 2019). In Japan, permeable pavements have been recommended as post-modern pavements for the design and development of resilient transportation infrastructure (Jamshidi et al., 2019).

Despite their wide usage in the USA, Europe, Asia and Australia, the utilisation of PPS as a stormwater management option in SIDS is scarce. Research evaluating the performance of PPS across Caribbean SIDS is very limited (Horsley Witten Group Inc. (HWG) and Centre for Watershed Protection Inc. (CWP), 2014). This research project addresses this gap in knowledge and presents PPS as a potential long-term, sustainable urban drainage option for flood risk reduction and improvement in urban stormwater runoff quality in SIDS. An in-depth literature survey has been presented to support and encourage the adoption of PPS as a proven sustainable stormwater control measure. Further, experimental evidence has been presented and evaluated to support the use of PPS in SIDS. This can most likely be significant as global warming, sea-level rise, change in weather patterns along with increasing urban development present new challenges for stormwater management authorities in SIDS. Existing conventional drainage systems in urban areas of most SIDS have proven to be inadequate and are not sustainable because of climate change. A lack of land and space, high costs and constraints such as underground utilities often restrict expansion of existing drainage infrastructure.

Sustainable development across developing countries should promote environmental preservation and conservation of the rapidly diminishing natural resources (Rao et al., 2007). PPS are typically designed and constructed using large quantities of quarried construction aggregates. Such volumes of construction materials may not always be available when

required. With the goal of promoting the sustainable use of natural materials, several countries, regions and municipalities across the world are accelerating their efforts towards formulating policies that promote the wide-scale recycling of waste products (Inyang, 2003, Lockrey et al., 2016, Akhtar and Sarmah, 2018). Advancement in infrastructural development provides significant opportunities for the use of waste and recycled materials, encouraging reduced waste disposal at landfills and/or environmental costs (Chang et al., 1999, Inyang, 2003, Cheeseman et al., 2005). The benefits of recycling in construction are shown systematically in Figure 1-2.

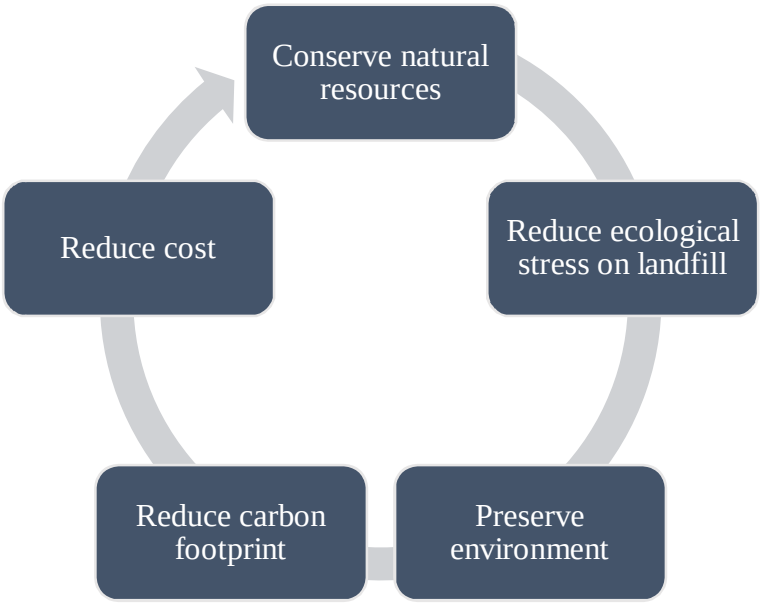

Figure 1-2 Benefits of recycling in construction
[adapted with permission from Behera et al. (2014)]

Numerous studies (Drake et al., 2013, Kayhanian et al., 2015, Rahman et al., 2015b, Weiss et al., 2019) have highlighted uncertainty and a knowledge gap regarding the performance of PPS consisting of recycled materials. Whilst several researchers (Nishigaki, 2000, Rizvi et al., 2010, Çetin, 2015, Khankhaje et al., 2017, Lu et al., 2019) have reported on the incorporation of recycled waste materials in permeable pavement concrete and asphalt surfaces, only a handful of studies (Sañudo-Fontaneda et al., 2014, Rahman et al., 2015b, Rodriguez-Hernandez et al., 2016) have reported on the incorporation of recycled materials as sub-base aggregates in permeable pavements. Moreover, these studies have each considered very limited performance evaluations. Rahman et al. (2015b), Rahman et al. (2015a) reported that Crushed Brick (CB) and Recycled Concrete Aggregates (RCA) from Construction and Demolition Waste (CDW) were suitable for use as sub-base materials in permeable pavements but the evaluation considered only geotechnical, hydraulic and few

water quality performances. Rodriguez-Hernandez et al. (2016) considered only the hydrological performance of permeable pavements when they used Recycled Aggregates (RA) from CDW as sub-base materials in permeable pavements and reported improved hydrological output in terms of attenuation, retained rainfall, peak outflow and time to peak. Sañudo-Fontaneda et al. (2014) used Basic Oxygen Furnace slag as sub-base materials in permeable pavements but only evaluated the water quality and permeability performances of the pavements. This research project addresses this gap in knowledge, producing new and original results and analysis. In addition to hydrological, hydraulic and water quality performance evaluations, this research project evaluates the structural integrity and long-term clogging behaviour of permeable pavements containing new/different recycled/recyclable materials. These performance evaluations are defined in this research project as follows:

1. Structural integrity refers to the load bearing capacity/ stiffness of the pavements.
2. Hydrological performance refers to the transformation of rainfall into discharge with specific focus on lag time, attenuation and retention capacity.
3. Pollutant removal focuses on the efficiency of the pavements to improve stormwater runoff quality. It also considers the impact of the varying sub-base materials on water quality.
4. Hydraulic conductivity and long-term clogging refer to the rate of stormwater infiltration into and through the pavement taking into consideration clogging from sediment accumulation/entrapment.

Specifically, three (3) recycled/recyclable materials namely, Crushed Concrete Aggregates (CCA), Carbon-Negative Aggregates (CNA) and Cement-bounded Expanded Polystyrene beads (C-EPS) were used to compare against traditionally-used natural materials (crushed basalt and quartzite aggregates). CCA and C-EPS were used as sub-base materials in permeable pavement rigs constructed for evaluation in the laboratory, whereas CNA were used to manufacture novel Concrete Permeable Pavement Blocks (CPPB) for use as the surface layer of the permeable pavements. CNA were considered but were not used as unbound sub-base aggregates in the rigs because they were found lacking in terms of strength, had a high water absorption percentage and contained an excessive amount of chlorides which had the potential to leach into the environment.

CCA are potential construction aggregates which were produced in the laboratory from the crushing of aged precast concrete cylinders. CCA consist of a stiff crushed aggregate core encapsulated by a relatively weak layer of mortar (Tatsuoka et al., 2013). The crushed

material was selectively screened to obtain a desired gradation. As SIDS urbanise and develop, it is projected that there will most likely be a significant increase in the amount of waste concrete available through demolition of aged and/or out-of-service concrete structures. Very limited information is available regarding the use of CCA in permeable pavements. CCA has previously been used in a permeable pavement in the laboratory (Bentarzi et al., 2013) but only as a water quality improvement option whereby CCA was mixed with compost to increase the retention of pollutants and stimulate biological treatment. Other construction applications of CCA include stone columns (Kawalec et al., 2017) and backfill material for pipe structures (Tatsuoka et al., 2013).

CNA are one form of artificially-engineered, lightweight aggregates manufactured from Municipal Solid Waste Incinerator (MSWI) ash using Accelerated Carbonation Technology (ACT) (Fernández Bertos et al., 2004, Li et al., 2007, Gunning et al., 2010). The technology utilises carbon dioxide to pelletise the MSWI ash into aggregates for construction (Gunning et al., 2009). The accelerated carbonation process captures more carbon dioxide from the waste than is used during plant processing; hence the development of a "carbon-negative" aggregate as per laboratory-based calculations. The solidified product contains permanently-bound carbon dioxide gas (Gunning et al., 2012). The raw materials used for this production are thermal residues; for example, fly ash and Air Pollution Control residue (APCr) from waste-to-energy plants. The CNA are grey, sub-rounded, homogeneous, and have a rough surface (Gunning et al., 2012). CNA were obtained from the manufacturing plant, Carbon8 Systems in Kent, UK in collaboration with the University of Greenwich, UK. CNA was selected because it is the first time in the Caribbean, as per the researcher's literature search, that a carbon-negative, artificial, commercial aggregate that was produced from Municipal Solid Waste (MSW), has been used and tested as a potential replacement for natural aggregates in Concrete Permeable Pavement Blocks (CPPB). Such recycling encourages reduced landfilling and presents opportunities to commercialise an alternative and effective MSW disposal option. It is noteworthy that the average MSW per capita generation rate for the Caribbean is 1.3 kg/capita/day with 83% of the waste landfilled (Kinnaman, 2010).

C-EPS is a novel, low strength porous material produced in the laboratory. The primary constituents are cement and EPS beads. EPS is a very low density foam which comprises of discrete air voids in a polymer matrix (Cook, 1983). The EPS particles are manufactured by thermal expansion of polystyrene particles saturated with n-pentane. EPS particles are microbiologically stable, float in water, swell in petroleum and demonstrate resistance to mineral acids (except for nitric acid) and bases (Sokolović et al., 2009). They are soluble in

organic solvents such as ketones and aromatic hydrocarbons and are thermally stable between 0 °C (32 °F) and 90 °C (194 °F). Toxicity of polystyrene depends on the content of the monomer, which can be easily removed by washing with water (Sokolović et al., 2009). EPS is usually deemed an environmental menace because it is not bio-degradable. However, it can easily be recycled into a product which can be utilised in practical sustainable construction (Mwasha et al., 2013). EPS is 100% recyclable and thousands of tonnes are recycled each year in developed countries such as the UK (Ngugi et al., 2017). The common characteristics, handling and uses of EPS has been discussed in detail by Mwasha et al. (2013). EPS beads can be regarded as a type of artificial, lightweight, low density (less than 30 kg/m^3) non-absorbent aggregate. In construction, they can be used to produce lightweight, low density concretes for building applications such as curtain walls, cladding panels and composite flooring systems (Cook, 1983).

This research project was undertaken to provide answers to the following questions:

1. What are the key parameters for consideration for widespread acceptance and adoption of PPS in SIDS?

2. What are the physical and chemical properties of the recycled/recyclable materials CCA, CNA and C-EPS?

3. Are CCA, CNA and C-EPS suitable for use as sub-base materials in permeable pavements?

4. How do the performances (bearing capacity, permeability, long-term clogging, attenuation and retention capacity, pollutant removal efficiency) of pilot-scale permeable pavement rigs that contain CCA and CEPS compare to rigs that contain natural aggregates (basalt and quartzite)?

5. Is the PCSWMM model able to accurately simulate the outflow from permeable pavements containing CCA and C-EPS in the sub-base?

6. What is the effect of CNA on the compressive and tensile strengths of concrete intended for use as solid concrete permeable pavement blocks?

1.2 Aims and objectives

This research comprises of two (2) main aims. The first aim is to present PPS as an available long-term, sustainable urban drainage option for flood risk reduction and improvement in

urban stormwater runoff quality in SIDS with greater emphasis on Caribbean SIDS. The second aim of the research is to evaluate the performance of permeable pavement systems (PPS) containing recycled/recyclable materials for Caribbean SIDS.

The primary objectives of the research are to:

1. Perform a comprehensive literature review and survey of PPS, challenges and opportunities of climate change and urban development in SIDS as well as the identification of key factors for consideration for widespread acceptance and utilisation of PPS in SIDS.
2. Assess the physical properties of the natural (basalt, quartzite) and recycled materials (CCA, CNA, C-EPS) and their behaviours in the laboratory.
3. Examine the chemical composition of recycled materials CCA, CNA and C-EPS and how they can be utilised.
4. Compare and evaluate in the laboratory, the performance of four (4) permeable pavement rigs; two containing recycled materials (CCA, C-EPS) and two made up of traditional materials (basalt, quartzite) in the following categories:
    a) Hydrological (lag time, attenuation and retention capacity)
    b) Hydraulic conductivity and long-term clogging
    c) Environmental (pollutant removal efficiencies)
    d) Structural integrity (stiffness and deflection profiles using PFWD testing)
5. Develop and calibrate hydrological rainfall-discharge models for each rig using the Computational Hydraulics International's (CHI) computer software, PCSWMM.
6. Examine the effect of CNA on the compressive and tensile strengths of concrete intended for use as novel Concrete Permeable Pavement Blocks (CPPB).

CHAPTER 2. LITERATURE REVIEW

2.1 Overview

This chapter presents a review of SIDS along with some of their challenges, constraints and issues relating to urban development and climate change. The chapter further collates and reviews ideas and research outputs from numerous studies worldwide, highlighting PPS as a form of sustainable urban drainage system. The review includes a literature survey of PPS and discusses key aspects for consideration when designing PPS for SIDS. A major part of this chapter has been published in the journal CLEAN – Soil Air Water and has been included in this thesis with permission from John Wiley and Sons. The article was further included in this journal's Global Recycling Day virtual issue which recognises and celebrates the important role that recycling plays in preserving natural resources (Henheik, 2019).

2.2 Small island developing states

2.2.1 Geography, weather and climate

Small Island Developing States (SIDS) represent a diverse and multicultural group of 38 United Nations (UN) Member States and 20 Non-UN Members/Associate Members of regional commissions located across the Atlantic, Pacific and Indian Oceans and the Caribbean, Mediterranean and South China Seas (UN-DESA, 2018). They are highlighted in Figure 2-1. They commonly enjoy a rich diversity of highly-endemic flora and fauna but limited natural resources.

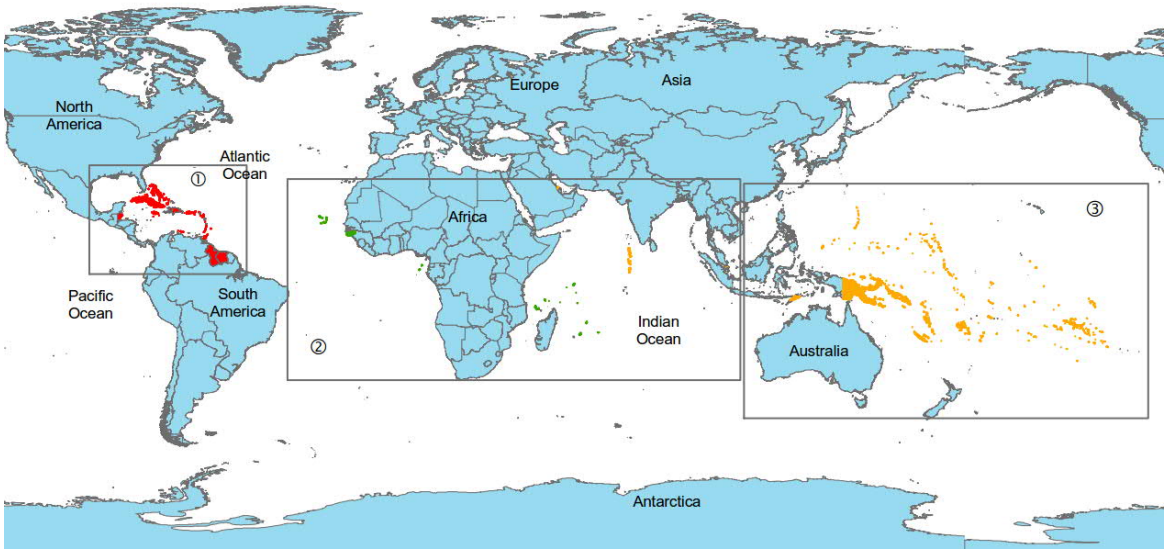

Figure 2-1 Map of Small Island Developing States (SIDS); Caribbean①, Atlantic Ocean, Indian Ocean, Mediterranean and South China Seas (AIMS)②, Pacific Islands③ [Reprint with permission from Monrose and Tota-Maharaj (2018)]

The climatic conditions of SIDS are generally characterised by large seasonal variability in rainfall throughout the regions. Seasonal temperature differences vary slightly for low-latitude islands but substantially for high-latitude islands (IPCC, 2007). The Caribbean SIDS have tropical marine climates, with more diurnal and local variations in temperature (22 – 33°C) rather than seasonal ones (Ekwue, 2010). There is a strong seasonal variation in rainfall distribution. Two distinct seasons exist; a dry season from January to May and a wet season from June to December which comprises of a hurricane season from June to November, where 75 to 80% of rainfall is received during the wet season (Ekwue, 2010, Global Water Partnership (GWP), 2014).

The climate of SIDS in the central Pacific is tropical and influenced by numerous contributing factors such the trade wind regimes, seasonally varying convergence zones such as the Inter-Tropical Convergence Zone (ITCZ) and the South Pacific Convergence Zone (SPCZ), sub-tropical high pressure belts and southern zonal westerlies, with El Niño Southern Oscillation (ENSO) dominating yearly variations (IPCC, 2007, Barnett and Campbell, 2010).

SIDS climate in the Indian Ocean is mostly influenced by the Asian Monsoon. Those of the Mediterranean are influenced mainly by the bordering lands whereby rainfall is predominantly received during the winter months of the Northern Hemisphere with prolonged summer droughts being experienced between four and five months (IPCC, 2007).Average annual rainfall depths and temperature variations amongst the various SIDS groups are presented in Figure 2-2. Insignificant variances are observed amongst the three (3) SIDS groups with an approximate mean rainfall of 2000 mm. The mean annual rainfall comparisons between SIDS and selected developed nations are presented in Table 2-1. It is noteworthy that most published studies on the field performance of Permeable Pavement Systems (PPS), originate from nations which receive less than 50% of SIDS' mean annual rainfall. This is significant and should be taken into consideration when designing PPS for SIDS.

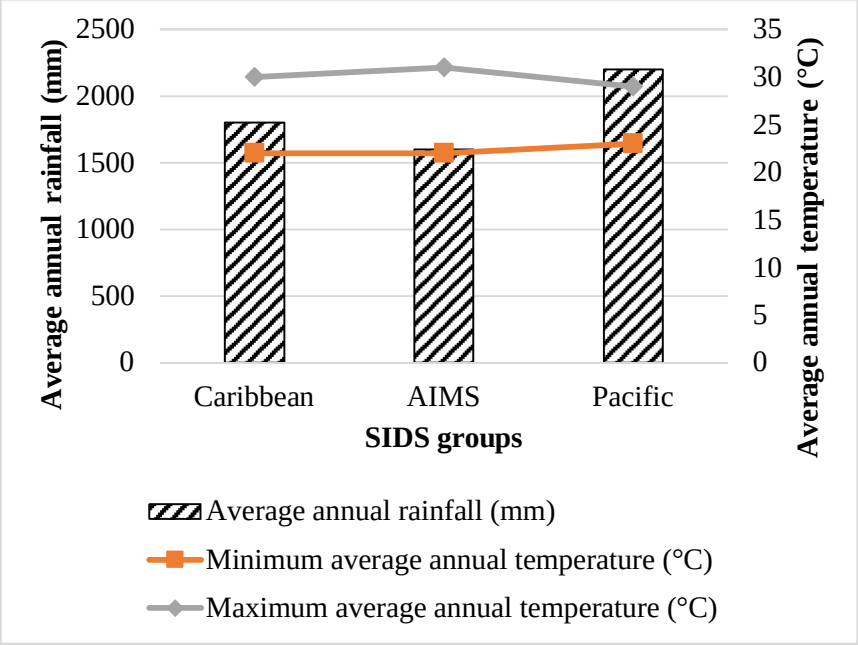

Figure 2-2 Average annual rainfall and temperature across SIDS groups
[Reprint with permission from Monrose and Tota-Maharaj (2018)]

Table 2-1 Average annual rainfall depths (mm) for selected nations
[Reprint with permission from Monrose and Tota-Maharaj (2018)]

Nation	**Mean Annual Rainfall (mm)**
SIDS	2000
United Kingdom*	1220
Spain*	635
France*	867
Australia*	534
Germany*	700
Canada*	537
United States*	715

*Source: (World Bank, 2018)

2.2.2 Challenges and constraints

SIDS, in their drive towards sustainable development, are confronted by numerous challenges and constraints of which ecological fragility and economic vulnerability dominate (Ghina, 2003). Naturally, most SIDS are geologically confined by coastal zones with small and isolated (such as archipelagic states) land extents of either volcanic derivation or coral based. These challenges often lead SIDS to be highly reliant on international trade and consequently are exposed to global economic variances (Ghina, 2003). Geographically,

most SIDS are extremely vulnerable to natural disasters such as hurricanes, cyclones, floods and droughts, all of which threaten lives, property, natural resources and critical urban infrastructure (UN-Habitat, 2015). The effects of these disasters are often extremely costly. Cyclones have accounted for 76% of the reported disasters in the Pacific island region from 1950 to 2004 with an average estimated cost per cyclone of US$ 75.7 million (UN-OHRLLS, 2009). Four (4) countries of the Caribbean (Dominican Republic, Grenada, Jamaica and the Bahamas) amassed an estimated US$2.2 billion in damages resulting from the 2004 Caribbean hurricane season which runs from June to November each year (UN-OHRLLS, 2009). The year 2004 was the worst for the Caribbean region over the last two decades in terms of estimated damage costs from cyclones (Acevedo Mejia, 2016). In contrast to larger territorial countries, a SIDS natural disaster can cause total collapse of economic networks, widespread environmental destruction and considerable and extensive disruptions in the social fabric of the affected SIDS (UN-OHRLLS, 2009).

Despite the numerous challenges faced by SIDS, there are a few common opportunities. These include tourism, aquaculture and fisheries, maritime "blue" economy, renewable energies such as wind, solar and geothermal to some extent, biodiversity and ecosystem-based adaptation (UN-OHRLLS, 2011).

Despite these common challenges and opportunities, it is noteworthy that SIDS vary politically, socially, culturally, in physical size and character or economic development (Nurse et al., 2014). The SIDS label is inconsistent given that not all descriptors are true for all SIDS. Papua New Guinea with an area close to 463,000 km^2, is almost twice New Zealand's size and could not be considered "small" compared to Tuvalu's 26 km^2. Belize, Guyana and Suriname are not surrounded by water, hence do not conform to the "island state" definition (Kelman and West, 2009). The Cayman Islands could not essentially be termed "developing" given that their economic data is superior to that of numerous European countries. Netherland Antilles and Montserrat are territories, as opposed to states, implying sovereignty (Kelman and West, 2009).

2.2.3 Urban development

The Asian Development Bank (ADB), refers to the term *urban* with regards to SIDS as a small town linked to villages bordering a coast, a small town connected by villages on an island, or a succession of islets (ADB, 2014). Approximately 38 million (59%) of the 65 million persons living in SIDS, reside in urban settlements (UN-Habitat, 2015). While there is a wide variation amongst SIDS with respect to the urban population, ranging from

Singapore and Nauru, standing at 100% (most urbanised) to Papua New Guinea with 13% and Trinidad and Tobago, W.I. with 8.5% (least urbanised), they share the common trend of increasing urbanisation (UN-DESA, 2010, UN-DESA, 2015). Listed in Table 2-2, are the comparative levels of urbanisation in the Caribbean, the Pacific islands, the world and More Developed Regions (MDR) for the period 1950 to 2014 in addition to 2050 projections. The Caribbean has experienced unprecedented urbanisation over the last few decades and is presently the world's most urbanised island region (Pelling and Uitto, 2001). Since the 1950s, urbanisation was already at 36% in the Caribbean with this figure increasing to 45.4% by 1970. By 2014 the percentage of people living in urban areas in the Caribbean increased significantly to 70% with projections of 81% by 2050 (UN-DESA, 2015).

For some SIDS, lack of land space available for development has forced development of coastal lands. This is the case for urban cities such as Port of Spain in Trinidad and Tobago, W.I. which has had to reclaim land for further expansion of the city (UN-Habitat, 2015).

Table 2-2 Comparative levels of urbanisation in the Caribbean, 1950–2050
[Reprint with permission from Monrose and Tota-Maharaj (2018)]

Year	**Percentage of total population living in urban areas**			
	Caribbean	**Pacific islands***	**World**	**MDR**
1950	36.1	9.0	29.6	54.6
1970	45.4	19.0	36.6	66.7
2014	70.0	23.0	53.6	78.0
2050	80.7	30.0	66.4	85.4

*Melanesia, Micronesia, Polynesia

2.2.4 Climate change

Climate change can have alternative meanings. This research follows that defined by the Intergovernmental Panel on Climate Change (IPCC) as a change in climate over time attributed to man-made activity or natural variability (IPCC, 2007). By distinction, the United Nations Framework Convention on Climate Change (UNFCCC), defines climate change as a change of climate accredited to human activity that interferes with the earth's atmosphere and which adds to natural climate variability observed over similar timelines (UN, 1992).

SIDS are particularly vulnerable to the impacts of climate change which include increased global temperatures, precipitation and sea level rise (Nurse et al., 2014). This was recognised in the Barbados Programme of Action (BPOA) for the Sustainable Development of SIDS

adopted in 1994 (UN, 1994). Global warming and the resulting sea level rise can become disastrous, threatening the existence and sovereignty of some SIDS whilst potentially reducing the land area in others (UN-Habitat, 2015). A recent study by Simon et al. (2016) suggested that five tiny vegetated islands of the Solomon Islands in the Pacific have disappeared due to rising sea levels and erosion. Islands such as the Maldives and the Marshall Islands in the Pacific could also become inundated given that their highest elevations are three (3) meters above sea level. According to UN-OHRLLS (2009), sea surface temperatures in oceans surrounding SIDS have been increasing by 0.1 °C per decade with projections exceeding 1.5 °C by the end of the 21st century. There have also been increases in extreme temperatures in the South Pacific and Caribbean regions. Rising sea levels have been estimated at 0.77 mm/yr in the Pacific region, 1.0 mm/yr in the Caribbean and 1.5 mm/yr in the Indian Ocean (UN-OHRLLS, 2009). Furthermore, according to UN-OHRLLS (2009) changes in rainfall patterns in the Caribbean could result in decreasing numbers of consecutive dry days with a subsequent increase in the number of heavy rainfall events in the Caribbean.

The progress of SIDS striving towards achieving sustainable development goals is under constant threat because of climate change (UN-Habitat, 2015). The urban centres, economic zones and agricultural lands of most SIDS are usually located in lowlands along coastal zones thereby exposing them to sea level rise, extreme tides and wave and surge events (UN-FCCC, 2007, Nurse et al., 2014). Nurse et al. (2014) presented a literature review on the observed impacts of climate change on human systems in SIDS. In this review Nurse et al. (2014) restated that in the case of atoll islands for instance, rapid urbanisation in city centres promoted unplanned developments at vulnerable locations.

Majority of SIDS experience problems regarding access to a reliable, safe, sustainable and affordable supply of potable water (UNEP et al., 2012). Water resources on SIDS are limited and particularly vulnerable to human-induced and natural stressors. At present, numerous SIDS share common problems associated with the reliability and availability of clean water. This is a serious problem for several SIDS today and one which is forecasted to increase in the future because of climate change (IPCC, 2008). Presented in Table 2-3 are water resource-related issues faced by individual SIDS groups.

Table 2-3 Water resource challenges faced by specific SIDS groups

[Reprint with permission from Monrose and Tota-Maharaj (2018)]

SIDS Group	Water Resource Related Issues
Caribbean	– Rainfall highly variable depending on wet or dry season – Deforestation – Conflicting land use activities within catchments – Reduced soil permeability due to erosion – Inefficient water distribution networks – Demands by rapid population growth and competing economic sectors
Pacific	– Reliable groundwater lenses absent – Polluted groundwater on larger atolls – Unregulated watershed developments cause mass sedimentation – Poor sanitisation – Fluctuating rainfall patterns – Salinisation – Inefficient water distribution networks
AIMS	– Fluctuating rainfall patterns – Significant runoff intensified by mountainous landscape – High soil porosity – Competing demands from tourism, industrial sectors and population growth

Climate change affects groundwater in many SIDS. Sea level rise is projected to widen the areas of seawater intrusion and salinisation of coastal groundwater, resulting in decreases in freshwater available at coastal zones in some SIDS. This becomes more critical in some SIDS as groundwater recharge decreases with changes in rainfall distribution. Further, groundwater resources on several SIDS, particularly low-lying carbonate islands are vulnerable because of several factors including limited land area, urbanisation and increasing demand over supply, decrease in surface water supply and pollution (Treidel et al., 2012).

Several SIDS have commenced implementation adaptation approaches to manage climate change. In Vanuatu, villagers who experienced frequent flooding and erosion were moved to higher grounds (UN-OHRLLS, 2009). The Virgin Islands, in its pursuit towards achieving low-carbon, climate resilient development, developed in 2012, *The Virgin Islands Climate*

Change Adaptation Policy which includes cost effective actions to adapt to the local impacts of climate change as well as the mitigation of carbon emissions (Penn, 2012). To mitigate the impacts of climate change on critical infrastructure, human settlements and water resources, the Government of the Virgin Islands (British) sought to develop and approve numerous policies. One such policy was to minimise impervious surfaces by using PPS for sidewalks and parking lots in an effort to reduce stormwater runoff (Penn, 2012). Others included utilisation of green roofs and other SUDS (Penn, 2012). Singapore's Active Beautiful Clean (ABC) Low Impact Development (LID) Waters Program implemented in 2006 will likely be impacted by larger, more intense rainfall events which may lead to modified design features to cope with the changing climate (Lim and Lu, 2016).

SIDS are not alone when it comes to climate change effects. More developed nations such as the Netherlands, for example, have been affected by sea level rise due to climate change resulting in obstructions in rainwater flow because of longer high tides. For the century prior to 2006, the sea level has risen by 200 mm with projections of 600 mm in the next century. Furthermore, climate change has affected rainfall patterns and heavier and more intense storms have been observed. To address these potential problems, the Netherland authorities recommended PPS with storing capacity as a possible solution (Boomsma and Huurman, 2006).

2.3 Urban stormwater runoff

In urban drainage watersheds, stormwater runoff is generated on impervious surfaces such as roads, roofs, sidewalks, parking lots, etc. or may also be generated on pervious surfaces if antecedent in-situ moisture conditions are high or if rainfall intensities or total rainfall depths exceed surface infiltration rates (Boyd et al., 1994, Pazwash, 2011).

Urban stormwater runoff is recognised as a major contributor to water pollution as contaminants deposited on impervious surfaces are washed off during rainfall events. Vital inorganic runoff pollutants include Total Suspended Solids (TSS) and heavy metals, particularly zinc, copper and lead (Brown and Peake, 2006, Göbel et al., 2007). Numerous studies have cited vehicular traffic, particularly tyre wear and brake lining abrasion as the major source of these metals (Davis et al., 2001, Adachi and Tainosho, 2004, Zanders, 2005). Mitigation of urban runoff pollution requires comprehension of the various runoff pollutant categories, their potential sources and possible effects. Table 2-4 lists a summary of the key classifications of urban runoff pollutants.

Table 2-4 Summary of urban pollutants

[adapted with permission from (Tota-Maharaj, 2010)]

Sediments	Organic and inorganic suspended solids; turbidity; dissolved solids	Suspended solids (100- 300 mg/l); total solids (100-3000 mg/l); turbidity (110-340 NTU)	Construction sites; urban and agricultural runoff; sewer systems; sewer pipelines; landfills; septic tanks	High turbidity, habitat alternation, recreational and aesthetic loss, contaminant transportation, hydrology, bank erosion
Nutrients	Nitrates; nitrites; ammonia; Organic nitrogen; phosphates; Total phosphorus	Ammonia-nitrogen (0.1-10 mg/l); nitrate-nitrogen (0.01-10 mg/l); total nitrogen (0.1-50 mg/l); total phosphorus (0.01-5 mg/l)	Urban and agricultural runoff; landfills; septic tanks; atmospheric deposition; soil erosion	Surface waters: algal overgrowth and blooms, ammonia toxicity. Ground water: Nitrate toxicity
Pathogens	Total coliforms; faecal coliforms; faecal streptococci; *Escherichia coli*; *Enterococcus*; viruses	Total coliforms (106-109); faecal coliforms (103-107 CFU/100ml); *Escherichia coli* (102-107 CFU/100ml); faecal streptococci (102-106 CFU/100ml);	Urban runoff; agricultural runoff; septic systems; poor sanitary connections; Combined Sewer Overflows (CSO); domestic and wild animals	Intestinal and gastrointestinal infections, ear infections, dysentery, typhoid fever, recreational and aesthetic loss
Organic enrichment	BOD; COD; TOC; Dissolved Oxygen	BOD (10-15 mg/l); COD (73-94 mg/l); TOC (80-220 mg/l)	Urban runoff; agricultural runoff; landfills; septic tanks; atmospheric deposition; soil erosion	Dissolved oxygen depletion, odours, toxicity levels for fish and other aquatic life, noxious weed proliferation
Toxic pollutants	Toxic trace metals; toxic organics; Poly-aromatic hydrocarbons	Total lead (0.01-5mg/l); total zinc (0.01-5 mg/l); total hydrocarbons (0.01-5 mg/l)	Urban runoff; agricultural runoff; pesticides; herbicides; hazardous waste sites; landfills; oil spills; hydrocarbon disposals, industrial discharges	Bioaccumulation in food chain organisms and potential toxicity to humans and other organisms

2.4 Sustainable urban drainage systems

Sustainable Urban Drainage Systems (SUDS) aim to protect and enhance natural water systems within urban developments, improve the quality of water draining from urban developments, reduce runoff and peak flows via development of on-site temporary storage measures for potential water reuse and minimisation of impervious areas, reduce potable water demands utilising stormwater as a resource through capture and reuse for non-potable purposes (gardens, irrigation, car washing, etc.) (Sharma, 2008, Stewart and Hytiris, 2008, Charlesworth and Warwick, 2012, Poleto and Tassi, 2012, Zhou, 2014, Woods Ballard et al., 2015). The philosophy of SUDS is therefore to replicate, as closely as possible, pre-development drainage through the minimisation of effects of development on runoff quantity and quality and maximising amenity and biodiversity (Woods Ballard et al., 2015). These objectives are shown in Figure 2-3. Quantity is achieved through the control of surface runoff at point sources and implementing stormwater techniques to reduce flooding. Quality is achieved through the reduction of pollutants within runoff. Amenity and biodiversity are based on social equity, environmental protection and prudent use of natural resources to sustain life (Woods Ballard et al., 2015, Hoang and Fenner, 2016).

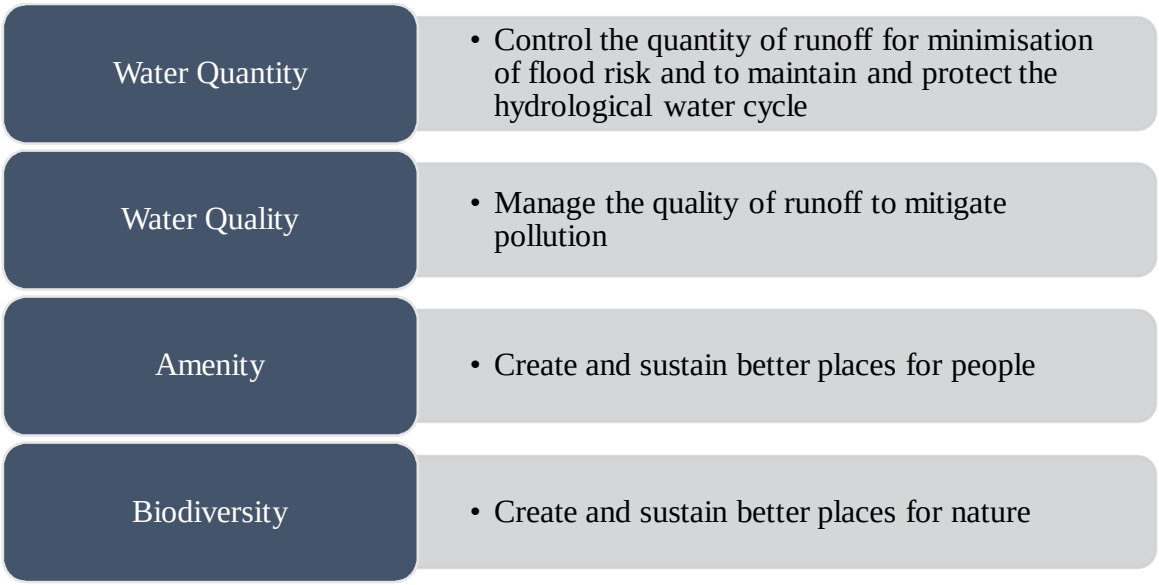

Figure 2-3 Sustainable Urban Drainage Systems (SUDS) objectives
[adapted with permission from Woods Ballard et al. (2015)]

SUDS provide three (3) main advantages. They decrease the risk of flooding, allow the natural disposal of water through infiltration and reduce the pollution of watercourses. Hesitancy in implementing such systems have included technical uncertainty in performance, lack of data, social perceptions and adoption and maintenance issues (Abbott and Comino-Mateos, 2003).

SUDS consist of several techniques designed to effectively manage surface water runoff at the source in a more sustainable manner than conventional drainage systems. Source control is defined by Pratt et al. (2002) as the control of runoff at or near its source. The relationship between source control and the overall surface water management train as described by Woods Ballard et al. (2007) is illustrated in Figure 2-4.

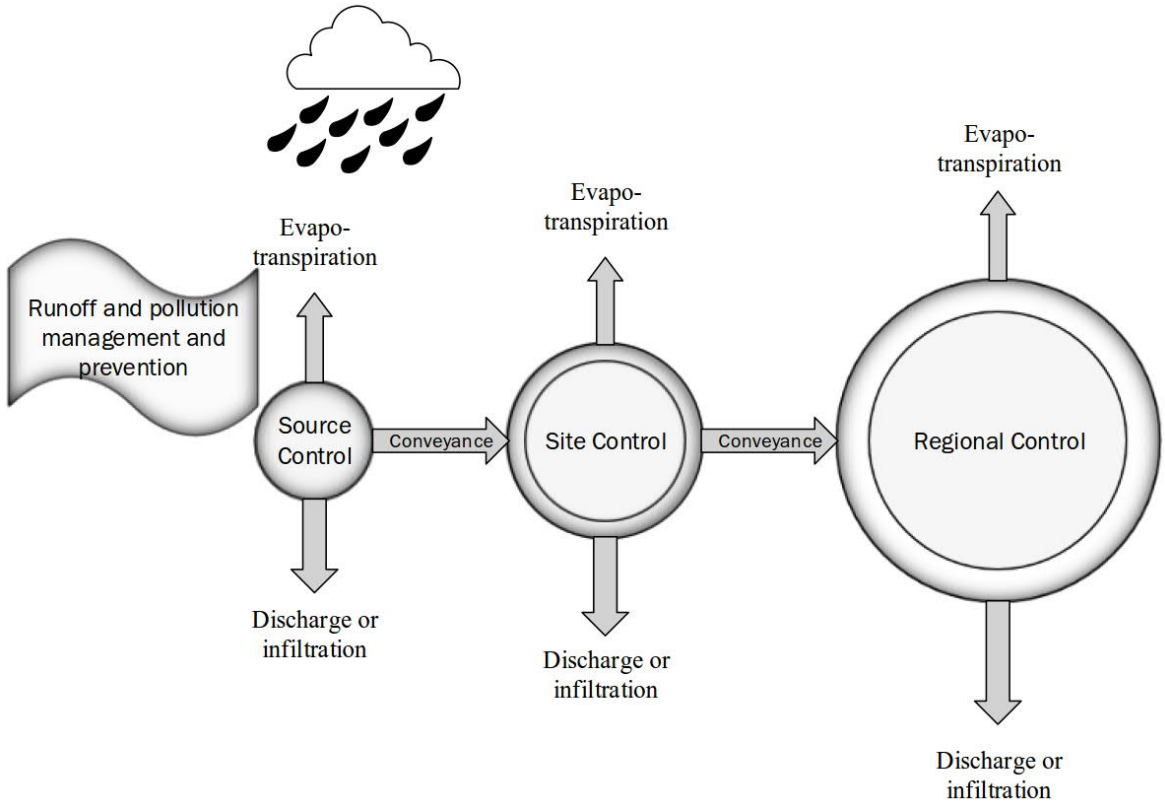

Figure 2-4 The relationship between source control and overall surface water management train

[adapted with permission from Woods Ballard et al. (2007)]

SUDS mimic natural drainage processes to treat, transport and attenuate runoff (Stewart and Hytiris, 2008). The terms SUDS, LID, WSUD, and Best Management Practice (BMP) refer to similar concepts (Fletcher et al., 2015, Cipolla et al., 2016). SUDS is used in Europe focusing on the maintenance of good public health, protection of water quality and preservation of biodiversity and natural resources for future needs (Henze et al., 1997a, Hellström et al., 2000, Willems et al., 2012). LID is used in the United States and Canada to describe an approach which aims at achieving stormwater management controls by fundamentally changing conventional site design to create an environmentally functional landscape that mimics natural watershed hydrological functions (Cheng et al., 2002). BMP in the United States and Low Impact Urban Design and Development (LIUDD) in New

Zealand are examples of similar approaches (Zhou, 2014). WSUD is used in Australia to mainly refer to a planning and engineering approach to achieve harmony between water and the urban environment through the sustainable integration of urban water management into the city landscape (Roy et al., 2008, Sharma et al., 2008, Joint Steering Committee for Water Sensitive Cities (JSCWSC), 2009).

The most prevalent SUDS include green or vegetated roofs, rainwater harvesting, filtration trenches, filter strips, swales, infiltration basins, constructed wetlands, retention ponds, detention ponds and permeable (also called porous or pervious) pavements (Cipolla et al., 2016).

2.5 Permeable pavement systems

2.5.1 Overview

The use of Permeable Pavement Systems (PPS) dates back to the early 1970s (Thelen et al., 1972). The technology allows for infiltration of stormwater runoff through pavement surfaces and into the underlying sub-base and into the foundation soils (if permitted), promoting pollutant removal and pre-development site conditions (Pratt et al., 2002, Tota-Maharaj, 2010). Typical applications include roadway shoulders, residential driveways, parking lots, sidewalks, bicycle lanes and pedestrian access (Pratt et al., 2002, Ferguson, 2005, Scholz and Grabowiecki, 2007). The vertical profile of a typical PPS is illustrated in Figure 2-5.

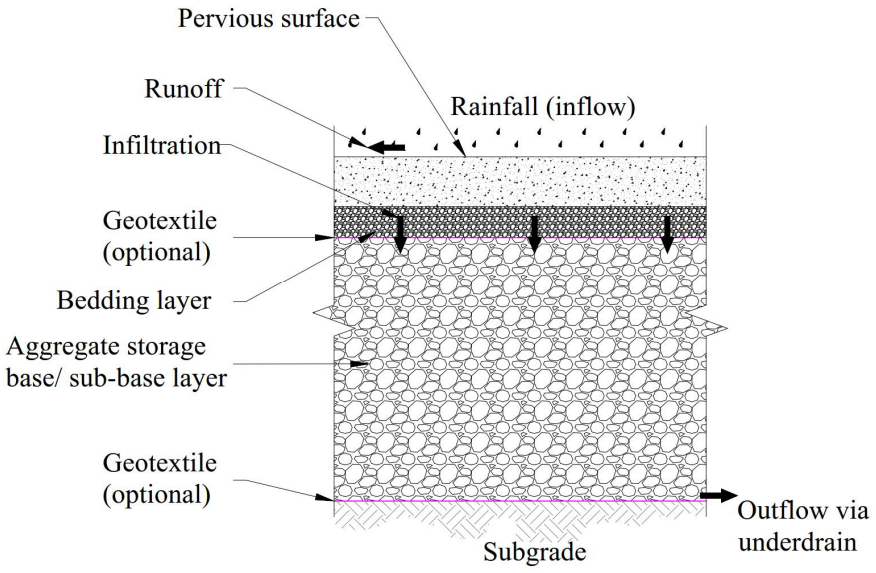

Figure 2-5 Vertical profile of typical permeable pavement systems with urban stormwater runoff

[Reprint with permission from Monrose and Tota-Maharaj (2018)]

2.5.2 Permeable pavement systems structure

The primary objectives and design requirements of PPS contrast with conventional pavements (Pratt et al., 2002, Pezzaniti et al., 2009, Charlesworth and Warwick, 2012). Conventional pavements, designed for use by vehicular traffic, are typically constructed in layers consisting of a rigid or flexible surface and one or more compacted aggregate sub-base/ base courses overlying a compacted subgrade (Pezzaniti et al., 2009). Stormwater is typically not permitted through the surface layer of conventional pavements. Permeable pavements, on the contrary, allow the infiltration of stormwater through the pavement structure (Diniz, 1980) thereby mimicking the natural soil environment. A cross section schematic of a permeable pavement system with optional geotextiles is shown in Figure 2-6. The structure typically consists of a permeable/pervious/porous paving surface and layers of coarse aggregate (sub-base and base) materials that function as a storage reservoir during rainfall events, a bedding layer which supports the paving surface and optional geotextile layer(s). Geotextiles, or filter fabrics as they are informally called, are typically polymer fabrics that inhibit the movement of small suspended particles in stormwater (Ferguson, 2005).

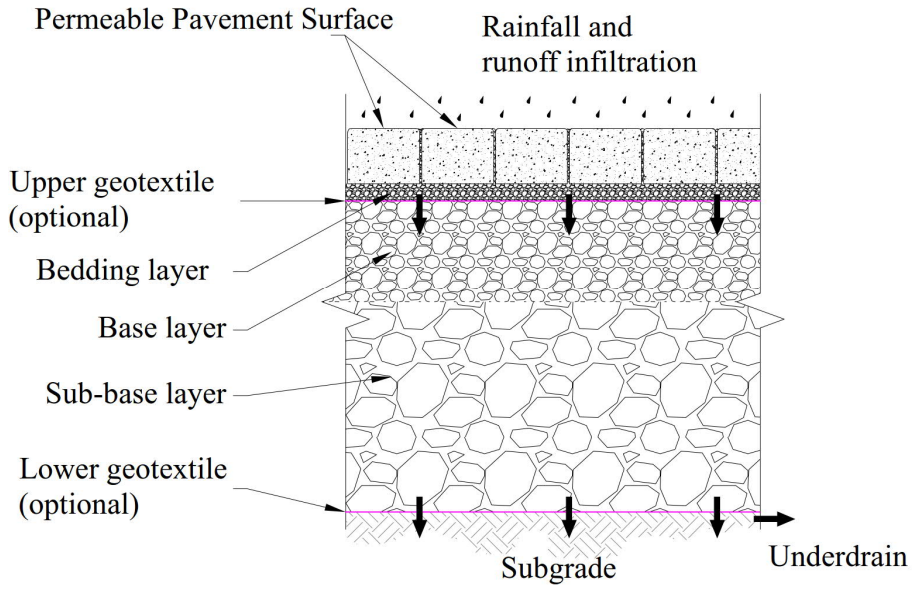

Figure 2-6 Cross section schematic of a permeable pavement system with geotextiles [Reprint with permission from Monrose and Tota-Maharaj (2018)]

Permeable pavements typically consist of natural aggregates with gradations based on ASTM C33, Specification for concrete aggregates (ASTM International, 2003). ASTM No.8 aggregate is typical for the bedding layer, ASTM No. 57 for base and ASTM No.2 for the

sub-base. For improved hydraulic and structural performance, these aggregates are typically clean, single-sized or open-graded and angular. The excessive voids between the aggregates permit high permeability usually in excess of 25 m/h (Ferguson, 2005). Unlike conventional pavements with aggregate base and sub-base layers that are constructed with compacted dense-graded aggregates, permeable pavement aggregate base and sub-base layers support loads primarily from friction and interlock between the aggregates (Ferguson, 2005). Underdrains and geotextile layers are optional depending on design requirements and in-situ subgrade (natural soil) permeability conditions.

The primary purpose of geotextiles in PPS is separation. They are often used to restrict the movement of fines into the aggregate storage reservoir (Ferguson, 2005). Furthermore, geotextiles assist in retaining pollutants and degrading oil (Newman et al., 2004, Tota-Maharaj et al., 2012, Scholz, 2013). Placement of a geotextile layer in PPS has, however, been inconsistent with some studies (Pratt, 1997, Lucke and Beecham, 2011a, Tota-Maharaj et al., 2012, Rahman et al., 2015b) proposing reasons either for or against them. Mullaney and Lucke (2013) conducted a literature review on the inclusion of a geotextile layer in PPS and reported some concerns. Geotextile layers were thought of as providing restrictions to the hydraulic conductivity (permeability) of PPS in addition to compromising the structural integrity of the pavement through the creation of a slip plane which reduced the friction between the various aggregate layers of the pavement. Either way, additional scientific evidence is required to support both arguments.

The typical design of PPS considers various boundary conditions for either no, partial or full infiltration into the in-situ subsoil (Tota-Maharaj, 2010). These boundary conditions are illustrated in Figure 2-7. When infiltration into the in-situ soil is not desired, an impermeable geotextile layer (geomembrane) is often used to separate the subsoil and the aggregate reservoir layer. An underdrain (perforated pipe) positioned at or near the bottom of the aggregate reservoir layer collects and conveys inflow to a desired outfall. This is often the case for permeable pavements installed over clayey subsoils with high shrink-swell potential and low permeability. These pavements are typically designed with a thicker aggregate reservoir layer for increased structural capacity (Hunt and Collins, 2008).

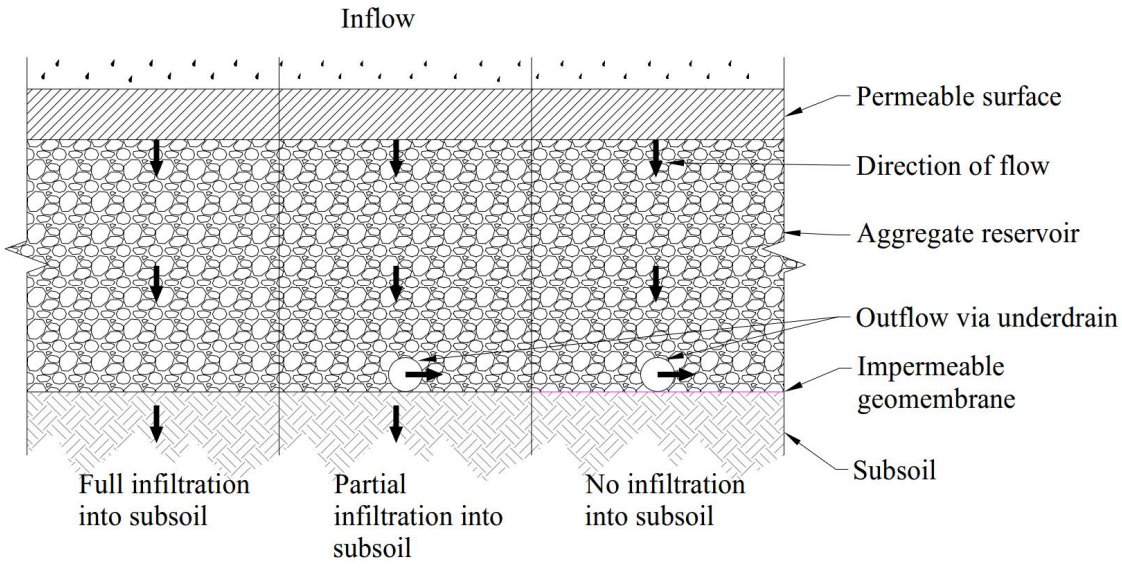

Figure 2-7 Permeable pavement infiltration boundary conditions
[adapted with permission from Interpave (2018)]

2.5.3 Types of permeable pavement systems

A variety of permeable pavements have been identified based on their surface layer which are either monolithic, modular or grid types. Monolithic permeable pavements facilitate infiltration of water through their surfaces. Examples include Porous Asphalt (PA) and Porous Concrete (PC). Modular pavements consist of concrete blocks placed adjacent to each other in various patterns with infiltration taking place through the joints between the blocks. The most prevalent modular units are Permeable Interlocking Concrete Pavers (PICP). Grid pavements consist of large gaps which facilitate infiltration. Examples include Concrete Grid Pavers (CGP) and Plastic Grid Pavers (PGP) (Collins, 2007).

Porous Asphalt (PA) is traditional hot mix asphalt with a reduced percentage of fines. The reduction in fines creates interconnected void spaces which facilitate infiltration of stormwater. Voids of approximately 22% have been reported by Van Heystraeten and Moraux (1990) for compacted PA. These voids increase skid resistance and reduce aquaplaning, splash, spray, noise level and light reflection (Van Heystraeten and Moraux, 1990). For improved structural integrity and temporary stormwater storage, an underlying base course layer is typically required (Ferguson, 2005).

Porous Concrete (PC) is concrete with a high porosity achieved due to the absence of fines thereby creating a highly interconnected void content (Sabnis and Obla, 2009). Typically, PC has a water to cementitious materials ratio of 0.35 to 0.45 with a void content of 15 to

25% (NRMCA, 2004). Due to the high void content, PC is lightweight with densities ranging from 1600 to 1900 kg/m^3. PC pavements are typically placed as a 100 to 200 mm thick mat with a gravel base to facilitate storage or infiltration. Compressive strengths of PC pavements are limited, ranging from 2.8 MPa to 28 MPa (NRMCA, 2004).

Permeable Interlocking Concrete Pavers (PICP) consists of manufactured modular concrete units of various shapes and sizes placed adjacent to each other in various patterns. Drainage is typically through small joints/ openings between the units which range from 3 to 13 mm. These openings usually comprise 8 to 20% of the surface area of the units and are filled with highly permeable 2 to 5 mm aggregates (Hunt and Collins, 2008). In the USA, PICPs conform to ASTM C936 (ASTM International, 2018b) which ensures that the pavers have a minimum depth of 65 mm and a compressive strength of 55 MPa. The compressive strength of concrete is taken as the maximum compressive load it can carry per unit area (Dhir and Jackson, 1996). Figure 2-8 illustrates the minimum compressive strengths required of block pavers in developed nations. Compressive strengths range from 40 MPa (New Zealand) to 60 MPa (Germany). PICPs, when designed and constructed adequately, are attractive, durable, easily repaired, require low maintenance and can withstand heavy vehicle loads (Kumar, 2014). Jamshidi et al. (2019) studied 47 years (1971–2018) of varying literature sources in Japan and reported that interlocking concrete pavers satisfied the structural, functional, social and environmental performances in addition to being highly rated by pavement users.

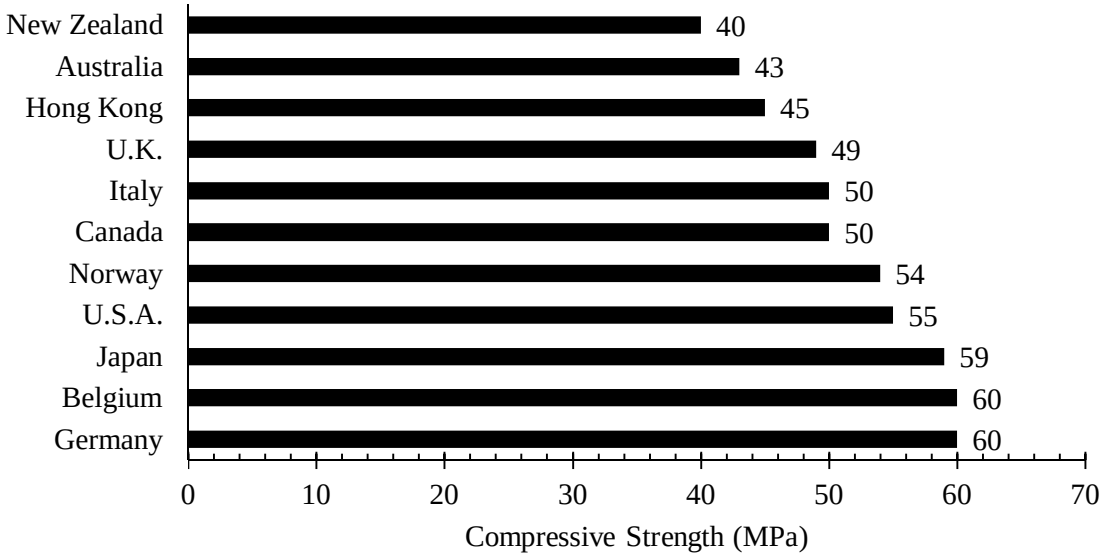

Figure 2-8 Minimum compressive strengths required of block pavers in various developed countries

[Reprint with permission from Monrose and Tota-Maharaj (2018)]

Concrete Grid Pavers (CGP) conform to ASTM C 1319, (ASTM International, 2014a), which defines concrete grids as having maximum dimensions of 610 mm long by 610 mm wide and a minimum nominal thickness of 80 mm (Hunt and Collins, 2008, Kumar, 2014). Open/void area percentage ranges from 20% to 50% and consists typically of topsoil and grass, sand, or aggregate (Hunt and Collins, 2008). Photoanalysis determined that CGP surface was approximately 30% open (Bean et al., 2007). A pavement structure utilising CGP, typically consists of fill media, a bedding sand layer (25 to 38 mm thick), a gravel base course layer and a compacted soil subgrade (ICPI, 2006).

Plastic Grid Pavers (PGP) also referred to as geocells, are made up of heavily-voided flexible plastic interlocking units which can be infilled with gravel, soil and grass that permit infiltration of stormwater. It is typical for a PGP design to include a sand bedding layer and a gravel base course layer to improve infiltration and storage. Grids are usually 90 to 98% open space when empty. As such, void space depends on the fill media (Ferguson, 2005).

Where PPS have been utilised, PICPs have been the preferred option primarily because of their superior structural capacity and infiltration performance, lower maintenance and ease of installation (Lucke and Beecham, 2011a).

2.5.4 Design of permeable pavement systems

In general, the success of a permeable pavement considers both its structural and hydrological characteristics. Structural design considers the pavement's load bearing capacity (Hein, 2014). To date, no standard structural design procedure has been adopted for all permeable pavement types (Weiss et al., 2019). Hydrological design considers the capacity required for infiltration, storage and detention of water as a sustainable stormwater management approach (Hein, 2014). The provision and maintenance of surface infiltration and storage capacity is fundamentally important to ensure that an adequate volume of stormwater is captured and treated (Scholz et al., 2014). The design process of permeable pavements has been well documented by several researchers (Leming et al., 2007, Hein et al., 2010, Hein, 2014, Weiss et al., 2019). The governing design is dependent upon which of the two designs (hydrological or structural) that provides the more conservative cross section (greater thickness of permeable sub-base). In this case, both structural and hydrological needs will be satisfied (Woods Ballard et al., 2015, Weiss et al., 2019). A summary of the various methods used in the hydrological and structural design of permeable pavements is presented in Table 2-5.

Table 2-5 Methods for hydrological and structural design requirements of permeable pavement systems

[adapted from Weiss et al. (2019)]

Hydrological Design	
Method	Details/ Design objective
Curve number method (NRCS, 1986)	Determines runoff depth of the design storm needed to be stored by the permeable pavement $$Q = \frac{(P - 0.2S)^2}{(P + 0.8S)}$$ where Q = runoff depth (mm), P = precipitation depth (mm) and S = maximum basin storage succeeding runoff (mm) $$S = \frac{25400}{CN} - 254$$ where *CN* is the Curve Number based on soil type and land use
Rational method	Determines peak flow of the design storm $$Q = HCiA$$ where Q = the peak flow rate of run-off (m^3/s, ft^3/s), C = the run-off coefficient for the surface (from 0 to 1.0), i = rainfall intensity (cm/hr, in/hr) and A = watershed area (hectares, acres). The unit conversion factor, H, is 0.0278 for metric units and 1.0 for English units.
PICP method (Smith, 2011)	Determine permeable pavement surface area and depth requirements Surface area of PICP is considered 100% pervious To avoid oversaturation of subgrade, maximum allowable storage time is first determined $$d_{max} = \frac{fT_s}{V_r}_{max}$$ where d_{max} = maximum base/subbase depth, f = final infiltration rate into the subgrade soil, T_s = maximum storage time and V_r = void ratio of the base/subbase (typically 0.4) For systems without underdrains two equations were developed for the volume of water stored in the base and subbase

	$$A_p = \frac{\Delta Q_c A_c}{V_r d_p - P + fT}$$ $$d_p = \frac{\Delta Q_c R + P - fT}{V_r}$$ where A_p = horizontal surface area of permeable pavement, ΔQ_c = depth of run-off from watershed flowing onto the pavement, A_c = contributing watershed area, V_r = void ratio of stone base and subbase, d_p = depth of stone base and subbase (excluding bedding course or pavers), R = ratio of the contributing area to the permeable pavement area, P = design storm run-off depth, f = final infiltration rate into the underlying soil and T = effective filling time of the base and subbase layers (assumed as 2 h for NRCS Type II storms). If the required depth > d_{max}, underdrains are required.
Los Angeles county method (LADPW, 2002)	This method has been utilised for pervious concrete. A computer program, *PerviousPave* incorporates a hydrologic design based on this method. The hydrologic design is in conjunction with structural design whereby the thickness of the concrete surface is determined from structural design and maintained during the hydrologic design. The subbase thickness is adjusted to meet the design storage requirements.
Computer modelling	Determines design storm flow rates and/or run-off volumes Various computer models can be used to perform hydrologic designs. Some of these include: – Storm Water Management Model (SWMM), developed by the U.S. Environmental Protection Agency – Hydrologic Engineering Centre – Hydrologic Modelling System (HEC-HMS), developed by the U.S. Army Corp of Engineers – HYDRUS, developed in collaboration with University of California, Riverside, USA
Structural Design	
Method / Source	Details/ Design objective

The American Association of State Highway and Transportation Officials (AASHTO) structural design guidelines for flexible pavements (AASHTO, 1993)	$$log\,W = Z_R \times S_0 + 9.36 \times log(SN + 1) - 0.02 + \frac{log\left[\frac{P_i - P_t}{P_i - 1.5}\right]}{0.4 + \frac{1094}{(SN+1)^{5.19}}}$$ $$+2.32 \times log(0.145 * M_R) - 8.07$$ where W = design traffic load in equivalent single axle loads (ESALs), Z_R = standard normal deviation associated with reliability level (factor of safety) R, S_0 = standard deviation, SN = structural number of the pavement, where SN = $\sum a_i d_i$, a_i = structural layer coefficient, d_i = layer thickness, P_i = initial serviceability, P_t = terminal serviceability and M_R = subgrade resilient modulus (kPa) One ESAL = 80 kN (18,000 lb) Reliability values of 0.75 or less can be assigned to low traffic volume roadways such as permeable pavements Subgrade soil strength quantified using the resilient modulus (M_R), California Bearing Ratio (CBR) or resistance (R-value)

2.5.5 Hydrological performance

PPS hydraulic characteristics generally contribute to four areas of hydrological control: peak flow, volume, hydrograph timing and duration (Fassman and Blackbourn, 2010). Numerous conditions should be considered when comparing results relating to the hydrological performance of PPS. The major factors include local climatic and in-situ soil conditions, depth of pavement structure, boundary drainage conditions and age of the PPS (Drake et al., 2013). Other conditions such as rainfall intensity and duration are also important and should be monitored. Spatial heterogeneity is typical for field-scale installations due to differential inputs, traffic loadings, drainage patterns and installation and maintenance conditions across the pavement surface (Drake et al., 2013).

Booth and Leavitt (1999), evaluated the long-term performance of four full-scale field PPS and reported an absence of surface runoff from all the PPS. Abbott and Comino-Mateos (2003) presented research on the hydraulic performance of an in-situ operational PPS in Wheatley, UK. They [Abbott and Comino-Mateos (2003)] reported an average 77.5%

surface runoff reduction for various storm events. In a 26-month monitoring study of a permeable parking lot consisting of two sections of PICPs, one CGP and one PC in Eastern North Carolina, USA, Bean et al. (2007) reported a reduction and at times an elimination of surface runoff. Collins et al. (2008) found that for the same area of study, PICPs and CGPs were able to retain up to 6 mm of rainfall with no runoff. Alyaseri and Zhou (2016) evaluated the effectiveness of permeable pavement in reducing the volume of stormwater in combined sewers and reported reductions in stormwater runoff of 36%, 13% and 46% from PC, PA and PICP pavements respectively.

Furthermore, in their studies, Rushton (2001), Hunt et al. (2002) used volumetric runoff coefficient (different from the Rational Method runoff coefficient) to assess the hydrological performance of permeable pavements. The average volumetric runoff coefficient, defined as the total runoff volume to the total depth of rainfall for conventional pavements, are typically in the order of 0.80 to 0.95 (Rushton, 2001). Hunt et al. (2002) reported average volumetric runoff coefficients ranging from 0.20 to 0.50 for a permeable paving parking lot with a concrete grid paver constructed over sandy soils in North Carolina, USA. Rushton (2001) found that for a permeable pavement section of a parking lot in Florida, USA, the average volumetric runoff coefficient was 0.10 as compared to 0.58 for an asphalt surface section.

Applied research by Pilgrim and Cordey (1992) used the runoff coefficient, as defined in the Rational Method, as the ratio of the peak rate of direct runoff to the average rainfall intensity to assess the hydrological performance of permeable pavements. In essence, this is the supply period of rainfall resulting in runoff after initial losses have occurred. Ball and Rankin (2010) found supply period runoff coefficients ranging from 0.04 to 7.33% for a pervious section of a suburban street in Manly, Australia. The comparable range for pervious surfaces is 5 to 35%. Furthermore, the installation of the pervious pavement section reduced the effective imperviousness of the catchment from 45% to 3% thereby restoring permeability to an urban catchment. A limitation when using volumetric runoff coefficients, results from the fact that different storms for the same PPS will have different volumetric runoff coefficients given that rainfall depths vary per storm event.

A handful of studies (Dreelin et al., 2006, Tyner et al., 2009, Fassman and Blackbourn, 2010) have reported on the hydrological performance of PPS over fine-grained soils with low permeability. Dreelin et al. (2006) evaluated porous pavement as a BMP for controlling stormwater runoff on fine-grained clay soils. They compared the performance of an asphalt parking lot with the performance of a porous pavement parking lot made up of grass pavers in Athens, Georgia, USA and reported that the porous lot produced 93% less runoff than the

asphalt lot. However, rainfall events were relatively small and of low intensity. Further, the reported percolation rates of the subgrade soils actually had high permeability from 48 to 167 mm/h. Fassman and Blackbourn (2010) investigated the hydrological performance of a 200 m^2 PPS constructed over clayey subgrade soils with an estimated permeability of 0.01 mm/d in New Zealand over a two (2) year period. The impermeable nature of the subsoils had little impact on the hydrological performance of the pavement. According to Fassman and Blackbourn (2010), the findings were 'exceptional' given that peak discharges from the underdrain were lower than modelled predevelopment discharges for most storm events. Tyner et al. (2009) measured exfiltration from pervious concrete through a clay subgrade soil at 8 mm/d and suggested that constructing features such as infiltration trenches and boreholes or scarifying the subgrade soil could enhance infiltration.

2.5.6 Water quality/ environmental performance

It is typical for stormwater runoff from urban areas to be laden with pollutants gathered from impermeable surfaces from a wide variety of anthropogenic activities and environmental processes (Ball and Rankin, 2010, Drake et al., 2013, Pilon et al., 2019). These include suspended solids, oils, heavy metals, organic matter, bacteria and nutrients. The origin of most of these pollutants is often from varying sources including decomposing litter, building materials, vehicle wear and traffic emissions. Left untreated, the quality of water in nearby watercourses and the environment in general is at risk (Scholz, 2013, Pilon et al., 2019).

Permeable pavements have been shown to reduce stormwater pollutants including heavy metals, motor-oil, sediments, bacterial contamination and some nutrients (Pratt et al., 1995, Brattebo and Booth, 2003, Bean et al., 2007, Li et al., 2017, Sounthararajah et al., 2017, Abdollahian et al., 2018, Jayakaran et al., 2019). However, the nutrient removal capabilities of permeable pavements are less understood (Hunt and Collins, 2008) with some studies (Day et al., 1981, Gilbert and Clausen, 2006, Bean et al., 2007, Collins et al., 2008) reporting varying results. Day et al. (1981); Bean et al. (2007) and Gilbert and Clausen (2006) reported removal of total phosphorous (TP), attributed to adsorption to sand and gravel sub-base materials, whilst a similar study (Collins et al., 2008) reported little change in TP concentrations. A handful of studies have shown a decrease in concentrations of all measured nitrogen species (NH_4-N, TKN and NO_3-N) (Pagotto et al., 2000, Gilbert and Clausen, 2006) whereas other studies have shown increases in certain forms of nitrogen concentrations or they remain unchanged (Day et al., 1981, Collins et al., 2008). These differences could be attributed to varying local environmental conditions. Permeable pavements have also been shown to be efficient attenuators for bacteria such as total coliforms, faecal streptococci,

Enterococci and *E. coli* (Tota-Maharaj and Scholz, 2010, Abdollahian et al., 2018, Selvakumar and O'Connor, 2018). Tota-Maharaj and Scholz (2010) reported that a permeable pavement was effective in removing *E. coli*, total coliforms and faecal streptococci by 98 to 99%. Selvakumar and O'Connor (2018) reported on the removal of faecal coliform, *Enterococci* and *E. coli* using PICP, PA and PC. Selvakumar and O'Connor (2018) found that PC removed faecal coliform, *Enterococci* and *E. coli* by 93%, 62% and 100% respectively; PA removed faecal coliform, *Enterococci* and *E. coli* by 94%, 100% and 100% respectively and PICP removed only *E. coli* by 39%. The authors attributed the near complete absence of microorganisms to the high pH (11) of the PA infiltrate which was previously reported by Brown and Borst (2015). Abdollahian et al. (2018) found that PICP with deep (2 m to 4 m) reservoirs removed *E. coli* by an average 69%.

PPS can act as powerful in-situ bioreactors that can reduce hydrocarbon contamination by 99% (Newman et al., 2002). The large surface area within the existing voids within the pavement structure creates a biological diverse micro-ecosystem capable of degrading pollutants such as oil leaks from automobiles (Ferguson, 2005). Pratt et al. (1999), evaluated the in-situ microbial bio-degradation of mineral oil within a full-scale laboratory model of a permeable pavement system over a 300-day period at Coventry University, UK. The authors reported that the pavement performed as an effective in-situ bioreactor, reducing petroleum contamination in the effluent by 97.6%. According to Pratt et al. (1999), nutrient supply is essential to maintain biodegradation efficiency. The authors used a slow-release fertiliser to provide a constant, low-level supply of nutrients to the biomass which promoted sustained oil-degradation within the structure. It is noteworthy that efficient use of nutrients must be ensured, otherwise there is danger that high levels in the effluent can lead to eutrophication problems in receiving waters. Newman et al. (2002) presented a paper which assessed the nature and biodiversity of microbes (microbial fauna) found within a laboratory-scale PPS after 4 years of continuous oil and simulated rainfall inputs. The authors reported 99 % efficiency in terms of oil retention.

2.5.7 Clogging and maintenance of hydraulic capacity

PPS have been commended by numerous studies (Brattebo and Booth, 2003, Bean et al., 2007, Collins, 2007, Beecham et al., 2012, Charlesworth et al., 2017) for the trapping of sediments and other pollutants during infiltration of stormwater runoff. However, this process can result in the clogging of the pavement surface leading to reduced infiltration rates. There is a perception that a conflict of interest exists that questions the appropriateness of the word ‘sustainable’ for permeable pavement (Butler and Davies, 2011). All

infrastructure including permeable pavements will require maintenance (Sansalone et al., 2012). Hence, permeable pavements, as with all filtration systems, will, over time, require removal of trapped solids. Some studies (Pratt et al., 1995, Borgwardt, 2006, Siriwardene et al., 2007, Lucke and Beecham, 2011a) have found that for PICPs, fine particles accumulate in the upper layer of the pavement joints and bedding layer aggregates. Finer particles trap larger particles resulting in increases in the rate of clogging (Balades et al., 1995). In a study conducted on 52 permeable pavement sites, Nicols and Lucke (2017) found that Particle Size Distribution (PSD) curves could not be used as a stand-alone tool to infer PICP clogging processes but found that fine particles of sizes 251 to 550 μm contributed to lower infiltration rate measurements. Charlesworth et al. (2017) found that after three (3) years of monitoring, most of the sediments were in the surface layer of a porous asphalt laboratory test rig.

Numerous researchers (Sansalone et al., 2008, Boogaard et al., 2014a, Winston et al., 2016) have shown an exponential decay of surface infiltration rate as a function of age of the permeable pavement (Figure 2-9). Emerson et al. (2010) reported that infiltration rates of permeable pavers were reduced by between one to two orders of magnitude after three (3) years of operation. Borgwardt (2006) reported that the infiltration performance of permeable pavements decreases in the order of a power of ten after a few years of operation. Categories of PICP pavement clogging and associated infiltration rates are listed in Table 2-6. These values could be used by engineers as a guide to assess clogging.

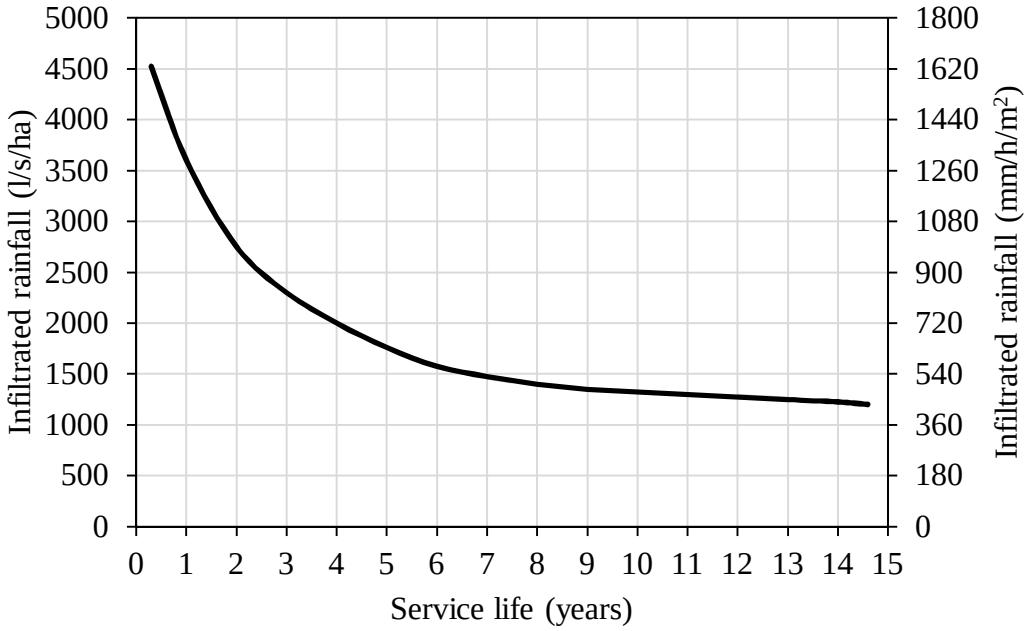

Figure 2-9 Permeable Pavement Surface infiltration rate with time
[Reprint with permission from Monrose and Tota-Maharaj (2018)]

Table 2-6 Categories of PICP pavement blockage and associated infiltration rates [Reprint with permission from Monrose and Tota-Maharaj (2018)]

Average Infiltration Rate (mm/h)	Blockage Category
>2000	Unblocked
30-2000	Medium Blocked
<30	Fully Blocked
97.2*	Minimum European PICP Infiltration Rate

*listed for reference purposes

Presently, there are no global standards for maintenance of PPS. Nevertheless, some field studies have used surface infiltration rate tests as a means of assessing clogging within PPS. ASTM D3385-09 Double-Ring or Single-Ring Infiltrometer tests (ASTM International, 2009b, ASTM International, 2009a) have been used in numerous field studies (Bean et al., 2004, Lucke et al., 2014, Nichols et al., 2014, Cipolla et al., 2016, Lucke et al., 2015, Kumar et al., 2016, Winston et al., 2016, Rocheta et al., 2017, Boogaard and Lucke, 2019). These tests utilise rings that are sealed to the pavement surface and filled with water. An average infiltration rate is recorded based on the time taken for the water to infiltrate through the pervious surface using either a constant or falling head (Boogaard et al., 2014b). These methods have, however, been reported as time consuming (Nichols et al., 2014, Lucke et al., 2015), costly, and not adaptable to be remotely monitored (Radfar and Rockaway, 2016b).

A similar method of evaluating degree of clogging in PICPs has been developed in Australia called the Stormwater Infiltration Field Test (SWIFT) (Lucke et al., 2015). The SWIFT test, according to Lucke et al. (2015) is simple, fast and inexpensive. It utilises a 20 L plastic bucket with a 40 mm diameter hole at its base and relies on counting the number of fully wetted concrete pavers. Immediate maintenance is required when more than 133 fully wetted bricks are counted. No maintenance is required if less than 29 fully wetted bricks are counted. A plan for maintenance within one to three (3) years is recommended if the number of fully wetted bricks counted is between 29 and 133.

Further, Lucke et al. (2015) compared infiltration results using the SWIFT to ASTM C1781M-14a and reported a strong correlation (Pearson's r = -0.714) between the two methods. Other similar methods include a specially designed Rainfall Simulation Infiltrometer Test (RSIT) (Nichols et al., 2014), the National Centre for Asphalt Technology (NCAT) permeameter (Cooley Jr, 1999, Li et al., 2013c, Lucke et al., 2014), the Falling Head Full Scale (FHFS) method and the Constant Head Full Scale (CHFS) method (Lucke et al., 2014). These two latter methods involve inundating a large area of pavement in the

form of a temporary dam so that the infiltration performance of whole sections of pavements can be measured simultaneously.

Additionally, Lucke et al. (2014) compared the infiltration performance of a seven-year-old PICP permeable pavement in the Netherlands using the FHFS, CHFS and Double Ring Infiltration Test (DRIT) methods. The authors reported that the infiltration results obtained using the FHFS test method were the most appropriate to represent the actual infiltration rate of the whole pavement surface tested. Li et al. (2013c) compared infiltration rates using the NCAT and ASTM C1701 methods and reported that both methods can reliably be used to measure the permeability of all pavement surface types. A major drawback of using ASTM and NCAT methods for conducting infiltration tests to predict maintenance requirements for permeable pavements is that these testing methods involve the transfer of infiltration rate results from a small area of pavement to that of the total pavement area (Lucke et al., 2014). This can produce inconsistent and erroneous results.

Several studies have reported high levels of spatial variability for different measurements conducted on the same pavement using similar or different methods. Nichols et al. (2014) examined the performance of two PICP surface infiltration rate methods: a modified DRIT and a specially designed Rainfall Simulation Infiltrometer Test (RSIT) and reported a 60 % variation in results. Lucke and Beecham (2011a) recorded infiltration rates ranging from 6 mm/h to 11,100 mm/h for twelve different locations of a PICP permeable pavement parking lot at the University of South Australia. The tests were performed after the parking lot had been in use for seven consecutive years.

Li et al. (2013c) compared infiltration rates using the NCAT and ASTM C1701 methods for six field-scale permeable surface types including PC, PA and PICP and recorded 50 to 90% lower readings using the ASTM C1701 method. Lucke, Boogaard & Van de Ven (2014) compared the infiltration performance of a seven year old PICP permeable pavement in the Netherlands using the FHFS, CHFS and DRIT methods and reported a wide variation in infiltration results ranging from 46 mm/h to 760 mm/h. Several reasons for these variations have been listed by Boogaard et al. (2014b). These include age, construction, maintenance, hydraulic ground conditions, environmental site conditions and pavement usage.

Other methods of evaluating clogging include visual assessments and installation of monitoring instruments to observe the water-movement rates in the bedding layer of the pavement. These other methods however, require multiple site visits and do not provide the

continuous performance measure necessary to determine the rate of change (Brown and Borst, 2013).

A more recent assessment of clogging in PPS is with the application of Time Domain Reflectometers (TDRs) and Water Content Reflectometers (WCRs), typically for PPS without drain pipes. The travel time (period) of an electromagnetic pulse of energy of known frequency as it travels back and forth through a conductive waveguide is measured by TDR sensors. When these sensors are inserted through a material of interest, the dielectric properties (or charge storing properties) of the surrounding material alter the travel time. As such, the Volumetric Water Content (VWC) of soils could be measured (Topp et al., 1980, Robinson et al., 2003). It must be noted that these sensors are only able to give an indication of VWC and are not able to estimate the moisture level within the granular reservoir of permeable pavements (Stander et al., 2013). Clogging can be evaluated through continuous recording of data from these sensors (Razzaghmanesh and Beecham, 2018). WCR sensors were first used in the aggregate storage layer under permeable pavements by Stander et al. (2013). The sensors successfully quantified the size and timing of the moisture front as inflow progressed through the various layers of a PPS. Brown and Borst (2013) successfully installed TDRs to measure spatial infiltration and assess clogging dynamics (demonstrate the progression of surface clogging from the upgradient edge) of PPS in Edison, New Jersey and Louisville, Kentucky of the USA. The pavements consisted of porous surfaces of either PICP, PC or PA over an open-graded sub-base reservoir of AASHTO No. 2 recycled concrete aggregate.

Regression models have also been used to assess and predict clogging. Yong et al. (2013) developed a regression model to predict physical clogging after a series of laboratory experiments and found that clogging was significantly correlated with runoff volume and flow rate. Sañudo-Fontaneda (2014) used linear regression models to understand the infiltration behaviour of laboratory permeable pavements under varying clogging scenarios. They correlated infiltration rate with pavement surface slope and runoff infiltration length and found that the runoff infiltration length was the most influential variable in all regression linear models obtained.

2.5.8 Reduction in urban heat island

Urban Heat Island (UHI) can be defined as the increase of the sub-surface, surface, or air temperatures observed in an urban environment compared to the relatively low temperatures of rural surroundings (Chow and Roth, 2006). High urban heat is mainly the result of

anthropogenic heat sources such as vehicles, power plants and air conditioners as well as re-radiated solar radiations stored in large concrete and asphalt infrastructure (Rizwan et al., 2008). Human thermal comfort, air quality and energy usage of nearby vehicles and buildings can potentially be affected by surface and near-surface heat islands (Li et al., 2013b).

The United States Environmental Protection Agency (US EPA), identifies cool pavements, in addition to cool roofs, as an urban heat island mitigating strategy (US EPA, 2008). Permeable pavements have been classified as 'cool' because of their ability to potentially reduce the temperatures of both pavements and air at or near the surface through evaporative cooling. Such evaporative cooling could potentially reduce pavement and consequent air temperature through latent head absorbed during the phase change of water from an aqueous to gaseous state. The cooling effect depends on the moisture content and evaporation rate (Li et al., 2013a). The amount of reflected solar radiation is reduced due to an increase in the amount of solar energy used in the adiabatic processes of evaporating moisture retained in the permeable pavement voids (Tota-Maharaj, 2010). In other words, these permeable pavements stay cool because they partition less solar absorption into thermal conduction than conventional/dry pavements do (Qin, 2015).

As air moves over the warmer pavement surface, heat is transferred to the near-surface air through convection whose rate is dependent upon the velocity and temperature of the passing surface-air, pavement roughness and the exposed surface area of the pavement (US EPA, 2008). Most permeable pavement surfaces are rough and contain more air voids than conventional pavements, thereby increasing their effective surface area exposed to air and introduces air turbulence or circulation over or within the pavement. The outcome is increased convective heat exchange between the pavement and air which promotes reduced temperatures of the pavement and moving near-surface air (Li et al., 2013a).

While permeable pavements' increased roughness and void structure can increase convection and the cooling effect, the possibility exists that their surface's net solar reflectance, thermal conductivity and heat capacity may also be reduced to the extent whereby increased surface temperatures may be produced (US EPA, 2008). Dry pervious/porous pavements have been shown to become hotter on the surface than conventional pavements, indicating the uncertainty of the permeable pavements' cooling effect without evaporation (Kevern et al., 2009, Li et al., 2013a).

Different types of permeable pavement surfaces have varying evaporative cooling effects. When grass is used as infill in Concrete Grid Pavers (CGP), the grass fosters evapotranspiration through roots which convey moisture from deeper soils to the surface. Dirt, soil, or gravel infilled CGP have very negligible cooling effects on the other hand (Asaeda and Ca, 2000, Takebayashi and Moriyama, 2009). Permeable pavers (PICP) have been observed to produce different results regarding temperature development (Qin, 2015). Asaeda and Ca (2000) studied the heating effects on the ground surface of permeable pavers and its characteristics during hot summer weather conditions in Japan and impacts on the thermal environment when compared to traditional asphalt pavements and found that the permeable surface was 9 °C, 14 °C and 9 °C cooler than the asphalt pavement at noon, twilight and midnight, respectively. Andersen et al. (1999) reported that permeable pavers with bedding material had greater daily evaporation rates over structures comprising surface blocks only, ranging from 22% to 122%. This suggested that the infiltration inlets were operating as wicks to allow moisture to move upwards from the substrate to the surface. The variations in increased evaporation percentages were attributed to the composition of the bedding material used. Li et al. (2013b) studied the use of porous asphalt (Caltrans standard 9.5-mm maximum size open-graded with conventional binder) for heat island mitigation at the University of California Pavement Centre test facilities in Davis and found that the porous asphalt pavements, under wet conditions, recorded reduced surface temperatures as compared to impermeable pavements.

2.5.9 Hydrological modelling of permeable pavements

A schematic depicting the hydrological processes occurring in a permeable pavement system is presented in Figure 2-10. These processes have been discussed in detail in literature (Zhang and Guo, 2014, Woods Ballard et al., 2015). Inflow in the form of direct rainfall or runon from adjacent subcatchments may either infiltrate through the pavement's surface zone and move down into the aggregate storage zone/reservoir or travel away from the pavement as surface runoff. Surface runoff will only occur provided that the rainfall/inflow intensity is greater than the permeability of the pavement layers. This seldom occurs as permeable pavements are usually constructed with high permeability. The percolation of water through the reservoir will result in a minor portion of water being adsorbed by the aggregates. The excess water will exit the pavement structure either via the underlying native subsoil if permitted or an underdrain. If the inflow rate exceeds the infiltration capacity of either of these exfiltration routes, the accumulation of water in the storage zone commences. The volume of water in the storage zone will continue to increase until the inflow has ceased or until the outflow rate exceeds the inflow rate. At the cessation of rainfall, the stored water

is depleted via infiltration into the native subsoil, exfiltration through the underdrain and evapotranspiration (ET).

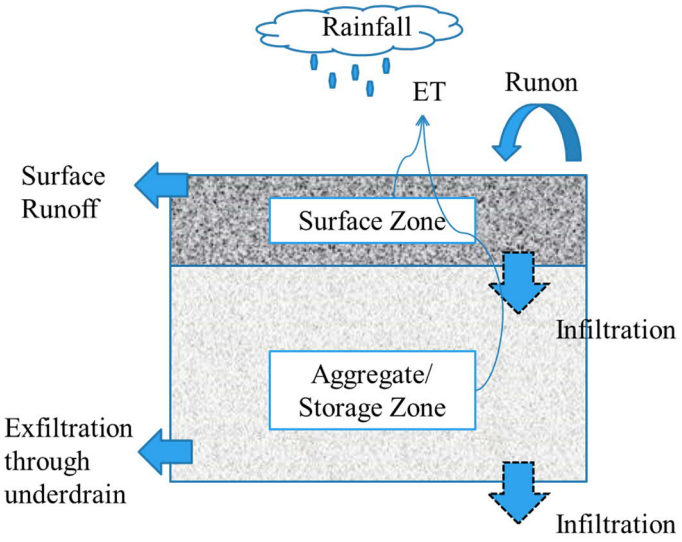

Figure 2-10 Schematic of the hydrological processes involved in a permeable pavement system
[adapted with permission from CHI and Rossman (2010)]

Modelling the hydrological processes of a permeable pavement system has been well presented in the literature (Lee et al., 2015, Huang et al., 2016). Commercially available computer software such as the Computational Hydraulics International (CHI) Personal Computer Stormwater Management Model (PCSWMM), which incorporates the US EPA's Stormwater Management Model (SWMM) engine, provide a LID module for the simulation of both runoff quantity and quality from various catchments. Eight LID types are defined under the LID module namely: bio-retention cell, rain garden, green roof, infiltration trench, permeable pavement, rain barrel and vegetative swale (Rossman, 2010, Rossman, 2015).

SWMM is often used for hydrodynamic sewer modelling and the analysis of LIDs (Goncalves et al., 2018). Jato-Espino et al. (2016b) used SWMM to model an urban catchment in Espoo, Finland and reported that permeable pavement systems of varying cross sections (PA, PC and PICP) had a statistically significant hydrological impact on the response of the catchment and reduced discharge by 50% when compared to scenarios based exclusively on conventional drainage systems. Kourtis et al. (2018) modelled the hydrological impact of permeable pavements (and green roofs) in a small catchment in Athens, Greece using SWMM and reported that the LID practices were effective in attenuating stormwater runoff at the source, thus reducing volume discharges and flooding. Guan et al. (2015) used SWMM to show that permeable pavements were able to reduce

flows to near predevelopment levels in a catchment located in the city of Espoo, Finland. The authors, however, suggested that full restoration of predevelopment flow regimes was not currently achievable.

2.5.10 Evaluation of structural behaviour

The majority of the literature on permeable pavements has focused on their role as a storm water management tool, while the structural assessment of permeable pavements has received much less attention (Vancura et al., 2011). For PICPs, such as those used in this research, different variables such as surface block shape, depth, laying patterns, size and orientation of jointing and interconnection, in addition to the quality of the base and sub-base reservoir materials play a vital role in the structural performance of these pavements (Toronto and Region Conservation, 2008, Murugan et al., 2016, Jamshidi et al., 2019). When designed and installed appropriately, PICPs have been shown to remain structurally sound under various loading and climatic conditions (Ferguson, 2005, Smith, 2011).

The Falling Weight Deflectometer (FWD) and Portable Falling Weight Deflectometer (PFWD) otherwise referred to as Lightweight Deflectometer (LWD) are often used in the field as dynamic, non-destructive testing equipment to obtain the load-deflection response of pavement systems subjected to impulse loading (Suleiman et al., 2011, Mallick and El-Korchi, 2017). The PFWD provides quick and direct measurement of a near-surface, composite modulus parameter. The mechanism of the PFWD has been well presented by Fleming et al. (2007) and Kim et al. (2007). The PFWD generates a force using a falling weight to create a deflection in the pavement equivalent to a moving vehicle with an axle load of approximately 1800 kg (4000 lbs) (Toronto and Region Conservation, 2008).

Very few studies (Toronto and Region Conservation, 2008, Suleiman et al., 2011, Vancura et al., 2011, Henderson, 2012), have reported on the use of deflectometer-type devices for evaluation of the structural integrity of permeable pavements. Vancura et al. (2011) used the FWD on pervious concrete in Minnesota to examine whether calibration of the empirical components of pavement analysis and design tools for pervious concrete, was different to that of a conventional concrete pavement. The authors compared the FWD deflection profiles of the pervious concrete pavements to those generated by the computer software ISLAB2005. Suleiman et al. (2011) used the FWD on a pervious concrete pavement at Iowa State University, USA with a 450 mm-thick aggregate base and reported smaller deflections and better uniform support than that of traditional concrete pavement.

A research team from the Toronto and Region Conservation (2008) used a PFWD to test the stiffness of a PICP section of a parking lot at Seneca College's King Campus a few kilometres north of Toronto, Canada. The researchers reported that the PICP exhibited seasonal changes in strength, with the winter period accounting for the highest elastic modulus values and lowest deflection values. The researchers based this finding on the pavements being stiffer and more structurally sound during the winter when the upper base layers are frozen. When compared to an asphalt pavement, the researchers found insignificant differences in strength.

Henderson (2012) used the PFWD to monitor the changes in the structural condition of five pervious concrete pavement sites and reported differences in structural capacity of the pavements over the monitoring period.

2.5.11 Permeable pavement research in SIDS

Research evaluating the performance of PPS across SIDS is limited to one report by Horsley Witten Group Inc. (HWG) and Centre for Watershed Protection Inc. (CWP) (2014), which listed few SIDS where PPS were used. These SIDS were St. Croix, St. Thomas and St. John of the US Virgin Islands of the Caribbean and American Samoa of the Pacific. The site at St. Croix was located at the University of the Virgin Islands Research and Technology Park as part of a "green" building initiative in combination with other LID practices such as vegetated bio-swales. PICP and grass-infilled PGP were the preferred pavement surface types for both sites. Some of these applications are illustrated in Figure 2-11. There was no information available appertaining to the performance of these PPS. Grass-infilled CGP (Figure 2-12), were used in a parking lot at the University of the West Indies, St. Augustine Campus, Trinidad, W.I. Similarly to the previous example, no information was available regarding the pavement structure or the performance of the pavement since being operational. It is noteworthy, however, that from the researcher's observation on site, it appeared that a significant section of the pavement was clogged, most certainly due to a lack of maintenance.

Figure 2-11 PPS in Caribbean islands (a) and (b) PICP with apertures at St. Croix, (c) and (d) PG in St. John, USVI

[Reprint with permission from Horsley Witten Group Inc. (HWG) and Centre for Watershed Protection Inc. (CWP) (2014)]

Figure 2-12 Grass-infilled concrete grid pavers at the University of the West Indies, St. Augustine Campus, Trinidad, W.I.

2.6 Considerations for use of permeable pavements in SIDS

Urban stormwater control in tropical zones where most SIDS are located is different to other regions of the world because of several factors including political instability, economic fragility, climate change vulnerability and infrastructural and maintenance challenges. Additionally, flooding remains a huge challenge for SIDS. The goal of maintaining an efficient and sustainable urban drainage system still applies. It is noteworthy, however, that

rainfall events in most SIDS are more frequent and of higher intensities than nations of temperate regions where permeable pavements have been used extensively. The literature survey presented previously attests to that. Consequently, the selection of appropriate LID strategies will require special consideration given the numerous variations amongst SIDS groups. Discussed below are some key factors for consideration if PPS are to be used successfully in SIDS.

2.6.1 Physical

2.6.1.1 **Structural integrity and loading applications**

The anticipated traffic loadings supported by the permeable pavement can be characterised according to AASHTO (1993) as Equivalent 80 KN (18,000 lb) Single Axle Loads (ESALs) and Average Daily Traffic (ADT) (Tennis et al., 2004). Permeable pavements in North America have typically been designed for applications not exceeding approximately 1 million ESALs (Smith, 2011). Traffic loadings in SIDS are expected be to significantly less than 1 million ESALs due to the lower traffic volumes, smaller parking lots and fewer heavy trucks.

2.6.1.2 **Design storms**

Design storm or design rainfall events are described in terms of rainfall intensity, duration and frequency (return period) of the event, for instance 25 mm/h for 1-hour with a frequency of 5 years (Pratt et al., 2002). For a given duration, a return period gives the probability that the maximum design rainfall event will be exceeded. It can also be expressed as an annual probability of exceedance. As an example, a return period of 100 years over a particular duration, means that on average, there is 1/100 or 1 percent probability that the maximum design rainfall event will be exceeded in any given year (Pratt et al., 2002). This does not mean that a 100-year storm event is limited to occurring only once every 100 years.

The design storm with the return period and intensity is usually supplied by the municipality or other regulatory agency depending on the flood risk level associated over a specific catchment. Rainfall Intensity-Duration-Frequency (IDF) maps or curves are typically referenced to establish the design storm (Smith, 2011). IDF curves and maps are typically available in numerous locations across the development world (Courty et al., 2019). Developing countries such as those across the Caribbean SIDS are challenged by a scarcity of IDF curves either because of the limited quantity of short-duration rainfall data available or because the few IDF curves that have been developed are generally not in the public domain (Lumbroso et al., 2011, Shrivastava, 2016). Moreover, Caribbean SIDS typically

consist of small catchments that are sensitive to high intensity, short duration storms that often result in flash floods. Cloudbursts (defined as rainfall intensity in excess of 100 mm/h over a short duration for example 15 minutes) along with spatial and temporal variations in rainfall often present further challenges. Under these circumstances, judgment, heuristics and transposition may be inevitable (Shrivastava, 2016).

Sañudo-Fontaneda (2014) conducted a study of IDF curves in 23 cities across several regions of the world for 100-year, 15-min storm events and reported major differences. Intensity values ranged from 50 mm/h (Vancouver, Canada), 100mm/h (London, UK), 200 mm/h (Washington, USA), 300 mm/h (Guatemala City, Guatemala) to 400 mm/h (Yongchun, China). The author also reported as an extreme case, Brisbane, Australia with intensities around 2,000 mm/h.

It is important that the appropriate design storm is selected when designing PPS because it establishes the volume or depth of rainfall which should be considered in the design (Leming et al., 2007). Permeable pavements need to be able to effectively capture the design storm event and discharge it in a controlled manner to the subgrade or drainage system (Woods Ballard et al., 2015). According to Leming et al. (2007), a permeable pavement system should be able to infiltrate most or all of the 2-year, 24-hour storm and that the performance of the system should be checked for at least the 10-year, 24-hour storm. The 2-year storm is often used as the service load storm for the catchment for water quality purposes. In any event, it is uneconomical to construct a permeable pavement system (or any conventional drainage system) that can cope with all rainfall events; periodic failure is accepted (Pratt et al., 2002). The risk of potential flooding should be evaluated for each permeable pavement installation whereby the level of risk attributed to the consequences of failure of the permeable pavement will decide the return period of the design storm (BSI, 2009a).

2.6.1.3 **Material selection and availability**

2.6.1.3.1 Recycled materials

Given the geological confinement of most SIDS, suitable aggregates may not be locally available for incorporation in PPS. Further, there is a growing demand for construction aggregates in SIDS as demand for housing and other public infrastructure increases with urbanisation. In Trinidad and Tobago, W.I. for instance, the demand for construction has seen a drastic increase during the past decade due to various industrial developments. However, in more recent times, the fluctuating prices of oil and natural gas which represents 35% of the Gross Domestic Product (GDP) of Trinidad and Tobago, W.I. (GoRTT, 2018),

has since resulted in a decline in construction activity. Nevertheless, the demand for civil engineering materials, construction aggregates in particular remain high (Lalla and Mwasha, 2014). In 2015, the Contractor on one of the major highway extension projects in Trinidad and Tobago, imported quarried aggregates by cargo ship from Canada; a journey of 3,785 km. Moreover, the cost of raw materials tends to increase as transportation costs increase (Behera et al., 2014). Some SIDS practice unsustainable methods of obtaining construction aggregates for meeting this demand. For instance, beach mining of aggregates is heavily practiced in the coral nation of Kiribati, one of the Pacific islands. This practice combined with climate change, improves the probability of damages and disasters associated with rising sea levels (Babinard et al., 2014). Other volcanic SIDS such as most of those of the Caribbean produce construction aggregates through quarrying. This practice of quarrying is unsustainable and presents an environmental challenge.

Preserving the environment and conserving the rapidly diminishing natural resources should be the core of sustainable development (Rao et al., 2007). SIDS nations should, therefore, consider the use of waste and recycled materials in PPS such as Construction and Demolition Waste (CDW), Crushed Brick (CB), Recycled Aggregates (RA), Crushed Concrete Aggregates (CCA), Recycled Concrete Aggregates (RCA), EPS and Lightweight Artificial Aggregates (LWAA) made from Municipal Solid Waste Incineration (MSWI) ash such as CNA. MSWI is, however, beyond the reach of most SIDS due to the high costs involved (Rand et al., 2000). Additionally, Kinnaman (2010) argues that incineration may not be appropriate for several SIDS for two main reasons. Firstly, MSW in these SIDS are not very combustible because of the high percentage of organic waste component which contain low levels of energy and high levels of moisture. Interestingly, Trinidad and Tobago, W.I., one of the more developed SIDS in terms of Gross Domestic Product (GDP) recorded only 27% organics in their waste characterisation study conducted in 2010 (SWMCOL, 2010). Secondly, Kinnaman (2010) mentions economies of scales in incineration whereby it becomes uneconomical for plants to operate at less than 1,100 tonnes of waste per day. Indeed Kinnaman (2010) suggested that Trinidad and Tobago, W.I. was able to capture these scale economies due to its large population; but smaller Caribbean SIDS such as Barbados, St. Lucia, Antigua and those of the Pacific fell well short.

Numerous researchers (Nishigaki, 2000, Poon and Chan, 2006, Cameron et al., 2013, Rahman et al., 2014, Garach et al., 2015, Murugan et al., 2016, Jindal and Ransinchung, 2018, Martinho et al., 2018) have reported using recycled waste materials in construction worldwide. CB, RCA and Reclaimed Asphalt Pavement (RAP) have been reported to be

suitable for pipe backfilling materials for stormwater and sewer pipes (Rahman et al., 2014). RCA and CB have been used for unbound sub-base materials (Poon and Chan, 2006, Cameron et al., 2013, Garach et al., 2015). Blast furnace slag has been found suitable for use in road sub-bases (Nishigaki, 2000). Tatsuoka et al. (2013) reported that well-compacted crushed concrete aggregate (CCA) can be used as backfill material for civil engineering soil structures requiring high stability. Murugan et al. (2016) used waste tyre crumb rubber to partially replace river sand in concrete block pavers in an attempt at improving the durability and sustainability of the blocks. LWAA have been used in several construction applications including lightweight concrete, lightweight blocks, lightweight geotechnical fill, insulation products, filters, and drainage. Their typical particle densities range between 0.8 to 2.0 g/cm^3. Particle densities of natural aggregates tend to range between 2.4 and 2.8 g/cm^3 (Cheeseman et al., 2005). Waste Glass (WG) has been used in pavements for several decades. Jamshidi et al. (2016) presented a thorough review of the use of WG on the structural performance, durability and sustainability of asphalt, concrete and concrete block pavements. Jindal and Ransinchung (2018) used RCA, industrial waste (fly ash) and agricultural wastes (rice husk ash and bagasse ash) in concrete pavements. Admixing industrial or agricultural wastes with pozzolanic properties enhances the strength and improves the durability of concrete thus making them as good as conventional concrete (Jindal and Ransinchung, 2018). Martinho et al. (2018) used RCA as substitutes of natural aggregates to produce asphalt mixtures.

The literature surrounding EPS in civil engineering and infrastructure applications is mostly devoted to lightweight EPS concrete whereby the mechanical properties of these materials are assessed. Normal aggregate is typically replaced with varying percentages of EPS beads depending upon structural requirements (density and strength) (Chen and Liu, 2004, Babu et al., 2005, Bouvard et al., 2007, Kan and Demirboğa, 2009, Xu et al., 2012, Kaya and Kar, 2016). Babu et al. (2005) examined the mechanical properties of lightweight concrete produced from EPS beads, cement, fly ash, sand and coarse aggregate. The concrete samples consisted of 50% fly ash by weight and EPS ranging from 0% to 66.5% of the total volume. Densities varied from 0.55 to 2.20 g/cm^3 and 28-day compressive strengths ranged from 0.55 to 22 MPa. Bouvard et al. (2007) studied the microstructure of cement-bounded, millimetre-size EPS beads. The authors reported very low density and compressive strength values ranging from 0.492 to 0.961 g/cm^3 and 0.8 to 9.2 MPa respectively. Kan and Demirboğa (2009), presented the results of an experimental study on the effects of using recycled waste EPS foam as a potential aggregate in lightweight concrete. The methodology involved replacement of natural aggregate with thermally-modified waste EPS forms in percentages

varying from 0 to 100% by volume. Compressive strengths at 28 days ranged from 12.6 to 23.3 MPa. Kaya and Kar (2016) examined the mechanical properties of lightweight concrete produced using waste EPS mixed with cement and Tragacanth resin. The resin content varied from 0.5%, 1% and 1.5% of the total volume. EPS ratios varied from 20 to 80% of the total volume. Compressive and tensile strengths at 28 days ranged from 0.5 to 16.9 and 0.2 to 1.4 MPa respectively. EPS blocks have been used worldwide as a type of geofoam lightweight fill material, typically used in embankments where the long-term applied stresses do not exceed circa 100 kPa (2000 lbs/ft^2) (Ngugi et al., 2017). EPS has further been used as a recycled material in asphalt. Baker et al. (2016) blended asphalt (bitumen) with recycled packaging waste polystyrene instead of common polymer. They suggested that the modified polystyrene-asphalt binder, had the potential of performing satisfactorily under hot climatic conditions and could be used for lightly-loaded areas such as playgrounds, training areas, parking lots and sidewalks.

Very few studies (Sokolović et al., 2009, Schöntag et al., 2015, Orlov et al., 2016, Osuagwu et al., 2018) have reported on the use of EPS as a filter material for water/wastewater treatment and no studies to the researchers' best knowledge have reported on the use of EPS in permeable pavements. Sokolović et al. (2009) used a laboratory pilot filter to investigate the efficiency of separation of iron hydroxide flocks from water through an EPS filtration bed. Schöntag et al. (2015) compared the pollutant removal efficiencies of rapid filters containing sand and anthracite media to that of polystyrene granules. The authors reported that the two filters achieved similar results. Additionally, the polystyrene granules did not release detectable amounts of styrene in the water and was recommended to be used as filter media. The authors did note, however, that monitoring for long term degradation and the possibility of leaching of styrene into the water was recommended. Orlov et al. (2016) argued that the cost of potable water treatment schemes is largely dependent on the cost of the filtration system and suggested that in Ukraine, filters made up of EPS as opposed to sand could provide savings in capital investment by 40–50%, in operating costs by 30–40% and in electricity by 7–9%. Osuagwu et al. (2018) used EPS as a viable adsorbent for the removal of iron from raw water. They reported 36% iron removal efficiencies within a contact time of 5 min.

Whilst several researchers (Nishigaki, 2000, Rizvi et al., 2010, Bhutta et al., 2013, Çetin, 2015, Jang et al., 2015, Tavares and Kazmierczak, 2016, Khankhaje et al., 2017, David et al., 2018, Lu et al., 2019, Monrose et al., 2019b, Yao et al., 2019) have reported on the incorporation of recycled waste materials in permeable pavement surfaces, very few studies

(Sañudo-Fontaneda et al., 2014, Rahman et al., 2015b, Rodriguez-Hernandez et al., 2016) have reported on the incorporation of recycled materials as sub-base aggregates in permeable pavements. Nishigaki (2000) used blast furnace slag in permeable paving blocks. Khankhaje et al. (2017) compared the effect of using two different sizes of Oil Palm Kernel Shell (OPKS) and Cockle Shell (CS) as partial replacement of natural coarse aggregate on the properties of pervious concrete pavement. Khankhaje et al. (2017) reported a decrease in compressive strength of the pervious concrete with increased shell contents but suggested that the values obtained satisfied the requirements for areas with low volume traffic such as parking lots. Rizvi et al. (2010) evaluated the use of RCA from old curb and gutter, sidewalks and sewers in pervious concrete pavement and found that up to 15% of virgin coarse aggregate could be replaced with RCA without affecting the structural and hydraulic performance of the pervious concrete. Çetin (2015) incorporated recycled household plastics (low density polyethylene) as a supplemental aggregate (1, 3, and 6%) in porous asphalt to produce a permeable plastic pavement. Tavares and Kazmierczak (2016) used RCA from construction and demolition waste in pervious concrete and found that mean 28–day compressive strengths were within the expected range (2.8 – 28 MPa or 400 – 4000 PSI) for pervious concrete. David et al. (2018) found similar performance characteristics when comparisons of compressive strength, density and surface infiltration rate of pervious concrete containing RAP and waste tire rubber were made with pervious concrete that was made up of natural aggregate without additions. Monrose et al. (2019b) used manufactured lightweight aggregates referred to as Carbon-Negative Aggregates in concrete block pavers and reported that CNA could replace natural coarse aggregates in these blocks by up to 100%. Rahman et al. (2015b) in a laboratory study, investigated the hydraulic performance and pollutants-removal efficiency of PPS using CB, RCA and RAP sub-base materials in combination with geotextile. They reported that the geotechnical and hydraulic properties of recycled waste materials in the pavement filter layers were consistent to that of typical quarry aggregates. Lu et al. (2019) replaced natural aggregate and bitumen with recycled ceramic aggregate and a bio-based polyurethane binder respectively in porous asphalt. Rodriguez-Hernandez et al. (2016) compared the runoff attenuation capacity and stormwater retention of permeable pavements containing limestone and RA from CDW in the sub-base and reported that the sub-base aggregate characteristics were proven to influence the attenuation capacity of permeable pavements.

Recycled waste materials obtain their physical and chemical characteristics from their sources, processing methods, and handling techniques which in turn determine their suitability for use in construction with respect to structural (strength and durability) and

environmental (leachability) requirements (Inyang, 2003). According to Arulrajah et al. (2013), different researchers have found that CDW materials possess few negative or detrimental effects because leachate release and existing heavy metals are within acceptable limits for civil engineering applications.

2.6.1.4 **Subgrade conditions**

Permeable pavements are designed for full, partial or no infiltration based on the in-situ soil infiltration rates or Hydrologic Soil Groups (HSG) (USDA and NRCS, 2009). Permeable pavements constructed over fine-grained soils (silts and clays) generally require thicker pavements than those constructed over coarse-grained soils (sands and gravels) (Hein, 2014). This is mainly because fine-grained soils tend to have a lower bearing capacity than coarse-grained soils which are capable of withstanding greater stresses without excessive deformation. The characterisation of the subgrade should consider, in addition to hydraulic design, its structural characteristics. California Bearing Ratio (CBR) has often been used to provide a measure of the structural support provided by the subgrade. The CBR values for varying subgrade soil types are listed in Table 2-7. The geologic composition of SIDS varies from either volcanic, coral atoll, raised coral atoll, reef island, or emergent limestone. Similarly, soil types vary in SIDS from either clays, loam or sandy soils. Infiltration of stormwater from permeable pavements into expansive clays, such as those present in the southern regions of Trinidad and Tobago and several other Caribbean SIDS, should be avoided. In such instances, designs may recommend a subgrade replacement layer such as sand or the addition of stabilisation additives such as cement or lime to the existing clay subgrade (Hein, 2014).

Table 2-7 California Bearing Ratio (CBR) values for varying subgrade soil types
[Reprint with permission from Monrose and Tota-Maharaj (2018)]

Subgrade soil type	Support	CBR
Fine grained soils such as silts and clays	Low	2.5–3.5
Sands and gravels with low amounts of fines	Medium	4.5 to 7.5
Sands and gravels with no fines	High	8.5 to 12

2.6.1.5 **Water Table**

Engineering guidelines recommend that permeable pavements be installed between 600 and 1000 mm above the maximum groundwater level (Hein, 2014, Horsley Witten Group Inc. (HWG) and Centre for Watershed Protection Inc. (CWP), 2014, Woods Ballard et al., 2015). This provides a depth of unsaturated soils that helps to ensure the infiltration performance

of the PPS in addition to protecting the underlying groundwater from possible contamination (Woods Ballard et al., 2015). Some urban cities in SIDS are located on coastal lowlands, which by nature, have high water table levels. Permeable pavements may not function well in these locations.

2.6.1.6 **Groundwater contamination**

The majority of published research focuses on impacts to surface runoff quality; however since several PPS include partial or full infiltration, potential groundwater contamination becomes a concern (Pitt et al., 1999). These concerns have been minimised since according to Wilson et al. (2003), the incorporation of an adequately designed and constructed impermeable geotextile at the base of the permeable pavement structure, should protect against any possible pollutant migration. Moreover, numerous long-term studies and simulations of PPS pollutant distributions have revealed low risks of subsoil pollutant accumulation and groundwater contamination (Legret and Colandini, 1999, Dierkes et al., 2002, Kwiatkowski et al., 2007). Groundwater is the major source of water for several low-lying coral islands such as the Maldives and Barbados and raised atolls such as Nauru, where freshwater lenses can vary in thickness and quality, depending on the rates of extraction and recharge from rainfall (UN-OHRLLS, 2009). Hence, protecting groundwater from contamination is crucial to those islands.

2.6.1.7 **Pavement slope**

Several SIDS have steep urban catchments which can have an impact on locations for installation of permeable pavements. While there have been numerous laboratory studies on the infiltration performance of permeable pavements on slopes up to 5% (Davies et al., 2002, González-Angullo et al., 2008) and 10% (Castro et al., 2007, Illgen et al., 2007), limited information has been published regarding field studies. Fassman and Blackbourn (2010) in their field study investigated permeable pavements installed on slopes between 6.0% and 7.4%. Lucke and Beecham (2011b) reported success when they investigated the infiltration performance of a field-scale PICP installed on slopes between 0 and 20%. They concluded that typical PICP design guidelines that recommend a maximum pavement slope of 5% were overly conservative. It must be noted however, that the test pavement used in their study was newly laid and had not yet experienced any pavement clogging. Should sloping ground be inevitable, internal check dams or berms can be incorporated into the subsurface to enable an even distribution of temporarily-detained subsurface flow as depicted in Figure 2-13. Underdrains may be placed at each dam location should there be a requirement for them (Kumar, 2014).

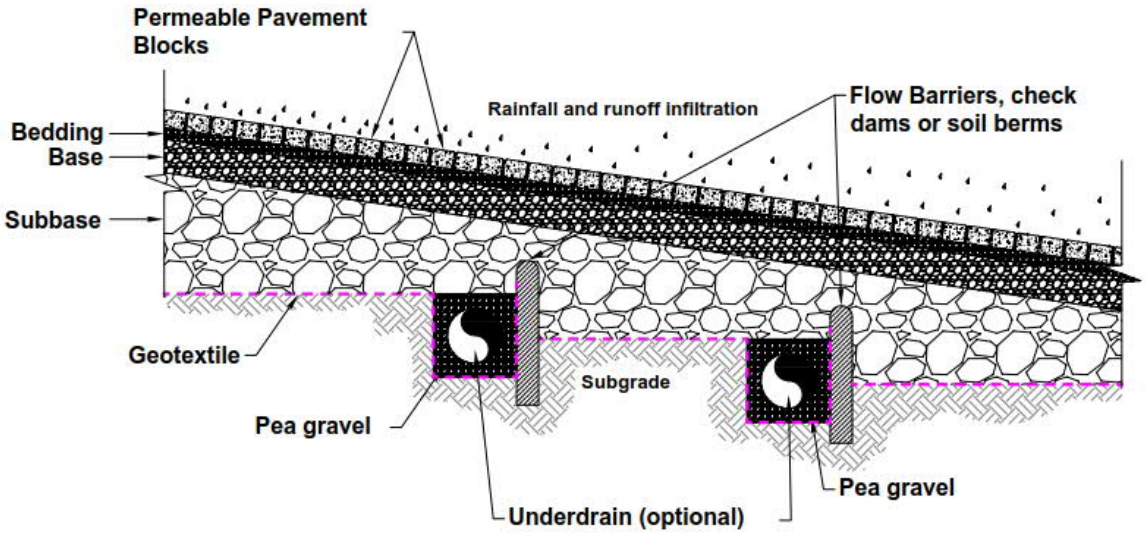

Figure 2-13 Flow barriers in PPS on sloping ground

[Reprint with permission from Monrose and Tota-Maharaj (2018)]

2.6.1.8 **Stormwater storage/ reuse potential**

Unlike most developed countries, the majority of SIDS do not utilise stormwater collection systems. Instead, stormwater is often channelled towards natural water courses such as rivers and oceans using conventional storm drains.

Despite significant yearly rainfall amounts in SIDS, there is an ever-present stress on their water resources (Cashman et al., 2009) primarily because of their small size, geology, topography, inadequate reservoir storage facilities, scarce financial resources, and climatic variations (Ekwue, 2010). Further, as many of these SIDS economies are heavily dependent on agriculture or tourism activities, both major consumers of freshwater (Gössling et al., 2012), economic losses are likely to result when these operations have to be discontinued (UNEP et al., 2012).

The use of PPS present opportunities for stormwater harvesting in many SIDS whereby partially-treated stormwater collected from the PPS can be used for non-potable purposes such as toilet flushing and external cleaning, thereby reducing the consumption of potable water, minimising water rationing and improving the availability of water resources (Antunes et al., 2016). Rainwater harvesting has been practiced in the Caribbean for many years; although it is now in decline. The mechanisms used for capture, conveyance and storage are building roofs, gutters and polythene tanks respectively (Dempewolf et al., 2015). Pratt (1999) suggested that permeable pavements could be used as a reservoir for stormwater treatment and storage for subsequent reuse. Nnadi et al. (2015) reported that a

permeable pavement system has the capability to recycle stormwater to a quality that meets the standards for use for agricultural irrigation irrespective of sub-base type.

2.6.1.9 **Clogging as a maintenance issue**

The importance of permeable pavement maintenance and its relevance to the integrated stormwater management agenda of urban SIDS cannot be stressed enough. The culture of poor maintenance practices of valuable infrastructure is still widespread throughout most SIDS. The unavoidable consequences of significant under-investment and neglect of stormwater management systems over many years are increasingly visible and is always a subject of considerable public concern.

2.6.2 Economic feasibility

2.6.2.1 **Initial and Life-cycle cost**

The financing and cost-recovery of urban drainage systems remain a challenge to many SIDS (Parkinson, 2002). Initial costs of PPS usually exceed those of conventional pavements, primarily due to PPS having thicker aggregate layers necessary to maximise stormwater storage and to provide enough structural support to accommodate vehicle loading. However, a life-cycle cost analysis may realise actual cost savings with PPS when compared to conventional pavements if a holistic approach is considered towards stormwater management systems. Savings and benefits include reduced need for conventional downstream stormwater infrastructure such as detention ponds and drainage ditches, less developable land consumed for stormwater ponds, improved aesthetics and reduced urban heat island effect (Ferguson, 2005, Dhalla and Zimmer, 2010).

Furthermore, there is often difficulty to install permeable pavements on a large scale due to high initial costs and infrastructural factors. As such, PPS are often combined with other stormwater management practices for entire catchments (Rahman et al., 2015b).

2.6.2.2 **Maintenance**

Periodic maintenance of PPS to ensure that they continue providing the necessary support to handle traffic loads, requires monitoring of the pavement for signs of distress which could alter the structural integrity of the pavement. Some of these distresses include clogging, depression, rutting, edge restraint damage, ravelling, cracking, excessive joint width, joint filler loss and horizontal creep (Hein, 2014).

As discussed previously in subsection 2.5.7, page 31, clogging is the most common challenge with permeable pavements. Numerous researchers have cited periodic maintenance as being fundamental to limiting clogging of PPS (Balades et al., 1995, Colandini et al., 1995, Dierkes et al., 2002, Yong et al., 2008, Pezzaniti et al., 2009, Blecken et al., 2017). Examples of maintenance techniques include manual removal of the upper 20 mm of fill material, mechanical street sweeping, regenerative air street sweeping, vacuum street sweeping, hand-held vacuuming, high pressure washing, and milling of porous asphalt (Field et al., 1982, Winston et al., 2016). Regenerative air street sweepers and vacuum trucks apply suction on the surface of the permeable pavement to dislodge dirt from the pavement joints, whereas mechanical sweepers only disperse debris from the surface. Mechanical street sweepers are increasingly being replaced by regenerative air street sweepers in municipal fleets in North America because they generate significantly less air pollution and remove finer sediment particles and associated pollutants from pavements (Sehgal et al., 2018). Some studies (Dierkes et al., 2002, Radfar and Rockaway, 2016a) have reported improvement in Surface Infiltration Rates (SIR) after applying various maintenance techniques to clogged permeable pavements. Dierkes et al. (2002) reported 1,500% improvement in infiltration rates after the use of cleaning vehicles consisting of high pressure cleaners with direct vacuum suction on a permeable pavement test site in Germany. Radfar and Rockaway (2016a) reported that average SIR increased after cleaning methods (street sweep trucks, pressurised air jets and hydro-excavator trucks) were used.

There are no global standards recommended by the PPS industry for the maintenance of PPS as previously mentioned in subsection 2.5.7, page 31. Numerous maintenance checklists (HydroSTON, 2019a, ICPI, 2019) are readily available from the PPS industry to be used as a guide for the installation and maintenance of permeable pavements. Routine street sweeping methods for PICP are often recommended by USA authorities, at frequencies up to three or more times per year. However, experience in Europe and Australia suggests that such regular frequency of maintenance is often unnecessary (Shackel, 2010). In the UK for example, Forterra (formally Hanson) Formpave (Formpave, 2016) and CIRIA's SuDS Manual (Woods Ballard et al., 2015) recommend regular sweeping to be carried out once or twice a year, typically in Spring and after leaf fall in Autumn as part of a regular maintenance schedule. Remedial actions such as remediating areas of rutting and depressions, replacement of damaged blocks and reapplication of jointing aggregates are further recommended as required. Formpave also recommends for PPS inspections within the first three months of installation, followed by annual inspections. In Australia, firms such as HydroSTON from HydroCon (HydroSTON, 2019b) which specialises in urban water

management, recommends regular removal of surface debris using readily available water/suction equipment. According to the Concrete Masonry Association of Australia CMAA (2010), in addition to occasional sweeping, the principal maintenance requirement for PICP is to maintain the joints to ensure that they are kept full of the jointing aggregate and to control weed growth.

Vacuum and street sweeping trucks are not readily available in SIDS and would attract significant importation costs. Vacuuming is therefore not recommended for SIDS facing economic challenges. Consequently, this eliminates the use of porous asphalt and porous concrete pavements given that vacuuming is the most effective maintenance option for these pavement types. The use of paver blocks is the preferred option in this regard, because maintenance options such as removal and replacement of the infill material (Dietz, 2007) are more in line with SIDS economics, having low start-up costs and can provide employment opportunities. Other relatively cheap options for PICP maintenance are through the utilisation of the hand-held power brush and the pressure washer (Sehgal et al., 2018).

2.6.3 Political environment

2.6.3.1 Institutional and legislative framework

Approximately 50% of SIDS use the common law system adopted from their former colonial administrator; England. Across these SIDS, governments are made up of a legislative arm which makes or repeals laws through the parliament, an executive arm which administers the laws and a judicial arm which interprets the laws. The remaining 50% uses the civil law system, which is a codified system of law that takes its origin from Roman law (Central Intelligence Agency, 2018).

These systems form part of the institutional and legislative framework in SIDS which are used to achieve various policies and goals. Urban stormwater management, as mentioned previously, remains a huge challenge for SIDS authorities. Drainage problems are usually not prioritised and are often dealt with in a reactive manner. For instance, expensive water treatment methods are applied to polluted water sources rather than preventing the pollution. Drainage channels are often cleared of solid wastes, rather than the solid waste problem being previously addressed (Reed, 2004).

Additionally, in the Caribbean for instance, institutions charged with enforcing policies surrounding existing stormwater management are often relaxed in their approach. This is evident in Caribbean SIDS such as Trinidad and Tobago, Guyana and St Lucia by the vast number of properties constructed on drain reserves and flood plains. Unplanned

development near urban cities is rampant and often exacerbates flooding problems (Thomas, 2013). There is an increasing demand for improved drainage in society. At the same time, a desire for a clean environment, preservation of nature and concern for the welfare of future generations is also progressively salient. Policy makers and politicians in the Caribbean must be cognisant of these conflicting desires along with the added benefits of adequately-managed SUDS as well as the various issues which may be confronted. This knowledge would seek to reduce the need for reactive spending and promote long-term integrated planning instead (Reed, 2004).

The implementation of successful PPS in SIDS depends heavily on aggressive enforcement of policies relating specifically to PPS and SUDS in general. There are currently no guidelines developed for PPS specifically targeting most SIDS. Singapore is perhaps one of the only exceptions. Developed nations such as the USA, UK and Australia are far ahead in this regard.

2.7 Municipal solid waste management in SIDS

Municipal Solid Waste (MSW) generation affects both developed and developing economies because of the increasing volumes of wastes generated on an annual basis. Management of this increasingly high mountain of MSW is crucial since it mitigates public health risks, contributes to sustained economic activity, and enhances public welfare. SIDS are mostly developing nations whereby increasing MSW generation is one of their major headaches. Additionally, problems relating to land scarcity, lack of economic resources and waste management expertise considerably reduces the waste management abilities in SIDS (UNEP, 1999).

Mohee et al. (2015) presented a useful review of the status of solid waste management in SIDS. Some key highlights of this review are as follows:

- Figure 2-14 compares MSW generation rates, Human Development Index (HDI) and Gross Domestic Product (GDP) per capita amongst the three SIDS groups. HDI measures the standard of living of a citizen, from 0 to 1. HDI and GDP per capita are used to explain the trend of waste generation in SIDS. SIDS average MSW generation is 1.33 kg/capita/day. The Caribbean and AIMS SIDS generate the largest quantities of wastes with averages of 1.61 kg/capita/day and 1.56 kg/capita/day respectively. The Pacific SIDS generate significantly less wastes at an average of 0.82 kg/capita/day. As observed in Figure 2-14, this trend follows the HDI and GDP per capita comparisons amongst SIDS. With higher standards of living and higher

GDP per capita, more goods and services are produced. This in turn leads to the generation of significantly larger volumes of MSW.

- Tourism is also linked to MSW generation. The higher the number of visitors, the more MSW is produced.
- In terms in waste composition, insignificant percent differences exist between the three SIDS groups as observed in Figure 2-15. Additionally, Figure 2-16 lists the average MSW composition in SIDS. The major fraction of MSW consists of organics (44%) followed by recyclables namely paper, plastics, glass and metals (total: 43%).
- Composting and anaerobic digestion appear to be the two most appropriate technologies for managing organic wastes in SIDS. The recyclables can be subjected to recycling or waste-to-energy techniques such as incineration.
- Despite the lack of landfill space in most SIDS, landfilling is routinely practised in numerous SIDS, primarily because of the absence of other waste management techniques and because it is relatively cheaper compared to other waste management options (Renou et al., 2008).

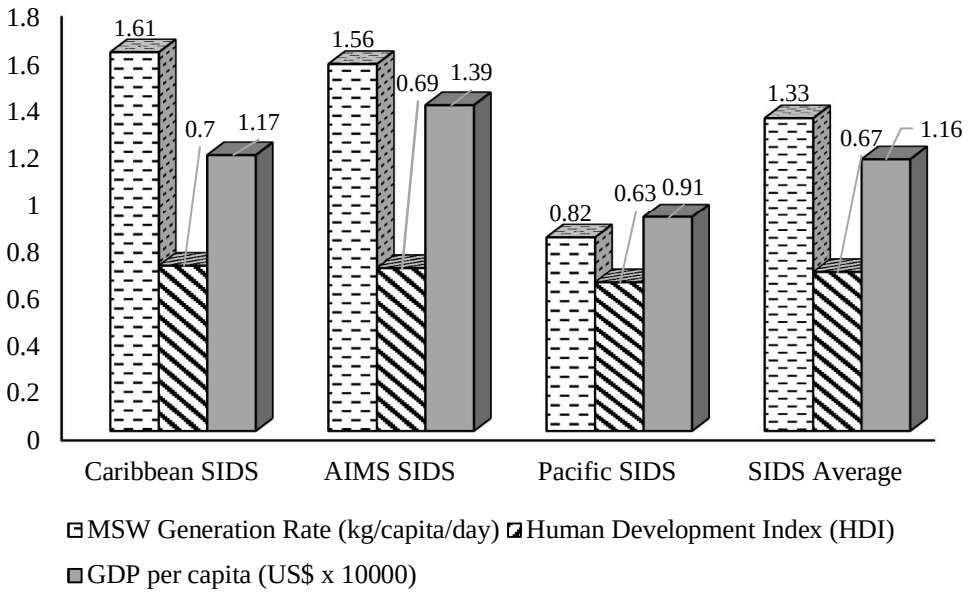

Figure 2-14 MSW generation rates, Human Development Index (HDI) and Gross Domestic Product (GDP) per capita amongst the three SIDS groups
[adapted with permission from Mohee et al. (2015)]

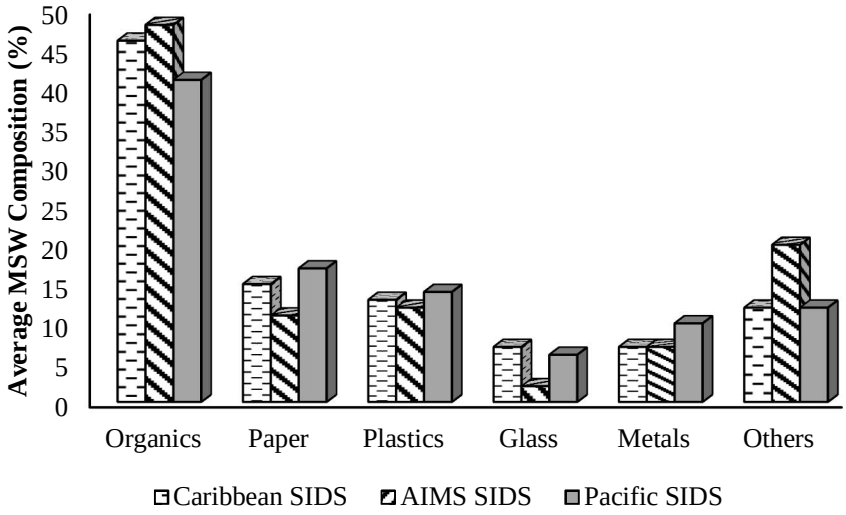

Figure 2-15 Comparison of MSW composition amongst SIDS groups
[adapted with permission from Mohee et al. (2015)]

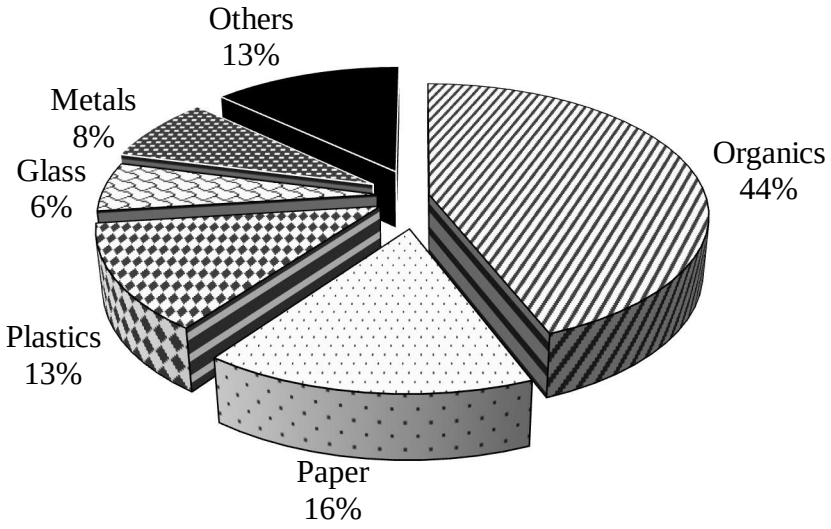

Figure 2-16 Average MSW composition in SIDS
[adapted with permission from Mohee et al. (2015)]

Going forward, this review section focuses on Caribbean SIDS in general, and two case study nations; Trinidad and Tobago, and St. Lucia, W.I. These are two different countries in terms of their size, population, culture, development status, economic and political landscape and waste generation.

The Caribbean comprises of mostly SIDS whereby the effects of improperly disposed waste is often amplified through indirect contamination of surface and groundwater, degradation of coastal and marine resources such as wetlands and coral reefs, limited land space for

housing and disposal facilities and insufficient financial resources for regulating and managing waste (Phillips and Thorne, 2013).

Waste management is not considered a priority public policy issue in the Caribbean. Far too often waste management competes with economic and social issues such as poverty, unemployment, education, health, infrastructure, fiscal and trade matters, crime and security (Phillips and Thorne, 2013).

The preferred waste disposal method in the Caribbean is landfills (Table 2-8) through various municipal collective programs. This has replaced the traditional practices of reusing valuable waste materials and composting organic waste materials (Kinnaman, 2010). Though there is evidence of several recycling initiatives across the Caribbean, the practice is on a small scale. Today, the scrap metals trading industry has evolved in several countries over the last decade but efforts to recycle plastic, paper, cardboard and glass have been mostly minute and sporadic (Phillips and Thorne, 2013).

Table 2-8 also shows the estimated average waste per-capita generation of selected Caribbean countries for selected years (2000, 2002). The average generation rate in the Caribbean at that time was 1.3 kg/capita/day with values ranging from 0.5 (Cuba) to 2.8 (BVI). It is noteworthy that tourism activities contribute towards daily waste production in the Caribbean. Kinnaman (2010) puts its impact at 10%. The waste characterisation for selected Caribbean countries for selected years (1999, 2000 and 2002) is provided in Table 2-9. Organics represent the largest percentage across the Caribbean (46.9%), followed by paper/cardboard (17.0%) and plastic (9.9%). These percentages are typical of most developing states.

Table 2-8 Waste Per-Capita Generation in Selected Caribbean Countries (2000, 2002) [adapted from Kinnaman (2010)]

Country	Generation (kg/day)	Percentage Landfilled	Percentage Incinerated
Caribbean[1]	1.3	83	2
Bahamas[1]	2.3	70	
Barbados[2]	0.9		
BVI[2]	2.8		
Cuba[1]	0.5	90	
Dominican Republic[1]	0.6	90	
Jamaica[2*]	1.0		
St. Lucia[1]	1.4	83	
St. Vincent and the Grenadines[2*]	0.7		

[1]Data from IPCC (2006)

[2]Data from Treasure (2003)

*Data from 2002

Table 2-9 Waste Characterisation of Selected Caribbean Countries (1999, 2000, 2002) [adapted from Kinnaman (2010)]

Material	Caribbean[1*] (%)	St. Vincent and the Grenadines[2***] (%)	Jamaica[2***] (%)	Barbados[2**] (%)	BVI[2**] (%)	Trinidad[2*] (%)
Organics	46.9	49.6	54.0	59.0	6.5	46.0
Paper/Cardboard	17.0	22.1	17.3	20.0	33.5	13.0
Wood	2.4	1.3			22.2	
Textiles	5.1	4.0	2.9		4.8	4.0
Rubber/Leather	1.9					
Plastic	9.9	8.4	11.8	9.0	6.3	12.0
Metal	5.0	3.8	5.3		8.6	7.0
Glass	5.7	5.6	4.3		18.1	6.0
C&D Materials		5.8				7.0
Other	3.5	0.3	3.2	12		5.0

[1]Dat from IPCC (2006)

[2]Data from Treasure (2003)

*Data from 1999

**Data from 2000

***Data from 2002

2.7.1 Case study 1–Trinidad and Tobago, W.I.

Trinidad and Tobago is a twin-island republic state located at the bottom of the Caribbean archipelago, with coordinates 10.5° North and 61.5° West. The combined land area of both islands is 5,128 km^2, of which Tobago occupies approximately 300 km^2. The total population is an estimated 1.35 million. Trinidad on its own is heavily industrialised with crude oil and natural gas as the main exports (CSO, 2010b). Tobago's revenue is generated mostly from tourism with financial inputs from Trinidad.

2.7.1.1 **Waste generation, collection and disposal**

Waste disposal in Trinidad and Tobago is managed by the Trinidad and Tobago Solid Waste Management Company (SWMCOL), a state-owned enterprise established in 1980 (Phillips and Thorne, 2013). Trinidad and Tobago's per capita waste generation is an estimated 1.5 kg/capita/day (SWMCOL, 2016) which is significantly over the 2016 average per capita waste generation of 0.99 kg/capita/day for Latin America and the Caribbean (Kaza et al., 2018). Comparatively, Europe and Central Asia and North America have average per capita waste generation values of 1.18 and 2.1 kg/capita/day respectively (Kaza et al., 2018). With an estimated population of approximately 1.35 million, 1.5 kg/capita/day equates to approximately 2000 tonnes of MSW being generated in Trinidad and Tobago per day (SWMCOL, 2016).

According to the Government of the Republic of Trinidad and Tobago GoRTT (2015), approximately 90% of MSW collection is performed by private contractors with the remaining 10% done by the public sector. Most of the MSW is disposed of via landfills. There are 9 operational disposal sites in Trinidad and Tobago (GoRTT, 2015). SWMCOL operates the three major landfills.

In 2010, Trinidad and Tobago generated an estimated 700,000 tonnes of MSW (SWMCOL, 2010). However, lower estimated figures of 558,617 and 514,834 tonnes for 2014 and 2015 respectively were received via Email correspondence from Juranwan-Richards (2016), Research and Information Officer, Department of Communications, Sales and Marketing, SWMCOL.

The GoRTT, through the Ministry of the Environment and Water Resources has established a policy to provide guidance for the creation of an enabling legislative and administrative framework to facilitate a 60% reduction of waste disposal at landfills by 2020 (GoRTT, 2015).

2.7.1.2 **Waste Composition/ Characterisation**

The results of the most recent waste characterisation study conducted in 2010 by SWMCOL through a Canadian consulting firm CBCL, are presented in Figure 2-17. Organics (27%), paper (19%), plastics (19%) and glass (10%) represented the largest waste quantities. It is noteworthy that there has been a drastic reduction in the quantity of organics produced over the last decade and a half. Table 2-9 reports Trinidad as producing 46% organic waste in 2000 which was at the time very consistent with most developing countries. Perhaps, as Trinidad's oil-rich economy grew over the last decade and a half, so did the disposable income of more of its population. In so doing, less persons were preparing meals at home but purchasing more processed and packaged foods resulting in increased production of paper, plastic and glass waste.

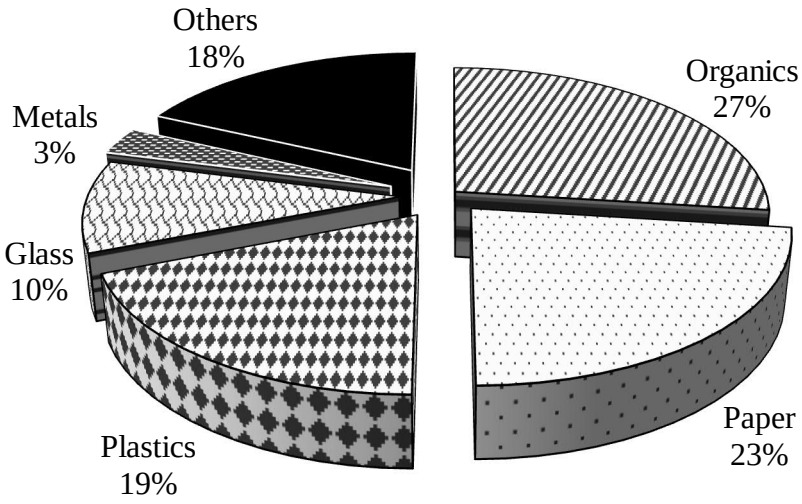

Figure 2-17 Solid Waste Characterisation for Trinidad and Tobago, 2010
[adapted from SWMCOL (2010)]

Marzolf et al. (2015) also analysed Trinidad's MSW characterisation in their Inter-American Development Bank (IDB)-funded report to the GoRTT. This report provided recommendations on policies for a sustainable energy future. They expressed amazement at the relatively small organic waste percentage found and suggested that Trinidad's MSW was a very dry waste consisting in large parts of plastic, foam boxes and other non-anthropogenic materials which corresponded more to European types of MSW more than to other tropical countries. As seen in Figure 2-18, Trinidad and Tobago's MSW composition is very similar to that of upper middle-income to high-income countries.

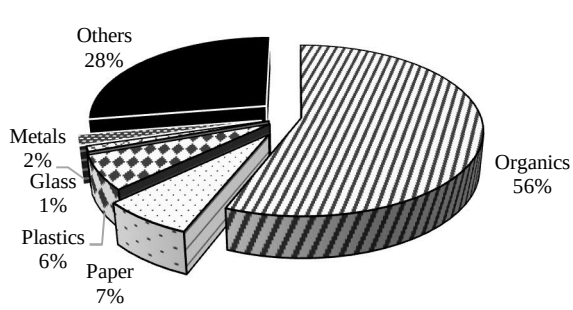

a. Low-income countries

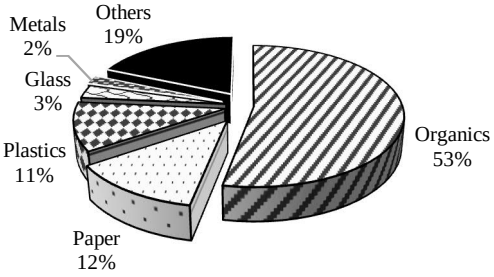

b. Lower middle-income countries

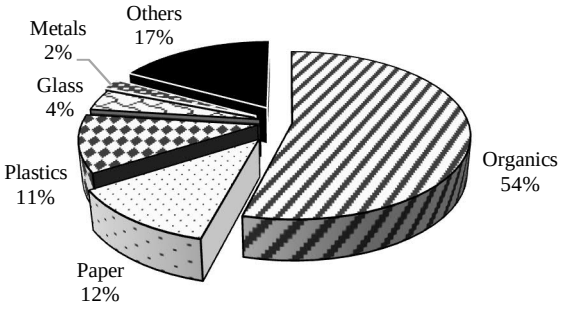

c. Upper middle-income countries

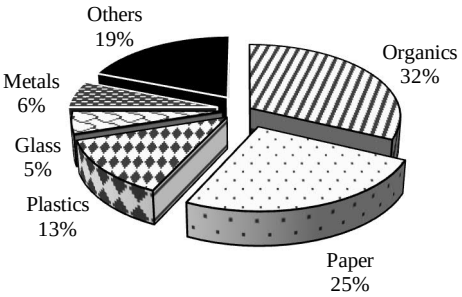

d. High-income countries

Figure 2-18 Typical MSW composition for low to high-income countries [adapted from Kaza et al. (2018) under a Creative Commons Attribution [CC BY 3.0 IGO] License]

2.7.1.3 **Costs to Public**

According to Phillips & Thorne (2013), the cost of handling MSW in Trinidad and Tobago was estimated at US$ 35.9 million (TT$ 226 million) in 2010. It was reported (Trinidad & Tobago Guardian, 2015) that it costs the GoRTT US$ 50.4 million (TT$ 321 million) per year to manage the island's waste collection and disposal. This represents a 40% increase in cost from 2010 to 2015. It was further reported that consideration should be given to imposing fees on citizens of Trinidad and Tobago for garbage disposal (Hunte, 2019).

2.7.2 Case study 2–St. Lucia, W.I.

St. Lucia forms part of the southern archipelago of the Caribbean island chain. It is geographically located north of Trinidad and Tobago with coordinates 14° North and 61° West (Phillips and Thorne, 2013). It has a land area of 616 km^2 and an estimated population of approximately 170,000 (CSO, 2010a). Tourism is the island's largest revenue earner.

The regulation, control and management of solid waste in St. Lucia falls under the purview of the St. Lucia Solid Waste Management Authority (SLSWMA), established in 1996. The Authority is mandated to provide coordinated and integrated systems for the collection, treatment, recycling and disposal of solid waste (SLSWMA, 2015). Presently, a majority of MSW is disposed of at two landfills; recycling is conducted, but on a small-scale by private companies.

2.7.2.1 **Waste generation, collection and disposal**

Records obtained from the publicly available Annual Reports of the SLSWMA from 2004 to 2015, reveal an average MSW production on the island of 77,919 tonnes per year with values ranging from 70,367 to 84,526 tonnes (SLSWMA, 2015). This is illustrated in Figure 2-19. Production fluctuates, but the trend is generally decreasing.

On a related issue, MSW generation rates in the island have remained relatively stable between 2010 and 2014 averaging approximately 1.1 kg/capita/day (SLSWMA, 2015). This rate has remained relatively constant over the last decade and a half.

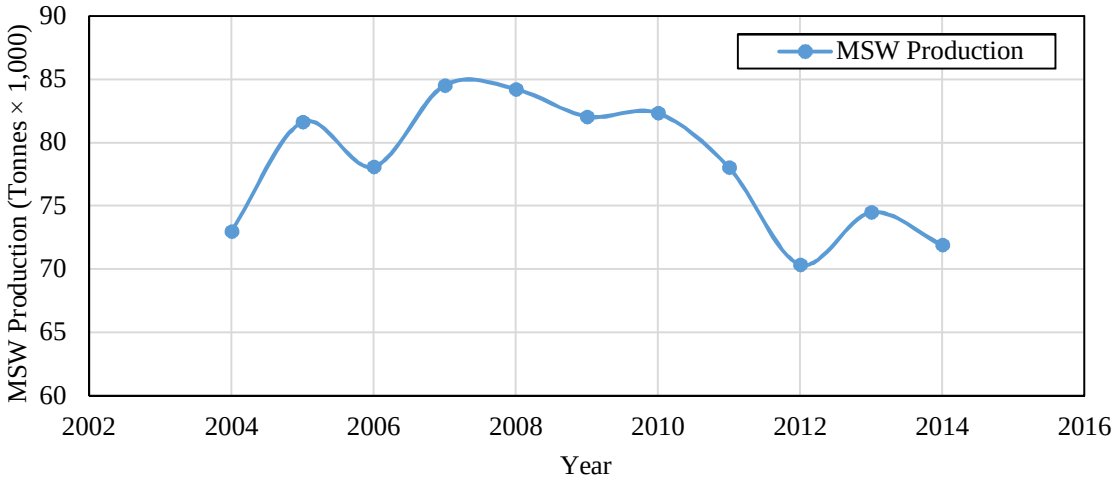

Figure 2-19 Yearly tonnage of waste disposal in St. Lucia between 2004 and 2015 [adapted from SLSWMA (2015)]

2.7.2.2 **Waste Composition/Characterisation**

MSW characterisation was first done in 2002 and repeated thereafter in 2008 (SLSWMA, 2002, SLSWMA, 2008). Nine (9) categories of wastes were identified. These were paper and paperboard, glass, metal, plastic, textiles, organics, CDW, special care wastes and other wastes. ASTM International (2016c) was used for characterisation. The results of these characterisation studies are presented in Figure 2-20. Organics and plastics were the largest

contributors for both years. There was a significant reduction in organics and an increase in plastics from 2002 to 2008.

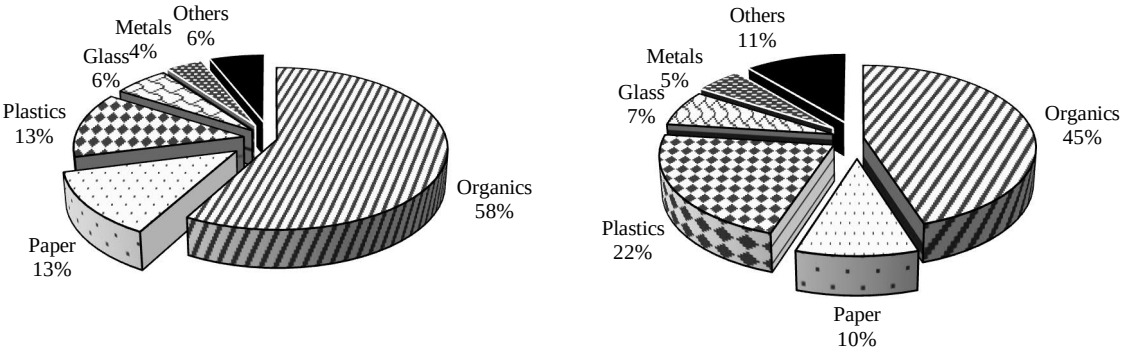

a. 2002 b. 2008

Figure 2-20 MSW characterisation in the Caribbean SIDS, St. Lucia
Source: (SLSWMA, 2002, SLSWMA, 2008)

2.7.2.3 **Cost to the Public**

The overall yearly cost of waste disposal in St. Lucia from 2007 to 2015 (SLSWMA, 2015) is presented in Figure 2-21. The average total cost for this 8-year period is USD $3,355,507 ranging from USD $2,687,370 to USD $3,890,037.

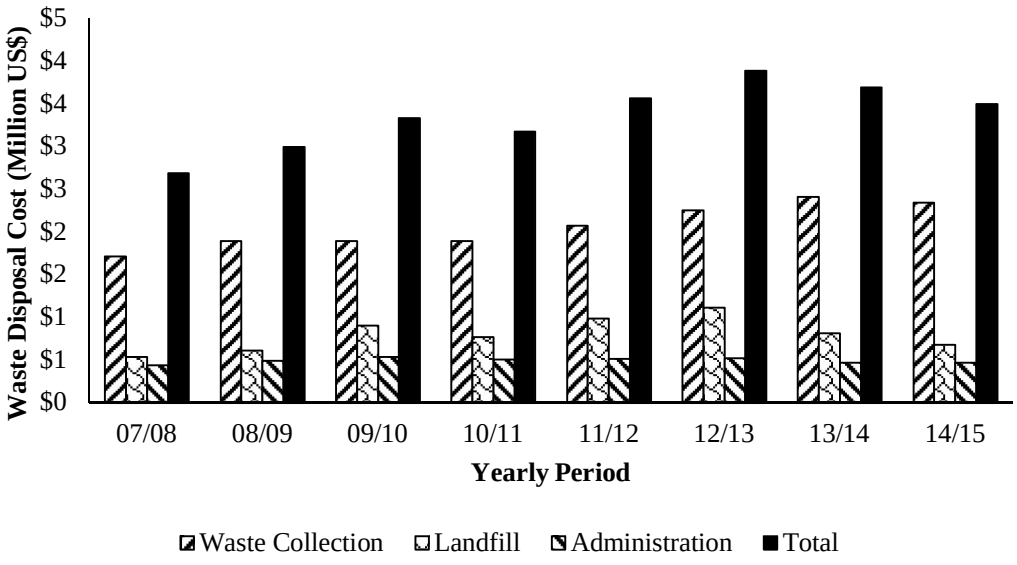

Figure 2-21 Overall cost of waste disposal in St. Lucia between 2007 and 2015
[adapted from SLSWMA (2015)]

2.8 Chapter summary

This chapter presented a comprehensive literature survey of PPS, evaluation of the impact of climate change and projections of urban development in SIDS as well as key factors worth considering for widespread acceptance and utilisation of PPS in SIDS (research question number 1 listed in Chapter 1). Numerous studies have reported successful applications of permeable pavements worldwide but mostly in developed countries such as the USA, UK and Australia. Permeable pavement installations are few across Caribbean SIDS. PPS reduce pollutants from infiltrating stormwater runoff, provide vital reservoir storage for potential reuse of stormwater and improve the hydrologic functions of various locations. Unlike most territorial states, the geographically and geologically confined nature of most SIDS present unique parameters for consideration when designing permeable pavements. The literature survey found that some of the most important parameters include traffic loads, design storms, cost, choice and availability of construction aggregates, permeability of existing soil at the intended location, depth of water table, potential for groundwater contamination, slope of pavements, stormwater reuse option, clogging, infrastructure maintenance and support from policy makers. Reluctance to implement PPS in SIDS may include technical uncertainty in performance, lack of reliable data as well as social perceptions. In addition to the lack of permeable pavement research in SIDS, the review also confirmed a research gap regarding the performance evaluation of permeable pavements containing recycled/recyclable sub-base materials. The following chapter provides details regarding the materials and test procedures used in this research project.

CHAPTER 3. EXPERIMENTAL METHODOLOGY

3.1 Overview

This chapter provides details regarding the materials and test procedures used in this research project. A summary of the research methodology is illustrated in Figure 3-1. Three (3) recycled materials were used, namely Carbon-Negative Aggregates (CNA), Crushed Concrete Aggregates (CCA) and Cement-bounded Expanded Polystyrene beads (C-EPS). CNA were used as a bound material in the production of Concrete Permeable Pavement Blocks (CPPB) for use as the surface layer of permeable pavements whilst CCA and C-EPS were used as sub-base materials in permeable pavement rigs. The performance (bearing capacity, permeability, long-term clogging, attenuation and retention capacity, pollutant removal efficiency) of rigs which contained natural aggregates (basalt or quartzite) was evaluated and compared to rigs containing CCA and C-EPS.

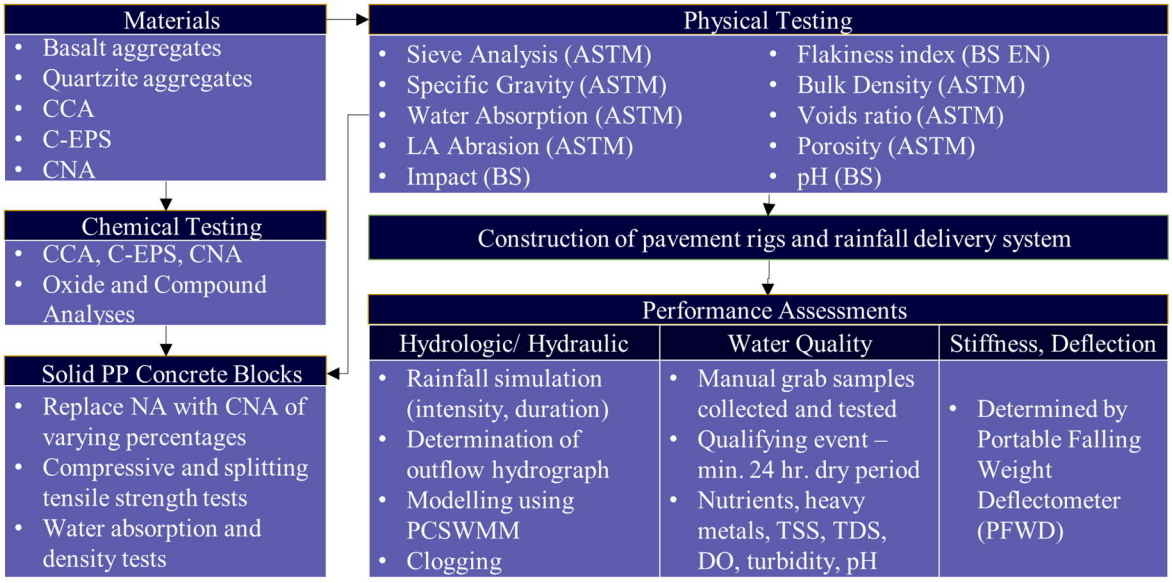

Figure 3-1 Flowchart showing overview of experimental research methodology

3.2 Materials

3.2.1 Basalt aggregates

Crushed basalt aggregates (Figure 3-2) were obtained from a quarry in St. Lucia, W.I. Basalt is naturally available in volcanic Caribbean SIDS such as St. Lucia, St. Vincent, Dominica and Grenada and is typically used in roadway bases and concrete works. The basalt aggregates are grey, angular and highly dense.

Figure 3-2 Crushed basalt aggregates, sourced from St. Lucia, 2016

3.2.2 Quartzite aggregates

Quartzite aggregates used in this research project, were sourced from a local quarry in Trinidad and Tobago, W.I. They are readily available and typically used in construction. Quartzite aggregates are classified as non-foliated metamorphic rock because of prehistoric exposure to extreme temperature conditions whereby deeply-buried, quartzite-rich sandstone was fused, leading to the formation of quartzite aggregates. Quartzite aggregates have low porosity and are highly weather-resistant (Mwasha, 2009). These aggregates are typically cream and brown in colour, rounded in shape and have smooth edges. A sample of the quartzite aggregates used is shown in Figure 3-3.

Figure 3-3 Quartzite aggregates, sourced from Trinidad, W.I., 2016

3.2.3 Carbon-negative aggregates

Carbon-Negative Aggregates (CNA) were supplied by the manufacturer, Carbon8 Systems Limited in Kent, UK in collaboration with the University of Greenwich, UK. The CNA, shown in Figure 3-4, were porous, grey, sub-rounded, homogenous and rough on the surface. As noted in subsection 1.1, CNA were used in an attempt at conserving natural aggregates and to introduce CNA to Caribbean SIDS as a potential construction product which can be commercialised.

Figure 3-4 Carbon-Negative Aggregates (CNA) sourced from the UK, 2017
[Reprint with permission from Monrose et al. (2019b)]

3.2.4 Crushed concrete aggregates

Crushed Concrete Aggregates (CCA) were manufactured locally in the laboratory by crushing and sieving concrete test cylinders. A Braun Chipmunk Crusher (Gilson Company Inc., Ohio, USA) was used for crushing. The CCA were angular, contained numerous sharp edges and light grey in colour. The crusher and samples of the CCA are shown in Figure 3-5. A selective sieving process was used to eliminate undesirable crushed materials. It is noteworthy that the CCA were made up of natural aggregates bounded by a hardened cementitious mortar. CCA were also selected as a possible replacement for natural aggregates and to also encourage recycling.

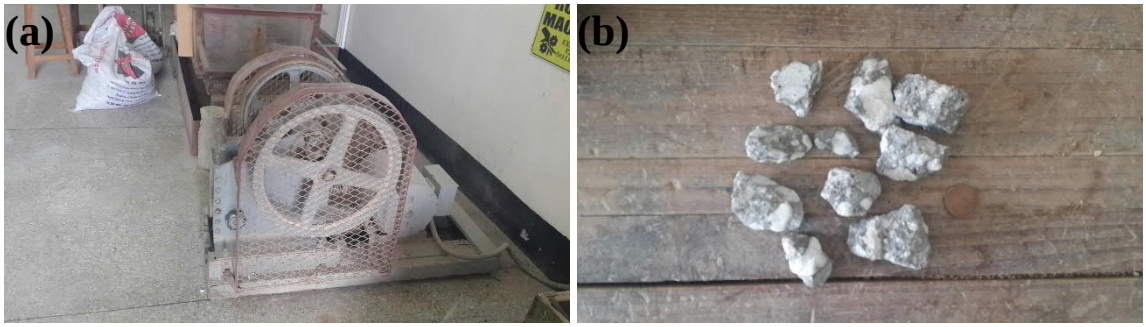

Figure 3-5 Production of CCA, December 2016 (a) Braun Chipmunk Crusher (b) Samples of CCA

3.2.5 Cement-bounded expanded polystyrene beads

An 8.09 kg, 450 × 420 × 250 mm Cement-bounded Expanded Polystyrene beads (C-EPS)porous block (Figure 3-6) for use as the sub-base layer in one of the rigs was prepared in the concrete laboratory at the University of the West Indies, St. Augustine Campus, Trinidad and Tobago, Department of Civil and Environmental Engineering. The materials used were Premium Plus Cement (PPC), which contains approximately 30% pozzolanic material and 70% Ordinary Portland Cement (OPC), tap water and EPS beads. The PPC was sourced from a local manufacturing plant (Trinidad Cement Limited, Claxton Bay, Trinidad, W.I.). PPC is manufactured in accordance with international standards (EN 197-1, 2011, ASTM International, 2017b). According to the manufacturer, PPC is an eco-friendly cement option whose production has significantly reduced the manufacturer's carbon footprint. The EPS beads were also sourced from a local supplier (Mecalfab Limited, O'meara Industrial Estate Arima, Trinidad, W.I.).

Prior to the production of the C-EPS block, four (4) trial mixes were prepared to obtain an optimum mix design. Mixes were evaluated based on hydraulic conductivity (permeability) and compressive strength characteristics. The mix designs used are presented in Table 3-1. The mixes ensured that excessive amounts of cement were not utilised. This was necessary to produce a filter material with adequate permeability. Mix No.4, chosen as the optimum, was used to produce the C-EPS block.

Figure 3-6 Block of C-EPS used as the sub-base layer in Rig 4, December 2016 [Reprint with permission from Monrose et al. (2019a)]

Table 3-1 Mix designs for C-EPS sub-base filter block

Mix. No.	Component mass (%)				Component mass (kg)				W/C ratio	EPS/C Ratio
	EPS	Water (W)	Cement (C)	Total	Total desired	EPS	Water (W)	Cement (C)		
1	15	25	60	100	1.0	0.15	0.25	0.60	0.4	0.3
2	20	30	50	100	1.0	0.20	0.30	0.50	0.6	0.4
3	10	30	60	100	1.0	0.10	0.30	0.60	0.5	0.2
4	14	30	56	100	1.0	0.14	0.30	0.56	0.5	0.3

3.2.5.1 **Hydraulic conductivity testing of C-EPS filter**

For each mix, three (3) 50 × 70 mm cylindrical samples (Figure 3-7) were prepared in PVC sample holders. These samples were used for hydraulic conductivity (permeability) testing using the falling head method (Das, 2010). The falling head permeability test allows water through a relatively short sample (usually soil, but C-EPS in this case). The falling head permeameter apparatus used is shown in Figure 3-8. The standpipe (burette) was filled with tap water to a predetermined head (h_1). Plumbers putty was used to seal around the top edge of the sample holder to prevent water from bypassing the sample. The valve was opened and the time, t (s), taken for the water to drop from the initial head, h_1, to a convenient head (h_2) was recorded. The hydraulic conductivity, k, was calculated from Darcy's law from Equation 3-1 (Das, 2010). This procedure was repeated three (3) times for each sample, after which the average hydraulic conductivity, k was calculated. Results of the average k of each sample mix are listed in Table 3-2. Average k values ranged from 1332 to 1764 mm/h. Numerous studies (Deo et al., 2010, Walsh et al., 2014, Andrés-Valeri et al., 2016, Amini et al., 2018,

Rama and Shanthi, 2018) have used the falling head permeability approach to assess clogging of porous concrete in the laboratory.

Figure 3-7 C-EPS samples for hydraulic conductivity testing, December 2016

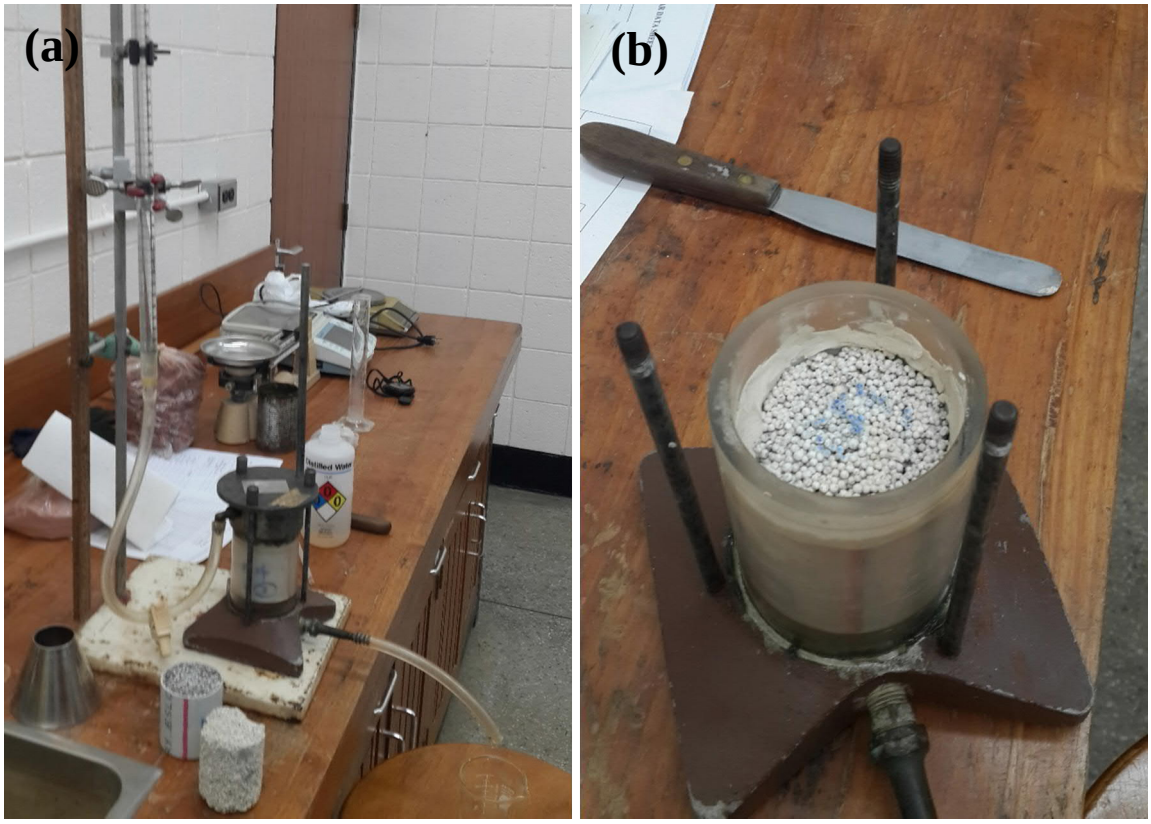

Figure 3-8 Falling head permeameter test for C-EPS samples, December 2016 (a) Standard laboratory falling head permeameter (b) C-EPS sample in permeameter
[Reprint with permission from Monrose et al. (2019a)]

$$k_f = \frac{aL}{At} ln \frac{h_1}{h_2} \quad (3\text{-}1)$$

Source: (Das, 2010)

where:

k_f = coefficient of permeability (cm/s),

a = cross-sectional area of the burette (cm^2)

L = sample length (cm)

A = cross-sectional area of the sample (cm^2)

t = time (s)

h_1 = initial head of water in the burette (cm)

h_2 = final head of water in the burette (cm) after time t

Table 3-2 Hydraulic conductivity (permeability) of C-EPS samples

Mix no.	Average hydraulic conductivity, k (mm/h)
1	1332
2	1692
3	1728
4	1764

3.2.5.2 **Compressive strength testing of C-EPS**

For compressive strength testing, two (2) 100 × 200 mm and six (6) 150 × 300 mm cylinder samples and six (6) 100 mm cube samples were prepared in accordance with BS EN 12390-3:2009 (BSI, 2009b) and ASTM C936 (ASTM International, 2018b) respectively. All samples were secured, de-moulded after 24 hours, labelled and cured in water at a standard temperature of 20 ± 1 °C for at least 28 days prior to testing. Low compressive strengths were expected, hence a Tinius Olsen tension and compression testing machine (Tinius Olsen TMC, Pennsylvania USA) was used as opposed to a traditional concrete compressive strength testing apparatus. Prepared samples and compressive strength testing are shown in Figure 3-9. All compressive strength results were less than 1.0 MPa.

(a) (b)

Figure 3-9 Compressive strength testing of C-EPS (a) Samples awaiting testing (b) Testing using Tinius Olsen tension and compression testing machine
[Reprint with permission from Monrose et al. (2019a)]

3.2.6 Physical testing of aggregates

The physical tests conducted on the aggregates along with their respective standards for testing are listed in Table 3-3. The details of each test are further described herein. The ASTM and BSI standards are two international standards typically used in pavement engineering which have been developed by traditional, reputable formal organisations (Mallick and El-Korchi, 2017). Hence, these standards were used in this research project.

Table 3-3 Physical tests performed on aggregates
[Adapted with permission from Monrose et al. (2019a)]

Test Name	**Source**
Sieve Analysis	ASTM C136 (2014c)
Specific Gravity and Absorption	ASTM C127 (2015)
Unit Weight and Voids in Aggregate	ASTM C29 (2016b)
Los Angeles (LA) Abrasion	ASTM C131 (2014b)
Aggregate impact value	BS 812 (1990)
Flakiness Index	BS EN 933-3 (2012)
Porosity	ASTM C29 (2016b)
pH	BS 1377 (2018)

3.2.6.1 **Sieve analysis**

Particle Size Distribution (PSD) or gradation of the aggregates was determined by sieve analysis in accordance with ASTM C136 (ASTM International, 2014c) using a Humboldt

"Mary Ann" Laboratory Sieve Sifter and 300 mm (12 in) sieves (Rainhart Co., Austin, Texas, USA). The sieve sizes ranged from 37.5 to 1.18 mm (1.5 in to No.16). Aggregates were prepared to meet ASTM classifications No.5, No.57 and No.8 for the sub-base, base and bedding layers respectively. These classifications are typically used in permeable pavements (Hunt and Collins, 2008). The aggregates were washed and dried at 105 °C for 24 h prior to sieve analysis. The mechanical sieve shaker and the rack of sieves used are shown in Figure 3-10.

Figure 3-10 Set up of sieve analysis rack in laboratory

3.2.6.2 **Specific gravity and water absorption**

Specific gravity (relative density), G_s and water absorption tests on the coarse aggregates were performed according to ASTM C127 (2015). Sampling excluded all material passing the 4.75 mm (No.4) sieve for base and sub-base aggregates and 2.36 mm (No.8) sieve for the bedding layer aggregates. Approximately 2 kg of aggregate samples were dried in the oven at a temperature of 110 ± 5 °C and then cooled in air at room temperature for at least 3 h. The aggregates were subsequently immersed in water at room temperature for 24 ± 4 h. The samples were then removed from the water, dried with an absorbent cloth and weighed. The results were recorded as the saturated-surface-dry mass in air (SSD_{air}). The SSD samples were then transferred to a water bath at 23 ± 2.0 °C and weighed. The results were recorded as the apparent mass in water. All entrapped air in the samples was removed prior to weighing by shaking the container while immersed. The SSD_{water} samples were subsequently dried in the oven at 110 ± 5 °C for 24 h, allowed to cool to room temperature and the mass determined. This mass was recorded as the mass of oven-dry sample in air. The specific gravity and absorption of the oven-dry sample were calculated from Equations 3-2 and 3-3 respectively.

Specific gravity (relative density), $G_s = \frac{A}{B-C}$ (3-2)

Absorption, % = $\frac{B-A}{A} \times 100$ (3-3)

where:

A = mass of oven-dry sample (g)

B = mass of SSD_{air} (g)

C = apparent mass of saturated sample in water (g)

Figure 3-11 Laboratory set up of specific gravity and water absorption apparatus

3.2.6.3 **Unit weight and voids**

Tests to determine the bulk density (unit weight), γ and voids in coarse aggregate were conducted in accordance with ASTM C29 (2016b). The dry-rodded method of testing was used. Laboratory equipment used included a 15.9 mm (5/8 in) diameter, 600 mm (24 in) long tamping rod, a weighing scale and a cylindrical metal mould with a minimum volume of 0.00283 m^3 (1/10 ft^3). The mould and weighing scale used are shown in Figure 3-12. Water at 29 °C was used to calibrate and verify the volume of the mould. The mould was filled progressively with coarse aggregates in one-third increments. Each layer of aggregate was rodded evenly over the surface with 25 strokes of the tamping rod. The final layer was

allowed to spill over and then was levelled using a straight edge. The combined mass of the mould filled with aggregate was then recorded. The procedure was repeated three (3) times and averaged. The bulk density and void content were calculated from Equations 3-4 and 3-5 respectively.

$$\gamma = \frac{A-B}{C} \tag{3-4}$$

where:

A = average mass of sample + mould (kg)

B = mass of mould in air (kg)

C = volume of mould (m^3)

γ = bulk density (unit weight) (kg/m^3)

$$\text{Void (\%)} = \frac{G_s \times \delta_w - \gamma}{G_s \times \delta_w} \tag{3-5}$$

Source: (Das, 2010)

where:

G_s = bulk specific gravity (kg/m^3)

δ_w= density of water (kg/m^3)

γ = bulk density (unit weight) (kg/m^3)

Figure 3-12 Testing apparatus for bulk density and voids of coarse aggregate

3.2.6.4 **Los Angeles abrasion**

The Los Angeles (L.A) abrasion test was conducted according to ASTM C131 (2014b). This test is a commonly-used test method to indicate aggregate toughness and abrasion characteristics. The L.A abrasion testing apparatus is shown in Figure 3-13. Samples were

prepared based on the gradings listed in Appendix A, page 221. Grade A was used for all samples except CNA where grade C was used. The test samples and the steel spheres were placed in the testing machine and rotated at a speed of 30 to 33 r/min for 500 revolutions. The samples were then sieved through the 1.70 mm (No. 12) sieve. The coarser material retained on the 1.70 mm (No. 12) sieve was washed, oven-dried at 110 ± 5°, allowed to cool and then weighed to the nearest 1 g. The percent wear (PW) was calculated to the nearest percent from Equation 3-6.

$$PW = \frac{A-B}{A} \times 100 \quad (3\text{-}6)$$

where:

A = mass of original test sample (g)

B = final mass of the test sample (g)

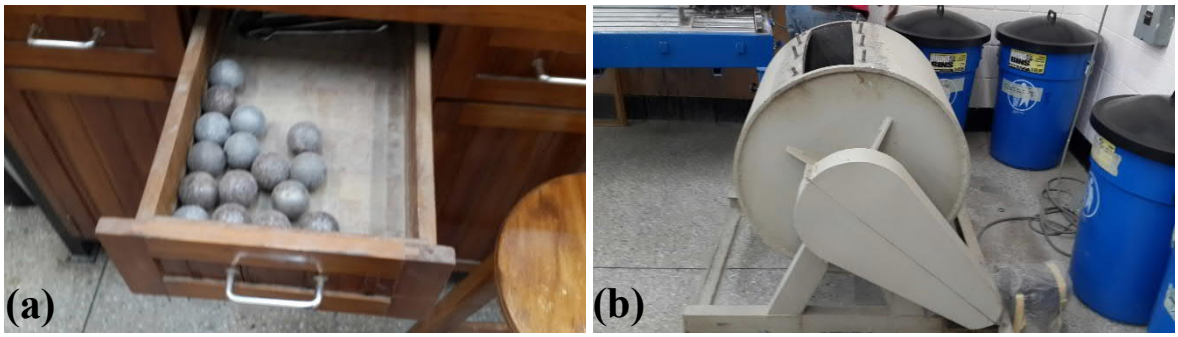

Figure 3-13 L.A abrasion apparatus (a) steel spheres (b) L.A testing machine

3.2.6.5 **Aggregate impact value**

Aggregate Impact Value (AIV) test was carried out to evaluate the resistance to deterioration after impact of aggregates. AIV was determined according to BS 812 (1990). Approximately 500 g of aggregates passing the 12.5 mm (1/2 in) sieve and retained on the 9.5 mm (3/8 in) sieve was used in the impact machine. Each test specimen was subjected to 15 impact blows from a 14 kg metal hammer free falling from a height of 380 mm (15 in). The specimens were then sieved through the 2.4 mm (No.8) sieve. The AIV apparatus used is shown in Figure 3-14. The AIV was calculated from Equation 3-7 (BSI, 1990).

$$AIV = \frac{W_1}{W_2} \times 100 \quad (3\text{-}7)$$

where:

W_1 = mass of sample passing No.8 (2.4 mm) sieve (g)

W_2 = original mass of sample (g)

Figure 3-14 Aggregate impact value testing apparatus

3.2.6.6 **Flakiness index**

The flakiness characteristics of the samples were determined according to BS EN 933-3 (2012). Approximately 3.5 kg of aggregates passing the 63 mm sieve and retained on the 6.3 mm sieve was sieved through the flakiness index special sieves with elongated apertures. The Flakiness Index (FI) was calculated to the nearest whole number from Equation 3-8 (BSI, 2012). Examples of sieves used for the determination of the flakiness index values are illustrated in Figure 3-15.

$$FI = \frac{M_2}{M_1} \times 100 \qquad (3\text{-}8)$$

where:

M_1 = sum of the masses of the individual size fractions and the flaky particles

M_2 = sum of the masses of all the flaky particles

(a) (b)

Figure 3-15 Flakiness index laboratory sieve setup

3.2.6.7 **pH**

pH values were determined in accordance with BS 1377 (2018). This method gives a direct reading of the pH value of a soil suspension in water. For the pH test, 30 g of a sample passing the 1.7 mm (No. 12) sieve was mixed with 75 mL of distilled water in a beaker. The suspension was stirred for at least 2 min and stored for at least 8 h. At the onset of the test, stirring of the suspension was repeated. pH measurements were subsequently taken using an Accumet Research AR10 pH meter (Fisher Scientific, Beverly, MA, USA) as shown in Figure 3-16.

Figure 3-16 Fisher Scientific Accumet Research AR10 pH meter with sample in laboratory

3.2.7 Chemical testing of the CNA, CCA and C-EPS

An external laboratory (Caribbean Industrial Research Institute [CARIRI], Macoya, Trinidad and Tobago, W.I.) was tasked with the examination and determination of the oxides and compounds present in the CNA, CCA and C-EPS. Oxide analysis was carried out using a Bruker-Axs X-ray Fluorescence spectrometer (XRF) model SRS 3400 (BRUKER AXS, Inc., Madison, Wisconsin, USA). An ELTRA CS2000 Carbon/Sulphur Determinator (ELTRA GmbH, Haan, Germany) was used to determine the percentage of Carbon and Sulphur present. Compound identification was carried out using a Bruker-Axs X-Ray Diffractometer (XRD) Model D8 Advance (BRUKER AXS, Inc., Madison, Wisconsin, USA). For each material, approximately 500 g of fines passing the 1.7 mm (No. 12) sieve was provided to CARIRI for analysis.

3.3 Material properties

3.3.1 Physical properties of aggregates

PSD or gradation curves of the unbound aggregates used in each rig are shown in Figure 3-17. The bedding course, base course and sub-base aggregates were graded to satisfy ASTM classifications No.8, No.57 and No.5 respectively. Based on the gradation curves, the coefficient of uniformity (C_u) and coefficient of curvature (C_c) values were calculated from Equations 3-9 and 3-10 (Erlingsson et al., 2009b) respectively. When C_u ranges between 4 and 6, the distribution is considered well graded. Conversely, when C_u is less than 4, the distribution is considered poorly or uniformly graded. The results presented show that the distribution of all aggregates was uniformly graded $(C_u < 4)$.

$$C_u = \frac{D_{60}}{D_{10}} \tag{3-9}$$

$$C_c = \frac{(D_{30})^2}{D_{10} \times D_{60}} \tag{3-10}$$

where D_{60}, D_{30} and D_{10} are the particle diameters corresponding to 60, 30 and 10% finer on the cumulative PSD curve, respectively.

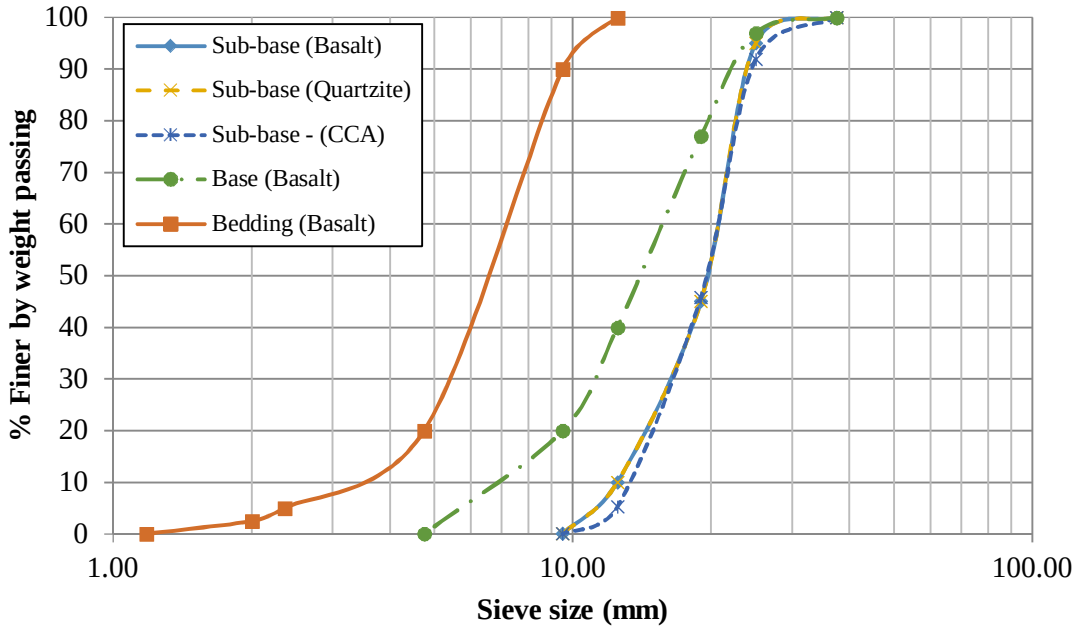

Figure 3-17 Particle Size Distributions (PSD) of unbound pavement aggregates used [Adapted with permission from Monrose et al. (2019a)]

The physical characteristics of the aggregates used are presented in Table 3-4. Full details of the physical tests are provided in Appendix A, page 221. The specific gravity of the CCA was as expected, lower than that of basalt and quartzite aggregates but greater than the typical requirement of 2.0 kg/m^3 (Rahman et al., 2015b). The specific gravity of CNA was approximately 40% lower than CCA confirming their lightweight characteristics. Water absorption of the CCA was significantly higher than that of basalt and quartzite aggregates but less than the typical requirement of 10% (Rahman et al., 2015b). Nevertheless, it fell at the low end of the 6 to 14% range of acceptable water absorption values for recycled materials in civil engineering applications (Poon and Chan, 2006). CNA recorded 23.6% water absorption which is consistent with values reported by Gunning et al. (2012). The CCA performed remarkably well under the L.A abrasion and impact tests with results better than the quartzite aggregates and below 50%. It must be noted that a significant portion of the abrasion was due to the disintegration of the cementitious paste (mortar) which surrounded the natural aggregates. CNA on the other hand, produced an L.A abrasion value of 66% which is not ideal for use in permeable pavements as unbound aggregates which depend on interlock and friction to provide structural support. The pH of the CCA and CNA were notably higher than the basalt and quartzite aggregates. This high pH value indicates high alkalinity which can be attributed to the chemical composition of the materials which were found to be rich in calcium oxide (CaO) and other compounds (Table 3-5). CCA pH results are consistent with results provided by Rahman et al. (2015a) but they reported slightly less alkaline values for RCA (10.5) and CB (9.5) and stated that these values were within expected limits. Based on these physical characteristics, CCA demonstrated potential for use as suitable construction material to substitute or add to traditional unbound aggregates in permeable pavement applications. CNA was not recommended and used as unbound sub-base materials from a structural point of view, primarily because of their high water absorption and L.A abrasion characteristics.

Table 3-4 Physical properties of aggregates

[Adapted with permission from Monrose et al. (2019a)]

Properties	Bedding	Base	Sub-base				CPPB
			Rig 1 - Basalt	Rig 2 - Limestone	Rig 3 - CCA	Rig 4 - C-EPS	CNA
ASTM grading classification	No.8	No.57	No.5	No.5	No.5	-	-
Coefficient of uniformity (C_u)	2.3	2.5	1.6	1.6	1.5	-	-
Coefficient of curvature (C_c)	1.3	1.1	0.8	0.8	0.9	-	-
Specific gravity, G_s (kg/m^3)	2.709	2.709	2.709	2.575	2.245	-	1.602
Water absorption (%)	1.2	1.2	1.2	0.8	7.1	-	23.6
L.A abrasion (%)	18	18	18	53	44	-	66
Impact (%)	16	16	16	38	42	-	-
Flakiness index (%)	1	1	1	3	-	-	-
Bulk density (kg/m^3)	1530	1559	1541	1504	1252	-	1159
SSD Bulk density (kg/m^3)	1548	1578	1559	1516	1341	-	1433
Voids ratio, e	0.433	0.422	0.429	0.414	0.44	-	0.27
Porosity, $n = \frac{e}{1+e}$ (%)	30	30	30	29	31	-	21
pH	8.51	8.51	8.51	8.28	12.26	-	11.56

3.3.2 Chemical properties of CNA, CCA and CEPS

Test results to determine the chemical compositions of the CNA, CCA and C-EPS using an X-ray fluorescence spectrometer (XRF) are presented in Table 3-5. CNA consisted predominantly of CaO at 49%, SiO_2 at 20% and Cl at 15%. CCA contained mostly CaO and SiO_2 at 29% and 62% respectively meanwhile C-EPS consisted predominantly of CaO, SiO_2 and C at 52%, 16% and 20% respectively. A copy of CARIRI's service project report is included in Appendix B, page 228. As per the report, the following approaches were taken:

1. Oxide analysis was performed using a Bruker-Axs X-Ray Spectrometer model SRS 3400 (BRUKER AXS, Inc., Madison, Wisconsin, USA). A standard-less method with an accuracy of ± 10% was used for measuring concentration of component parts.
2. An ELTRA CS2000 Carbon/Sulphur Determinator (ELTRA GmbH, Haan, Germany) was used to determine the percentage of Carbon and Sulphur present in the samples.
3. Oxides calculation was conducted using the mathematical model that is part of the analyser software which is based on simple oxide forms which may not necessarily be present in the sample.
4. Compound identification was performed using a Bruker-Axs X-Ray Diffractometer (XRD) Model D8 Advance (BRUKER AXS, Inc., Madison, Wisconsin, USA).

Table 3-5 Oxide composition of the recycled materials

[Adapted with permission from Monrose et al. (2019a)]

Oxide (wt.%)	CCA	C-EPS	CNA
CaO	28.72	52.04	48.69
SiO_2	62.12	16.14	19.65
Cl	< LLD	0.08	14.58
Na_2O	< LLD	< LLD	3.87
C	1.2	20.09	2.75
Al_2O_3	3.66	3.58	2.64
K_2O	0.39	0.12	2.34
Fe_2O_3	2.45	4.68	1.74
S	0.31	0.8	0.89
ZnO	< LLD	< LLD	0.79
P_2O_5	0.19	0.2	0.73
MgO	0.63	1.47	0.66
TiO_2	0.17	0.3	0.38
PbO	< LLD	< LLD	0.13
MnO	0.03	0.08	0.07
SrO	0.1	0.21	0.04
Cr_2O_3	0.02	0.05	0.04
ZrO_2	0.01	0.01	0.01
WO_3	< LLD	0.13	<LLD

LLD–Lower Limit of Detection

3.4 Design and construction of permeable pavement rigs

The permeable pavement rigs were designed in accordance with technical guidance from literature sources (Scholz and Grabowiecki, 2007, Collins et al., 2008, Smith, 2011, Drake et al., 2013, Woods Ballard et al., 2015, Bentarzi et al., 2016). Moreover, numerous institutions worldwide have provided general guidance relating to the design and construction of permeable pavements. In the UK, BS 7533-13 (BSI, 2009a) offers guidance on the design of permeable pavements. Likewise, the Interlocking Concrete Pavement Institute ICPI (2016) has also provided industry guidance for PICP in the USA and Canada. Similarly, in Australia, the Concrete Masonry Association of Australia (CMAA) has several available design guidance manuals on permeable paving (CMAA, 2016). Each of these standards provides similar recommendations relating to site boundary conditions, pavement structure (layer thickness, aggregate gradations) and pavement usage. Nevertheless, the use of permeable pavements as a stormwater management option is scarce across Caribbean SIDS. Consequently, only certain recommendations from these industry guidelines along with previous studies relating to aggregate gradations and pavement layer thicknesses were adopted in this research. It is noteworthy, that the permeable pavement rigs were intended to simulate permeable pavements designed for low speed, lightly trafficked surfaces such as parking lots, pedestrian access ways, bicycle paths and so forth.

Four (4) 450 × 420 × 610 mm (18 × 16.5 × 24 in) permeable pavement rigs were constructed from 19 mm (3/4 in) construction plywood as a tanked and enclosed system. The rigs were made watertight by inserting a 2 mm thick layer of commercially available PVC based pond liner on the inside. Three (3) 12.5 mm (1/2 in) PVC outflow pipes were inserted through one face of each rig at varying heads of 50, 250 and 480 mm (2, 10 and 19 in), above the base of the rigs. Three (3) of the test rigs are shown in Figure 3-18.

Figure 3-18 Three of four permeable pavement test rigs in the laboratory, December 2016 [Reprint with permission from Monrose et al. (2019a)]

The rigs were made up of an 80 mm (3.1 in) deep I-Paver interlocking concrete block surface, a 50 mm (2.0 in) deep bedding layer, a geotextile layer, a 100 mm (4.0 in) deep base course layer and a 250 mm (10.0 in) deep sub-base layer. The I-Pavers were supplied by the concrete block manufacturer, Abel Building Solutions (Arouca, Trinidad, W.I.). Each block paver unit measured 80 × 197 × 143 mm (3.1 × 7.8 × 5.6 in) and weighed 4.35 kg (9.6 lbs). Typically, these paver blocks are designed and installed in the Caribbean with little to no gaps. However, the design was modified by increasing the width of the gaps (2 to 13 mm) to facilitate increased infiltration of water to the underlying pavement layers (Figure 3-19). As mentioned previously in subsection 2.5.3, PICPs typically consist of joint spacing or gaps ranging from 3 to 13 mm which constitute between 8 and 20% of the pavement surface area. Moreover, the Interlocking Concrete Pavement Institute (ICPI, 2016) recommends that for pedestrian applications joint widths should not exceed 15 mm (¾ in). As the individual paver units themselves are not permeable, the joint spacing or gaps provide the necessary permeability. An increase in joint spacing is generally associated with an increase in hydraulic conductivity (permeability). The percent perviousness (porosity) of the surface of the pavement rigs used in this research project was estimated at 15%. This estimation was determined by dividing the joint-fill area by the total surface area of the pavement. Areas

were determined using the computer software AutoCAD 2018. While increasing joint width is advantageous for increased permeability, excessive joint width could lead to possible movement of the surface blocks after use, therefore reducing the surface stiffness. A ruler and measuring tape were used to measure the head of water above the surface of the concrete blocks. A three-dimensional (3-D) schematic of structure of the rigs is shown in Figure 3-20.

(a)

(b)

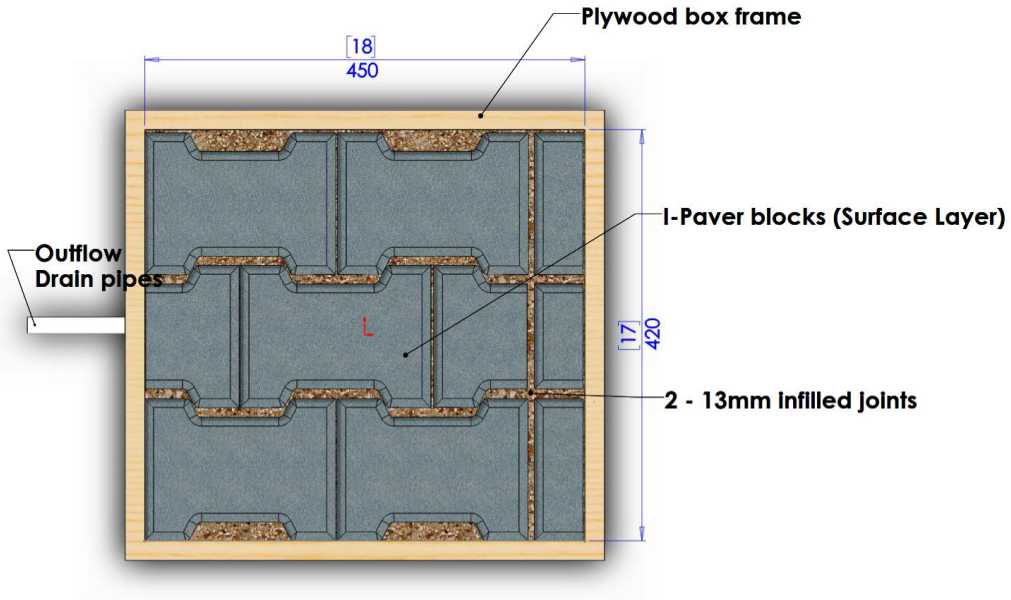

(c)

Figure 3-19 Plan view of installed I-Paver blocks; (a) Typical local installation with narrow joints (b) Installation with wider joints in the test rigs (c) Schematic layout

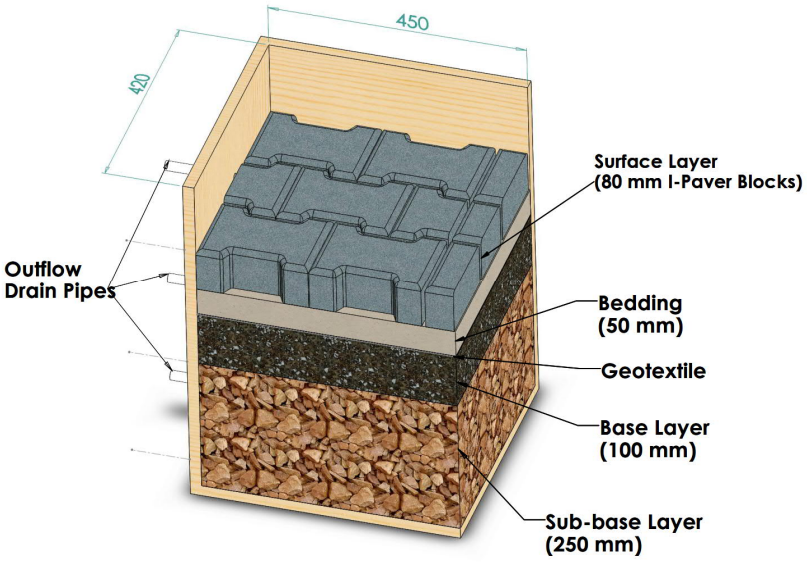

Figure 3-20 3-D schematic of the permeable pavement structure

The bedding layer was made up of 5 mm (No. 4 sieve) ASTM-classified No.8 washed fine aggregate. The base course layer was formed of 12.5 mm (1/2 in sieve) ASTM-classified No. 57 washed aggregate. The sub-base layer consisted of either 19 mm (3/4 in sieve) ASTM-classified No.5 aggregate or the novel C-EPS block. The different sub-base materials used in the pavement rigs along with their sources are listed in Table 3-6. CNA were considered but were not used as unbound sub-base materials in the rigs for two main reasons.

1. Physical properties: CNA did not display adequate strength to be used as unbound sub-base aggregates in the pavement rigs. The physical characteristics of the CNA presented in Table 3-4, showed that the CNA were porous and highly susceptible to crushing. Specifically, L.A abrasion values and water absorption values were 66% and 23.6% respectively. These characteristics are not ideal for use in permeable pavements as unbound aggregates which depend on interlock and friction to provide structural support.

2. Chemical properties: Table 3-5 showed that CNA consisted of 14.6% chlorides. High chloride content is toxic to the environmental. There was potential for these chlorides along with heavy metals to leach into the environmental should CNA be used as unbound aggregates in the pavement rigs.

Table 3-6 Sub-base materials in permeable pavement rigs

Rig No.	Sub-base material	Source
1	Basalt aggregates	Quarry from St. Lucia, W.I.
2	Quartzite aggregates	Quarry from Trinidad, W.I.
3	CCA	Prepared in laboratory
4	C-EPS	Prepared in laboratory

For all rigs, a nonwoven geotextile layer (Figure 3-21a) was placed between the bedding layer and the aggregate base course layer. The properties of the geotextile layer are listed in Table 3-7. The Minimum Average Roll Value (MARV), as defined in ASTM D4433 (ASTM International, 2018c), is a manufacturing quality control tool used to provide purchasers/users a 97.7% degree of confidence that any samples will exceed reported values. Numerous researchers have reported on the ability of geotextiles to improve short-term pollutant removal efficiency (Tota-Maharaj et al., 2012, Rahman et al., 2015b) as well as improving infiltration and attenuation of stormwater (Nnadi et al., 2014).

A commercially available biaxial geogrid (Figure 3-21b) with an ultimate tensile strength of 19.2 kN/m was placed between the C-EPS block and the aggregate base course layer in Rig 4. The purpose of the geogrid was to reinforce the pavement and to reduce the load transferred to the C-EPS block. The physical and mechanical properties of the geogrid are listed in Table 3-8.

Table 3-7 Mechanical and hydraulic properties of nonwoven geotextile
[Reprint with permission from Monrose et al. (2019a)]

Property	Test Method	MARV
Mechanical Properties		
Grab Tensile Strength (N)	ASTM D4632	912
Trapezoid Tear Strength (N)	ASTM D4533	356
CBR Puncture Strength (N)	ASTM D6241	2224
Hydraulic Properties		
Apparent Opening Size (mm)	ASTM D4751	0.18
Permittivity (s^{-1})	ASTM D4491	1.4
Flow Rate ($l/min/m^2$)	ASTM D4491	3870
UV Resistance after 500 h (% strength)	ASTM D4355	70

(a) (b)

Figure 3-21 Geosynthetics used in pavement rigs (a) nonwoven geotextile used in all rigs; (b) Biaxial geogrid used in Rig 4

Table 3-8 Physical and mechanical properties of the biaxial geogrid

Property	**Value**
Aperture Dimensions (mm)	25
Minimum Rib Thickness (mm)	1.27
Tensile Strength @ 2% Strain (kN/m)	6.0
Tensile Strength @ 5% Strain (kN/m)	11.8
Ultimate Tensile Strength (kN/m)	19.2
Junction Efficiency (%)	93
Flexural Stiffness (mg-cm)	750,000
Aperture Stability (m-N/deg)	0.65

3.5 Inflow (Water) delivery system

A purpose-built Rainfall Simulation Infiltrometer (RSI), designed and built from guidance from literature (Nichols et al., 2014), was used to deliver water to the rigs as water droplets that mimic the characteristics of natural rainfall. Numerous studies (Nnadi et al., 2015, Alsubih et al., 2017, Sounthararajah et al., 2017, Mai et al., 2018) have successfully used rainfall simulation techniques for practical research in urban drainage. The RSI was constructed of 12.5 mm (1/2 in) PVC pipes, valves and fittings. It was designed to be simple, lightweight and portable as it was required to be manually positioned over the permeable pavement rigs. It consisted of an outer frame measuring 610 × 610 × 1830 mm (24 × 24 × 72 in) along with an inner ring which matched the external dimensions of the rig. This inner ring was surrounded by a clear plastic sheet which served to mitigate loss of inflow to the pavement. At the top of the PVC frame were six 12.5 mm (1/2 in) horizontal PVC pipes

(parallel to the surface of the rigs) spaced 60 mm (2.4 in) apart. To facilitate rainfall simulation, a series of 3 mm (0.1 in) diameter holes spaced 50 mm (2.0 in) apart were drilled into the underside of these pipes. Prior to hitting the pavement surfaces, water droplets were simulated by breaking the flow of the water jets from the perforated PVC pipes using a pair of horizontal insect screen wire mesh sheets placed 300 mm (12 in) below the perforated PVC pipes. Water was conveyed to the RSI via a 19 mm (3/4 in) rubber hose connected to a submersible pump stationed inside a 100 L mixing tank. A Stir-Pak variable-speed heavy-duty mixer (Cole-Parmer, IL, USA) was included in the tank during accelerated clogging simulation tests. A valve and an inline flowmeter (Gardena®, Ulm, Germany) were used to control and measure the inflow rate. The flowmeter measured total volume (L) and flowrates (L/min). A schematic and laboratory layout of the experimental set up are shown in Figure 3-22 and Figure 3-23 respectively.

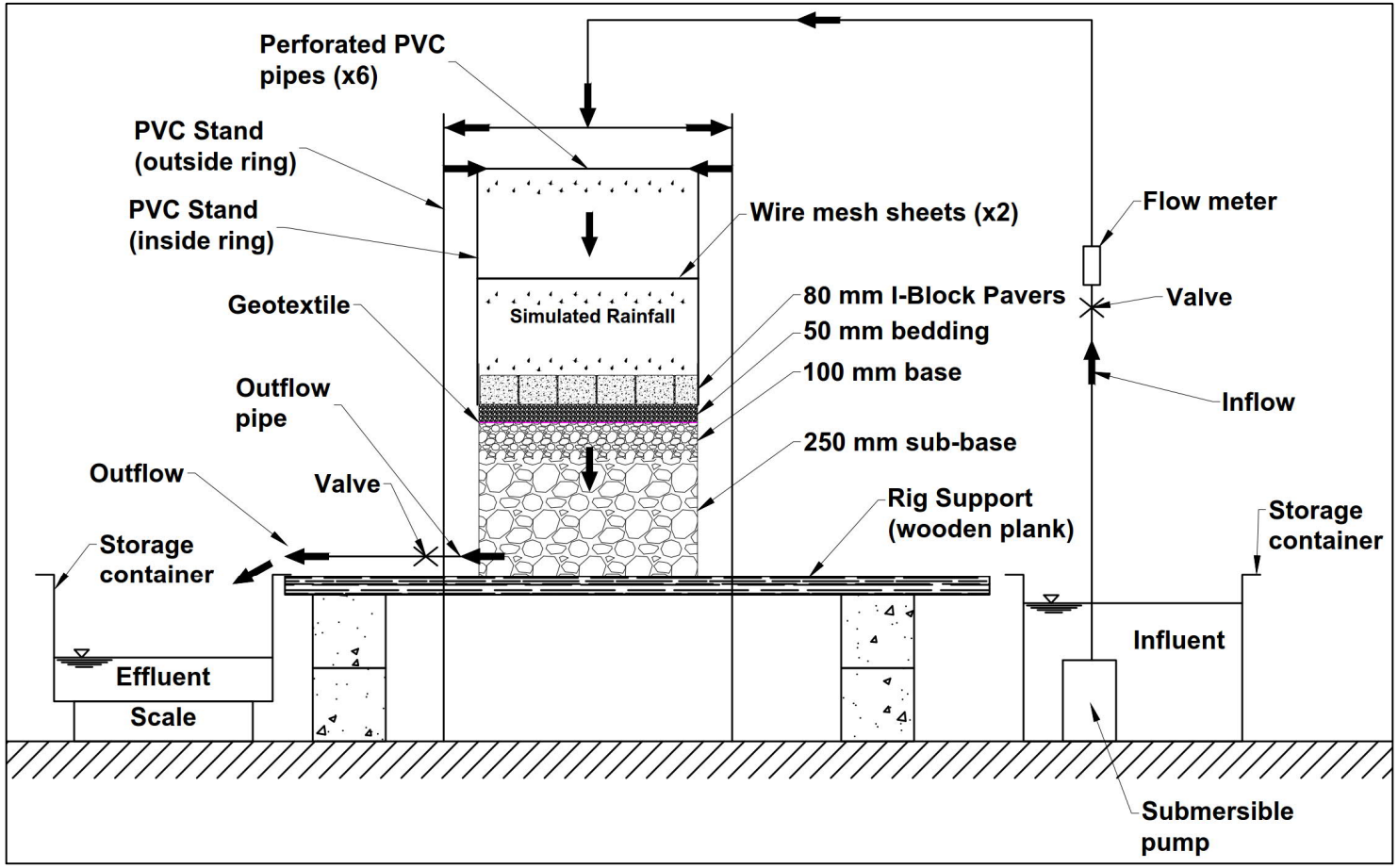

Figure 3-22 Schematic of permeable pavement laboratory set up

[Reprint with permission from Monrose et al. (2019a)]

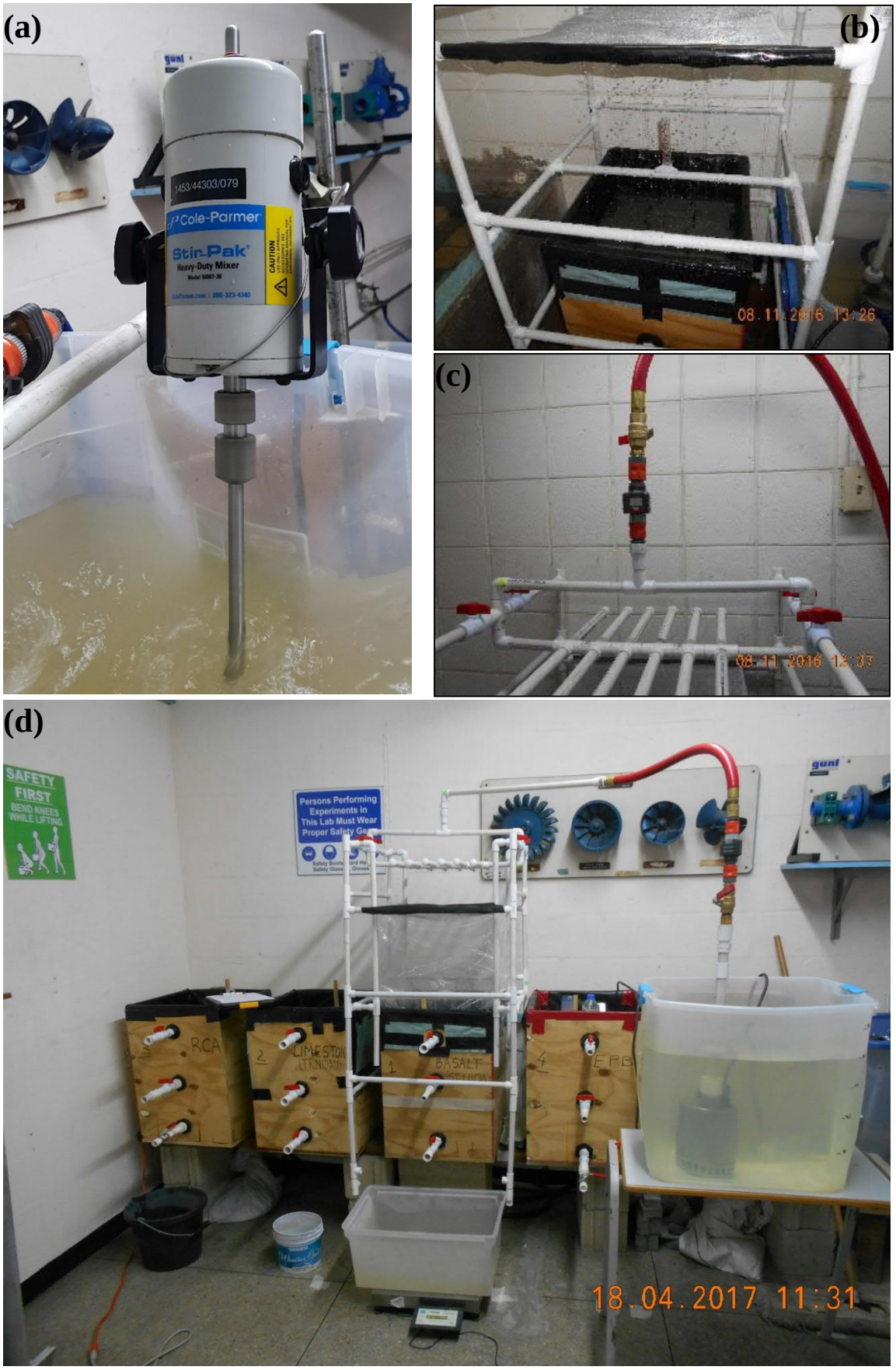

Figure 3-23 Layout of permeable pavement laboratory rigs; (a) heavy-duty mixer, (b) simulated raindrops, (c) Gardena® flowmeter (d) laboratory set up

3.5.1 Calibration of RSI flowmeter

The RSI's inline flowmeter was calibrated prior to the start of rainfall simulations to establish the relationship between the flowmeter readings and the actual inflow measurements. The calibration process occurred using the same tap water and under the same laboratory conditions which were used for hydrological response assessments of the rigs. The calibration process was repeated throughout the simulations. The following steps were taken to achieve this.

1. The density of the water was determined by measuring the mass of water in a known volume. Density (D) = Mass (M) / Volume (V)
2. Rainfall simulation was performed during a 15-min period over an empty container whereby the mass of water was recorded at 1-minute intervals. At the same time, the flow readings from the flowmeter were also recorded.
3. The mass of water recorded was converted to actual volume from the relationship, V = D/M
4. A scatter plot showing the relationship between the flowmeter volume and the actual measured volume was plotted using the computer software, Microsoft Excel. A calibration example is illustrated in Figure 3-24. In this example, the calibration equation is presented as Equation 3-11.

$$V_{Fl} = 1.3475 V_m \quad (3\text{-}11)$$

where:

V_{Fl} = Flowmeter volume (L)

V_m = Measured volume (L)

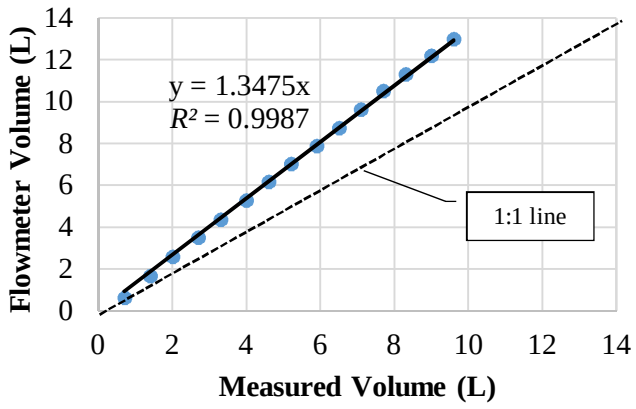

Figure 3-24 Flowmeter calibration graph showing relationship between flowmeter volumes and measured volumes

3.6 Experiment 1–Hydrological performance of the pavement rigs

These practical experiments sought to examine the hydrological response of the permeable pavement rigs to varying event-based inflow (rainfall) intensities and durations. The experiment provided a greater insight into the impact of recycled/recyclable materials as sub-base components of permeable pavements on their attenuation and retention capacity of stormwater. Very few literature sources (Rodriguez-Hernandez et al., 2016) are available on the impact of recycled/recyclable sub-base materials on the attenuation and retention capacity of permeable pavements.

The custom-built RSI was used for supplying rainfall input (tap water) to the rigs. All rainfall and discharge measurements were recorded simultaneously at 1-min intervals. Discharge was measured through continuous recording of the mass of water which exited the rigs at the outlet and collected in a container placed beneath the outlet. A VA-30 kg ACCULAB digital weighing scale (Acculab has since ceased business operations) was used for this purpose. A data logger was not used as none was available at the time of the experiments. Attempts to maintain a near constant rainfall intensity during the experiments were often difficult to achieve because the inflow controlling valve required manual adjustments to achieve a specified flowrate. Andersen et al. (1999) reported similar difficulties and sources of error at attempts to produce constant rainfall intensities during hydrological simulations.

For all simulated rainfall events, the discharge pipe was at an offset of 50 mm from the base of the rigs. Simulations were performed with water already occupying the 50 mm storage depth below the discharge pipe therefore negating any additional capacity for storage below the discharge pipe. For all rigs, a constant duration of 15 min was used during each rainfall simulation. All rainfall intensities exceeded 0.75 L/min ([238 mm/h] based on a plan area of 0.189 m^2). There was difficulty achieving lower flow rates from the flowmeter. Drainage structures are usually designed for a 50-year return period storm in Trinidad and the Caribbean by extension. The 5-min 50-year storm for a catchment in north Trinidad is circa 200 mm/h. Hence, the minimum 15-min storm used in the simulations have exceeded typical design conditions in the Caribbean. Fourteen (14) rainfall events were simulated for Rigs 1 to 3 and eleven (11) events for Rig 4. There was a total of 53 rainfall events simulated over a 6-month period from December 2016 to May 2017. The minimum antecedent dry period before simulated storm events was 24 h. Other researchers have also used 24 h (Alsubih et al., 2017) whilst some have used two weeks (Rodriguez-Hernandez et al., 2016).

The experiments were kept indoors wherein atmospheric conditions remained relatively constant. Average temperatures during the day was approximately 27 °C (81 °F). The evaporation impact from the rigs was considered negligible during rainfall events therefore no evaporation data was collected. Additionally, the hydrological analyses excluded minor losses from absorption of water by the surface blocks and/or the pavement aggregates. To minimise the impact of these losses, the results of the initial simulated events were excluded from analyses although the expected impact was insignificant given the high rainfall intensities, small surface area and short rainfall durations.

The following values were obtained for all hydrological simulations:

- Total rainfall volume (mm)
- Rainfall duration (min)
- Average rainfall intensity (L/min) and (mm/h)
- Lag time (min)
- Discharge volume during rainfall (L) and (m^3)
- Total discharge volume (L) and (m^3)
- Maximum retention (storage) capacity (mm) and (%)
- Retention/storage after discharge
- Runoff (if any) (mm)

Volume (L) was converted to depth (mm) by dividing by the surface area of the rigs (0.189 m^2). Similarly, rainfall intensity was converted from L/min to mm/h by also dividing by the surface area of the rigs. For instance, 1.0 L/min is equivalent to 317 mm/h (0.06 m^3/h / 0.189 m^2). Lag time was measured as the time delay from the onset of rainfall to the onset of discharge. The discharge, *Q*, was deemed to have ceased when the cumulative mass of discharge did not increase by more than 0.02 g at the succeeding time step (1 min). Storage/retention volume during rainfall was calculated from the water balance equation (Equation 3-12). The retention/storage volume during rainfall gives the maximum retention/storage capacity which is determined at the end of the equilibrium state (Lin et al., 2014).

$$\Delta S = R - Q \tag{3-12}$$

where:

ΔS = storage or retention volume during rainfall (mm)

R = rainfall input (mm)

Q = discharge volume during rainfall (mm)

Moreover, the results obtained were statistically analysed using the IBM software Statistical Package for the Social Sciences (SPSS) version 20 (IBM, 2011). Descriptive statistics and the Mann-Whitney U two-independent samples tests were used for the analysis of lag time and retained rainfall values. A 95% confidence interval was used for all statistical analyses. Results and discussions of the hydrological response assessments are presented in Chapter 4.

3.7 Experiment 2–Water quality performance

Because of the scarcity of literature sources, it is evident that a research gap exists involving the assessment of water quality performance (pollutant removal efficiency) of PPS whereby recycled/recyclable materials are incorporated as sub-base materials in permeable pavements. This subsection discusses the means and methods used to evaluate the water quality performance of the permeable pavement rigs.

3.7.1 Sampling and testing methods

Rather than using synthetic stormwater to assess the pollutant removal efficiencies of the pavement rigs as used in numerous studies (Tota-Maharaj and Scholz, 2010, Myers et al., 2011, Rahman et al., 2015b, Sounthararajah et al., 2017, Jayakaran et al., 2019), this research project utilised natural stormwater runoff samples extracted during rainfall events at various locations across Trinidad, W.I. In doing so, a manual “grab” method of collecting samples of stormwater runoff was used. Grab samples are discrete samples of fixed volume taken to represent local conditions in the flow (Butler and Davies, 2011). Attempts were often made to capture representative “first flush” samples. These “first flush” samples typically contain the largest percentage of the total contaminant loadings especially in small catchment areas with predominantly impervious surfaces and which experience high intensity storms (Geosyntec Consultants and Wright Water Engineers, 2009). These high intensity rainfall events are commonplace in Trinidad and across most Caribbean SIDS especially during the wet season (June to December). First flush samples were not always obtained due to difficulties in estimating the timing of rainfall events. This made weather forecasting a crucial aspect of the sampling efforts.

A total of thirty (30) individual 100 L grab samples were collected from rainfall events between December 2016 and August 2018. Five (5) 20 L polyethylene buckets were used in this regard. Trinidad has an annual rainfall depth of approximately 2000 mm. There is a strong seasonal variation in rainfall whereby 75 to 80% of rainfall is received during the wet

season (June to December). The remaining 20 to 25 % is received during the dry season (January to May) (Monrose and Tota-Maharaj, 2018).

Captured stormwater runoff samples were applied uniformly over the rigs using the purpose-built RSI at intensities ranging from 1.0 to 2.0 L/min. Outflow (effluent) exited at the outlet of the permeable pavement rigs and was permitted to flow for several min (7 to 10 min) prior to collection in 300 ml sampling bottles for analysis. Throughout the stormwater application events, the influent (raw stormwater) was continuously stirred to ensure particles remained in suspension. The collected outflow samples were analysed immediately or refrigerated at 4 ºC to minimise any changes in the physio-chemical properties of the samples prior to analyses. An example of stormwater runoff collected from one of the rainfall events is shown in Figure 3-25.

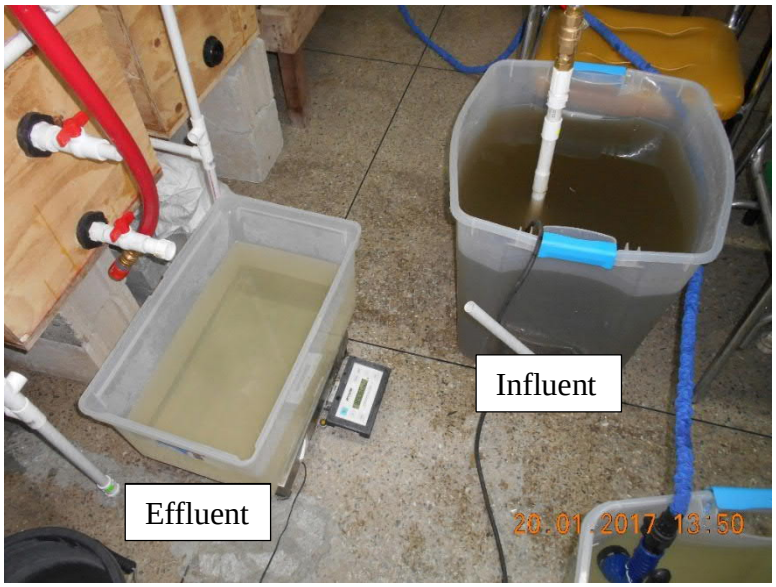

Figure 3-25 Example of stormwater influent and effluent samples

3.7.2 Water quality analyses

The pollutant removal efficiencies of the four (4) rigs was compared through analysis of various influent and effluent water quality parameters – pH, Chemical Oxygen Demand (COD), Dissolved Oxygen (DO), Electroconductivity (EC), turbidity, Total Suspended Solids (TSS), Total Dissolved Solids (TDS), Nitrate-Nitrogen (NO_3-N), reactive phosphorous (PO_4^{3-}), sulphates (SO_4^{2-}), copper (Cu), zinc (Zn), manganese (Mn), iron (Fe), lead (Pb) and Chromium (Cr). All water quality sample analyses were in accordance with the American Public Health Association standard methods for the examination of water and wastewater (APHA, 1998). The water quality analyses were conducted at the Process Engineering laboratory of the University of Trinidad and Tobago (UTT), Department of Utilities Engineering, Point Lisas, Trinidad, W.I. and at the environmental laboratory of the

University of the West Indies, St. Augustine Campus, Department of Civil and Environmental Engineering, St. Augustine, Trinidad, W.I.

Table 3-9 identifies the standard methods used in this research project and the Minimum Detectable Levels (MDL) for each parameter. pH was measured using an Orion 3 Star benchtop meter (Thermo Scientific, Beverly, MA, USA). DO was measured using a YSI 5000 Benchtop DO Meter and probe (YSI, Yellow Springs, OH, USA). A Jenway 4520 Conductivity meter (Jenway, Staffordshire, UK) was used to measure electroconductivity (µS/cm). A Hach Colorimeter (DR/820) (Hach, Loveland, CO, USA) was used to measure NO_3-N (mg/L), SO_4^{2-} (mg/L), PO_4^{3-} (mg/L), and turbidity (Nephelometric Turbidity Units [NTU]). The concentration of NO_3-N (mg/L) was determined by a cadmium reduction method using Hach NitraVer5 Nitrate reagent powder pillows. SO_4^{2-} (mg/L) was measured by the SulfaVer 4 Method using Hach SulfaVer 4 sulphate reagent powder pillows. PO_4^{3-} (mg/L) was measured by the Amino Acid method using Hach Molybdate and Amino acid reagents. The Absorptometric method was used to measure turbidity. COD was analysed using a Hach DRB200 Reactor block (Hach, Loveland, Colorado, USA) (for sample digestion) and a Hach Spectrometer (DR/5000) TNT 822 COD vial (Hach, Loveland, CO, USA). COD was measured rather than BOD due to ease of measurement and the correlation between the two parameters. A similar approach was taken by Pilon et al. (2019) for evaluating the effect of porous concrete on water quality parameters in Alcoa, TN, USA. TDS (mg/L) and TSS (mg/L) were measured using a 0.45 µm Whatman filter paper. Total metal concentrations in water were analysed from flame Atomic Absorption Spectrometry (AAS) using an Analytik Jena NovAA 400 Atomic Absorption Spectrometer (Analytik Jena AG, Germany) in accordance with the US EPA method 200.2. The samples were acidified with nitric acid (HNO_3) and hydrochloric acid (HCl), then digested for 2.5 h at 95 °C and cooled prior to analyses.

Table 3-9 Laboratory analysis methods and their Minimum Detection Levels (MDL)
[Adapted with permission from Monrose et al. (2019a)]

Water Quality Parameter	**Method**	**MDL**
pH	SM 4500-H+B	-
Chemical COD (mg/L)	HACH TNT 822	20
DO (mg/L)	SM 4500-OG	0
NO_3-N (mg/L)	HACH Cadmium Reduction Method	0.3
PO_4^{3-} (mg/L)	HACH Amino Acid Method	0.02
SO_4^{2-} (mg/L)	HACH SulfaVer 4 Method	2
Turbidity (NTU)	HACH Absorptometric Method	0
TDS (mg/L)	SM 2540C	5
TSS (mg/L)	SM 2540D	0.5
Conductivity (µS/cm)	SM 2510B	1
Cu (mg/L)	US EPA Method 200.2	0.001
Zn (mg/L)	US EPA Method 200.2	0.01
Mn (mg/L)	US EPA Method 200.2	0.01
Fe (mg/L)	US EPA Method 200.2	0.01

3.7.3 Data analysis

Statistical analyses of the results were also performed using SPSS version 20 (IBM, 2011). Descriptive statistics, tests for normality using goodness-of-fit statistics, one-way analysis of variation (ANOVA), Pearson's correlations and the Mann-Whitney U two-independent samples tests were used for the analysis of all water quality parameters. A 95% confidence interval was used for all statistical analyses. Boxplots and bar charts were used to examine and present variations and/or similarities in mean pollution concentration results. Mean pollutant removal efficiencies were calculated from Equation 3-13.

$$\text{Removal efficiency (RE) (\%)} = \left(\frac{C_{in}-C_{out}}{C_{in}}\right) \times 100 \qquad (3\text{-}13)$$

where:

C_{in} = inflow (influent) concentration (mg/L)

C_{out} = outflow (effluent) concentration for individual samples (mg/L)

3.8 Experiment 3–Hydraulic conductivity and long-term clogging

Variations in the permeability of PPS are significantly affected by the testing methods used. Accelerated Simulation Technique (AST) was used to simulate clogging, over a 10-year period, of the four (4) permeable pavement rigs. Pratt (1990) pioneered accelerated rainfall

and sediment accumulation application techniques on laboratory-based PICP models. Numerous researchers (Borgwardt, 2006, Siriwardene et al., 2007, Pezzaniti et al., 2009, Yong et al., 2013, Nichols et al., 2015, Ahn et al., 2018) have since used AST along with hydraulic conductivity measurements for assessing the clogging patterns of laboratory-scale permeable pavements. These studies used a variety of sediment types including natural and silica-based sediment.

Semi-synthetic stormwater made up of tap water and fine sediments (300 µm in diameter) were used as the clogging agent. The fine sediments were sourced from a local quarry. The PSD curve of the sediments is shown in Figure 3-26. The purpose-built RSI was used to supply the semi-synthetic stormwater to the rigs. The 300 µm fine sediments were chosen because numerous studies (Balades et al., 1995, Nicols and Lucke, 2017) have reported that finer materials contribute disproportionally to accelerated clogging of permeable pavements. As argued by Alsubih et al. (2017), it is obvious that utilisation of a single sediment type and size is not necessarily representative of the full range of sediment loads that a real-world permeable pavement would be exposed to. Nevertheless, given the general uncertainties regarding the influence of sediment on the hydraulic capacity of permeable pavements, consideration of a more complex sediment input approach would unnecessarily complicate the intent and analysis of the experiment.

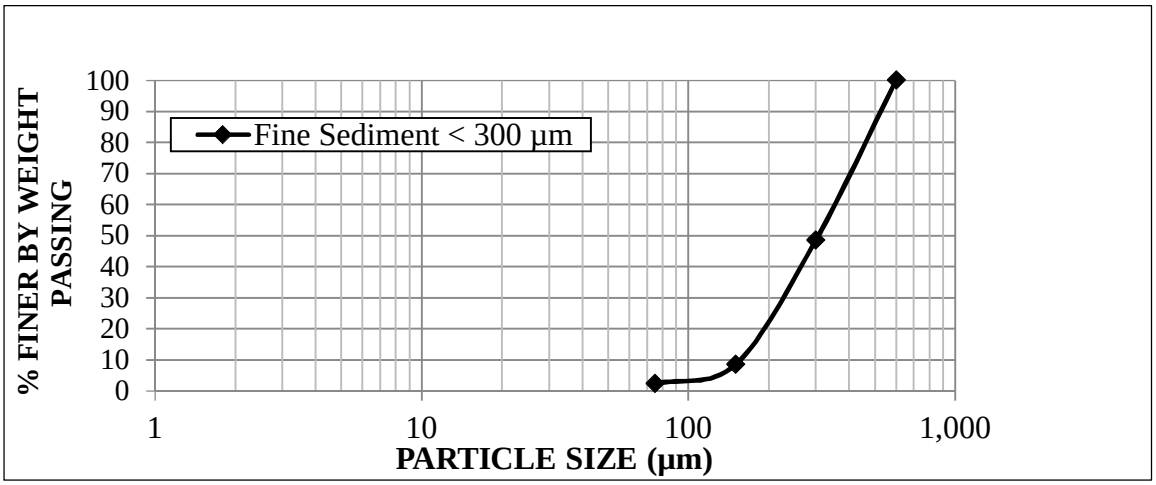

Figure 3-26 PSD of the sediments used to clog the experimental rigs

The clogging pattern of the permeable pavement rigs was determined from yearly hydraulic conductivity measurements over an accelerated 10-year period. This assumes that, in practice, most permeable pavement installations will receive additional sediment at every rainfall event. Inflow volumes into the permeable pavement test rigs were calculated from the product of the plan surface area (0.189 m^2) of the rigs and the yearly rainfall depth as illustrated in Equation 3-14. The Caribbean region has an average annual rainfall depth of

approximately 2000 mm (Monrose and Tota-Maharaj, 2018). Hence, with each rig having a surface area of 0.189 m^2, an inflow stormwater volume of 378 L (2000 mm × 0.189 m^2) was required to deliver the equivalent of one year's rainfall to the rigs. This value was rounded up to 400 L for ease of measurement.

$$R = \frac{V}{A} \tag{3-14}$$

where:

R = rainfall depth (mm)

V = volume of water (L)

A = surface area (m^2)

Based on a review of previous studies (Pezzaniti et al., 2009, Nichols et al., 2015), an average suspended sediment (SS) loading of 200 mg/L or 80 g/400 L was used in this study.

The hydraulic conductivity of the test rigs was determined after each year of simulated SS loading. A falling head permeability test (Erlingsson et al., 2009a) was used for this purpose. With the outlet valve closed, the pavement rigs were saturated with tap water up to a predetermined head above the surface of the pavement. The time taken for the water level to drop by a predetermined head was measured using a stopwatch and recorded. The hydraulic conductivity (permeability) was then calculated from Darcy's law as a falling head test from Equation 3-15 (Das, 2010). A minimum 24-h drying period was set for each rig prior to performing the hydraulic conductivity tests. A schematic of the details of the hydraulic conductivity testing is shown in Figure 3-27. Variation in sediment accumulation from year 1 to year 10 of the accelerated clogging simulation of one of the rigs is shown in Figure 3-28.

$$k = \frac{L}{t} ln \frac{h_1}{h_2} \tag{3-15}$$

where:

k = coefficient of permeability (cm/s),

L = sample length (cm)

t = time (s)

h_1 = initial head of water above the pavement surface (cm)

h_2 = final head of water dropped (cm) after time t

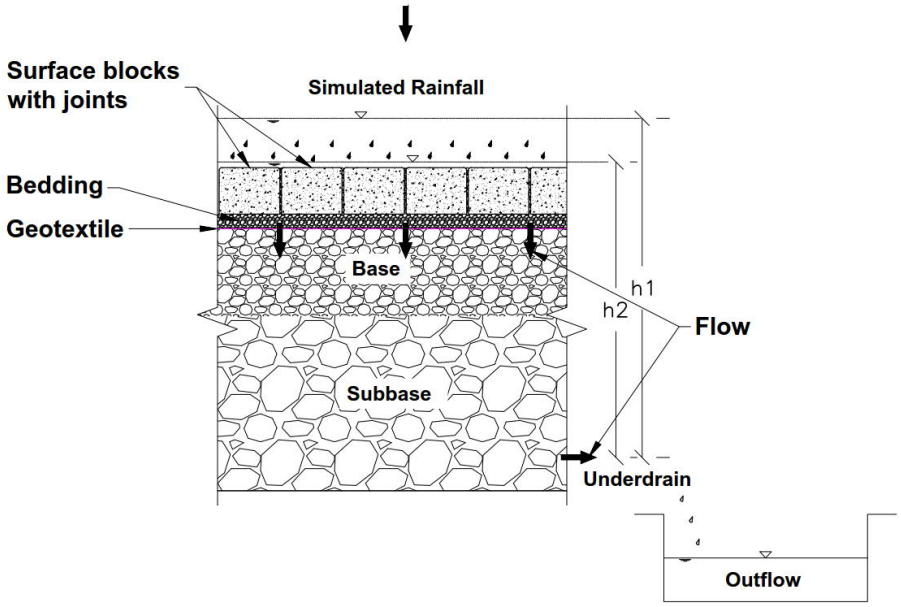

Figure 3-27 Details of hydraulic conductivity testing of the permeable pavement rigs

(a) (b)

Figure 3-28 Accelerated clogging simulation example (a) Year 1 (b) Year 10

Statistical analyses of the results were performed using SPSS version 20 (IBM, 2011). Pearson's correlations and regression models were used to test the hypothesis that the hydraulic conductivity of permeable pavements decreases over time because of clogging. A 95% confidence interval was used for all statistical analyses. The variables used in the regression models were hydraulic conductivity (dependent variable) and service life/age of permeable pavement (independent variable).

3.9 Experiment 4–Stiffness modulus and deflection testing

Surface modulus and deflection profiles of the permeable pavement rigs were assessed using a PRIMA 100 Portable Falling Weight Deflectometer (PFWD) (Sweco Denmark, A/S, formally Grontmij A/S). Figure 3-29 shows a schematic and photograph of the PRIMA 100 PFWD used in this research project. As mentioned previously in subsection 2.5.10, the

PFWD is a non-destructive testing apparatus that is used to evaluate the structural integrity of pavements. It is modelled after the FWD but uses a much lighter weight making it portable and able to be manually operated. The relationship between load and deflection, created by the free falling weight, is measured using the PFWD (Kim et al., 2007, Grontmij A/S, 2012). The PRIMA 100 PFWD consisted of a 300 mm (12 in) diameter base (loading) plate with a sensor and a falling weight (10 kg sliding hammer) which was dropped onto the plate from a height of 850 mm (33.5 in). The base incorporates two sensors: a load cell and a geophone (velocity transducer). The PFWD was positioned in order to ensure good surface contact and the test was done at the centre of the permeable pavement rigs. All measurements were recorded, interpreted, calculated and stored in a Personal Digital Assistant (PDA) device connected to the PRIMA 100 device via a wireless Bluetooth connection. The deflections were measured at the centre of the loading plate. A total of six (6) PFWD measurements were taken for each rig set up. All measurements were performed under identical conditions for all rigs. The first two (2) drops were excluded from analyses as they were considered seating. An average value of the remaining four drops for each rig was used to establish the mean surface modulus and deflection.

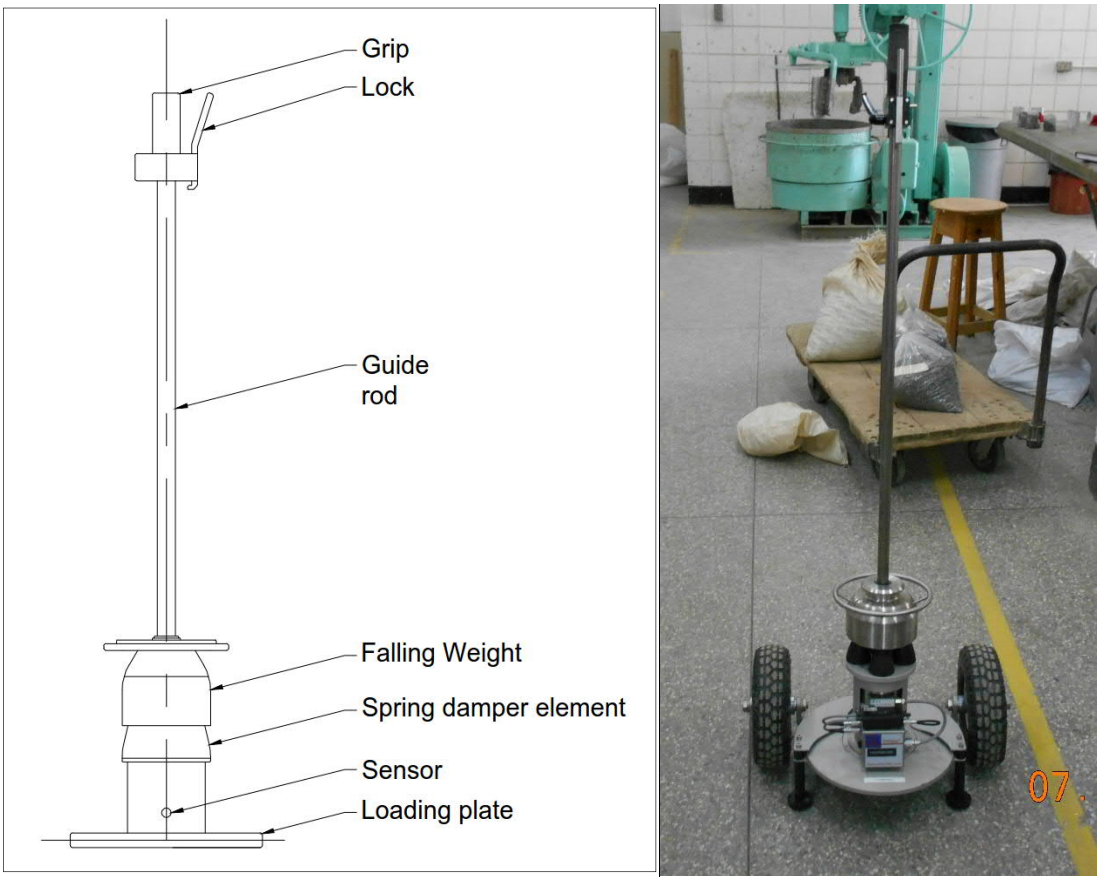

(a) (b)

Figure 3-29 PFWD used in study (a) schematic (b) actual at University of the West Indies, St. Augustine Campus, Trinidad, W.I.

3.9.1 Analysis Technique

During testing, the load is applied to the surface of the rigs via the base plate. The resulting force and velocity/time histories are measured above and below the centre of the plate by the load cell and geophone, respectively. The corresponding displacement/time history is automatically obtained via integration (internal to the device) of the velocity record. The output includes respective time histories and peak values of the applied load and ensuing deflection, as well as an estimated value of the surface modulus, E_0 (Hoffmann et al., 2004). E_0 is based on the Boussinesq solution relating the static deflection of an elastic half-space subjected to an axisymmetric surface loading according to Equation 3-16 (Stamp and Mooney, 2013). This analysis is illustrated in Figure 3-30.

$$E_0 = \frac{f(1-v^2)F_{pk}}{\pi r_0 w_0} \tag{3-16}$$

where:

E_0 = Surface Modulus

v = Poisson's ratio

F_{pk} = Peak applied load

r_0 = Radius of loading plate

w_0 = Peak vertical deflection

f = Stress distribution factor

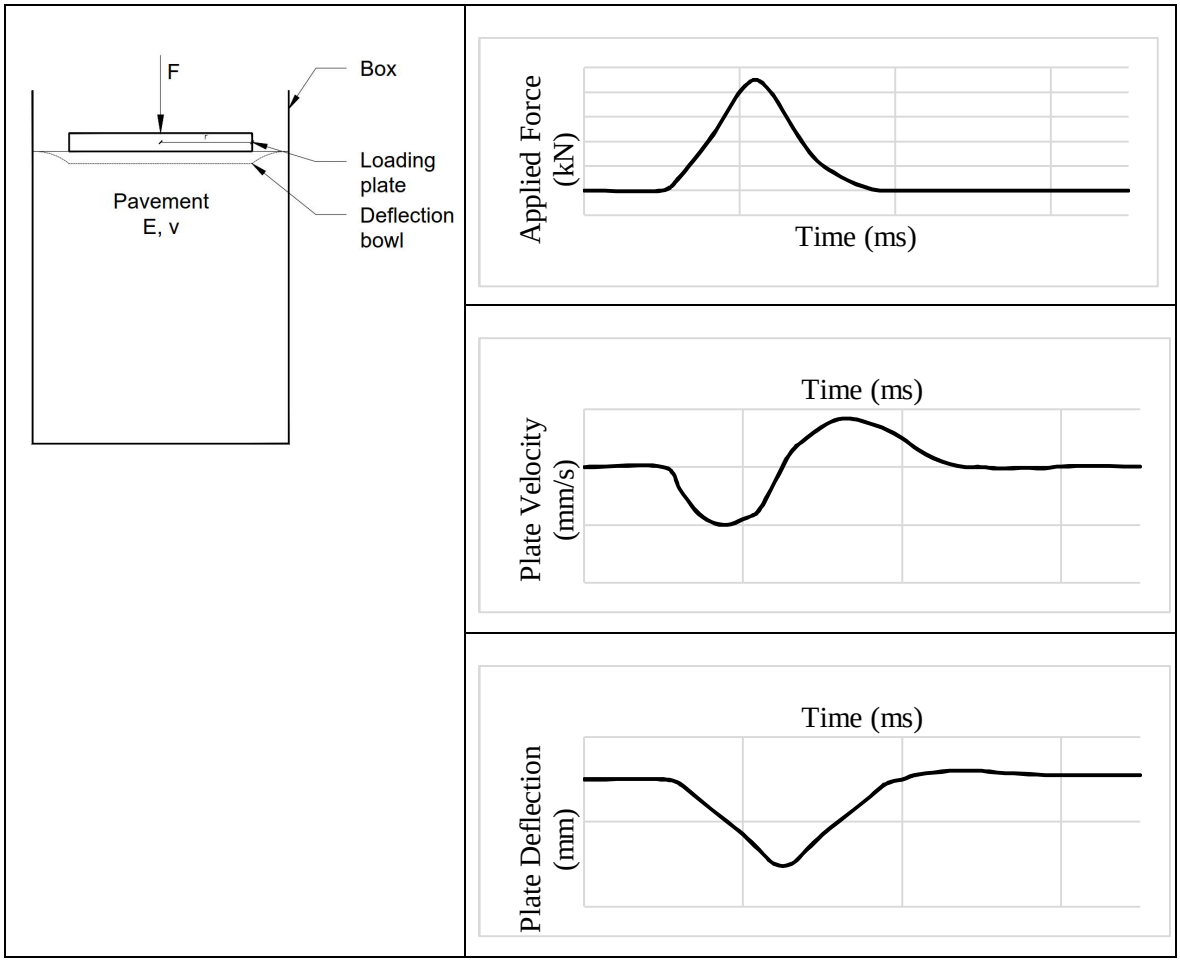

Figure 3-30 PFWD testing analysis schematic and typical time history profiles [adapted with permission from Mooney and Miller (2009)]

The configuration of the rigs provided a 60 mm (2.4 in) maximum distance between the side of the boxes and the edge of the PFWD loading plate. For laboratory studies involving PFWD testing using one geophone, an exact minimum distance between the edge of the loading plate and the wall of the test box is not set as various researchers have suggested different values. Alshibli et al. (2005) suggested a distance of 150 mm (6 in) but did not present any theoretical reasons. Rafiei et al. (2012) reported 400 mm (16 in) based on finite difference software (FLAC) modelling of the PFWD dynamic loading on a sandy gravel material (650 mm deep), in which the falling mass was 15 kg, the drop height was 500 mm, the loading plate diameter was 300 mm and the boundary conditions considered vertical displacement at the side of the box and fixed at the bottom. Considering that the permeable pavement rigs used in this research project were different in terms of physical and geotechnical characteristics, along with the use of a 10 kg falling mass, these results reported by Rafiei et al. (2012) are most likely not applicable. Moreover, numerous factors influence PFWD results including plate size and rigidity, loading rate, buffer stiffness and shear

strength of the pavement foundation materials (White et al., 2007, ASTM International, 2011).

Nevertheless, as illustrated in Figure 3-30, deformations are larger directly under the footprint of the loading plate and gradually decrease towards the walls of the boxes. With regards to the depth of the test boxes, previous studies (Mooney and Miller, 2009, Senseney et al., 2014, Tirado et al., 2017), have found that the effective depth of influence during PFWD testing is 1.2 – 1.4 times the diameter of the loading plate. Hence, the 480 mm depth of pavement used for all rigs in this research project allows PFWD values up to 420 mm below the surface of the pavements. On the basis of these observations, it is suggested that boundary effects due to the test boxes are negligible in this research project. Boutet et al. (2011) suggested that boundary effects may be negligible after they found that the deformations along the wall of a test container were always 10% or lower than that under the PFWD loading plate.

Reports from the literature survey showed that PFWD testing of permeable pavements is uncommon and limited to field installations of permeable pavements. Despite the lack of literature sources, the methodology of utilising the PRIMA 100 PFWD was practical to evaluate and compare the stiffness and deflection of the pavement rigs under ‘as-built” conditions in the laboratory. The PRIMA 100 device was capable of providing composite stiffness or surface modulus values which take into consideration the different sub-base materials in each of the four (4) permeable pavement rigs.

3.9.2 Impact stiffness modulus

Impact Stiffness Modulus (ISM) is defined as the ratio of the applied load (kN) to its corresponding deflection at the centre sensor as defined by Equation 3-17 (Steinert et al., 2005). A higher ISM value implies better support capacity (Lin et al., 2016).

$$ISM = \frac{P}{D_c} \tag{3-17}$$

where:

P = Applied load (kN)

D_c = Surface deflection at centre of PFWD censor (mm)

3.10 Chapter summary

This chapter has described the materials and methods used to assess the physical and chemical properties of CCA, CNA and C-EPS and their suitability for use in permeable pavements. This chapter also gave a detailed account of the materials and methods used to evaluate and compare the performance (bearing capacity, permeability, long-term clogging, attenuation and retention capacity, pollutant removal efficiency) of pilot-scale permeable pavement rigs that contained natural aggregates (basalt or quartzite) to rigs containing CCA and C-EPS. The results of these performance evaluation experiments are presented in Chapter 4. In terms of the suitability of the recycled/recyclable materials, both CCA and C-EPS were found suitable for use as sub-base materials in PPS. However, C-EPS was recommended for use in pavements with no vehicular traffic because of its relatively low compressive strength (< 1.0 MPa). CNA were found unsuitable because they lacked strength (66% L.A Abrasion), had high water absorption (23.6%) and could leach excessive amounts of chlorides and other compounds into the environment. CNA was instead used in a bound application for the production of novel Concrete Permeable Pavement Blocks (CPPB) for use in the surface layer of permeable pavements. The methodology and results for this experiment are presented in Chapter 6. The following chapter presents, analyses and discusses the results of the four performance evaluation experiments.

CHAPTER 4. PERFORMANCE EVALUATIONS OF PERMEABLE PAVEMENT RIGS

4.1 Overview

This chapter presents, analyses and discusses novel results obtained from experiments highlighted in Chapter 3. Some researchers (Drake et al., 2013, Kayhanian et al., 2015, Rahman et al., 2015b, Weiss et al., 2019) have opined that more scientific research is required to reduce uncertainty and a knowledge gap regarding the performance (structural integrity, hydrological, pollutant removal, hydraulic conductivity and long-term clogging) of permeable pavements consisting of recycled materials. The discussions herein can most likely reduce these uncertainties. A major component of the water quality performance evaluation has been published in the journal Road Materials and Pavement Design. The remaining performance evaluations have been submitted for publication as articles in the journals, Journal of Hydrologic Engineering and International Journal of Pavement Research and Technology.

4.2 Hydrological performance evaluation

The results of experiments carried out to determine the hydrological response of the permeable pavement rigs to varying high intensity and short duration rainfall events, are analysed and discussed herein. It must be noted that results and conclusions drawn are limited to laboratory conditions as described previously in subsection 3.6. Thus, factors that can influence the long-term hydrological performance of permeable pavements such as clogging and possible geometrical changes to the pavement structure based on usage were not considered in this subsection. The influence of clogging on hydraulic conductivity is discussed in subsection 4.4.

As noted previously in subsection 3.6, fourteen (14) rainfall events were simulated for Rigs 1 to 3 and eleven (11) rainfall events were simulated for Rig 4. No surface runoff was observed from any of the simulated rainfall events. Descriptive statistics of the hydrological response outputs to rainfall from each rig are listed in Table 4-1. For all rigs, mean inflows ranged from 343 to 476 mm/h. Full details of the hydrological response outputs of all simulated rainfall events are listed in Appendix C, page 235.

Table 4-1 Descriptive statistics of hydrological response outputs from each test rig

Statistic	Rig No.	Rainfall (Inflow)		Discharge (Outflow)		Storage (Retention)	
		Depth	Average Intensity	Lag time	Volume at rainfall cessation	Volume at rainfall cessation	
		(mm)	(mm/h)	(min)	(mm)	(mm)	(%)
Min	Rig 1	60.95	243.46	1.0	44.80	16.15	16
	Rig 2	59.40	237.26	1.0	44.26	15.14	16
	Rig 3	63.59	254.00	1.0	47.14	15.84	17
	Rig 4	71.12	284.07	1.0	54.76	16.36	13
Median	Rig 1	84.59	337.88	1.5	67.10	18.17	21
	Rig 2	76.65	296.52	1.5	61.18	16.50	20
	Rig 3	94.58	377.77	1.0	76.80	17.90	19
	Rig 4	106.93	427.10	2.0	82.64	26.32	23
Max	Rig 1	418.22	1670.44	2.0	352.09	66.13	26
	Rig 2	130.87	522.72	2.0	110.18	21.19	30
	Rig 3	223.43	892.42	2.0	176.24	47.19	26
	Rig 4	272.44	1088.20	3.0	235.78	36.67	35
Mean	Rig 1	117.70	470.20	1.5	94.97	22.74	21
	Rig 2	86.53	342.97	1.5	69.14	17.39	21
	Rig 3	104.60	417.80	1.3	83.86	20.74	20
	Rig 4	119.12	475.79	2.0	93.36	25.76	23
Standard Deviation	Rig 1	91.91	367.12	0.5	79.00	13.06	4
	Rig 2	24.36	98.95	0.5	22.89	2.17	4
	Rig 3	40.35	161.15	0.5	32.91	7.94	3
	Rig 4	55.53	221.81	0.5	50.70	7.02	5

4.2.1 Hyetograph-Hydrograph analysis

4.2.1.1 **Shape**

Figure 4-1 provides examples of hydrographs and hyetographs along with their respective cumulative hydrographs for one rainfall simulation event for each rig. Hyetographs and hydrographs were drawn to examine the response of discharge to rainfall intensity over time. They provide valuable hydrological information regarding attenuation, storage, lag time and discharge. Figures 4-1a, 4-1c, 4-1e, 4-1g show the hyetographs and hydrographs and figures 4-1b, 4-1d, 4-1f, 4-1h illustrate the cumulative flow hydrographs that indicate peak discharge, lag time and maximum storage capacity (Lin et al., 2014). It is noteworthy that the hydrographs have a similar shape for all rigs which signify that the discharge responses to rainfall are similar and that the hydrological performances amongst the rigs are comparable. In these examples highlighted, the rainfall simulation experiments were

performed at an average rainfall intensity of circa 1.5 L/min (475.5 mm/h). A 15 min rainfall duration was used during each simulation. Discharge measurements were discontinued when the cumulative mass of the measured outflow did not increase by 0.02 g at the next time-step (1-min). The gap between the cumulative inflow and discharge hydrographs confirm that the pavements are storing water within their structure. All hyetographs and hydrographs for all simulated events are provided in Appendix D, page 239.

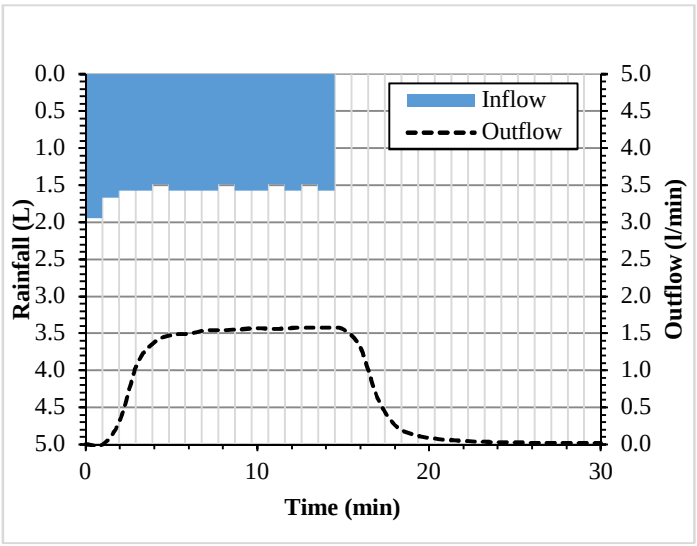

(a)

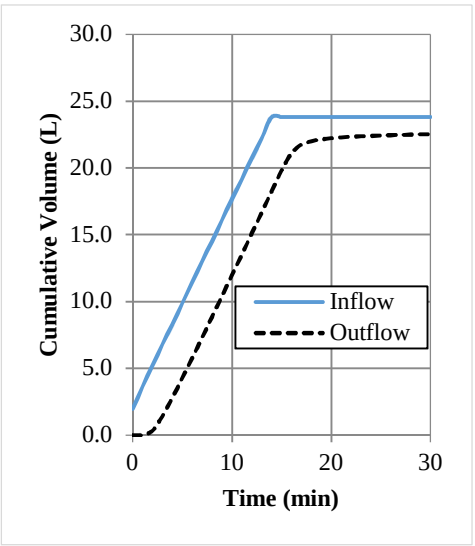

(b)

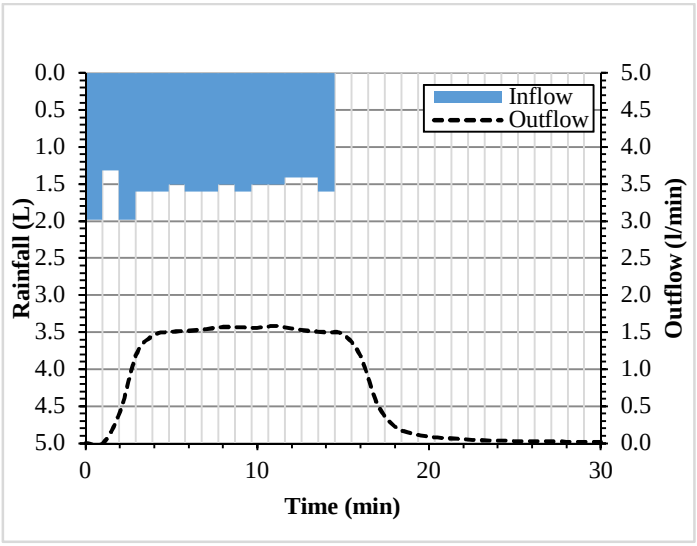

(c)

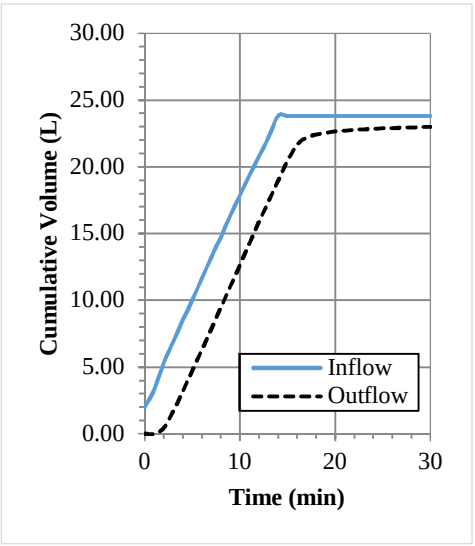

(d)

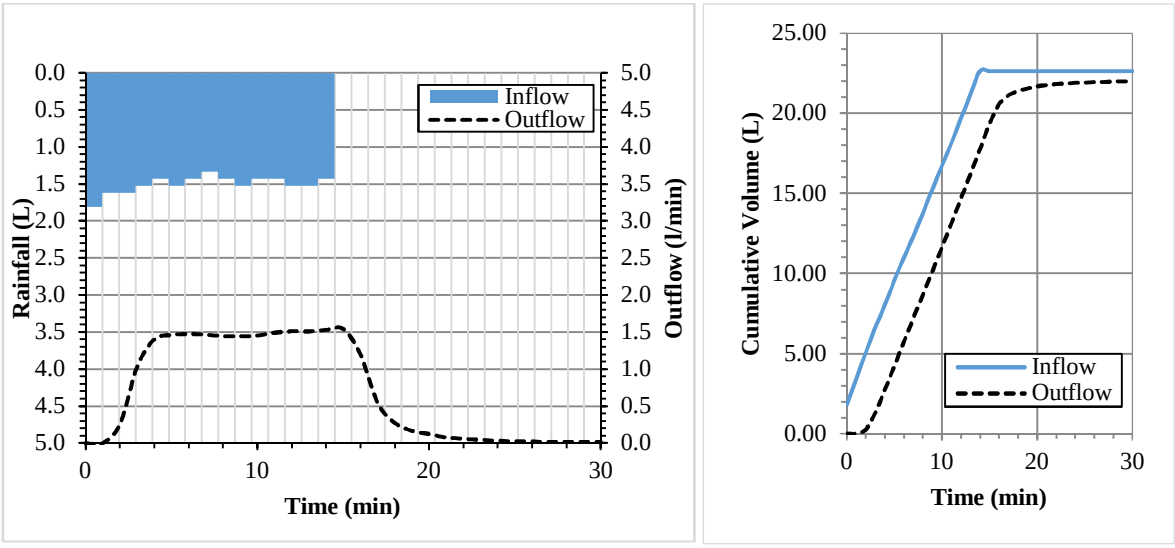

(e) (f)

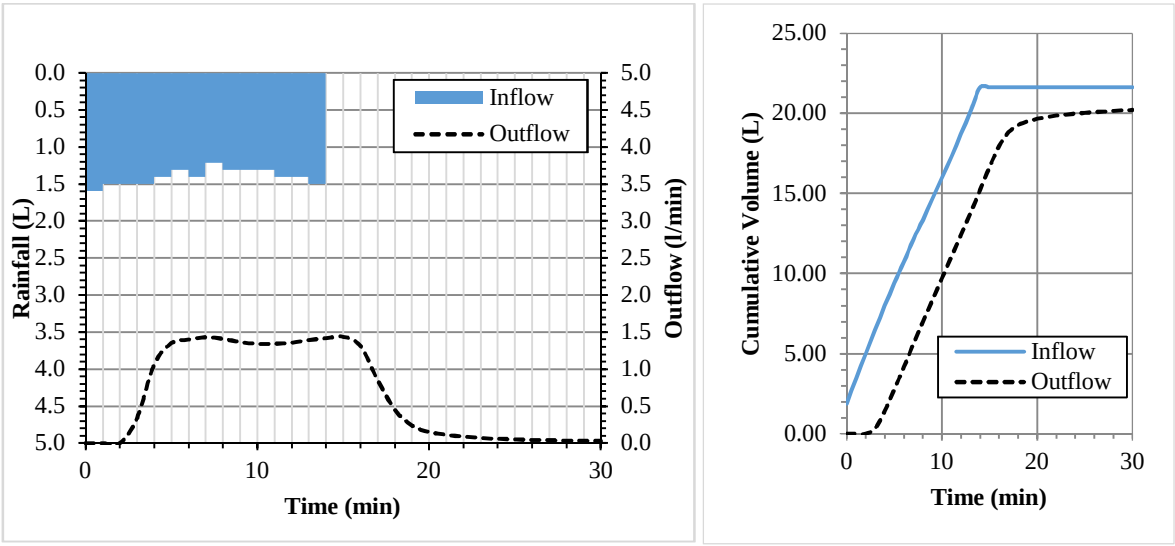

(g) (h)

Figure 4-1 Example of rainfall hyetographs, discharge hydrographs and cumulative hydrographs for one rainfall event per rig type: (a-b) Rig 1, (c-d) Rig 2, (e-f) Rig 3, and (g-h) Rig 4

It is noteworthy from Figure 4-1, that measured rainfall intensities for the simulated rainfall events were not constant resulting in outflow hydrographs with multiple peaks. As mentioned previously in subsection 3.6, attempts at maintaining near constant rainfall intensities were often difficult to accomplish because of the need to manually adjust the inflow controlling valve to achieve a specified flowrate. Nevertheless, near constant rainfall intensities were obtained during some simulations. Supposing the rainfall events were simulated in the laboratory with a constant intensity distribution over the duration (for instance 200 mm/h to 400 mm/h) of the rainfall events, the only difference would have been

an outflow hydrograph with a constant peak period of uniform flow (equilibrium depth of water within the pavement structure (Bateni et al., 2019)).

4.2.1.2 **Lag time and maximum retention capacity**

Lag time (delay between start of rainfall and start of discharge) and retained rainfall are governed by rainfall intensity, antecedent conditions, infiltration capacity of the pavement and the pavement thickness (Lin et al., 2014, Park et al., 2014). The maximum storage (retention) capacity is effectively the maximum volume of water retained in the pavement reservoir at the cessation of rainfall (Lin et al., 2014, Park et al., 2014). Scatter plots of the average lag time and maximum retained rainfall results obtained from the four (4) rigs are shown in Figure 4-2 and Figure 4-3 respectively.

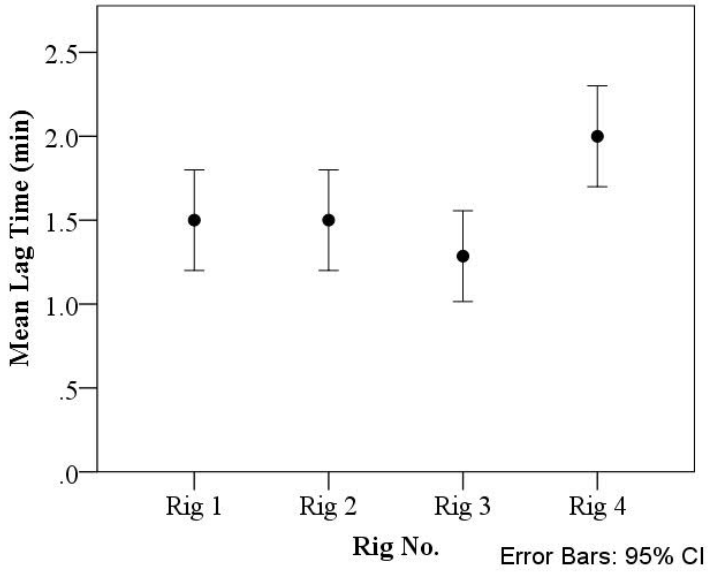

Figure 4-2 Scatter plots with error bars of the average lag time per rig

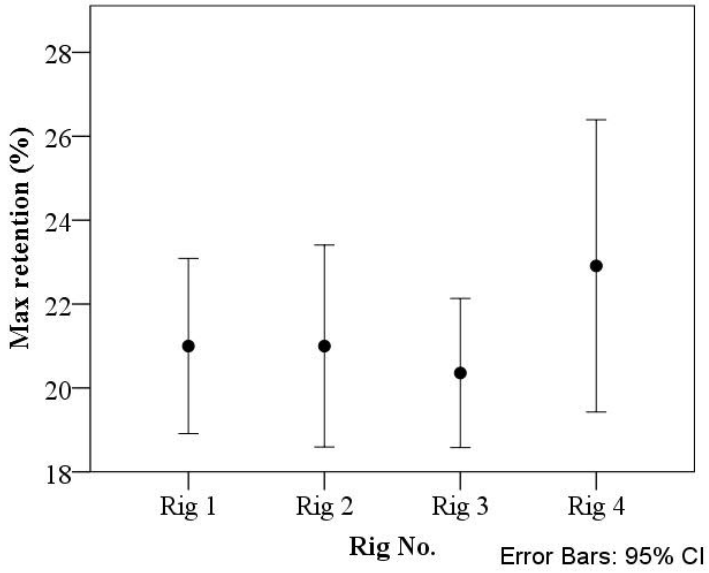

Figure 4-3 Scatter plots with error bars of the average maximum retention capacity per rig

It can be observed that Rigs 1 and 2 (with natural materials in the sub-base) produced similar mean lag times (1.5 min) and maximum retained rainfall values (21%) whereas Rigs 3 and 4 (with recycled/recyclable materials in the sub-base) produced mean lag times and maximum retention values which were slightly lesser or greater than values obtained from Rigs 1 or 2. Rig 3 recorded a mean lag time of 1.3 min whereas Rig 4 had a mean lag time of 2.0 min. Maximum retention values for Rigs 3 and 4 were 20 and 23% respectively. It must be noted that these lag times and storage values were obtained from high mean intensity rainfall events ranging from 340 mm/h (Rig 2) to 475 mm/h (Rig 4). The variations in lag times observed amongst the rigs can most likely be attributed to the porosity of the sub-base materials. Park et al. (2014) reported that materials with higher porosities produced shortened lag times. Rig 4 on the other hand, contained a monolithic block of C-EPS filter material (see Figure 3-6, page 69) in the sub-base whose infiltration rate was less than that of basalt aggregates, quartzite aggregates or CCA. This reduced infiltration rate was the most likely reason for the higher lag time and increased retained rainfall values from Rig 4. There was an expectation that Rig 3, which contained CCA, would have produced higher lag times and retained rainfall values than Rigs 1 and 2 because of the higher water absorption of the CCA. However, this was not the case, confirming that the CCA became fully saturated after the first few rainfall simulation events. Rodriguez-Hernandez et al. (2016) used Recycled Aggregates (RA) from Construction and Demolition Waste (CDW) in the sub-base of permeable pavements in the laboratory. They reported high lag time and retain rainfall values during initial rainfall simulations on the permeable pavements and attributed the high lag time and retained rainfall values to the high water absorption of the RA. Numerous studies (Andersen et al., 1999, Alsubih et al., 2017, Ioannidou and Arthur, 2018) have reported varying amounts of retained rainfall during simulation experiments. Alsubih et al. (2017) and Ioannidou and Arthur (2018) reported in a laboratory study on a 1 m^2 permeable pavement that more than 40% of the total rainfall was retained within the pavement structure for all rainfall events. In these studies, however, the total pavement thickness was 780 mm which included a 300 mm sand fill subgrade layer. The pavement structure used in this research as described earlier in subsection 3.4, has a plan area of 0.2 m^2 and a depth of 480 mm with no sand fill subgrade layer. Andersen et al. (1999) reported that 55% of a 1 hour, 15 mm/h storm event could be stored in a 0.36 m^2 permeable pavement in the laboratory. Rodriguez-Hernandez et al. (2016) also reported that depending on the materials used, PPS provide different stormwater retention capacities in terms of lag time and retained rainfall volumes.

Antecedent dry periods prior to simulated rainfall events ranged from 24 h to circa two weeks for each rig. During these times, the pavement rigs, after having drained the previous rainfall event, experienced some loss of moisture stored within the pavement rigs' surface and structure through evaporation. Lag time results showed no variations based on these antecedent drying spells. This result was expected as stated in subsection 3.6 for three main reasons.

1. The experiments were kept indoors wherein atmospheric conditions remained relatively constant.

2. The impact of moisture loss through evaporation (drying) from the rigs was considered negligible because of the size of the rigs.

3. Rainfall events were of high intensity and short duration.

The graphical plots showing the relationship between maximum storage capacity and rainfall intensity for each rig are presented in Figure 4-4. The graphs show that maximum storage capacity, expressed as a volume (l/m^2 or mm) increased linearly with increasing rainfall intensity for all rigs. This is in agreement with results presented by Lin et al. (2014) who studied the relationship between inflow and outflow through permeable pavements. They attributed this result to the increase in inflow while outflow was constrained since the maximum flow rate capacity had been reached.

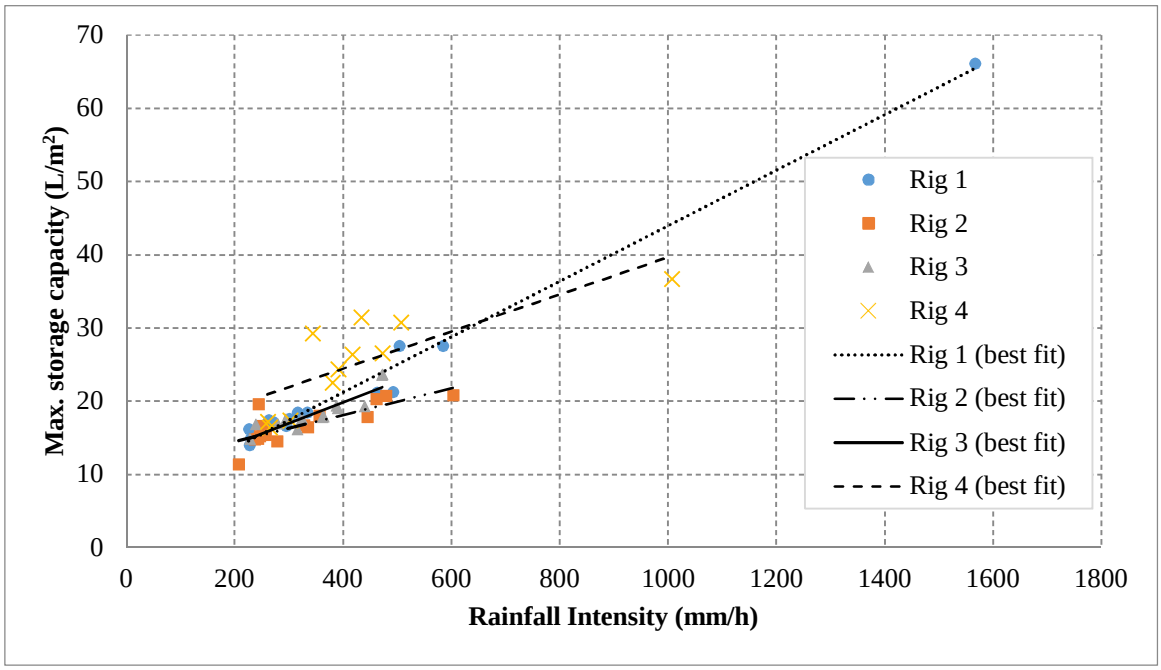

Figure 4-4 Relationship between maximum storage volume and rainfall intensity per rig

Statistical analysis of the lag time and retained rainfall values in SPSS showed that the distributions were not normal ($p < 0.05$). Therefore, a non-parametric statistical analysis was performed to assess whether there were any statistical differences between the results obtained. Specifically, Mann-Whitney U two-independent samples tests at a confidence level of 95% were selected. The results of these tests are listed in Table 4-2. No significant differences ($p > 0.05$) between lag time values were obtained for Rigs 1, 2 and 3. However, Rig 4 when compared with all other rigs had significantly higher lag time values ($p < 0.05$). In terms of retained rainfall, the results showed that there were no significant differences ($p > 0.05$) amongst the four (4) rigs.

Table 4-2 Mann-Whitney U two-independent samples tests among lag time and retained rainfall results between rigs, significant values ($p < 0.05$) formatted in ***bold italics***

	Rig 1 vs. Rig 2		Rig 1 vs. Rig 3		Rig 1 vs. Rig 4		Rig 2 vs. Rig 3		Rig 2 vs. Rig 4		Rig 3 vs. Rig 4	
	M-W U	A Sig.	M-W U	A Sig.	M-W U	A Sig.	M-W U	A Sig.	M-W U	A Sig.	M-W U	A Sig.
Lag time	98.000	1.000	77.000	.254	42.000	***.023***	77.000	.254	42.000	***.024***	27.000	***.002***
Retained rainfall	90.000	.711	92.000	.780	58.500	.295	91.000	.745	58.000	.296	45.500	.081

M-W U–Mann-Whitney U
A Sig.–Asymptotic Sig. (2-tailed)

The results showed that under high intensity (> 250 mm/h) and short duration (15 min) simulated rainfall events, the attenuation and retention capacity of the permeable pavement rigs were not significantly influenced by the sub-base component provided that the discharge rate from the pavement exceeded the inflow rate. On the contrary, some studies (Andersen et al., 1999, Rodriguez-Hernandez et al., 2016) have shown that sub-base aggregates do influence the attenuation and retention capacity of permeable pavements. These studies however, used significantly lower simulated rainfall intensities and longer durations. Rodriguez-Hernandez et al. (2016) used 50 mm/h simulated rainfall events for 1 h whilst Andersen et al. (1999) used a mean 15 mm/h simulated rainfall events for 1 h.

4.3 Water quality performance evaluation

This subsection presents and discusses results regarding the pollutant removal efficiencies of the rigs. The overall variations of influent and effluent water quality parameters are presented, and performances of the rigs are assessed by evaluating the concentration of each parameter.

4.3.1 Influent runoff characteristics

Table 4-3 presents descriptive statistics (range, mean [$\overline{x}$], standard deviation [σ] and standard error of the mean [$\sigma_{\bar{x}}$]) along with the Maximum Permissible Level (MPL) of water

pollutants discharged into the environment according to the Trinidad and Tobago Environmental Management Authority (EMA) and the United States Environmental Protection Agency (US EPA) for the influent runoff samples. Mean, standard deviation and standard error of the mean are calculated from Equations 4-1, 4-2 and 4-3 respectively (Mac Berthouex and Brown, 2002). No traces of lead (Pb) or chromium (Cr) were detected in any of the influent samples.

$$\text{Mean, } \overline{x} = \frac{\sum x}{n} \tag{4-1}$$

$$\text{Standard deviation, } \sigma = \sqrt{\frac{\sum (x-\bar{x})^2}{n}} \tag{4-2}$$

$$\text{Standard error of the mean, } \sigma_{\bar{x}} = \frac{\sigma}{\sqrt{n}} \tag{4-3}$$

where x is the sample parameter and n is the number of samples.

Table 4-3 Influent concentrations from December 2016 to August 2018 (n = 30)
[Adapted with permission from Monrose et al. (2019a)]

Parameter	**Range**	$\overline{x}$	$\sigma_{\bar{x}}$	σ	**MPL**	
					EMA[a]	**US EPA[b]**
pH	6.70–10.40	8.10	0.20	1.10	6-9	6-8.5
COD (mg/L)	35.1–119	70.88	4.35	21.76	250.0	-
DO (mg/L)	5.67–8.46	7.19	0.20	0.75	> 4	> 4
NO_3-N (mg/L)	0–6.50	1.49	0.30	1.52	-	-
PO_4^{3-} (mg/L)	0.6–4.90	1.90	0.22	1.09	5.0	-
SO_4^{2-} (mg/L)	0–77	17.80	4.15	20.73	-	-
Turbidity (NTU)	6–184	57.25	11.07	54.21	5.0	≤ 29
TDS (mg/L)	22–400	196.82	23.17	108.69	-	≤ 1000
TSS (mg/L)	18–386	131.95	24.97	114.43	50.0	-
EC (µS/cm)	43.3–477	168.10	20.60	102.80	-	≤ 1275
Cu (mg/L)	0–0.23	0.04	0.07	0.01	0.5	0.5
Zn (mg/L)	0.05–0.19	0.10	0.05	0.01	2.0	1.0
Mn (mg/L)	0–0.63	0.16	0.22	0.04	0.5	-
Fe (mg/L)	0.1–1.34	0.38	0.24	0.05	3.5	1.0

[a]EMA for inland surface water (EMA, 2001)

[b]US EPA for Class IV Agricultural water supplies (US EPA, 2018)

4.3.2 Statistical Analysis

4.3.2.1 Test for normality

The one-sample Kolmogorov-Smirnov and Shapiro-Wilk goodness-of-fit tests were used to test for normality. These statistical measures were used to determine whether a given distribution is significantly different from the one hypothesised based on the assumption of a normal distribution (Kottegoda and Rosso, 2008). The results of these tests using SPSS are presented in Table 4-4. Output water quality data from each rig is presented in Appendix E, page 266. Water quality parameters where the null hypothesis is true, follow a normal distribution if the *p*-value > 0.05 and are formatted as ***bold italics***. The distribution required transformation where $p < 0.05$. The *p*-value is a number between 0 and 1 which helps determine the significance of a hypothesis test (Lyman Ott and Longnecker, 2010). Since the bulk of the data violated conditions for data normality, which limited the use of standard parametric testing, non-parametric statistical tests were utilised.

Table 4-4 Test for normality using one-sample Kolmogorov-Smirnov and Shapiro-Wilk goodness-of-fit tests. Normal distribution ($p > 0.05$) formatted in ***bold italics***
[Adapted with permission from Monrose et al. (2019a)]

Water Quality Parameters	Influent		Effluent							
			Rig 1		Rig 2		Rig 3		Rig 4	
	K-S	S-W	K-S	S-W	K-S	S-W	K-S	S-W	K-S	S-W
pH	***0.200***	***0.195***	***0.200***	***0.533***	***0.200***	***0.234***	***0.200***	***0.126***	***0.200***	***0.531***
COD (mg/L)	***0.200***	***0.448***	***0.200***	***0.162***	0.011	0.025	***0.073***	***0.286***	***0.081***	***0.087***
DO (mg/L)	***0.149***	***0.527***	***0.185***	***0.378***	***0.107***	***0.374***	0.002	0.001	***0.200***	***0.200***
NO_3-N (mg/L)	0.002	0.000	0.001	0.000	0.011	0.001	0.001	0.000	***0.200***	***0.251***
PO_4^{3-} (mg/L)	0.000	0.001	0.000	0.003	***0.103***	0.016	0.016	0.038	0.019	0.039
SO_4^{2-} (mg/L)	0.001	0.000	***0.158***	0.007	0.007	0.002	0.014	0.004	0.000	0.000
Turbidity (NTU)	0.005	0.001	0.000	0.000	0.000	0.000	0.048	0.003	0.012	0.005
TDS (mg/L)	***0.200***	***0.304***	***0.200***	***0.648***	***0.074***	***0.198***	***0.200***	***0.806***	***0.200***	***0.661***
TSS (mg/L)	0.001	0.001	0.001	0.000	0.004	0.000	0.000	0.000	0.030	0.009
EC (µS/cm)	***0.078***	0.010	***0.117***	***0.129***	0.044	0.022	0.000	***0.465***	***0.200***	***0.873***
Cu (mg/L)	0.000	0.000	0.000	0.000	0.000	0.000	0.000	0.000	0.000	0.000
Zn (mg/L)	***0.070***	0.011	***0.063***	0.017	***0.064***	0.017	0.001	0.001	0.048	0.031
Mn (mg/L)	0.000	0.000	0.000	0.000	0.000	0.000	0.000	0.000	0.000	0.000
Fe (mg/L)	***0.057***	0.000	***0.074***	0.001	0.016	0.000	***0.200***	***0.543***	0.028	0.031

K-S: Kolmogorov-Smirnov

S-W: Shapiro-Wilk

4.3.2.2 **Analysis of variance**

Analysis of variance (ANOVA) is a method of testing at least two treatments to determine whether any known differences between sample means can be attributed to chance or whether the means of the sampled populations are different (Mac Berthouex and Brown, 2002, Kottegoda and Rosso, 2008). The one-way ANOVA in SPSS was used to determine whether there were any statistically significant differences between the means of the water quality parameters from at least two of the rigs. The results are presented in Table 4-5. The null hypothesis suggests that the means of each water quality parameter is the same across all rigs. The null hypothesis was rejected ($p < 0.05$) for all parameters except COD, NO_3-N, turbidity, TSS and the heavy metals.

Table 4-5 One-way ANOVA between effluent samples from each rig; significant values ($p < 0.05$) formatted in ***bold italics***

[Adapted with permission from Monrose et al. (2019a)]

Water quality parameters	**All rigs**		
	Sum of Squares	**F**	**Sig.**
pH	444.467	438.766	***0.000***
COD (mg/L)	198.368	0.208	0.890
DO (mg/L)	2.922	4.880	***0.005***
NO_3-N (mg/L)	10.672	1.943	0.128
PO_4^{3-} (mg/L)	9.748	4.778	***0.004***
SO_4^{2-} (mg/L)	7.331×10^3	10.389	***0.000***
Turbidity (NTU)	3.326×10^3	0.887	0.451
TDS (mg/L)	2.179×10^6	32.044	***0.000***
TSS (mg/L)	4.017×10^3	0.383	0.766
EC (µS/cm)	8.515×10^7	295.393	***0.000***
Cu (mg/L)	0.001	0.068	0.977
Zn (mg/L)	0.002	0.340	0.796
Mn (mg/L)	0.024	0.207	0.891
Fe (mg/L)	0.001	0.009	0.999

4.3.2.3 **Correlation analysis**

The bivariate Pearson's correlation function in SPSS was used to evaluate the strengths of the relationships between the varying pavement rigs (sub-base variations) and the effluent parameter concentrations. The Pearson's correlation coefficient, *r*, was used to determine the strength of the correlations, if present, whilst the *p*-values determined the significance of the

relationships (Lyman Ott and Longnecker, 2010). The results of the bivariate correlation analysis using Pearson's coefficients are presented in Table 4-6. A 95% confidence level was used. The results showed that all pavement rigs were significantly correlated ($p < 0.01$) with the water quality parameters in all cases except COD, NO_3-N, turbidity, TSS and the heavy metals ($p > 0.05$). These results support the ANOVA results presented in Table 4-5.

Table 4-6 Pearson's correlation coefficients relationship between water quality parameters between rigs

[Adapted with permission from Monrose et al. (2019a)]

	Rig No.	
	r	Sig. (2-tailed)
pH	0.886	0.000
COD (mg/L)	0.068	0.744
DO (mg/L)	0.437	0.001
NO_3-N	0.117	0.396
PO_4^{3-}	-0.361	0.003
SO_4^{2-}	-0.490	0.001
Turbidity (NTU)	0.000	0.999
TDS (mg/L)	0.681	0.000
TSS (mg/L)	-0.106	0.344
EC (µS/cm)	0.884	0.000
Cu (mg/L)	-0.032	0.756
Zn (mg/L)	-0.050	0.630
Mn (mg/L)	-0.002	0.986
Fe (mg/L)	0.017	0.873
Rig No.	1.000	

To further analyse the significance of the distribution of water quality parameter results between each pair of rigs, the non-parametric Mann-Whitney U two-independent samples test at a confidence level of 95% was used. According to Jayakaran et al. (2019), the Mann-Whitney U two-independent samples test has documented strengths and has been widely used in the analyses of stormwater quality data. The results of these analyses are listed in Table 4-7. It is noticeable that for all parameter distributions, there were no significant differences ($p > 0.05$) between the distributions for Rigs 1 and 2, both of which contained natural aggregates in their sub-base layer. The distributions were therefore statistically equal between Rigs 1 and 2 for all parameters. There was significant evidence ($p < 0.05$) to show

that the distribution of 43% of the water quality parameters were different between rig groups 1 vs. 3; 1 vs. 4; 2 vs. 3 and 2 vs. 4. To this end, the distribution of all water quality parameters except COD, NO_3-N, turbidity, TSS and the heavy metals were significantly different ($p < 0.05$) between a rig which contained natural aggregates in the sub-base to a rig containing recycled material. This was not surprising given the composition of the recycled materials. Comparisons between Rigs 3 and 4 which contained CCA and C-EPS respectively, showed that the distribution of 36% of the water quality parameters were significantly different ($p < 0.05$).

Table 4-7 Results of Mann-Whitney U Test from effluent water quality parameter values between rigs, significant values ($p < 0.05$) formatted in ***bold italics***

[Adapted with permission from Monrose et al. (2019a)]

	Rig 1 vs. Rig 2		Rig 1 vs. Rig 3		Rig 1 vs. Rig 4		Rig 2 vs. Rig 3		Rig 2 vs. Rig 4		Rig 3 vs. Rig 4	
	M-W U	A Sig.	M-W U	A Sig.	M-W U	A Sig.	M-W U	A Sig.	M-W U	A Sig.	M-W U	A Sig.
pH	275.0	.467	0.0	***.000***	0.0	***.000***	0.0	***.000***	0.0	***.000***	161.0	***.015***
COD (mg/L)	300.0	.808	285.0	.594	223.5	.390	304.5	.877	237.0	.574	246.0	.716
DO (mg/L)	94.0	.854	46.5	***.018***	33.0	***.003***	46.0	***.017***	32.5	***.003***	88.5	.662
NO_3-N (mg/L)	308.5	.938	220.5	.074	215.0	.200	235.0	.132	208.5	.155	172.0	***.028***
PO_4^{3-} (mg/L)	243.0	.176	159.5	***.003***	126.5	***.002***	210.5	***.047***	156.0	***.011***	235.5	.398
SO_4^{2-} (mg/L)	254.5	.260	141.0	***.001***	45.0	***.000***	189.0	***.016***	81.0	***.000***	164.0	***.015***
Turbidity (NTU)	263.5	.613	240.0	.322	223.5	.517	256.0	.509	210.0	.339	188.5	.148
TDS (mg/L)	210.0	.452	78.0	***.000***	15.5	***.000***	62.5	***.000***	12.0	***.000***	103.0	***.006***
TSS (mg/L)	209.5	.782	193.0	.489	162.0	.447	202.0	.641	166.0	.517	182.5	.855
EC (µS/cm)	269.0	.399	1.0	***.000***	0.0	***.000***	1.0	***.000***	0.0	***.000***	15.0	***.000***
Cu (mg/L)	307.0	.910	308.0	.926	236.0	.532	312.5	1.00	242.0	.629	242.0	.629
Zn (mg/L)	305.5	.891	257.0	.277	246.5	.723	271.5	.422	251.0	.807	242.0	.647
Mn (mg/L)	285.0	.749	283.0	.717	250.0	.961	307.0	.910	243.0	.646	237.0	.548
Fe (mg/L)	289.0	.826	284.0	.580	253.0	.834	259.0	.412	228.0	.585	257.0	.903

M-W U–Mann-Whitney U

A Sig.–Asymptotic Sig. (2-tailed)

4.3.3 Water quality results

4.3.3.1 **pH**

pH determines the acidity or alkalinity of a water/wastewater sample by measuring the fraction of hydrogen (H^+) and hydroxyl (OH^-) ions present in the sample (Sawyer et al., 2003, Tota-Maharaj, 2010). Figure 4-5 shows box and whiskers plots for influent and effluent pH values for the rigs. Influent values ranged from 6.7 to 10.4 with a mean of 8.1 ± 1.1 (Table 4-3). Notable differences in mean effluent values were observed between the rigs with natural materials to those with recycled materials. The ANOVA (Table 4-5) showed significant variations of pH ($p < 0.01$) across the rigs. This confirms the pattern of pH distribution observed in Figure 4-5. Mean effluent pH values from Rig 1 (7.8 ± 0.1) and Rig 2 (7.9 ± 0.1) were neutral as compared to the alkaline mean effluent pH values from Rig 3 (12.0 ± 0.1) and Rig 4 (12.3 ± 0.1). The high pH values from Rigs 3 and 4 can be attributed to the dissolving of calcium hydroxide, $Ca(OH)_2$ from the hardened cement paste as the stormwater percolates through the sub-base materials. The $Ca(OH)_2$ was produced from cement hydration and the soluble metal alkalis present in cement (Dhir and Jackson, 1996). The cementitious CCA and C-EPS sub-base materials were shown to be rich in CaO (lime) and other compounds (Table 3-5). A similar explanation was provided by Zhang et al. (2018) for the reported high pH values obtained from permeable pavements with porous concrete and cement brick surfaces. However, the effluent pH from porous concrete surfaces tend to decrease over time due to the carbonation of the porous concrete. Guidelines for reuse of stormwater for domestic use or irrigation set a pH range of 6 to 9 (US EPA, 2012). Outflow from Rigs 3 and 4 would therefore most likely not be suitable for these types of reuse without further treatment. However, permeable pavements with high pH effluents can be beneficial and behave like a buffer for acidic rainfall events (Collins et al., 2010, Kazemi and Hill, 2015, Razzaghmanesh and Borst, 2019). Effluent pH from permeable pavements is highly reflective of the composition of the materials used within the pavement structure. Numerous studies have reported increases in pH effluents from permeable pavements consisting of porous concrete (Collins et al., 2010, Drake et al., 2014, Crookes et al., 2017, Vadas et al., 2017, Zhang et al., 2018, Pilon et al., 2019), porous asphalt (Jayakaran et al., 2019, Razzaghmanesh and Borst, 2019), slag sub-base aggregates (Sañudo-Fontaneda et al., 2014) and calcite sub-base aggregates (Reddy et al., 2014).

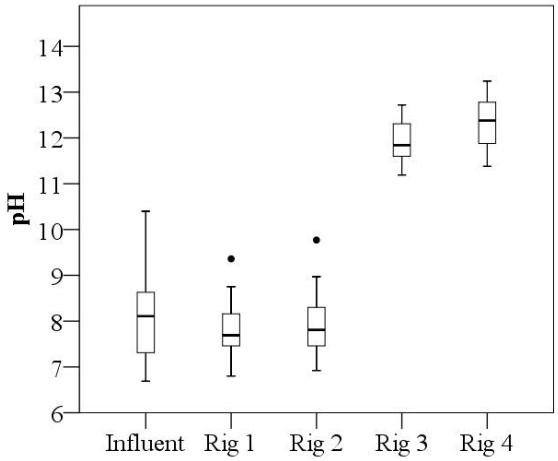

Figure 4-5 Box and whiskers plots for pH values for influent and effluent from each rig [Reprint with permission from Monrose et al. (2019a)]

4.3.3.2 **Electroconductivity**

Electroconductivity (EC) or conductivity, measured in microsiemens per centimetre (µS/cm), is a measure of the concentration of dissolved ions/salts present in a given solution (Sawyer et al., 2003, Tota-Maharaj, 2010). It is a measure of the ability of water to conduct an electric current and is sensitive to variations in dissolved solids, mostly mineral salts (Chapman and Kimstach, 2002). Conductivity itself is not an aquatic or human health concern, but because it is easily measured, it can serve as an indicator of other water quality issues (Tota-Maharaj, 2010). Mean EC concentrations and removal efficiencies for all rigs are presented in Figure 4-6. The results showed that EC values increased for all rigs. Rig 1 and Rig 2 had slight increases (33.5% and 17.2% respectively) whereas significant increases were observed from Rig 3 and Rig 4 (908% and 1895% respectively). These variations were confirmed by ANOVA (Table 4-5) which showed significant variations in mean EC values ($p < 0.01$) across the rigs. In general, the increases can be attributed to the dissolution of ions and other mineral fractions on the surface of the materials within the pavement structure (Myers et al., 2009). The composition of basalt and quartzite aggregates in the sub-base of Rigs 1 and 2 respectively, did not permit high levels of dissolution of ions. This was not the case for the CCA and C-EPS in Rigs 3 and 4 respectively. As with high pH, EC values were high from Rigs 3 and 4 most likely because of the richness of CaO and other metal compounds present in the CCA and C-EPS (Table 3-5).

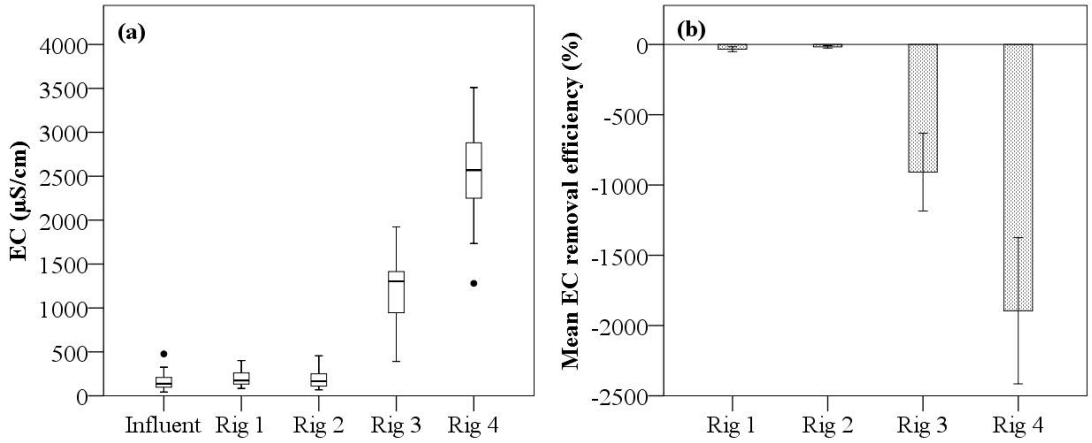

Figure 4-6 Electroconductivity results (a) box and whiskers plots for influent and effluent from each rig (b) bar charts for mean removal efficiencies

[Reprint with permission from Monrose et al. (2019a)]

4.3.3.3 **Sediments**

4.3.3.3.1 Total suspended solids

Total Suspended Solids (TSS) are the organic and inorganic solid matter maintained in suspension and retained upon evaporation and drying at 103 to 105 °C, when a sample is filtered through filter paper with a pore size of approximately 0.45 µm (Sawyer et al., 2003, Alley, 2007, Butler and Davies, 2011). The finer fractions of suspended solids (<63 µm) are extremely effective pollutant carriers. High concentrations of suspended solids pose harmful threats to receiving water, including increased turbidity and interference with numerous types of fish and aquatic invertebrates (Butler and Davies, 2011). Box and whiskers plots for influent and effluent TSS values along with average removal efficiencies are presented in Figure 4-7. Influent TSS concentrations ranged from 18 to 386 mg/L with a mean of 131.95 ± 114.43 mg/L. Mean effluent TSS concentrations ranged from 46.50 ± 40.02 mg/L (Rig 4) to 64.48 ± 63.82 mg/L (Rig 1). The ANOVA (Table 4-5), Pearson's correlation tests (Table 4-6) and the Mann-Whitney two-independent samples tests (Table 4-7) showed no statistical significant differences ($p > 0.05$) between rigs with respect to TSS effluent concentrations. As expected, TSS removal percentages were relatively high for all rigs. TSS removal in permeable pavements is highly credited to sedimentation and mechanical filtration through the pavement structure. The entrapment (and thus removal) of most sediments is largely dependent on the size of the particulate matter and occurs within the top layers of the pavement structure (Brown et al., 2009, Lucke and Beecham, 2011a). Rig 1 had the lowest removal percentage of 52% whilst Rig 4 has the highest rate of 64%. Rigs 2 and 3 had removal percentages of 53% and 58% respectively. Based on the clarity of the samples collected, Rig 4 was seen to produce the highest TSS removal rates. Additionally, the

increased filtration surface area of the C-EPS in the sub-base of Rig 4 provided for increased filtration of particulate matter. The presence of a geotextile layer between the bedding layer and the base course layer in all rigs also contributed to the removal of TSS. Numerous studies (Pratt, 1997, Tota-Maharaj et al., 2012, Rahman et al., 2015b) have reported improved TSS removal efficiencies when geotextiles have been used in permeable pavements. Brown et al. (2009) assessed the processes and characteristics of solids removal in two types of permeable pavements in Canada and found that both pavement types removed 90% to 96% of suspended solids. Pilon et al. (2019) reported a 97% removal of TSS from a pervious concrete section of a parking lot in Alcoa, TN, USA.

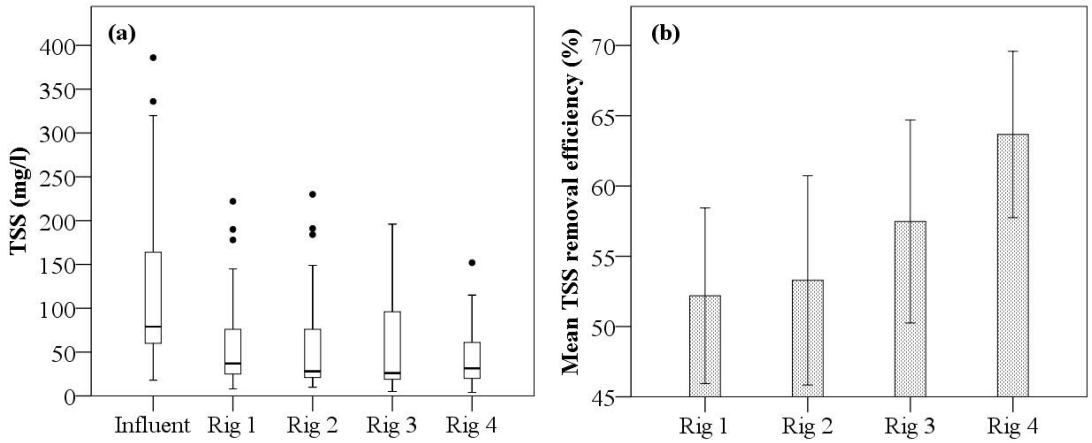

Figure 4-7 TSS results (a) box and whiskers plots for influent and effluent from each rig (b) bar charts for mean removal efficiencies

[Reprint with permission from Monrose et al. (2019a)]

4.3.3.3.2 Total dissolved solids

Total Dissolved Solids (TDS) are the inorganic salts and dissolved materials in the filtrate from the TSS test (i.e. with a diameter < 0.45 µm) (Alley, 2007, Butler and Davies, 2011). Water with a high dissolved-solids content tends to have adverse impacts on irrigated crops, plants and grasses (Sawyer et al., 2003). Box and whiskers plots for influent and effluent TDS values along with average removal efficiencies are presented in Figure 4-8. Influent TDS values ranged from 22.00 to 400.00 mg/L with a mean of 196.82 ± 108.69 mg/L. Effluent TDS removal percentages were negative for all rigs. TDS increased by 48% from Rig 1, 31% from Rig 2, 212% from Rig 3 and 387% from Rig 4. These variations were confirmed by ANOVA (Table 4-5) which showed significant variations in mean TDS (p < 0.01) across the rigs. In general, TDS is directly related to EC (Chapman and Kimstach, 2002) and as such the negative removal rates for TDS can be attributed to the dissolution of ions and other mineral fractions on the surface of the materials within the pavement structure (Myers et al., 2009) similarly to EC. As with high pH and EC, TDS values were high from

Rigs 3 and 4 most likely because of the richness of CaO and other compounds present in the CCA and C-EPS (Table 3-5).

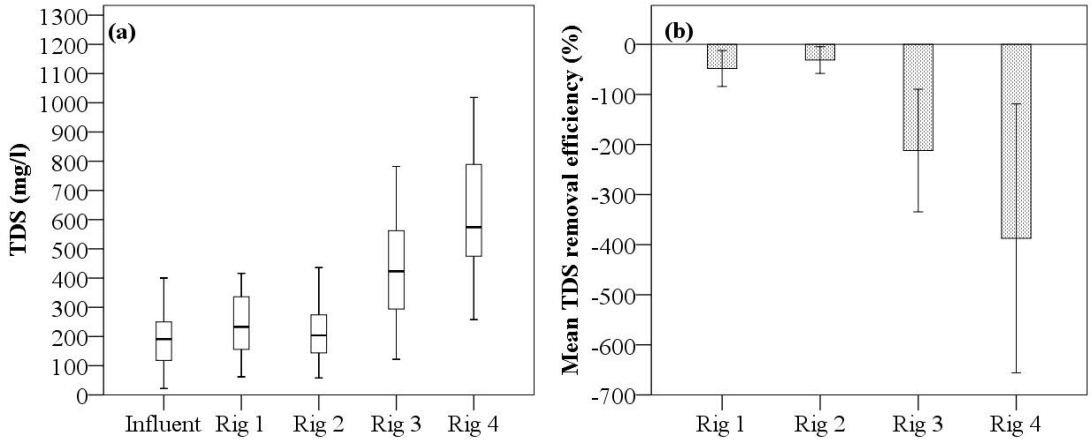

Figure 4-8 TDS results (a) box and whiskers plots for influent and effluent from each rig (b) bar charts for mean removal efficiencies

[Reprint with permission from Monrose et al. (2019a)]

4.3.3.3.3 Turbidity

The turbidity or cloudiness, of water may be defined as the interference of light passing through water by suspended matter such as silt, clay, organic matter, organic compounds, or dissolved inorganics (Sawyer et al., 2003, Alley, 2007, Hammer and Hammer Jr., 2007). Suspended particles can be a significant health concern when heavy metals and hydrophobic chemicals such as pesticides adsorb to the particles (AWWA, 2011). Box and whiskers plots for influent and effluent turbidity values along with average removal efficiencies are presented in Figure 4-9. Influent turbidity values ranged from 6 to 184 mg/L with a mean of 57.25 ± 54.21 mg/L. The ANOVA (Table 4-5), Pearson's correlation tests (Table 4-6) and the Mann-Whitney two-independent samples tests (Table 4-7) showed no statistical significant difference ($p > 0.05$) between rigs with respect to turbidity effluent values. All rigs had positive removal rates for turbidity with Rig 4 recording the highest (57%) and Rig 3 the lowest (10%). Rigs 1 and 2 reduced turbidity by 37% and 31% respectively. Some studies (Tota-Maharaj and Scholz, 2010, Chowdhury et al., 2016) have reported turbidity removal rates in excess of 90% from permeable pavements (with residence times in excess of 24 h) while Pilon et al. (2019) reported no significant change in turbidity removal rates.

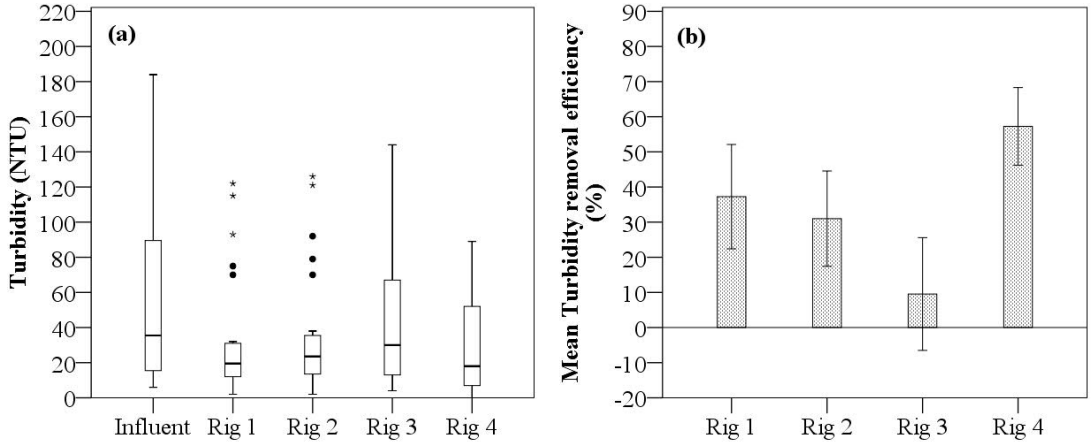

Figure 4-9 Turbidity results (a) box and whiskers plots for influent and effluent from each rig (b) bar charts for mean removal efficiencies

[Reprint with permission from Monrose et al. (2019a)]

4.3.3.4 **Organic content**

4.3.3.4.1 Chemical oxygen demand

Chemical Oxygen Demand (COD) measures the organic strength of wastewaters in terms of the total quantity of oxygen required for oxidation to CO_2 and H_2O (Sawyer et al., 2003). The COD is widely used as a measure of the susceptibility to oxidation of the organic and inorganic materials present in water bodies (Chapman and Kimstach, 2002). Box and whiskers plots for influent and effluent COD concentrations along with average removal efficiencies are presented in Figure 4-10. Influent COD concentrations ranged from 35.1 to 119.0 mg/L with a mean of 70.9 ± 21.8 mg/L. The ANOVA (Table 4-5), Pearson's correlation tests (Table 4-6) and the Mann-Whitney U two-independent samples tests (Table 4-7) showed no significant difference ($p > 0.05$) between rigs with respect to COD effluent concentrations. COD removal was similar amongst all rigs, ranging from 4.2% (Rig 2) to 7.2% (Rig 1). Rigs 3 and 4 reduced COD by 4.5% and 6.5% respectively. The decrease in COD can most likely be attributed to the aerobic conditions and the subsequent oxidation of pollutants and organic material within the permeable pavement rigs. This is in agreement with findings presented by Pilon et al. (2019) who reported 36% reduction in COD from a porous concrete section of a parking lot in Alcoa, TN, USA. Zhang et al. (2018) found that after 48 h residence time, a permeable pavement containing shale bricks at the surface removed COD by approximately 46%. Balades et al. (1995) reported that COD was reduced by a porous pavement by 80 to 90%.

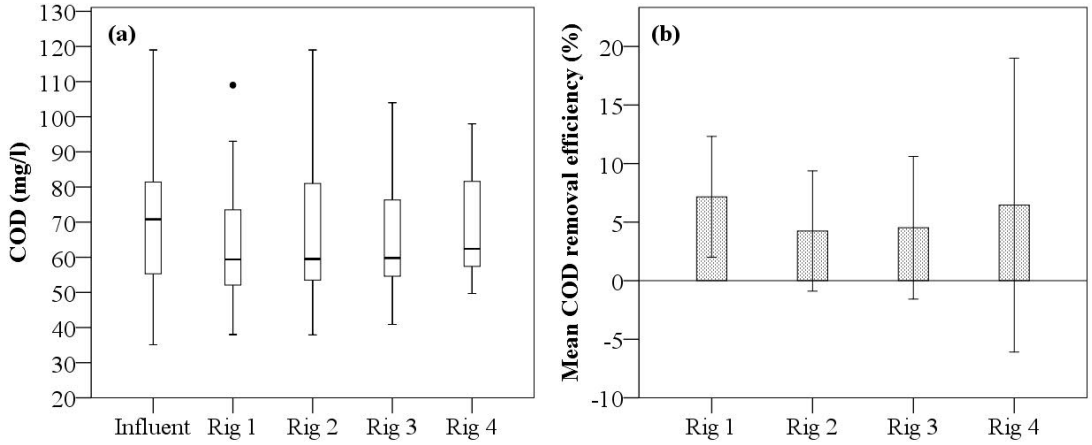

Figure 4-10 COD results (a) box and whiskers plots for influent and effluent from each rig (b) bar charts for mean removal efficiencies

[Reprint with permission from Monrose et al. (2019a)]

4.3.3.4.2 Dissolved oxygen

Dissolved Oxygen (DO) determination measures the amount of dissolved (or free) oxygen present in a water or wastewater sample (Hammer and Hammer Jr., 2007). In liquid wastes, DO determines whether the biological changes result from aerobic or anaerobic organisms (Sawyer et al., 2003). Oxygen is essential to all forms of aquatic life, including those organisms responsible for the self-purification processes in natural waters. In freshwaters, DO at sea level ranges from 15 mg/L at 0 °C to 8 mg/L at 25 °C. Concentrations less than 5 mg/L may threaten the functioning and survival of biological communities and below 2 mg/L may lead to the death of most fish (Chapman and Kimstach, 2002). Mean DO influent and effluent concentrations and removal efficiencies are presented in Figure 4-11. Influent DO values had a mean of 7.19 ± 0.75 mg/L ranging from 5.67 to 8.46 mg/L. The ANOVA (Table 4-5) showed significant differences in DO ($p < 0.01$) across the rigs. DO was slightly reduced by 2% in Rigs 1 and 2. Rigs 3 and 4 on the contrary, produced a slight increase in DO by 3% and 5% respectively. This result was not expected and required further research.

Further DO analysis was conducted on Rig 4 which sought to determine the most likely cause of increased DO concentrations. A modified approach was taken whereby six different influent samples of varying DO concentrations were poured into and stored in Rig 4 for residence times ranging from 4 to 26 days for each sample. Results of the effluent DO concentrations are presented in Figure 4-12. All DO concentrations increased (except for the case of distilled water) from their initial values to an average constant value of circa 7.5 mg/L. DO values increased by 200% in some samples. It is common for the DO of stored water in permeable pavements to deplete as residence time increases (Kazemi and Hill, 2015)

because of microbiological activity. However, no odours signifying microbiological decay were detected during sampling events from Rig 4. Additionally, microbiological activity was not expected due to the high pH environment (Selvakumar and O'Connor, 2018). The increased DO concentration results were once again inconclusive and requires continued further research.

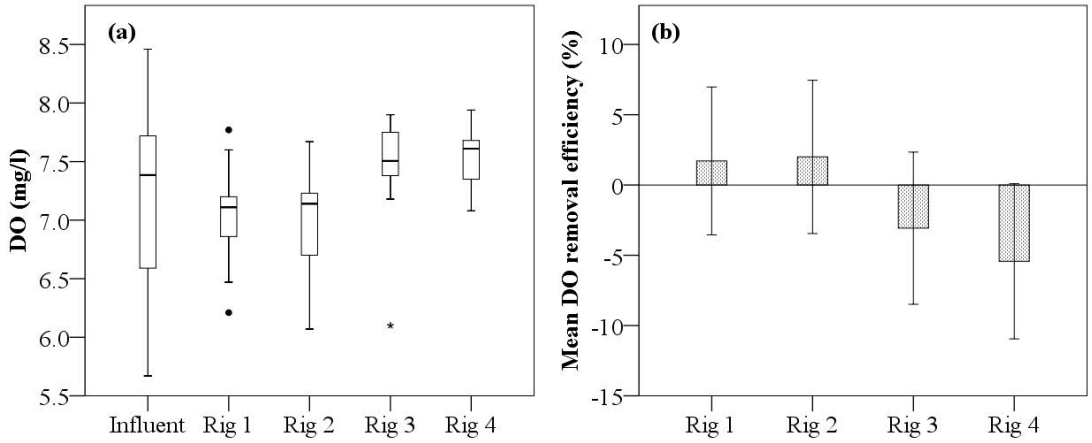

Figure 4-11 DO results (a) box and whiskers plots for influent and effluent from each rig (b) bar charts for mean removal efficiencies

[Reprint with permission from Monrose et al. (2019a)]

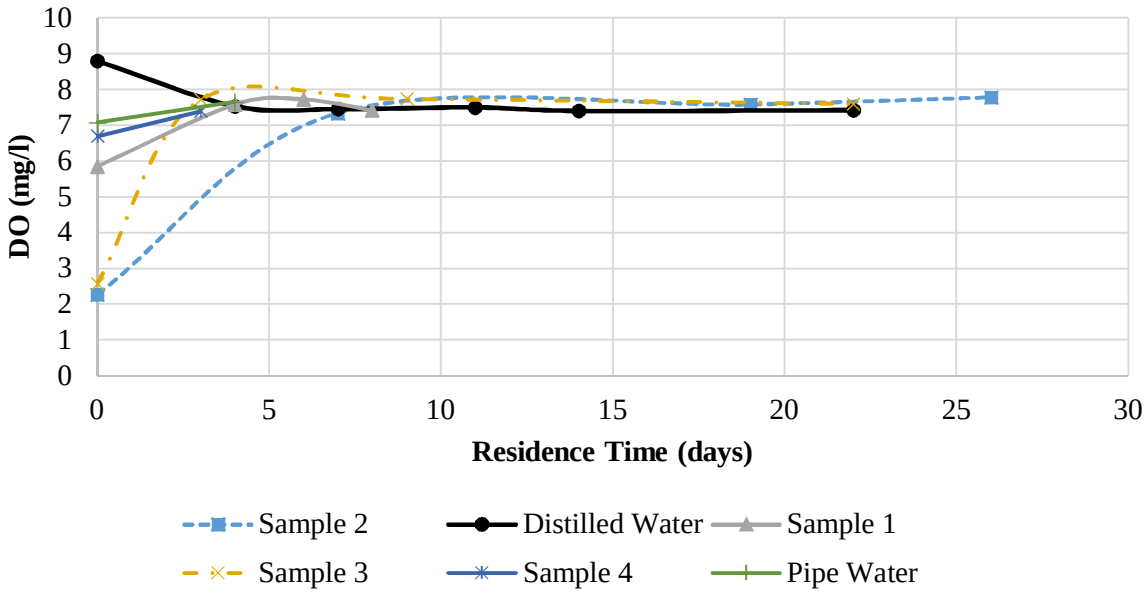

Figure 4-12 Variation of DO concentrations over time for Rig 4

[Reprint with permission from Monrose et al. (2019a)]

4.3.3.5 **Nutrients**

4.3.3.5.1 Nitrate-Nitrogen (NO_3-N)

Nitrogen, which exists in four main forms (organic, ammonia, nitrite and nitrate) is of historical environmental concern in water which has led to the regulation of its concentration in surface waters for decades. Excessive levels of nitrogen, when discharged into receiving waters, can promote the growth of undesirable aquatic plants such as algae and floating macrophytes (Sawyer et al., 2003, Butler and Davies, 2011). Box and whiskers plots for influent and effluent NO_3-N concentrations along with average removal efficiencies are presented in Figure 4-13. Influent NO_3-N concentrations ranged from 0 to 6.50 mg/L with a mean of 1.49 ± 1.52 mg/L. NO_3-N concentrations from Rig 4 were slightly higher than the other three rigs. The ANOVA (Table 4-5), Pearson's correlation tests (Table 4-6) and the Mann-Whitney two-independent samples tests (Table 4-7) showed no statistical significant difference ($p > 0.05$) between rigs with respect to NO_3-N effluent concentrations. No rigs removed NO_3-N except for Rig 3. Rig 1 increased NO_3-N by 27%, Rig 2 by 21% and Rig 4 by 98%. Rig 3 reduced NO_3-N by 20%. Water infiltrating through permeable pavements tend to cause increases in NO_3-N (James and Shahin, 1998) which could be attributed to aerobic conditions that were likely present throughout the pavement allowing ammonium-nitrogen (NH_4-N) to be nitrified to NO_3-N (Collins et al., 2010, Tota-Maharaj and Scholz, 2010, Drake et al., 2014, Razzaghmanesh and Borst, 2019). Denitrification of nitrate (NO_3-) into nitrogen gas [$N_{2(g)}$] requires anoxic conditions which are unlikely to be present in a permeable pavement structure given that these pavements are designed to be free draining (Drake et al., 2014). Hence, it is not clear as to why Rig 3 removed some amount of NO_3-N. Numerous studies (James and Shahin, 1998, Bean et al., 2007, Collins et al., 2010, Drake et al., 2014, Braswell et al., 2018, Razzaghmanesh and Borst, 2019), which have compared runoff from conventional asphalt pavements to effluent discharges from permeable pavements, have reported increased NO_3-N concentrations. However, a few studies (Pagotto et al., 2000, Gilbert and Clausen, 2006) have shown a reduction in NO_3-N concentrations.

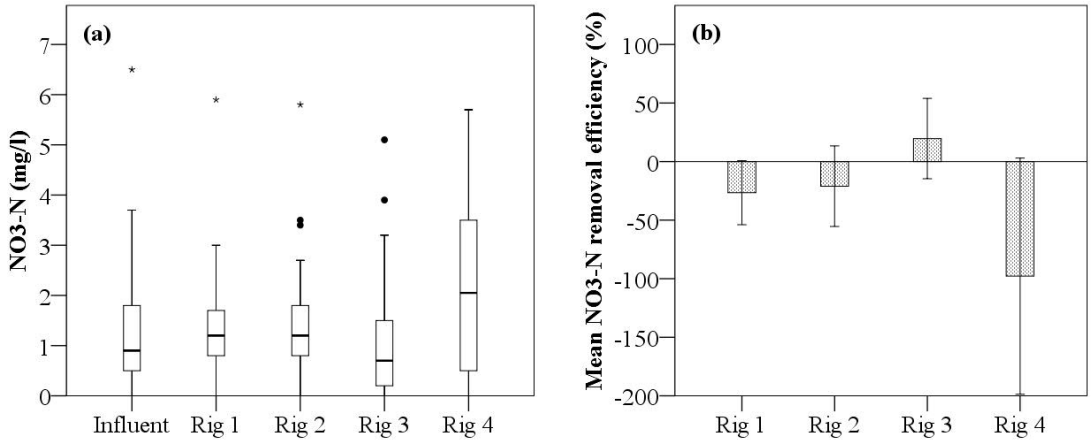

Figure 4-13 Nitrate-Nitrogen results (a) box and whiskers plots for influent and effluent from each rig (b) bar charts for mean removal efficiencies

[Reprint with permission from Monrose et al. (2019a)]

4.3.3.5.2 Reactive Phosphorous (PO_4^{3-})

Phosphorous is an essential nutrient for living organisms and is present as both dissolved and particulate species in water. High levels of phosphorous in water may lead to eutrophication and algal growth (Chapman and Kimstach, 2002). Box and whiskers plots for influent and effluent PO_4^{3-} concentrations along with average removal efficiencies are presented in Figure 4-14. Influent PO_4^{3-} concentrations ranged from 0.60 to 4.9 mg/L with a mean of 1.90 ± 1.09 mg/L. Mean effluent PO_4^{3-} concentrations ranged from 1.39 ± 0.82 (Rig 4) to 2.20 ± 0.0.79 (Rig 1). The ANOVA (Table 4-5) showed significant variations of PO_4^{3-} ($p < 0.01$) across the four (4) rigs. Rigs 1 and 2 recorded slight increases in PO_4^{3-} of 22% and 9% respectively, while Rigs 3 and 4 had reductions of 18% and 33% respectively. The increases in PO_4^{3-} from rigs 1 and 2 can most likely be ascribed to the decomposition of organic matter present in the rigs. The removal of PO_4^{3-} from Rigs 3 and 4 can be attributed to the formation of phosphate salts from the reaction of PO_4^{3-} ions and the cementitious sub-base materials which lead to adsorption by the cementitious components. Wang et al. (2014) used cementitious materials for the sequestration of phosphorous from wastewater and reported removal rates of 80% for phosphorus concentrations ranging from 20 to 1000 mg/L. Agyei et al. (2002) removed PO_4^{3-} ions from aqueous solutions using fly ash, slag and Ordinary Portland Cement (OPC) and found that the rate and removal efficiency of PO_4^{3-} was linked to increasing CaO and/or Ca^{2+} ions in the adsorbents released into solution via hydration and dissolution. This is in agreement with the results presented in Figure 4-14 given that the percent of CaO (Table 3-5) was greater in C-EPS (Rig 4) than CCA (Rig 3). Deng and Wheatley (2018) reported that 2–5 mm Recycled Concrete Aggregate (RCA)

removed more than 90% of phosphorous from effluent and suggested that RCA could be used for both wastewater treatment and phosphorous recovery.

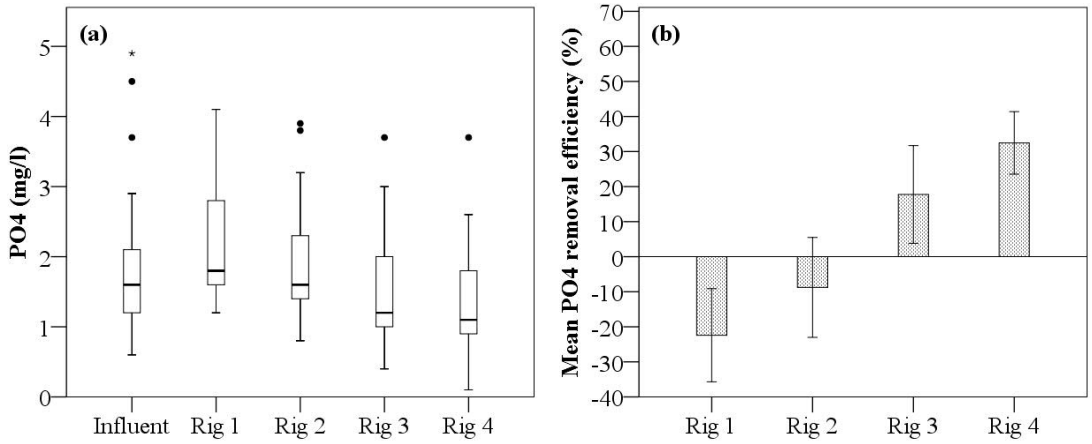

Figure 4-14 Reactive phosphorous results (a) box and whiskers plots for influent and effluent from each rig (b) bar charts for mean removal efficiencies
[Reprint with permission from Monrose et al. (2019a)]

4.3.3.5.3 Sulphate (SO_4^{2-})

Surface waters tend to contain SO_4^{2-}. Sources include atmospheric deposition of oceanic aerosols, leaching of sulphur compounds, industrial discharges or atmospheric precipitation. Bacteria can use sulphate as an oxygen source which is converted to hydrogen sulphide (H_2S, HS^-) under anaerobic conditions (Chapman and Kimstach, 2002). Box and whiskers plots for influent and effluent SO_4^{2-} concentrations along with average removal efficiencies are presented in Figure 4-15. Influent SO_4^{2-} concentrations ranged from 0 to 77 mg/L with a mean of 17.8 ± 20.73 mg/L. The ANOVA (Table 4-5) showed significant variations of SO_4^{2-} ($p < 0.01$) across the four (4) rigs. Rigs 1 and 2 recorded significant increases in SO_4^{2-} (121% and 66% respectively) while Rig 3 and Rig 4 recorded 33% and 74% reductions in SO_4^{2-} respectively. Increases in SO_4^{2-} from Rigs 1 and 2 can most likely be attributed to the dissolution of SO_4^{2-} ions from the aggregates as water infiltrated through the rigs. Pilon et al. (2019) found a 157% increase in SO_4^{2-} from a pervious concrete pavement installed as a parking stall in Alcoa, TN, USA. They attributed this increase to the degradation of hydrocarbons or other organic compounds within the pavement structure or the creation of SO_4^{2-} by oxidation of another form of sulphur such as sulphide (S^{2-}). The high removal rates of SO_4^{2-} by Rigs 3 and 4 on the other hand, can most likely be attributed to the reaction of SO_4^{2-} ions and the cementitious sub-base materials leading to the formation of calcium sulphate ($CaSO_4$) and other salts which adhere to the sub-base materials. This reaction is essentially an attack by the SO_4^{2-} ions on calcium hydroxide [$Ca(OH)_2$], tricalcium aluminate (C_3A) and hydrated aluminate phases of the cement paste. The $Ca(OH)_2$ can convert to

$CaSO_4$ as per Equation 4-4 and further to the subsequent growth of ettringite crystals as per Equation 4-5 (Miron and Magaña, 2017).

$$Ca(OH)_2 + {SO_4}^-{}_{aq.} \rightarrow CaSO_4.2H_2O \quad (4\text{-}4)$$

$$3CaSO_4.2H_2O + C_3A + 25H_2O \rightarrow 3CaSO_4.C_3A.31H_2O \quad (4\text{-}5)$$

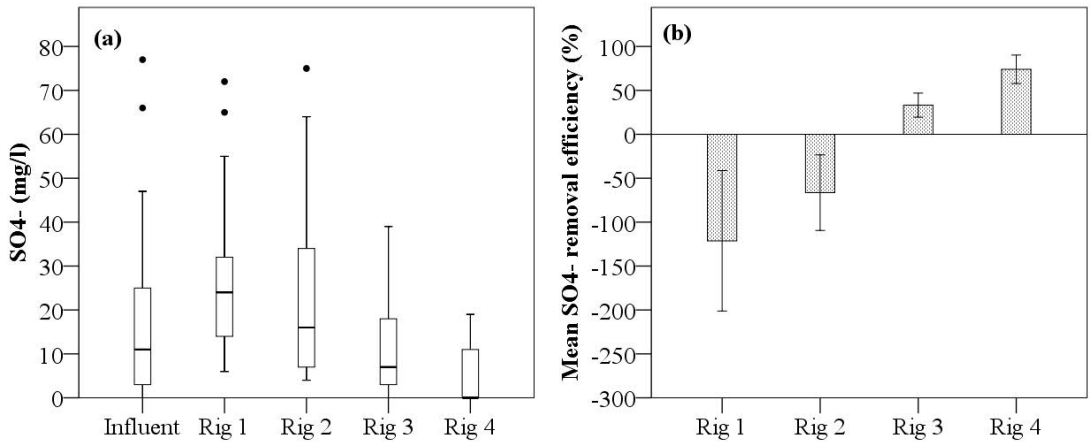

Figure 4-15 Sulphate results (a) box and whiskers plots for influent and effluent from each rig (b) bar charts for mean removal efficiencies

[Reprint with permission from Monrose et al. (2019a)]

4.3.3.6 **Metals**

Metals such as Mn, Zn and Cu when present in trace concentrations support aquatic life in natural waters. However, these same metals when discharged into natural receiving waters at increased concentrations, may pose severe toxicological effects on humans and the aquatic ecosystem (Chapman and Kimstach, 2002). Metals transported by stormwater runoff exist in dissolved, suspended and colloidal forms. These forms could transfer between each other in the aqueous environment (Liu and Borst, 2018). Box and whiskers plots for influent and effluent metal (Cu, Zn, Mn, Fe) concentrations along with average removal efficiencies are presented in Figure 4-16. For all metals, influent mean concentrations were less than the MPL of water pollutants discharged into the environment according to the Trinidad and Tobago Environmental Management Authority (EMA) and the US EPA (Table 4-3). The ANOVA (Table 4-5), Pearson's correlation tests (Table 4-6) and the Mann-Whitney U two-independent samples tests (Table 4-7) showed no statistical significant difference ($p > 0.05$) between rigs with respect to all metal effluent concentrations. For all rigs, all metal removal rates were negative except for Rigs 3 and 4 which removed 5% and 10% of Zn respectively and Rig 2 which removed 2% of Fe. Cu increased by 16% from Rigs 1 to 3 and 6% from Rig 4. Zn increased by 7% and 10% from Rig 1 and Rig 2 respectively. Mn had the largest

increases; Rig 1 increased Mn by 38%, Rig 2 by 119%, Rig 3 by 135% and Rig 4 by 71%. Fe was increased by 1% from Rig 1, 11% from Rig 3 and 20% from Rig 4. These varying increases in effluent metal concentrations were most likely due to small amounts of metals leaching from the aggregates into the infiltrate. Liu and Borst (2018) reported increases in metal concentrations in permeable pavement infiltrates from a 9-year old PICP parking lot in Edison, New Jersey USA. They suggested that leaching from the surface material of the permeable pavement was one of the most likely causes for the increase.

Heavy metal removal rates from stormwater are dependent on the type and volume of bedding materials in the PPS, the influent metal concentrations and the infiltration rate (Sounthararajah et al., 2017). The low metal removal rates found can most likely be attributed to the low influent metal concentrations (Table 4-3) and high infiltration rates. Removal rates more than 50% are typically reported from permeable pavement effluent samples (Pagotto et al., 2000, Dierkes et al., 2002, Myers et al., 2011). Nevertheless, low heavy metal removal rates from permeable pavements have also been previously reported. Beecham et al. (2012), found that when field stormwater was poured onto a 0.145 m^2 plan area permeable pavement rig, containing a 300 mm (12 in) thick, 20 mm gravel sub-base layer, removal efficiencies were 2.9%, 9.4%, 38.9%, and 18.2% for Cu, Pb, Zn, and Ni respectively. The authors attributed the low metal removal rates to the influent concentrations being close to or below detection limits. The removal of Zn from the Rigs 3 and 4 was most likely due to the presence of dissolved calcium carbonate ($CaCO_3$) which caused the Zn to precipitate as zinc oxide (ZnO) and possibly zinc carbonate ($ZnCO_3$) (Aziz et al., 2001). Various studies (Reddy et al., 2014, Thomas et al., 2015) have shown that Zn cations are strongly sorbed by a $CaCO_3$ surface. Reddy et al. (2014) reported 78% to 98.9% removal of Zn from stormwater runoff using a calcite filter material.

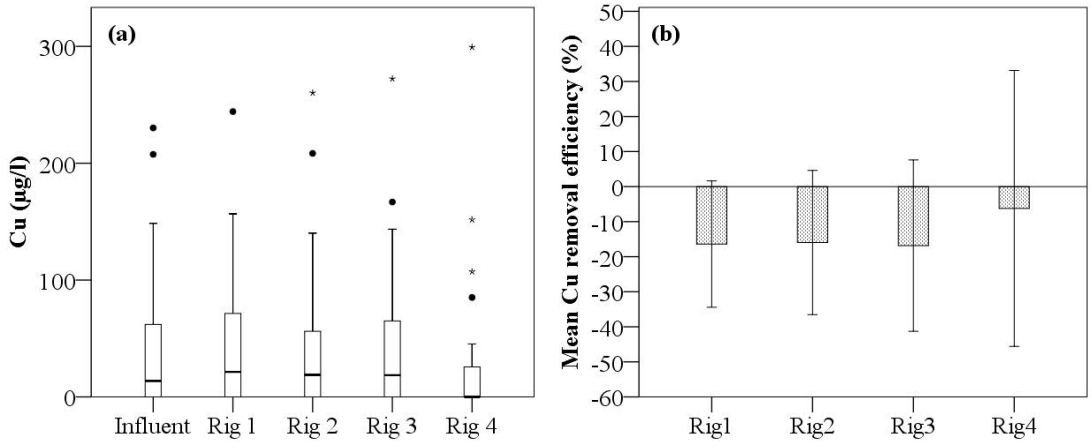

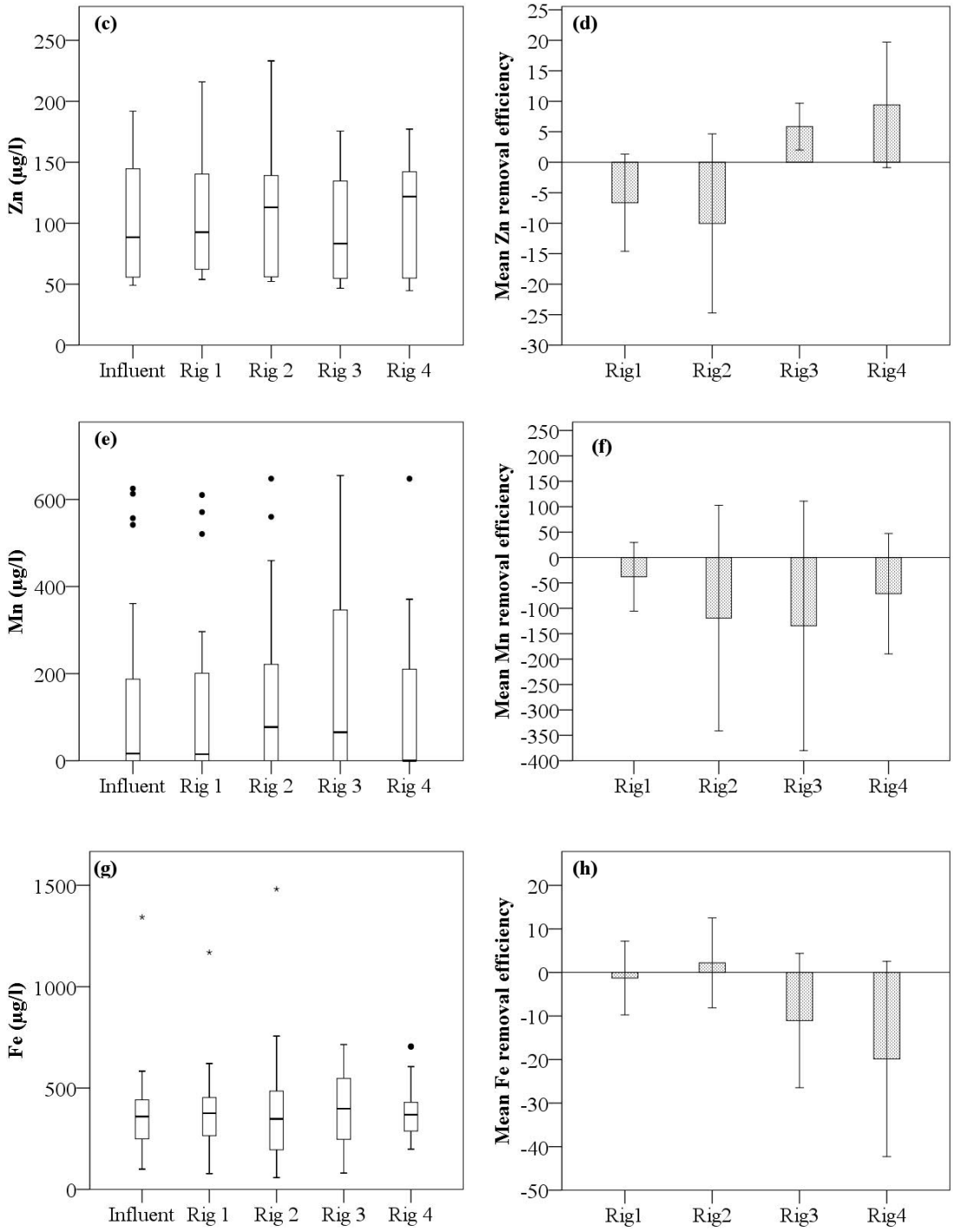

Figure 4-16 Metals box and whiskers plots for influent and effluent from each rig and bar charts for mean removal efficiencies, (a–b) Cu, (c–d) Zn, (e–f) Mn, (g–h) Fe

4.3.3.7 **Summary**

The water quality performance experiments targeted the efficiency of the pavements to improve stormwater runoff quality. It also took into consideration, the impact of the varying sub-base materials on outflow water quality. For these tests, stormwater runoff was collected from various municipalities and applied to the rigs using the RSI. Overall, differences in pollutant removal performances were observed between the rigs. Rigs 3 and 4 containing CCA and C-EPS respectively, were shown to yield higher removal rates for suspended solids, nutrients, and Zn. However, noticeable increases in pH, TDS, EC measurements, Cu, Mn and Fe were noted from these rigs. Despite the apparent negative removal efficiencies reported, all mean pollutant concentrations were within the Maximum Permissible Levels (MPLs) of water pollutants discharged into the environment (Table 4-3) according to the EMA (2001) and the US EPA (2018). In this regard, the CCA and C-EPS performed satisfactorily as sub-base materials in the permeable pavement rigs.

4.4 Hydraulic conductivity and long-term clogging evaluation

This subsection presents and discusses the hydraulic conductivity (permeability) and long-term clogging pattern of the four (4) rigs when subjected to 10 years of accelerated sediment loading. It is important that researchers and practitioners in SIDS across the Caribbean understand the clogging process of PPS and can reasonably estimate when PPS will require maintenance. The methodology was presented in Chapter 3, subsection 3.8.

4.4.1 Reduction in hydraulic conductivity due to clogging

The infiltration capacities and clogging pattern of the permeable pavement rigs based on calculated hydraulic conductivity changes after 10 years of accelerated simulation of semi-synthetic stormwater made up of tap water and fine sediment are shown in Table 4-8 and Figure 4-17. Hydraulic conductivities were predictably high at the commencement of the tests taking into consideration that the rigs were constructed with joints (2–13mm) containing ASTM No.8 bedding stone. It is noteworthy that the rigs were previously subjected to a series of stormwater runoff samples during the water quality performance assessment phase of this research project. Consequently, background solids were already trapped within the rigs prior to the commencement of accelerated simulation clogging tests. These trapped solids did not appear to significantly influence the hydraulic conductivity test results given the high values obtained at the commencement (year 0) of the accelerated clogging tests. The values presented in Table 4-8 and graphs shown in Figure 4-17 show an exponential decline in hydraulic conductivity as a function of service life (clogging) of the permeable pavement rigs. Hydraulic conductivities were reduced by 45%, 44%, 50% and 51% in Rig 1, Rig 2, Rig 3 and Rig 4 respectively. Greater reductions were not obtained over the 10-year accelerated period, most likely because some joints remained with relatively few sediment accumulations as well as some sediments remained over the surface of the concrete block pavers rather than getting trapped within the joints between the pavers. The pattern of exponential decline in hydraulic conductivity agrees with previous studies (Borgwardt, 2006, Sansalone et al., 2008, Boogaard et al., 2014a, Winston et al., 2016).

Table 4-8 Hydraulic conductivity results of the pavement rigs from accelerated clogging simulations using falling head method

Year	Hydraulic conductivity, k (mm/h)			
	Rig 1	**Rig 2**	**Rig 3**	**Rig 4**
0	5780	5994	5138	4516
1	5057	5138	4316	3605
2	4559	4760	3630	3351
3	4204	4316	3269	3004
4	3900	3996	2997	2723
5	3720	3853	2864	2640
6	3557	3720	2790	2562
7	3407	3637	2675	2454
8	3372	3557	2631	2387
9	3269	3443	2589	2293
10	3205	3372	2549	2234

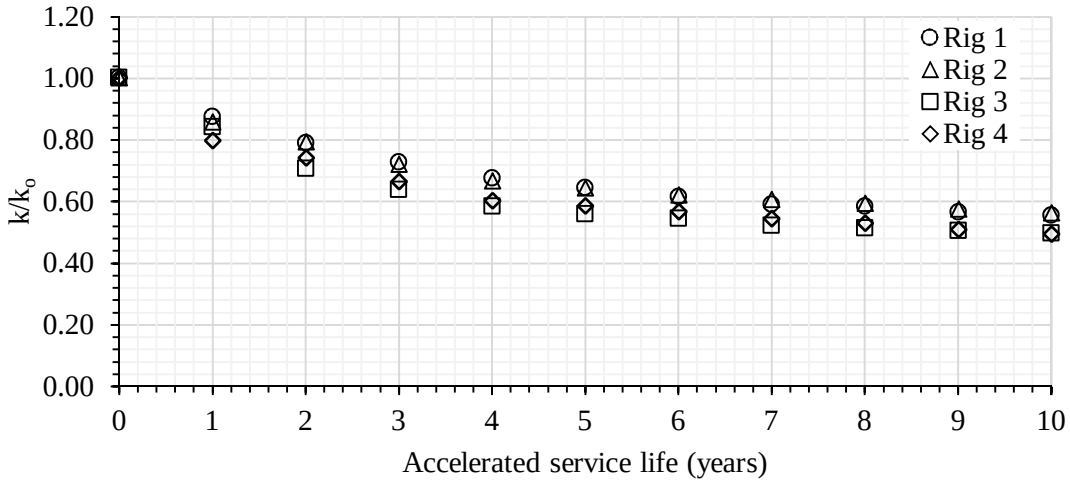

Figure 4-17 Reduced hydraulic conductivity coefficients of the pavement rigs

Reductions in the rigs' hydraulic conductivities for each succeeding year (Figure 4-18) were found to be of a similar pattern and rate for all rigs. This observance was not surprising due to the similarity in pavement structure of the rigs above the sub-base layer. The rigs were also subjected to the same clogging agent under similar rainfall application rates. Numerous studies (Pratt et al., 1995, Borgwardt, 2006, Siriwardene et al., 2007) have found that for PICPs, fine particles accumulate in the upper layer of the pavement joints and bedding layer resulting in clogging. The variation in sub-base materials most likely had insignificant influence on the hydraulic conductivities of the rigs.

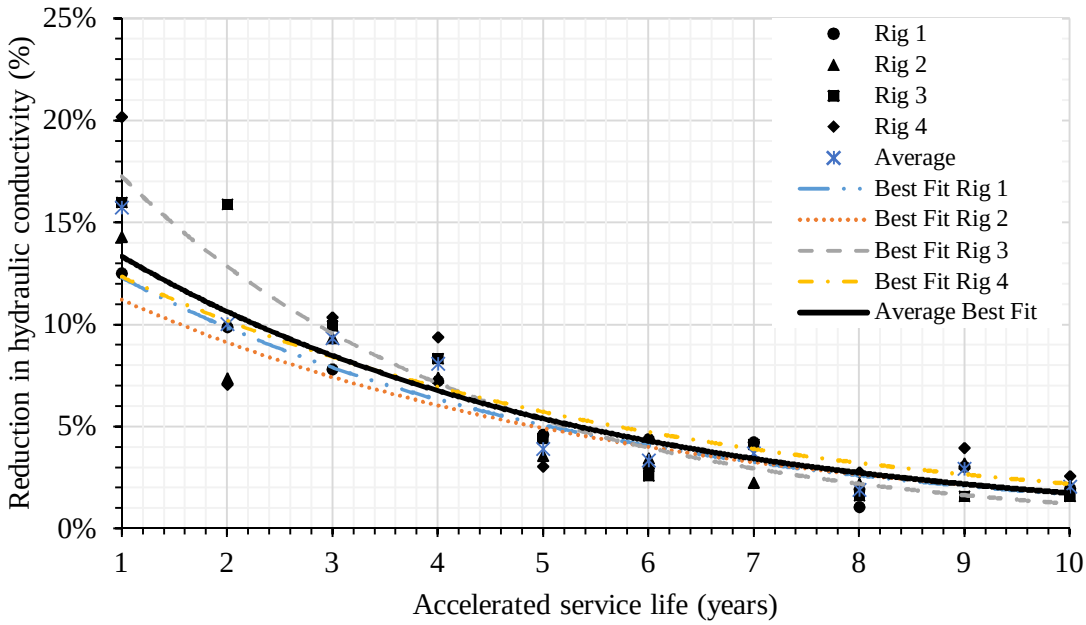

Figure 4-18 Observed yearly percent reduction in hydraulic conductivities of the rigs

4.4.1.1 **Statistical analysis**

4.4.1.1.1 Correlation analysis

Pearson's correlation in SPSS was used to test the hypothesis that aged permeable pavements without maintenance have reduced hydraulic conductivities because of clogging. The results presented in Table 4-9, show that for all rigs, there is a significant ($p < 0.01$) negative correlation between hydraulic conductivity and service life (age) of the pavements. The correlations are also strong (0.88 to 0.93).

Table 4-9 Pearson's correlation coefficients for hydraulic conductivity and service life of each pavement rig

		Hydraulic Conductivity, k				**Year**
		Rig 1	**Rig 2**	**Rig 3**	**Rig 4**	
Year	Pearson Correlation	-0.931	-0.920	-0.880	-0.905	1
	Sig. (2-tailed)	.000	.000	.001	.001	

4.4.1.1.2 Regression analysis

The details of the regression models done in SPSS are presented in Table 4-10. Both linear and exponential regression models were analysed at a 95% confidence level. In all cases, the exponential regression model simulated a better fit of the observed values as indicated by the higher R^2 values which ranged from 0.84 (Rig 3) to 0.91 (Rig 1). Graphical illustrations of the exponential regression models are shown in Figure 4-19.

Table 4-10 Regression models for all permeable pavement rigs analysed under accelerated clogging simulations

Rig No.	Equation	Regression Model	R^2
1	Linear	$k = -232.045A + 5162.955$	0.87
	Exponential	$k = 5191.810e^{-.056A}$	0.91
2	Linear	$k = -228.482A + 5304.773$	0.85
	Exponential	$k = 5323.052e^{-.052A}$	0.90
3	Linear	$k = -220.409A + 4324.591$	0.77
	Exponential	$k = 4313.997e^{-.064A}$	0.84
4	Linear	$k = -189.191A + 3834.045$	0.82
	Exponential	$k = 3846.884e^{-.062A}$	0.89

where:

k = hydraulic conductivity

A = Age (service life) of pavement based on accelerated sediment accumulation

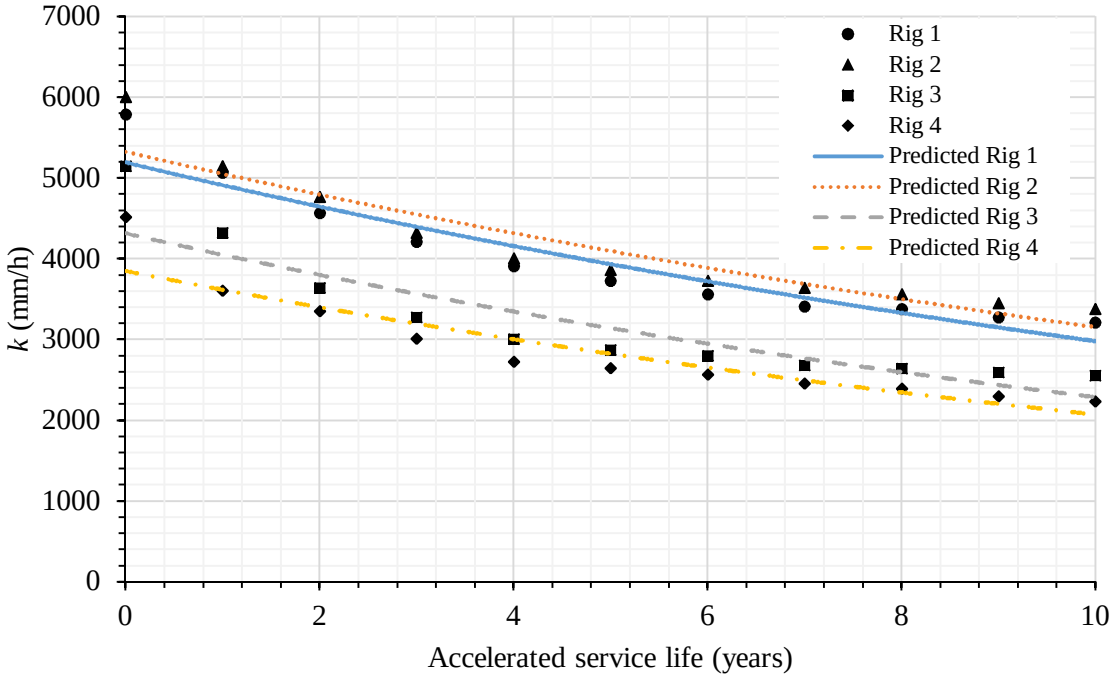

Figure 4-19 Exponential regression model for the pavement rigs under accelerated sediment accumulation scenarios

4.5 Structural performance evaluation

This subsection evaluates results regarding the structural integrity or load bearing capacity of the permeable pavement rigs. Non-destructive evaluation of the structural response of the pavement rigs was done through Portable Falling Weight Deflectometer (PFWD) testing.

4.5.1 Bearing capacity (Stiffness modulus and deflection)

As noted earlier in subsection 3.4, permeable pavements are typically designed for low speed, low volume traffic surfaces such as parking lots and pedestrian walkways. Despite this bearing capacity limitation, it is crucial that permeable pavements remain structurally sound throughout their life cycle. This experiment sought to evaluate and compare the stiffness and deflection of the pavement rigs under ‘as-built” conditions in the laboratory using a PRIMA 100 PFWD. The PFWD test was described earlier in subsection 3.9. In general, the test involved dropping a 10 kg weight onto the surface of the pavement rigs and sensors measure the deflection and stiffness of the pavement at the centre of the loading. An example of the PRIMA 100 PFWD on one of the rigs is shown in Figure 4-20. It must be noted that the permeable pavement rigs were subjected to a series of water quality, hydrological and accelerated clogging tests, prior to deflectometer testing. The rigs were not subjected to any additional loading other than that provided by the PFWD, hence changes in the structural capacity of the rigs over time were not monitored and are outside the scope of this research.

Figure 4-20 PFWD testing on one of the permeable pavement rigs in the laboratory

Descriptive statistics of the deflection and surface modulus results of the PFWD tests conducted on the rigs are presented in Table 4-11. Bar charts of the mean deflection and surface modulus results obtained are further shown in Figure 4-21. The general trend observed from the results best corresponds to a power function with a negative exponent (Figure 4-22) whereby larger surface modulus values corresponded to lower deflection values and vice versa. The results were as expected with Rig 1 recording the lowest mean deflection (493 µm) and the highest surface modulus (53 MPa) whilst Rig 4 recorded the highest deflection (1095 µm) and the lowest surface modulus (24 MPa). There was an expectation that Rig 1, which contained crushed basalt aggregates, would have produced the lowest deflection and highest surface modulus results. As per the physical properties presented earlier in Table 3-4, basalt aggregates were of the highest quality strength-wise, hence the expected results.

Table 4-11 Deflection and surface modulus PFWD test results

Parameter	Rig No.	Mean	Std. Deviation	Std. Error	Minimum	Maximum
Deflection (µm)	1	492.75	10.05	5.02	484.00	507.00
	2	681.25	7.37	3.68	672.00	690.00
	3	872.75	9.81	4.91	865.00	887.00
	4	1095.50	14.57	7.29	1080.00	1114.00
Surface Modulus (MPa)	1	53.48	1.10	0.55	51.90	54.40
	2	38.65	0.45	0.23	38.10	39.20
	3	30.15	0.31	0.16	29.70	30.40
	4	24.05	0.34	0.17	23.60	24.40

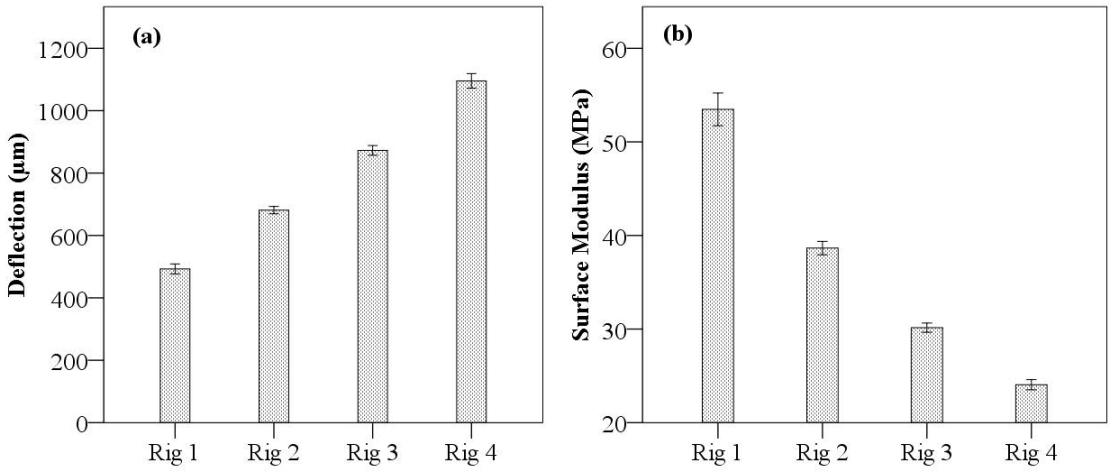

Figure 4-21 Bar chart bearing capacity PFWD test results (a) deflection (b) surface modulus

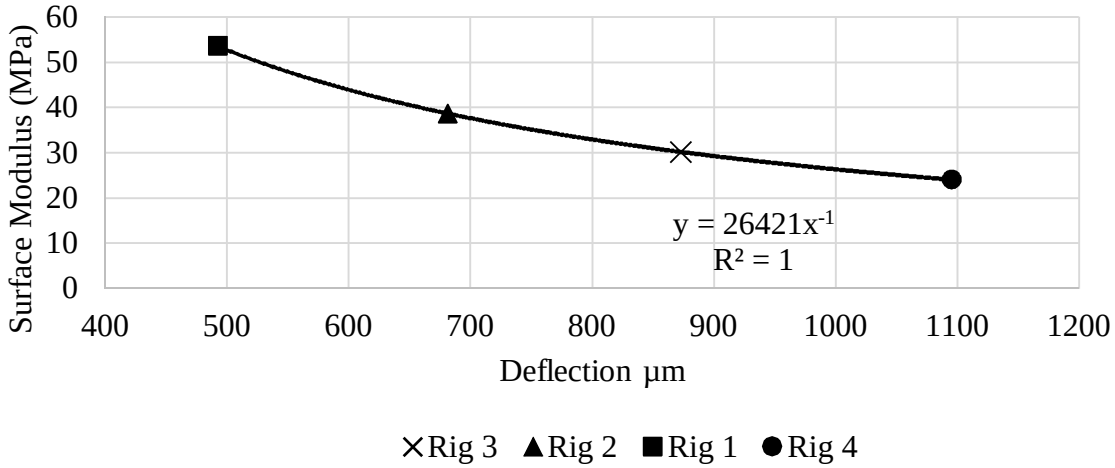

Figure 4-22 Variation of surface modulus and deflection amongst the pavement rigs

The graphs presented in Figure 4-23 and Figure 4-24 demonstrate the shapes of the applied load and the deflection bowl respectively for the structural response of the rigs using the PRIMA 100 PFWD. It is noted that the peak values of the deflection signals for all rigs lag the respective peak forces. Some studies (Hoffmann et al., 2004, Fleming et al., 2007) have reported this trend, which, according to Hoffmann et al. (2004) is due to the effects of inertia.

Figure 4-24 highlights a section of the deflection plots with large negative deflection values (in cloud). As shown in Figure 4-25 (a), such response type provides an indication of incomplete compaction or excessive moisture within the test rigs which is characteristically expected with permeable pavements. Poor compaction in the test rigs would have produced deflection response profiles like that shown in Figure 4-25 (c). Nevertheless, permeable pavements, unlike conventional pavements which typically consist of one or more layers of densely compacted aggregate courses, rely on frictional resistance created by the interlock of one or more layers of unbound aggregates. It is important that densification/compaction of this aggregate reservoir in permeable pavements be kept to a minimum to maintain adequate voids within the structure for water storage capabilities. Fleming et al. (2007) evaluated the effect of increasing compaction of a layer of sand on the PFWD deflection response and reported that in its loose and partly compacted state, the deflection response appeared to show significant permanent deflection but when well compacted or with a carefully prepared contact surface, the deflection response was considered more akin to that expected whereby the deflection returns almost to zero.

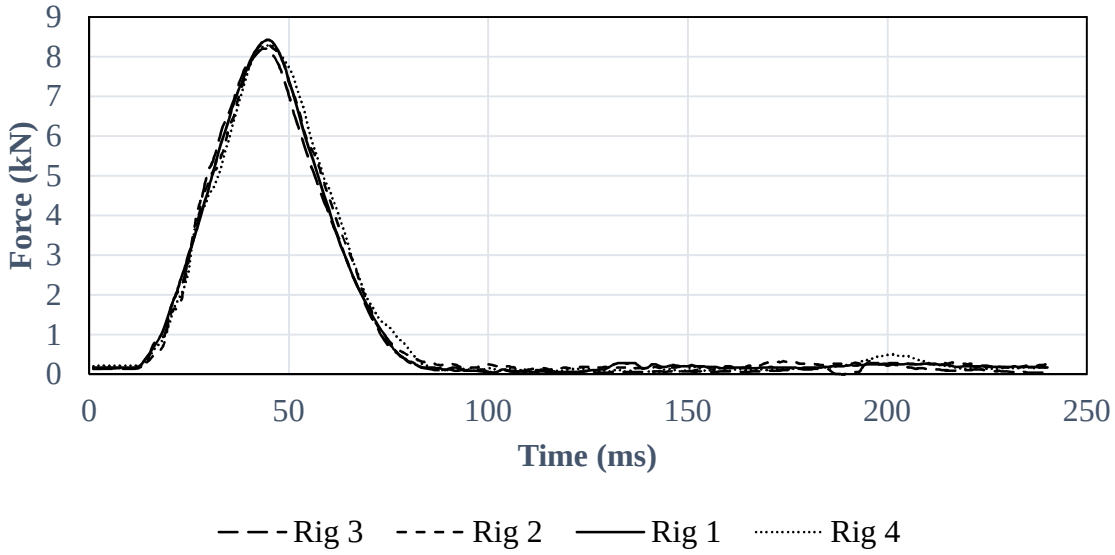

Figure 4-23 Force signal response from the PRIMA 100 PFWD for each rig

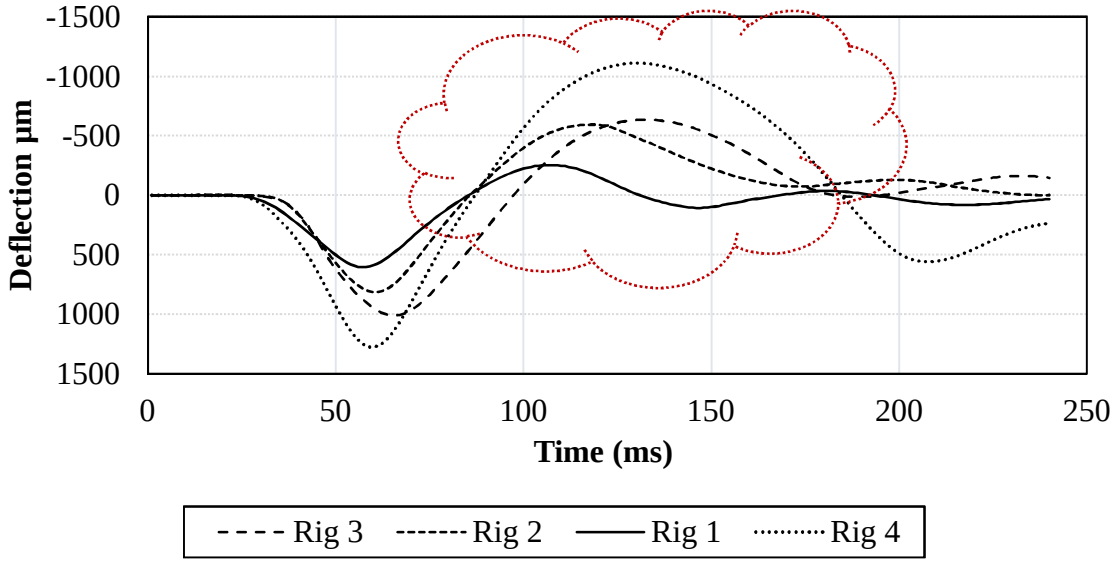

Figure 4-24 Deflection response output from PRIMA 100 PFWD for each rig

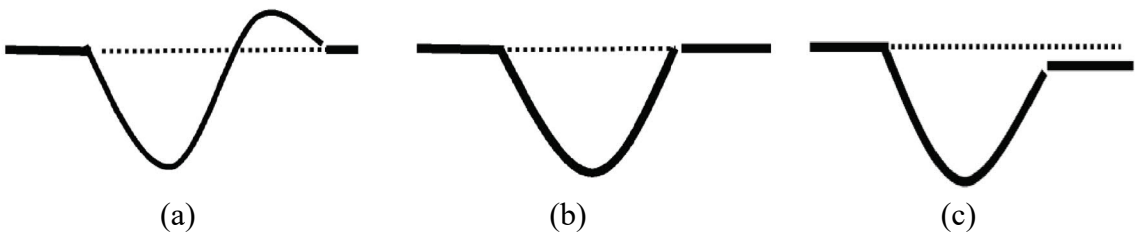

Figure 4-25 Typical deflection responses from Prima 100 PFWD Software (a) Incomplete compaction (loose material) or excessive moisture (b) Ideal (c) Poor compaction [adapted from Grontmij A/S (2012)]

Figure 4-26 illustrates the Impact Stiffness Modulus (ISM) values of the varying permeable pavement rigs. ISM was previously defined in subsection 3.9.2, page 104. ISM values varied between rigs ranging from 7.5 × 10^{-3} kN/mm (Rig 4) to 17.1 × 10^{-3} kN/mm (Rig 1). Rigs 2 and 3 recorded values of 12.3 × 10^{-3} kN/mm and 9.3 × 10^{-3} kN/mm respectively.

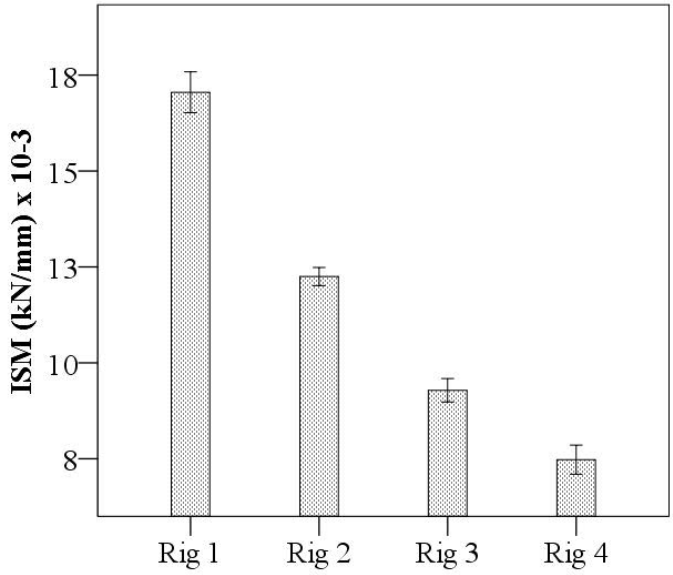

Figure 4-26 Impact stiffness modulus of the permeable pavement rigs

4.6 Chapter summary

This chapter presented, analysed and discussed the results obtained from the four performance assessment experiments of the pilot scale rigs. A summary of the results is presented herein. Hydrological performance evaluations targeted experiments which investigated the influence of high intensity (> 250 mm/h) and short duration (15 min) rainfall events on the lag time, attenuation and retention capacity of the permeable pavement rigs. The results showed that lag times were not significantly different between the rigs except for Rig 4 which had longer lag times. In terms of retained rainfall, there were no significant differences amongst the rigs. The pollutant removal efficiencies of the rigs were evaluated using natural stormwater runoff collected from different locations in Trinidad, W.I. as influent. Effluent was collected for analysis after 7–10 min of discharge. Significant differences ($p < 0.01$) were found in pH, EC, TDS, DO, PO_4^{3-} and SO_4^{2-} across all rigs whereas no significant differences ($p > 0.05$) were found with respect to TSS, turbidity, COD, NO_3-N, Zn, Cu, Mn and Fe. Rigs containing CCA and C-EPS produced significant increases in pH, EC and TDS measurements but produced improvements in DO, TSS, turbidity, COD, PO_4^{3-} and SO_4^{2-}. All mean values except pH were, however, within the Maximum Permissible Levels (MPLs) of water pollutants discharged into the environment

according to the Trinidad and Tobago Environmental Management Authority (EMA) and the United States Environmental Protection Agency (US EPA). The hydraulic conductivity and long-term clogging behaviour of the rigs were evaluated through the yearly accelerated simulation of 10 years of accumulated natural sediment. The results showed a similar pattern of exponential decline in hydraulic conductivity for all rigs. Pearson's correlation found that for all rigs, there was a significant ($p < 0.01$) negative correlation between hydraulic conductivity and service life (age) of the rigs. Regression analysis found that the exponential regression model, rather than a linear regression model simulated a better fit of the observed values and that all rigs displayed a similar pattern of regression. The structural integrity and load-bearing capacity of the permeable pavement rigs was evaluated using non-destructive Portable Falling Weight Deflectometer (PFWD) testing. The results showed significant differences amongst rigs. Rig 1 had the lowest deflection (493 µm) and the highest surface modulus (53 MPa) whilst Rig 4 had the highest deflection (1095 µm) and lowest surface modulus (24 MPa). The results of the as-built PFWD testing have demonstrated that CCA and C-EPS can maintain the structural integrity of permeable pavements when used as sub-base materials. However, due to lower stiffness and higher deflection values obtained from Rig 4 which contained C-EPS it is recommended that Rig 4 be used as pavements only in non-traffic areas such as building aprons, sidewalks, footpaths, landscapes, pedestrian access and bicycle lanes. The conclusion drawn from this chapter is that CCA and C-EPS can be suitable for use in permeable pavements. This answers research question number 3 listed in Chapter 1. The following chapter describes hydrological modelling of the pavement rigs.

CHAPTER 5. HYDROLOGICAL MODELING OF PERMEABLE PAVEMENT SYSTEMS

5.1 Overview

This chapter is aimed at producing event rainfall-discharge models for the four (4) permeable pavement rigs using the Computational Hydraulics International's (CHI) Personal Computer Stormwater Management Model (PCSWMM) computer software. Data used to calibrate and validate the models was taken from the simulated hydrological performance assessments presented previously in subsection 4.2. High intensity, short duration rainfall events (at least 50-year return period) were simulated. The models were capable of accurately predicting the discharge response of the pavement rigs to rainfall events. Maximising the fit between observed and simulated discharge at the outlet of the rigs meant that effective parameterisation and calibration was crucial.

5.2 Model development

The rainfall-runoff simulation model PCSWMM version 7.0.2330 (CHI, 2017) was used to simulate and evaluate the hydrological response of each pavement rig to laboratory simulated rainfall events. PCSWMM is a Geographic Information System (GIS) based spatial decision support system for the US EPA's SWMM engine. PCSWMM was selected because it includes a specific (and identical) SWMM version 5.1.011 LID module called LID Control Editor (Figure 5-1) with adequate capabilities of modelling the hydraulics and geometry of permeable pavements (Rossman, 2015). The LID editor allows the assessment of the simulation of permeable pavements on the impact of urban drainage (Jato-Espino et al., 2016a) which can be useful for urban drainage planners and specialists. This LID module also allows for the modelling of seven other types of SUDS. It is noteworthy that the module lacks the capability to route water through the individual reservoirs layers of the pavement structure (Elliott and Trowsdale, 2007). Rather, the hydrological model considers the aggregate layers as a lumped structure.

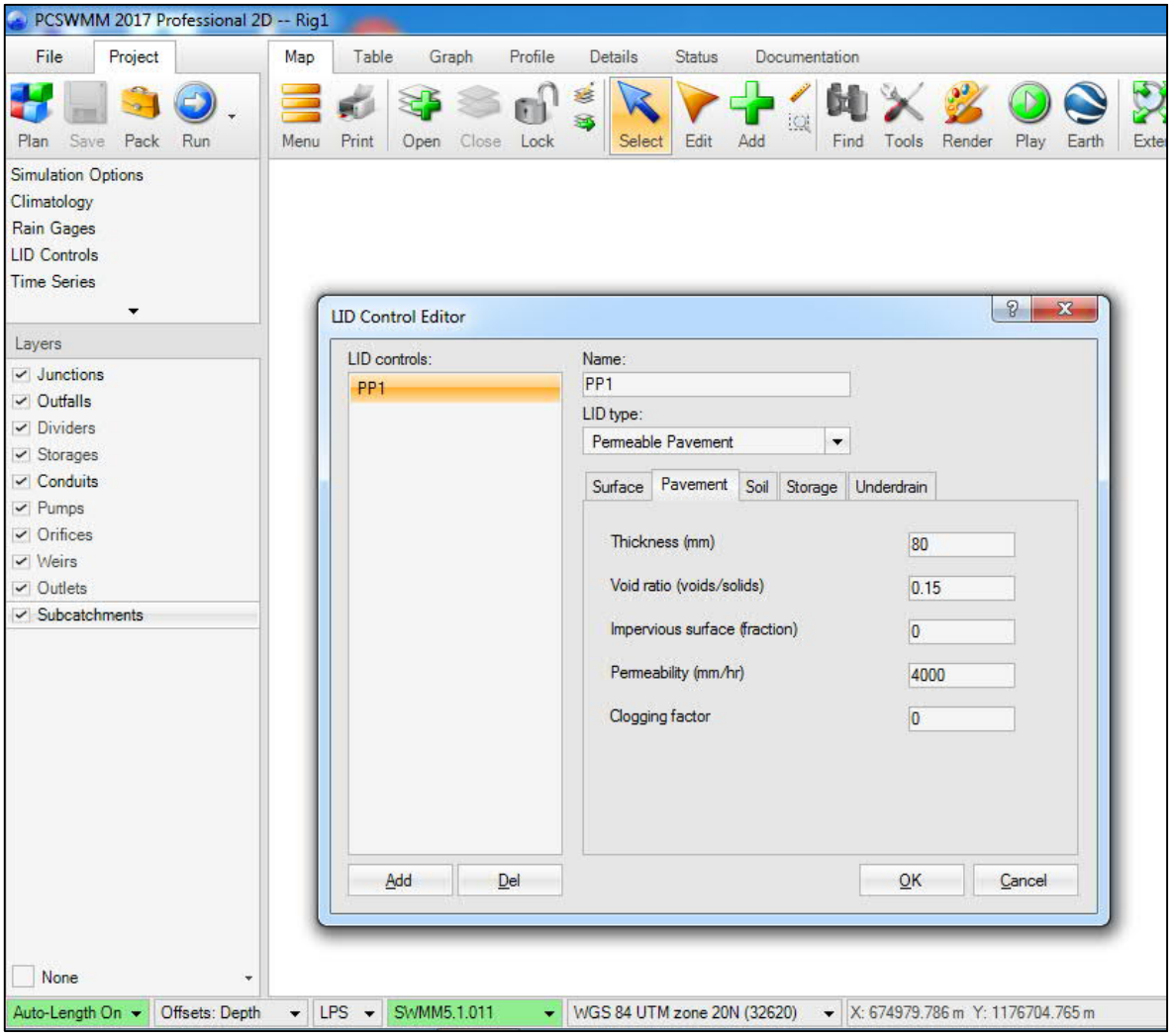

Figure 5-1 Screenshot of LID Control Editor in PCSWMM

5.2.1 SWMM model theory

SWMM is a widely used, dynamic rainfall-runoff model applicable for simulating single event or long-term (continuous) performance of runoff quantity and quality from primarily urban areas. SWMM conceptualises a typical urban drainage system as a series of water and material flows between four major environmental compartments namely: atmosphere, land surface, groundwater/sub-surface and transportation/conveyance. The model is a physically based, discrete-time simulation model which employs principles of conservation of mass, energy and momentum where appropriate (Rossman, 2015). A flow chart of the processes modelled by SWMM is illustrated in Figure 5-2. Details of each of these processes (hydrologic, hydraulic, water quality, treatment and LID) and the governing equations are provided in SWMM's reference manuals volumes I, II and III (Rossman, 2016, Rossman and Huber, 2016a, Rossman and Huber, 2016b).

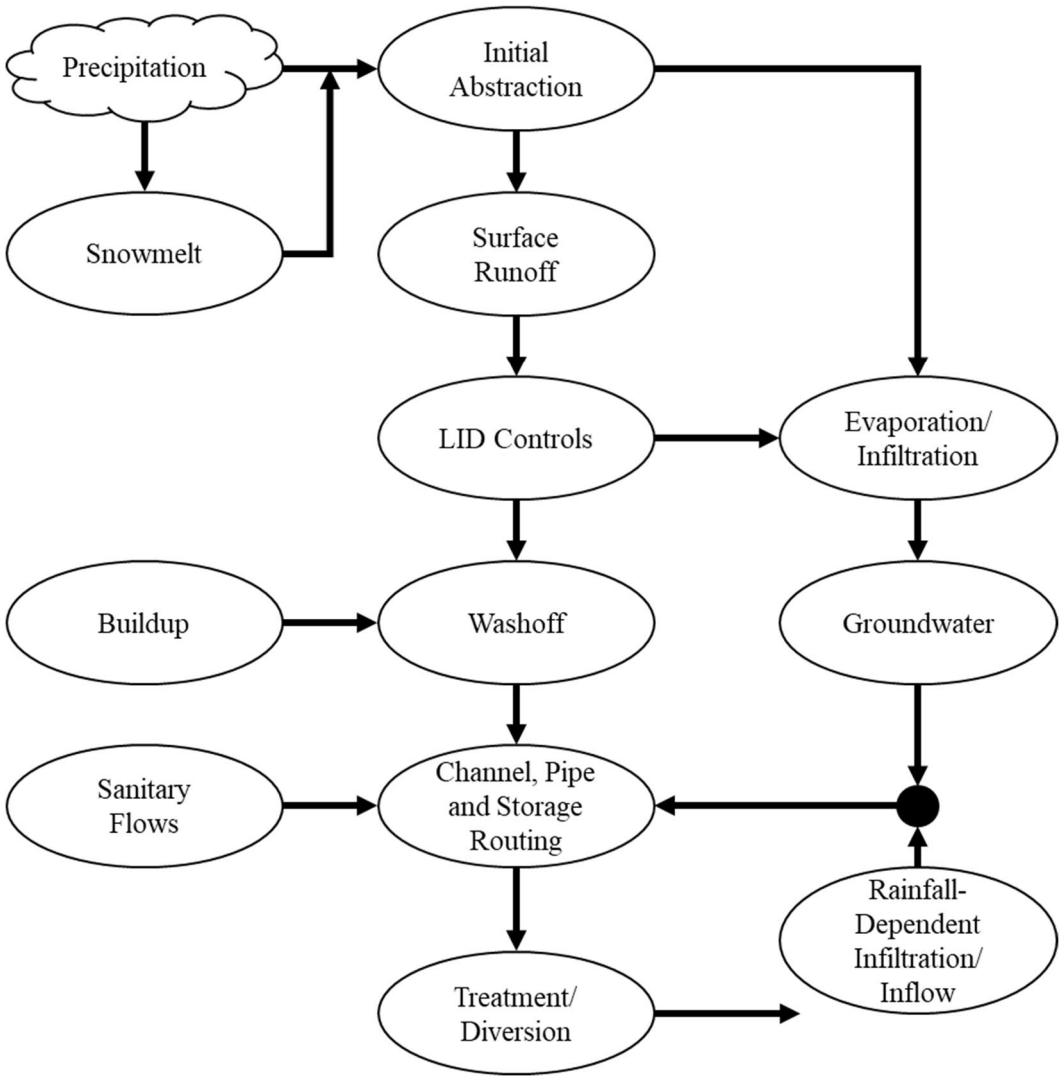

Figure 5-2 Flow chart of the processes modelled by SWMM
[adapted with permission from Rossman and Huber (2016a)]

A schematic of the SWMM surface runoff conceptual model is illustrated in Figure 5-3. The model estimates runoff based on a collection of subcatchment areas that receive precipitation and generate runoff and pollutant loads. Each subcatchment is treated as a nonlinear reservoir, which receives inflows from precipitation and generates outflows and losses based on the assigned catchment parameters such as area, average slope, flow width, imperviousness, depression storage, and Manning's roughness (Guan et al., 2015). The capacity of the nonlinear reservoirs is represented by a maximum depression storage value, which characterises both the pervious and impervious areas. Surface runoff occurs only when the depth of water in the reservoir exceeds the maximum depression storage, d_s, in which case the outflow is given by the Manning's equation. The subcatchment water depth, d, is continuously updated over time through the numerical solution of the water balance equation over the subcatchment. Either a NRCS (SCS) CN based approach, the Green-Ampt equation, or one of two variants of Horton's infiltration model can be used for modelling

infiltration in pervious areas. For each of the infiltration models, there are a number of physical and conceptual parameters which must be specified. Horton's equation describes the infiltration capacity into the soil as an exponential decaying function of time, but in the SWMM model, the integrated form for the cumulative infiltration is used to prevent undue reduction in infiltration capacity for low-intensity rainfall events. The Green-Ampt equation is a two-stage approach which considers both effects of the volume of water to be infiltrated and the moisture condition of the surface soil on the infiltration (Wang and Altunkaynak, 2012, Nipper, 2016, Fry, 2017). Detailed formulations for the NRCS (SCS) CN, Horton or Green-Ampt approaches are available in the SWMM manual (Rossman, 2015).

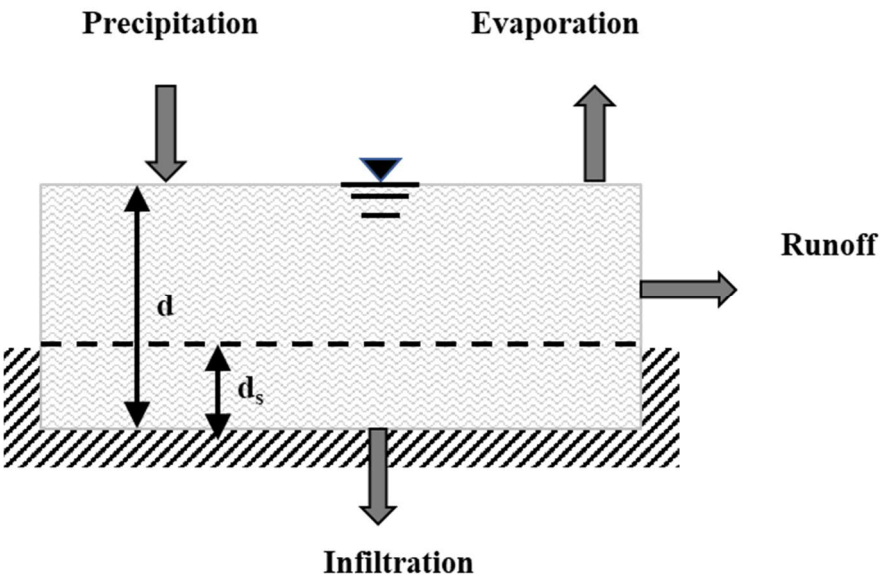

Figure 5-3 Schematic of SWMM surface runoff conceptual model
[adapted with permission from Rossman (2015)]

In the SWMM model, runoff is routed through a conveyance system of pipes, channels, storage/treatment devices, pumps and regulators. SWMM tracks the quantity and quality of runoff generated within each subcatchment, and the flow rate, flow depth, and quality of water in each pipe and channel during a simulation period comprised of numerous time steps. Routing within conduits is governed by the conservation of mass and momentum equations for gradually varied, unsteady flow (i.e., the Saint Venant flow equations). There are three types of water routing models in SWMM: steady flow routing model, kinematic wave routing model and dynamic wave routing model. In the steady flow routing method, a hydrograph is routed through the drainage system without change in shape and only accounts for the lagging effects. In kinematic wave routing, the continuity equation and a simplified

form of the momentum equation is used whereby flow is permitted to propagate in the downstream direction only as downstream conduits have no effect on upstream conduits. The dynamic wave routing method on the other hand, uses the continuity equation and a complete form of the momentum equation and flows can propagate in both downstream and upstream directions (Zhang, 2009, Rossman, 2015, Rossman and Huber, 2016a).

The SWMM model considers LID controls as part of its Subcatchment object, where each control is assigned a portion of the subcatchment's impervious area whose runoff it captures. This is because LID is a distributed stormwater runoff source control measure which utilises surface and landscape modifications located on or adjacent to impervious areas that generate most of the runoff in urbanised areas. Various design variables affect the hydrological performance of LID controls. These include the properties of the media contained within the LID unit, the depth of the media layers, the hydraulic capacity of any underdrain system utilised and the surface area of the LID unit (Rossman, 2016).To model LID hydrology, SWMM treats LID controls as an additional type of discrete element, using a process-based representation of their behaviour that is sufficiently accurate for the simulation of dynamic rainfall events in a computationally efficient method. LID controls are represented by a combination of vertical layers as illustrated previously in Figure 2-10 (subsection 2.5.9, page 38). During a simulation, SWMM executes a moisture balance that tracks and quantifies the water movement between and stored within each LID layer (Rossman, 2015). It does so by solving a set of flow continuity equations that describe the change in moisture content in a particular layer over time. The simple form of the continuity equation presented in Equation 5-1, is described as the difference between the inflow and outflow water flux rates, expressed as volume per unit area per nit time. Details of the governing equations within the LID controls of SWMM are available in the SWMM's reference manual volume III (Rossman, 2016).

$$\frac{\partial d}{\partial t} = i + q_0 - e - f - q_1 \qquad (5\text{-}1)$$

Where i is the rainfall intensity [L/T], q_0 is runon from adjacent subcatchments [L/T], e is the evaporation rate [L/T], f is the infiltration rate [L/T], and q_1 is the runoff rate [L/T] (Rossman, 2016).

5.2.2 Hydrological model setup and parameterisation

Four (4) separate SWMM models were created; each representing one of the pilot scale permeable pavement rigs. Each model comprised one subcatchment, a junction, a conduit (pipe) and an outlet as illustrated in Figure 5-4. For each model, the permeable pavement LID occupied the full subcatchment. LID parameters were inputted through the SWMM LID Control Editor.

For permeable pavements, the SWMM LID Control Editor consists of five tabbed data entry process layers namely surface, pavement, soil, storage and underdrain. The surface layer represents the ground surface that receives direct rainfall and runon from adjacent up-gradient land areas, stores excess inflow in depression storage and generates surface runoff. The pavement layer describes the characteristics of the particular pavement used. The soil layer is the engineered soil mixture used to support vegetative growth in bioretention cells. In this case the soil layer is not applicable. The storage layer is the mattress of crushed aggregates, gravel or porous material that provides hydrologic storage. The underdrain pipe is an outlet which conveys water from storage (Fleischmann, 2014). A description of the parameters required under each of these process layers along with typical range of values are provided in the SWMM User's Manual (Rossman, 2015). The components and parameters used in the LID module are listed in Table 5-1. The parameters were estimated through a combination of laboratory data and guidance from the typical ranges provided by Rossman (2015) along with literature sources (Zhang and Guo, 2014, Jato-Espino et al., 2016a). The surface and pavement layer parameters were kept constant for all rigs. The concrete block pavers were 80 mm in depth as described in subsection 3.4. The voids between the concrete blocks was estimated at 15%, hence 85% impermeable. A clogging factor was considered as negligible and was not included in the models because of the short duration of the simulations. An average 4000 mm/h permeability value was used for all rigs. The storage parameters were obtained from the properties of the materials as described in subsection 3.3, page 79. Seepage was not included in the models because sub-soil was not included as a component of the rigs. Underdrain parameters were estimated through model calibration.

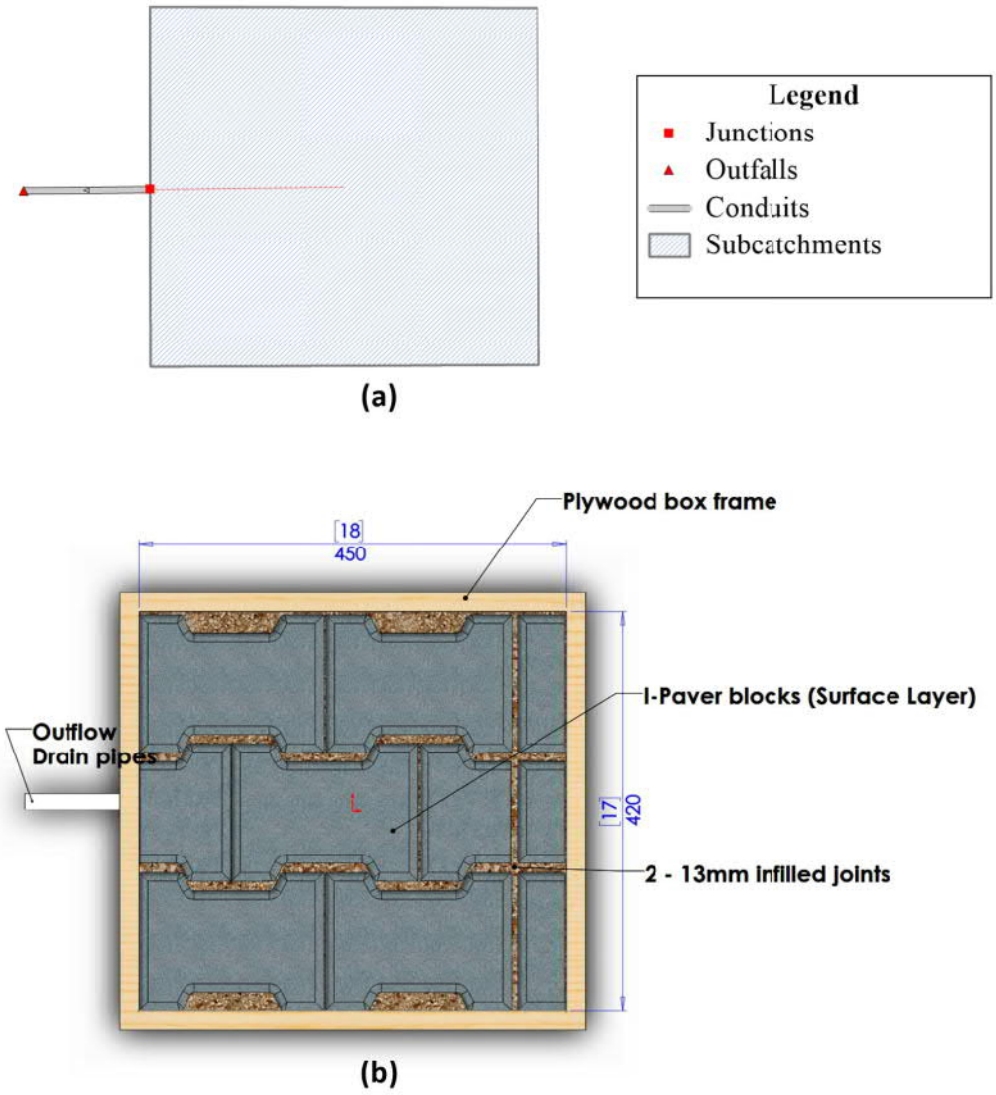

Figure 5-4 PCSWMM model setup: (a) model components (b) Plan view schematic of rig (illustrated previously in Figure 3-19c)

Table 5-1 Components and parameters used in the SWMM permeable pavement LID module to characterise each permeable pavement rig

LID Control Component	**Parameter**	**Rig 1**	**Rig 2**	**Rig 3**	**Rig 4**
Surface Layer	Berm height (mm)	0	0	0	0
	Vegetative volume (fraction)	0	0	0	0
	Surface roughness (Manning's *n*)	0.030	0.030	0.030	0.030
	Surface slope (%)	1	1	1	1
Pavement Layer	Thickness (mm)	80	80	80	80
	Void ratio (voids/solids)	0.15	0.15	0.15	0.15
	Impervious surface (fraction)	0.85	0.85	0.85	0.85

	Permeability (mm/h)	4000	4000	4000	4000
	Clogging factor	0	0	0	0
Storage	Thickness (mm)	350	350	350	350
	Void ratio (voids/solids)	0.50	0.45	0.45	0.50
	Seepage rate (mm/h)	0	0	0	0
	Clogging factor	0	0	0	0
Underdrain	Drain coefficient (mm/h)	20	20	16	16
	Drain exponent	0.85	0.85	0.85	0.85
	Drain offset height (mm)	25	25	25	25

5.2.3 Model calibration and validation

Model calibration is required when the required parameters cannot be accurately estimated (Moriasi et al., 2007). With the use of observed rainfall and outflow data, the optimal parameter values are found as a result of a systematic search process which yield the best fit between the observed and simulated outflow (Yener, 2006).

Model validation is a process whereby the calibrated model parameters are used to simulate runoff over an independent period outside the calibration period given that enough data is available (Moriasi et al., 2007). In circumstances where data is lacking, validation may be performed using shorter periods within an available dataset (Vaze et al., 2012).

Model calibration was accomplished using a split events approach where six (6) events per rig were used for calibration and four (4) to eight (8) events used for validation. The calibration procedure involved manually adjusting sensitive parameters individually in PCSWMM until errors between the observed and simulated discharge hydrographs were minimised. The following parameters were adjusted during the model calibration: storage void ratio, drain coefficient, drain exponent and drain offset height. The calibration was completed when either the best match between observed and simulated hydrographs was obtained or when the parameter value exhausted its range limits (Rosa et al., 2015). Calibration becomes more difficult as the specified ranges for feasible model parameter values increase (Cooper, 2002). Unavailability of relevant data complicates the parameterisation process tremendously resulting in randomly estimating conceptual values.

5.2.4 Model evaluation criteria/ Goodness-of-fit measures

Several performance measures are available to evaluate the accuracy of hydrological models. Visual assessment and commonly used goodness-of-fit statistical metrics were used to evaluate the relationship between observed flows and PCSWMM simulations. The statistical

metrics used were the Nash-Sutcliffe Efficiency coefficient (NSE) (Nash and Sutcliffe, 1970), coefficient of determination, R^2 and the Root-Mean-Square-Error (RMSE). Numerous researchers (Guan et al., 2015, Rosa et al., 2015, Brunetti et al., 2016, Kourtis et al., 2017, Turco et al., 2017) have often used these goodness-of-fit measures for evaluating the overall fit of hydrological models. The NSE and R^2 coefficients indicate how well the plot of observed verses simulated data matches each other. The NSE is a normalised statistic that determines the relative magnitude of the residual variance compared to the measured data variance (Nash and Sutcliffe, 1970). The NSE, which ranges from minus infinity to 1.0 (with the higher values indicating better agreement) is the ratio of the mean square error to the variance in the observed data, subtracted from unity and is given by Equation 5-2 (Legates and McCabe, 1999).

$$NSE = 1 - \frac{\sum_{t=0}^{T}(Q_o^t - Q_m^t)^2}{\sum_{t=0}^{n}(Q_o^t - \overline{Q}_o)^2} \tag{5-2}$$

R^2, is the square of the Pearson's product-moment correlation coefficient such that $R^2 = r^2$. It describes the proportion of the total variance in the observed data that the model can explain. R^2 ranges from 0.0 to 1.0, with the higher values indicating better agreement, and is represented by Equation 5-3 (Legates and McCabe, 1999).

$$R^2 = \left(\frac{\sum_{t=0}^{T}(Q_o^t - \overline{Q_o}) \cdot (Q_m^t - \overline{Q}_m)}{\sum_{t=0}^{T}(Q_o^t - \overline{Q}_o)^2 \cdot \sqrt{\sum_{t=0}^{T}(Q_m^t - \overline{Q}_m)^2}} \right)^2 \tag{5-3}$$

RMSE indicate error in the units (or squared units) of the constituent of interest, which aids in analysis of the results. The RMSE measured the deviation between the simulated discharge and the observed discharge. A zero (0) value indicates perfect simulation of the observed values (Moriasi et al., 2007). RMSE is given by Equation 5-4.

$$RMSE = \sqrt{\frac{\sum_{t=0}^{T}(Q_o^t - \overline{Q}_o)^2}{n}} \tag{5-4}$$

The variables from Equations 5-2, 5-3 and 5-4 are defined as follows:

Q_o^t = observed discharge at time t

Q_m^t = modelled discharge at time t

$\overline{Q}_o$ = mean of observed discharges

$\overline{Q}_m$ = mean of modelled discharges in the time series T

n = total number of observations

5.2.5 Sensitivity analysis

Sensitivity analysis was performed in order to identify which parameters would be most effective in improving the correlation between observed and simulated results (Moriasi et al., 2007, Rosa et al., 2015). Model parameters were ranked based on their contribution to the overall error in model predictions. Sensitivity analysis can be either local or global. Local sensitivity analysis involves changing individual parameters separately while keeping the others constant whereas global sensitivity analysis allow all model input parameters to vary over their ranges simultaneously (Haan, 2002). Three (3) types of sensitivity analysis coefficients can be used in both local or global sensitivity analyses namely:

(1) Absolute Sensitivity (AS) defined by Haan (2002) as Equation 5-5
(2) Relative Sensitivity (RS) defined by Haan (2002) as Equation 5-6
(3) Deviation Sensitivity (DS) defined by McCuen (2003) as Equation 5-7

$$AS = \frac{\partial O}{\partial I} \tag{5-5}$$

$$RS = \frac{\partial O/O}{\partial I/I} = \frac{\partial O}{\partial I} \cdot \frac{I}{O} \tag{5-6}$$

$$DS = \Delta O = \frac{\partial O}{\partial I} \Delta I \cong \frac{\Delta O}{\Delta I} \Delta I \tag{5-7}$$

where:

O = original model output value
I = original input parameter value
∂O = difference between the original and model output
∂I = difference between the original and adjusted input parameter value
ΔO = change in output value
ΔI = change in input parameter value from its baseline

For each rig, a local sensitivity analysis was adopted whereby individual parameters were manually changed over a range of ± 50% of the baseline value. The three (3) performance measures, NSE, R^2 and RMSE described in subsection 5.2.4 were used as sensitivity functions and because they were dimensionless, the AS coefficient (Equation 5-5) was used to compare the sensitivity analyses results. The LID module parameters namely, storage void ratio, drain coefficient, drain exponent and drain offset height were used to conduct the sensitivity analysis using one rainfall event used for calibration of the model for each rig.

5.3 Model results

5.3.1 Calibration and validation

Initial and calibrated values for the four (4) LID module parameters of each rig that proved to be significant regarding matching observed and simulated discharges are listed in Table 5-2. Further details regarding the sensitivity of these parameters are discussed further in subsection 5.3.3.

Table 5-2 Calibrated and initial parameters for each rig based on sensitivity to the model outputs

Parameter	Range	Rig 1		Rig 2		Rig 3		Rig 4	
		Initial value	Cali. value	Initial value	Cali. value	Initial value	Cali. value	Initial value	Cali. value
Storage void ratio	0.4–0.6	0.5	0.5	0.5	0.45	0.5	0.45	0.4	0.5
Drain coefficient	15–20	15	20	15	20	15	16	15	16
Drain exponent	0.5–1.0	0.5	0.85	0.5	0.85	0.5	0.85	0.5	0.85
Drain offset height (mm)	0–50	0	25	0	25	0	25	0	25

Figure 5-5 represents flow comparison graphs along with their respective scatter graphs for one (1) of six (6) calibration events for each rig. Flow comparison graphs compare the simulated and observed hydrographs whilst the scatter graphs compare the simulated flow value for each time step against the observed flow for the same time step. The graphs show that for all rigs, the observed discharges were very well simulated. Low flows were however under-estimated in all cases. All flow comparison hydrographs and associated scatter graphs are presented in Appendix F, page 268.

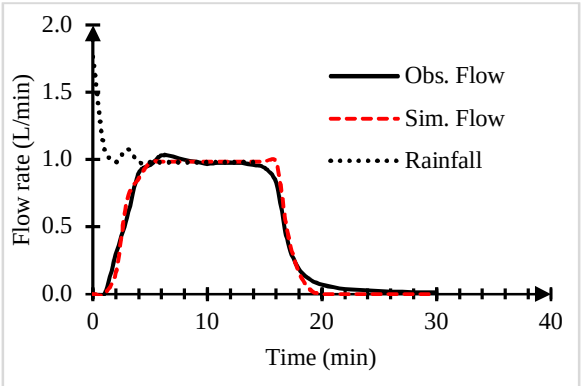

(a)

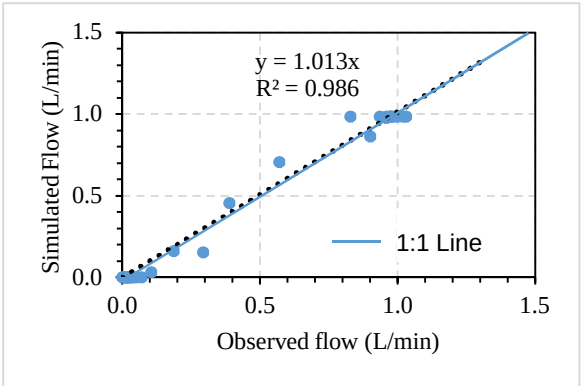

(b)

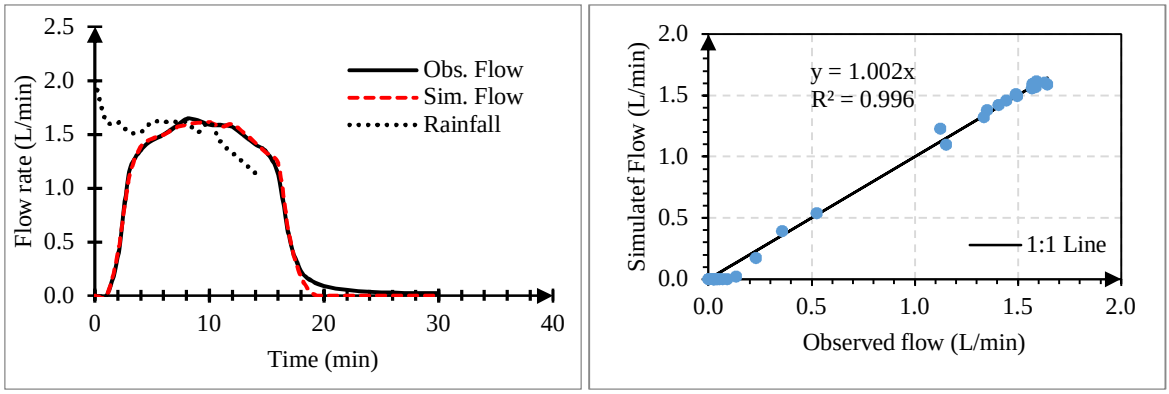

(c) (d)

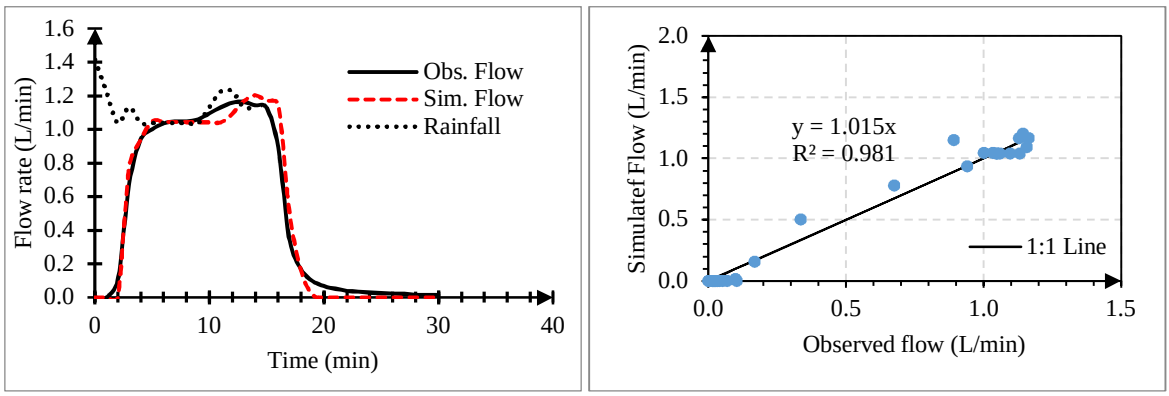

(e) (f)

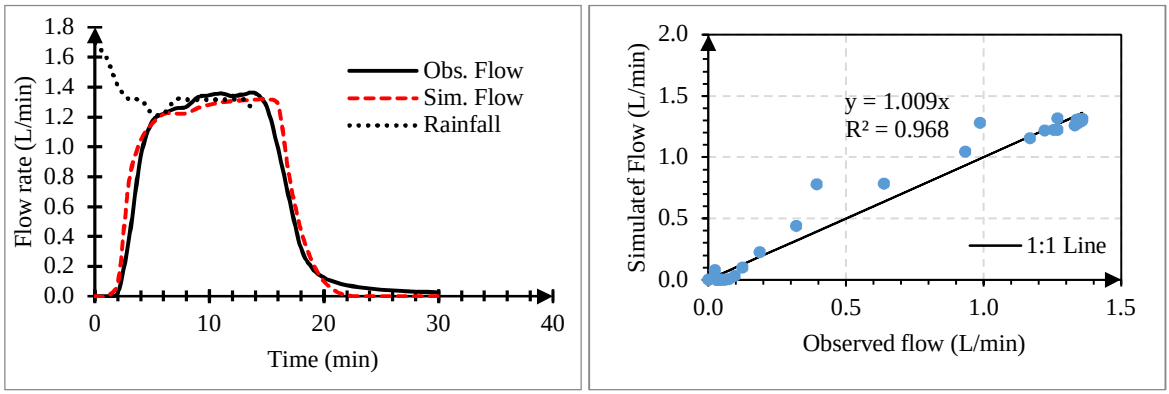

(g) (h)

Figure 5-5 Comparison between observed and simulated outflows for one of six calibration events (a) Rig 1 Flow hydrographs (b) Rig 1 Scatter graph (c) Rig 2 Flow hydrographs (d) Rig 2 Scatter graph (e) Rig 3 Flow hydrographs (f) Rig 3 Scatter graph (g) Rig 4 Flow hydrographs (h) Rig 4 Scatter graph

5.3.2 Model evaluation/ Goodness-of-fit measures

Table 5-3 and Figure 5-6 present results obtained from the four (4) rigs for the calibration and validation events according to goodness-of-fit measures NSE, R^2 and RMSE. For the calibration simulations, R^2 which is typically used, ranged from 0.985 to 0.996 for Rig 1, 0.975 to 0.997 for Rig 2, 0.970 to 0.994 for Rig 3 and 0.968 to 0.989 for Rig 4. These results

along with the NSE and RMSE show excellent model results. Dongquan et al. (2009) suggested that an NSE greater than 0.5 indicates acceptable model performance for SWMM simulations. The high values of the goodness-of-fit measures in calibration assure the data quality in terms of consistency between the rainfall and discharge observations (Guan et al., 2015). It is noteworthy that Rig 4 had the least desirable model results for all three (3) statistical measures. This can most likely be attributed to the C-EPS block in the sub-base of Rig 4 for which the model was not designed to consider. Nevertheless, the model results from Rig 4 were indeed quite satisfactory.

Table 5-3 Mean statistical performance measures for each rig obtained during the calibration and validation events

Rig No.	NSE		R^2		RMSE	
	Calibration	**Validation**	**Calibration**	**Validation**	**Calibration**	**Validation**
1	0.987	0.976	0.990	0.979	0.004	0.007
2	0.980	0.978	0.986	0.982	0.004	0.004
3	0.984	0.975	0.988	0.977	0.004	0.007
4	0.975	0.948	0.978	0.953	0.006	0.011

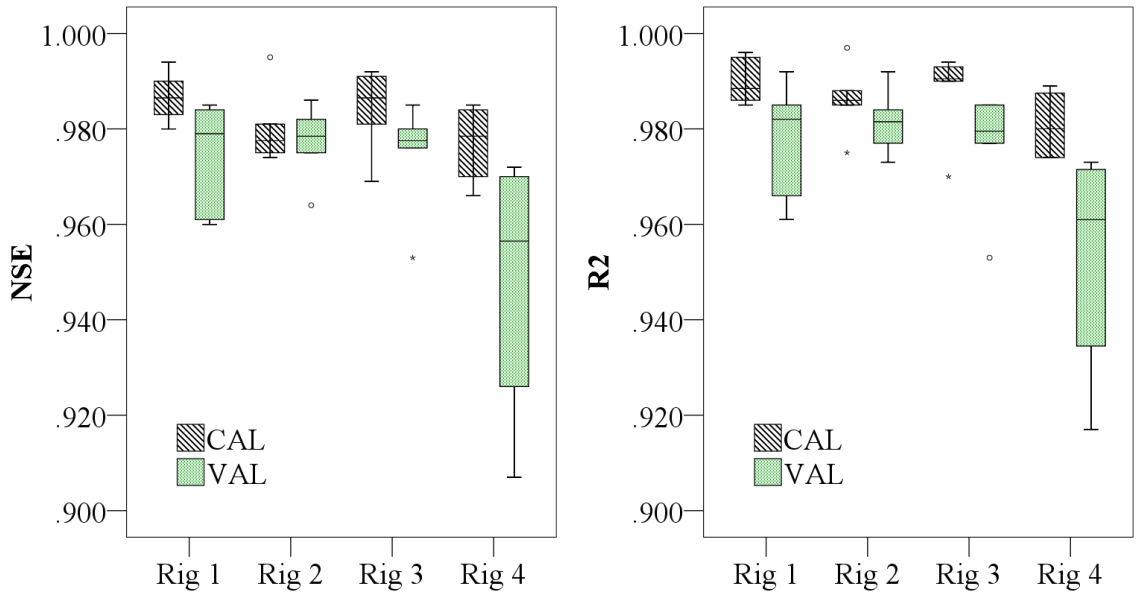

(a) (b)

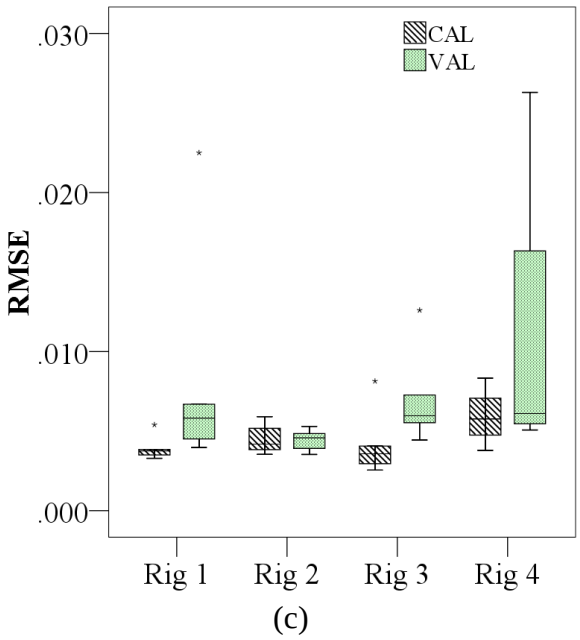

(c)

Figure 5-6 Box and whiskers plots with the values of NSE, R^2 and RMSE for each rig during the calibration (CAL) and validation (VAL) events (a) NSE, (b) R^2 and (c) RSME

5.3.3 Sensitivity analysis results

As previously mentioned in subsection 5.2.5, the Absolute Sensitivity (AS) coefficient (Equation 5-5) was used to compare the sensitivity analyses results. Full details of these results are available in Appendix G, page 284. Figure 5-7 compares the sensitivity analysis results for R^2 amongst the four (4) rigs based on parameter changes of ± 50% of the baseline value. The results found that for all rigs, the drain exponent parameter was the most sensitive LID parameter followed by storage void ratio. Drain coefficient and drain offset height were not sensitive parameters. Adjusting these parameters by ± 50% had an almost negligible effect on the quality of the modelled outflows.

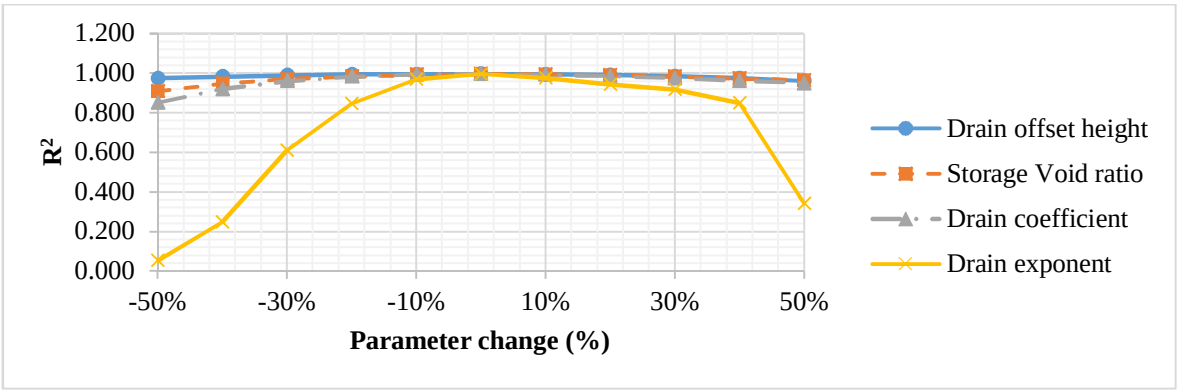

(a)

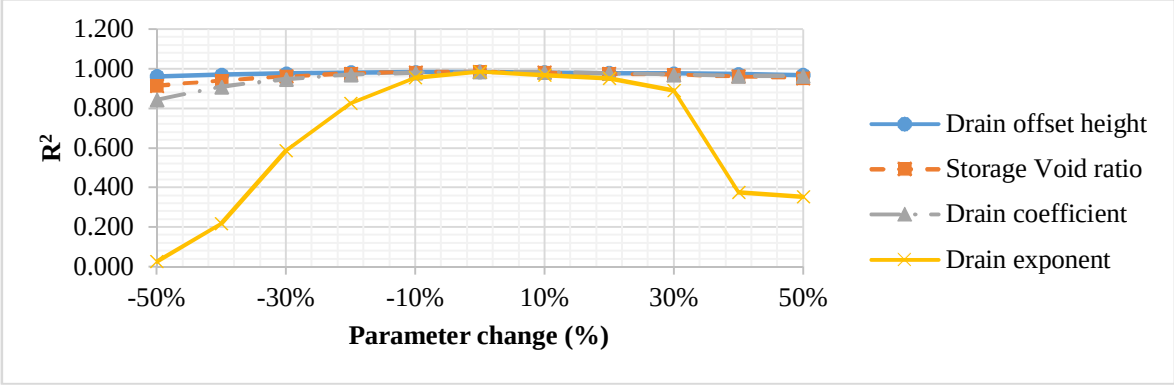

(b)

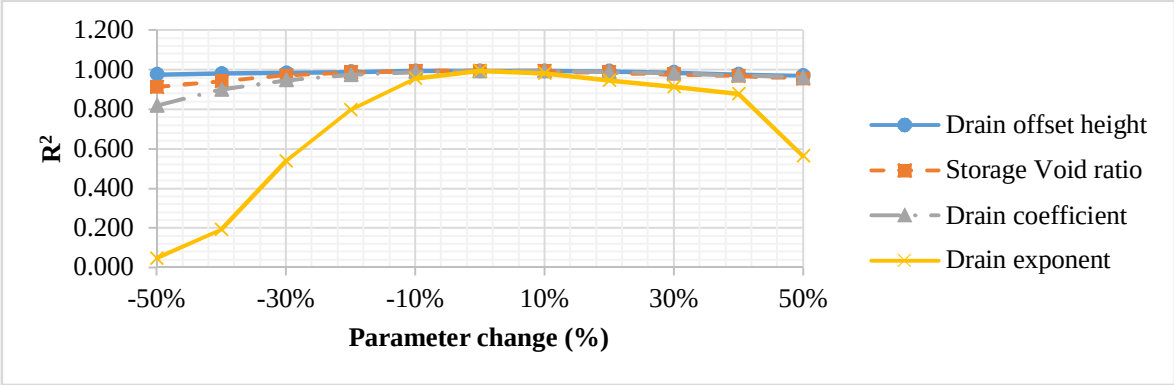

(c)

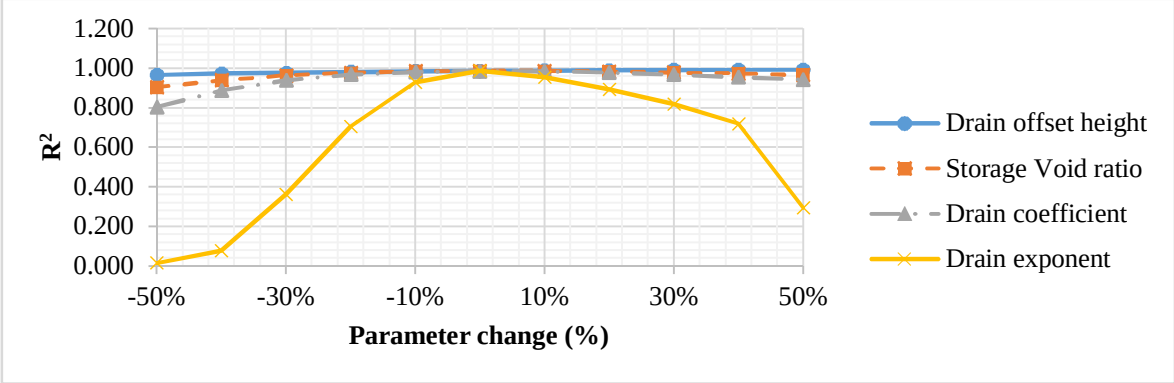

(d)

Figure 5-7 Comparison of sensitivity analysis results for R^2 amongst the four rigs (a) Rig 1 (b) Rig 2 (c) Rig 3 (d) Rig 4

The nature of the sensitivity of the four (4) parameters based on the selected variance range on the discharge hydrograph is illustrated in Figure 5-8. As with Figure 5-7, the Drain exponent LID parameter had the greatest influence on the gradient of the both the rising and falling limbs of the modelled hydrograph. Increasing the drainage exponent by ± 50% of its

baseline value, resulted in the hydrograph quickly rising and flattening off. A change of ± 10% had insignificant impact on the hydrograph. Variation in the value of the other three (3) LID parameters had minor influence on the modelled hydrograph but in a different way. A reduction in storage void ratio parameter value by 50% caused the hydrograph to begin rising earlier. Other changes again had minor influence.

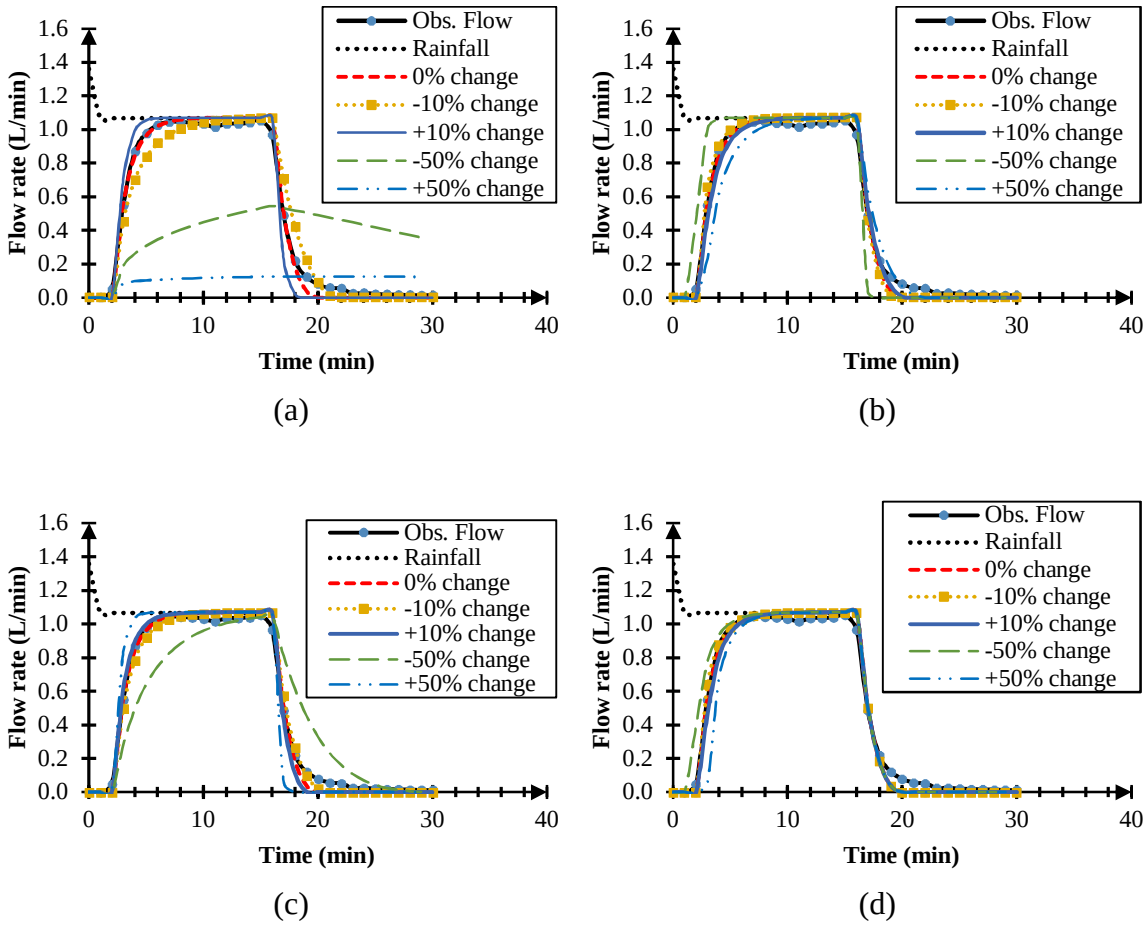

Figure 5-8 Selected modelled discharge hydrographs using parameters at calibration and adjusted parameters at ± 10% and ± 50% for selected parameters (a) Drain exponent (b) Storage void ratio (c) Drain coefficient (d) Drain offset height

5.4 Chapter summary

In this chapter, rainfall-discharge models of each of the pilot scale permeable pavement rigs were developed, calibrated and validated using the Computational Hydraulics International's (CHI) PCSWMM computer software. The models developed, determined whether PCSWMM was able to accurately simulate outflow from permeable pavement rigs that contained recycled and non-traditional sub-base materials (CCA, C-EPS). PCSWMM includes a specific and identical US EPA's SWMM LID module with adequate capabilities of modelling the hydraulics and geometry of permeable pavements. The models were calibrated and validated using data obtained from the simulated hydrological performance

assessments presented previously in subsection 4.2, page 106. High-intensity, short-duration rainfall events (at least 50-year return period) were simulated. Parameter values were estimated based on guidance from literature and from the results obtained from the previous hydrological performance experiments. The results found that for all rigs, the drain exponent parameter was the most sensitive LID parameter followed by storage void ratio. Excellent model results according to goodness-of-fit measures NSE, R^2 and RMSE were obtained for the four (4) rigs during model calibration and validation. Additionally, comparison of modelled and observed hydrographs revealed excellent fits for all rigs. PCSWMM was therefore able to satisfactorily model the outflow from all pavement rigs with similar accuracy. This chapter has provided greater insight into the hydrological modelling of permeable pavement rigs containing CCA and C-EPS and has demonstrated that PCSWMM can be used to accurately model their discharge response to high-intensity, short-duration rainfall events. Research question number 4 listed in Chapter 1 is therefore answered. The following chapter examines the physical and mechanical characteristics of concrete consisting of CNA for use as permeable pavement blocks.

CHAPTER 6. PRODUCTION AND EVALUATION OF LOW CARBON CONCRETE PERMEABLE PAVEMENT BLOCKS

6.1 Overview

The literature shows that a research gap exists regarding evaluations of the performance of artificial, lightweight aggregates when used in concrete to produce Concrete Permeable Pavement Blocks (CPPB). This chapter examines the physical and mechanical characteristics of concrete consisting of Carbon-Negative Aggregates (CNA) for use as CPPB in permeable pavements. This chapter builds on work done by Gunning et al. (2009) to whom credit is given to for the production of the CNA. The methodology involves substituting natural aggregates (NA) by mass, with CNA at percentages of 0, 15, 30, 50, 75 and 100. Compressive and splitting tensile strengths after 28 days and water absorption tests are evaluated and compared. The mix designs ensured that cement and fines content remained unchanged irrespective of the NA/CNA ratio. The major component of this chapter has been published in (the) International Journal of Pavement Engineering and has been included in this thesis with permission from Taylor & Francis.

6.2 Materials and methods

6.3 Materials

Premium Plus Cement (PPC), which contains approximately 30% pozzolanic material and 70% Ordinary Portland Cement (OPC), as described previously in subsection 3.2.5 was used in the production of all concrete mixes. Ordinary tap water was used in all mixes. Quarried basalt aggregates were used as natural aggregates. CNA was supplied by the manufacturer, Carbon8 Systems located in Kent, UK. Natural aggregates and CNA were used in the mixes as per ASTM C33 (ASTM International, 2016a) and ASTM C330 (ASTM International, 2017a) respectively. Natural 'river' sand (NS) constituted most of the fine aggregate component in the mixes. Conplast SP430 super plasticiser was used to improve the workability of the concrete mixes. The physical properties of the coarse and fine aggregates are presented in Table 6-1. The physical properties of the CNA and the natural aggregates contrast sharply as seen in Table 6-1. CNA are categorised as lightweight because of a low bulk density value below 1200 kg/m^3 (González-Corrochano et al., 2009). The particle size distributions of the aggregates were determined in accordance with ASTM C136 (ASTM International, 2014c) and are presented in Figure 6-1. The gradations of the CNA and the natural aggregates for concrete were obtained as per ASTM C330 (ASTM International, 2017a) and ASTM C 33 (ASTM International, 2018a) respectively.

Table 6-1 Physical properties of aggregates and fines

[Reprint with permission from Monrose et al. (2019b)]

Property	**Specification**	**Sand**	**NA**	**CNA**	**Typical value**
Specific Gravity, G_s (kg/m^3)	ASTM C127 (2015)	-	2.709	1.602	
Water absorption (%)	ASTM C127 (2015)	-	1.2	23.6	<10
L.A abrasion (%)	ASTM C131 (2014b)	-	18	66	
Impact (%)	BS 812 (1990)	-	16	-	
Bulk Density (Loose) (kg/m^3)	ASTM C29 (2016b)	1736	1530	1141	
Fineness modulus		3.19	5.71	4.69	3.2–4.2
Coefficient of uniformity (c_u)		4	2	8	>4
Coefficient of curvature (c_c)		1	1	1	$1 \leq Cc \leq 3$
Voids ratio		-	0.433	0.285	
Porosity (%)		-	30	22.2	
pH	BS 1377 (2018)	-	8.51	12.26	6–11

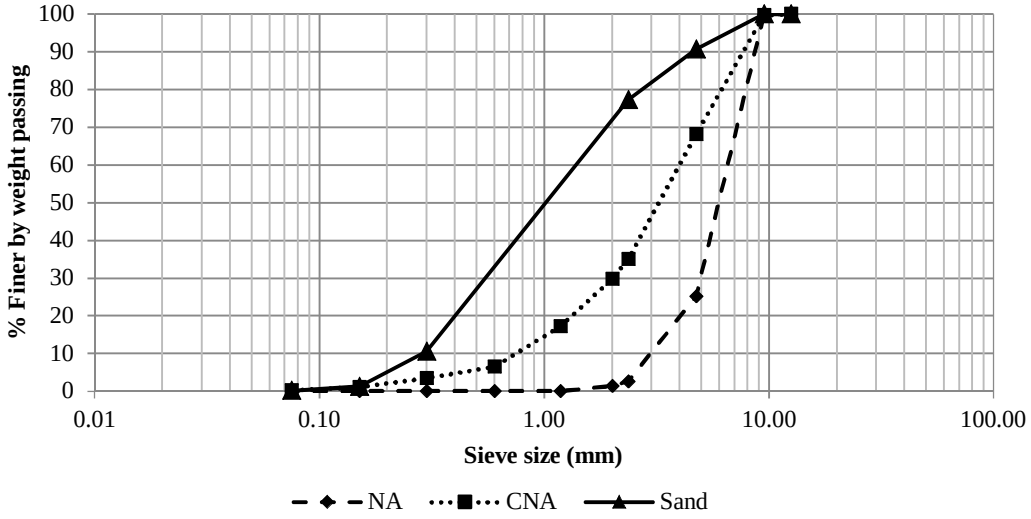

Figure 6-1 Particle Size Distributions (PSD) of aggregates and fines

[Reprint with permission from Monrose et al. (2019b)]

6.3.1 Methods

6.3.1.1 **Production of concrete samples and concrete permeable pavement blocks**

Six (6) different concrete mixes were produced whereby natural aggregates were replaced with CNA by mass in varying percentages of 0, 15, 30, 50, 75 and 100. All mixes were prepared in a 50 dm^3 capacity rotary mixer in the laboratory. Increased natural aggregate replacement had a negative effect on the workability of the fresh concrete because of the higher water absorption of the CNA. Consequently, the water-cement ratio was increased as

the CNA percentages increased. The additional water was predetermined based on the water absorption of the CNA. Alternatively, the CNA could have been pre-soaked to saturation (Kockal and Ozturan, 2011) or pre-wetted (Jiajun et al., 2006, ACI, 2013) prior to mixing. For all mixes, the fresh concrete slump values were measured immediately after mixing. The mix compositions and slump values of all concrete mixes are listed in Table 6-2.

For each mix, four (4) 100 × 200 mm cylinder samples, five (5) 100 mm cube samples and four (4) 200 × 100 × 80 mm CPPB were prepared in accordance with BS EN 12390-3:2009 (BSI, 2009b) and ASTM C936 (ASTM International, 2018b) respectively. All samples and blocks were secured, de-moulded after 24 h, labelled and cured in water at a standard temperature of 20 ± 1 °C for 28 days before testing. A total of 54 samples and 24 CPPB were prepared. Some of the samples are shown in Figure 6-2.

Table 6-2 Composition of various concrete mixtures

[Reprint with permission from Monrose et al. (2019b)]

Mix	CNA %	Cement (kg)	Sand (kg)	NA (kg)	CNA (kg)	Water (kg)	Super plasticiser (ml)	Slump (mm)	W/C ratio	A/C ratio
Control	0	8	16	24	0	3.2	50	10	0.4	3
CNA15	15	8	16	20.4	3.6	4.0	50	15	0.5	3
CNA30	30	8	16	16.8	7.2	4.0	50	5	0.5	3
CNA50	50	8	16	12	12	5.0	50	5	0.6	3
CNA75	75	8	16	6	18	6.0	50	10	0.8	3
CNA100	100	8	16	0	24	6.0	50	0	0.8	3

W/C–water/cement ratio

A/C–aggregate/cement ratio

Figure 6-2 Concrete samples consisting of CNA

6.3.1.2 **Hardened concrete samples**

6.3.1.2.1 Compressive and splitting tensile strength tests

The 28-day compressive strength of the cube samples was measured in accordance with BS EN 12390-3:2009 (BSI, 2009b). The splitting tensile strength tests of the cylinder samples were performed according to ASTM C 496 (ASTM International, 2017c). The compressive and splitting tensile strength testing machine used (Engineering Laboratory Equipment Ltd, UK) is shown in Figure 6-3.

Figure 6-3 Concrete compressive and splitting tensile strength testing machine in laboratory

6.3.1.2.2 Density and water absorption

Density and water absorption were determined in accordance with ASTM C642 (ASTM International, 2013).

6.3.1.2.3 Micro-structural observations through SEM

A Scanning Electron Microscope (SEM) equipped with an Edax Energy Dispersive System (EDS) and Gatan Digscan imaging system shown in Figure 6-4, was used to examine the micro-structure and bonding or Interfacial Transition Zone (ITZ) (Scrivener et al., 2004) between the aggregates and the cementitious paste. A total of two (2) small (< 10 mm in diameter) samples were taken from split concrete samples for examination. Samples from the control mix and the CNA100 mix were used. Several attempts were made prior to retrieving suitable samples without affecting the ITZ. A Denton Vacuum Desk II Sputter

Coater, shown in Figure 6-5, was used to gold coat the samples for better electrical conductivity prior to placement in the electron microscope. The microscope was operated at medium vacuum and 10–30 kV accelerating voltage with magnifications ranging from X20 to X3000. All micrographs were digitised to 768 × 768 pixels.

Figure 6-4 Scanning Electron Microscope
[Reprint with permission from Monrose et al. (2019b)]

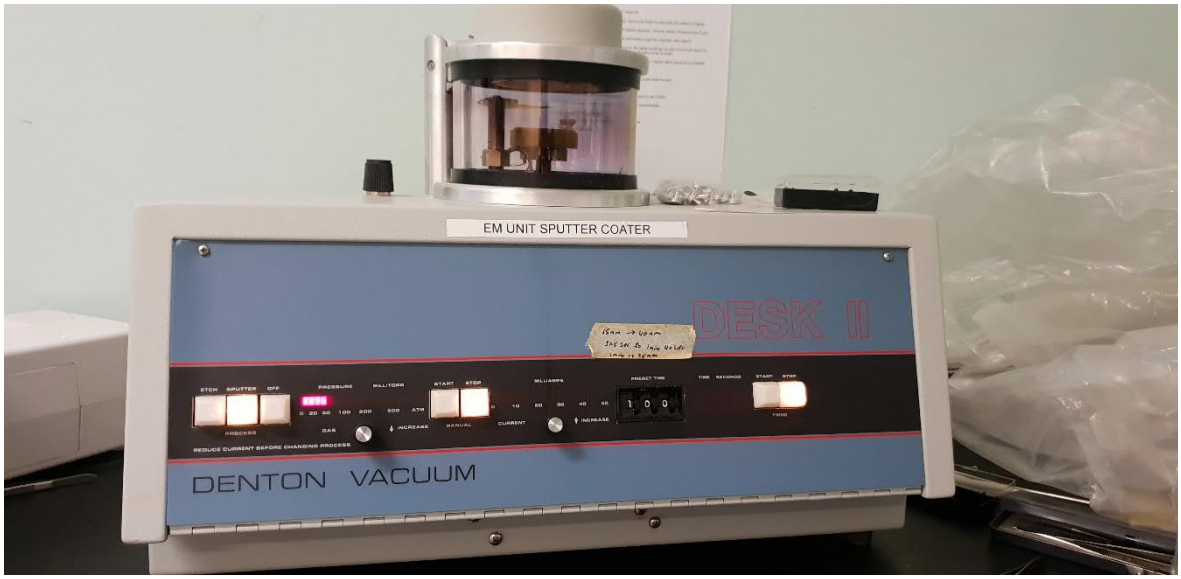

Figure 6-5 Denton Vacuum Desk II Sputter Coater
[Reprint with permission from Monrose et al. (2019b)]

6.4 Results and discussion

6.4.1 Density and water absorption

The relationship between %CNA replacement and average 28-day Saturated Surface Dry (SSD) densities is presented in Figure 6-6. As seen from Figure 6-6, density values decrease with increases in %CNA. Equation 1 represents the best fit for these density results. This relationship can be attributed to the lower specific gravity of the CNA compared to that of the natural aggregates. Additionally, the spherical shape of the CNA reduced the packing density of the concrete mixtures. The natural aggregates on the other hand, were predominantly angular and fractured, thereby increasing the packing density of the mixes. The average 28-day SSD densities ranged from 2211 kg/m^3 (100% CNA mix) to 2591 kg/m^3 (0% CNA mix). Concrete with dry densities between 2000-2200 kg/m^3 is considered as semi-lightweight (Abouhussien et al., 2015).

$$w_c = -3.98CNA + 2578 \quad (6\text{-}1)$$

where w_c is average 28-day saturated surface dry density (kg/m^3) and CNA is the percentage of carbon-Negative aggregates added by mass.

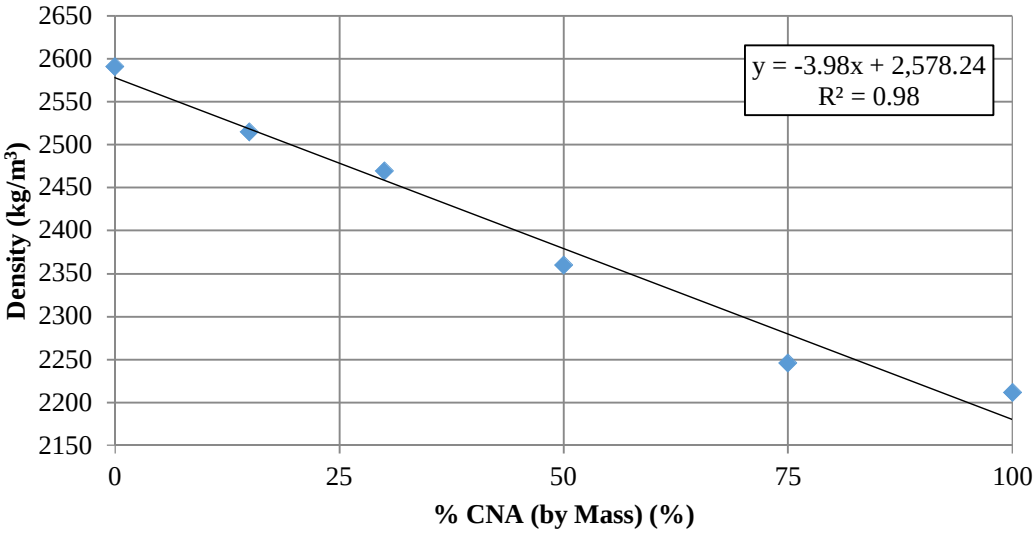

Figure 6-6 Relationship between average 28-day (SSD) density and percent CAN [Reprint with permission from Monrose et al. (2019b)]

Water absorption results are presented in Figure 6-7 and Figure 6-8. As shown in Figure 6-7, for all mixes, the average water absorption percentages increased rapidly during the first 20 minutes of saturation, then gradually flattened off at a slight positive gradient after 2 hours until the end of the test at 24 h. It can be seen from Figure 6-8, that water absorption increased

with increases in CNA percent. These water absorption results can be attributed to the high porosity and high-water absorption of the CNA. The average 24-hour water absorption percentages of the various concrete mixes ranged from 1.66 (0% CNA mix) to 9.17% (100% CNA mix). Although absorption is not used as a measure of quality of concrete, most good concretes have absorption below 10% (Gencel et al., 2012).

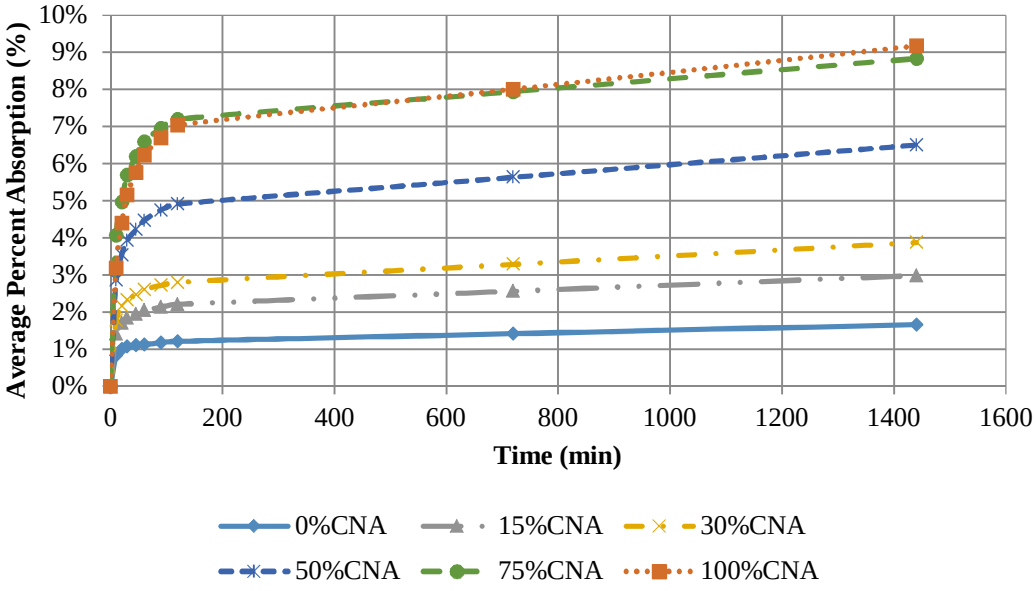

Figure 6-7 Water absorption rate for the various concrete mixes

[Reprint with permission from Monrose et al. (2019b)]

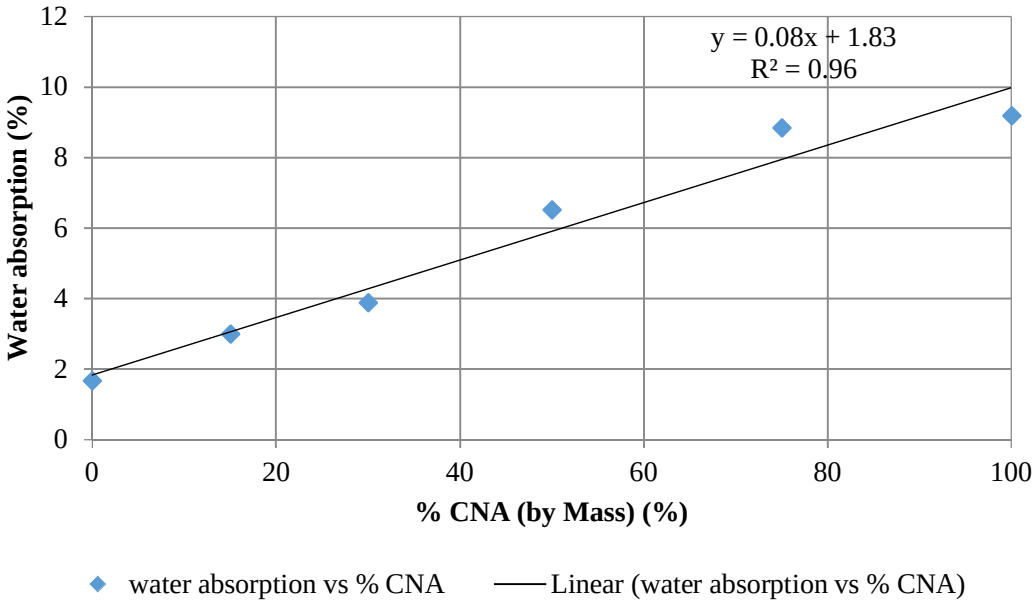

Figure 6-8 Relationship between water absorption and percent CAN

[Reprint with permission from Monrose et al. (2019b)]

6.4.2 Compressive strength

Figure 6-9 shows the relationship between average 28-day compressive strength values and %CNA. It is important that CPPB have satisfactory compressive strengths as the durability of CPPB depends heavily on the quality and strength of the paving block (Murugan et al., 2016). Compressive strengths decreased exponentially with increasing %CNA. Values ranged from 68.8 MPa (0% CNA mix) to 18.5 MPa (100% CNA mix). The reduction in compressive strength is primarily because the CNA have a significantly lower crushing resistance and density as compared to the natural aggregates. Equation 6-2 represents the best fit for the results obtained.

$$f_{cu} = 66.87e^{-0.01CNA} \quad (6\text{-}2)$$

where f_{cu} is cube compressive strength (MPa) and CNA is the percentage of Carbon-Negative Aggregates added by mass.

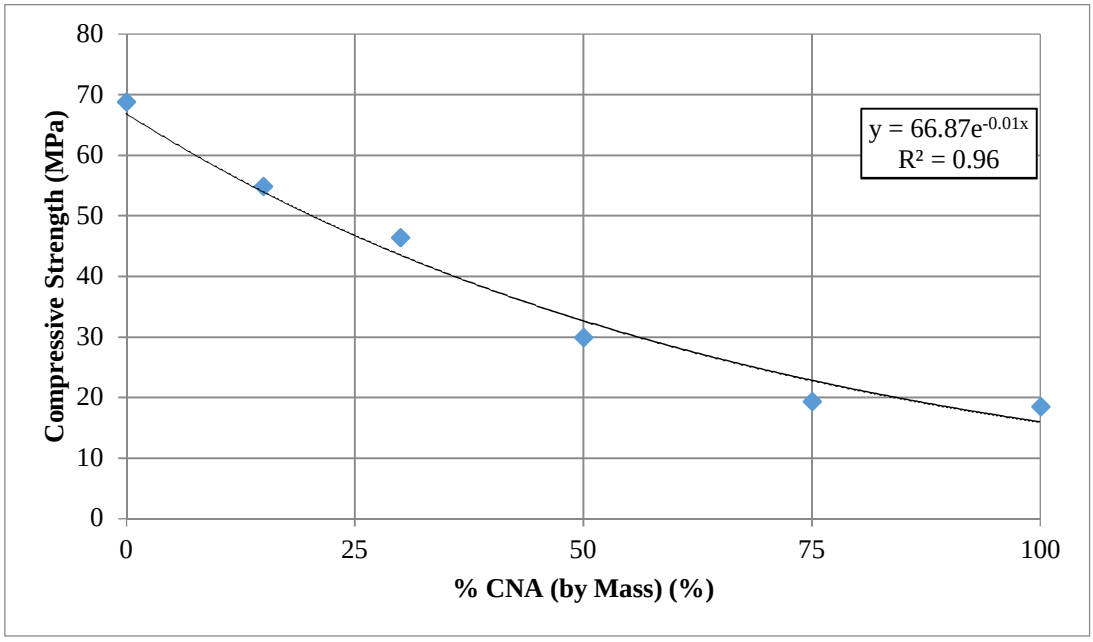

Figure 6-9 Relationship between 28-day compressive strength and %CNA
[Reprint with permission from Monrose et al. (2019b)]

Figure 6-10 and Figure 6-11 show the relationships between compressive strength and percent water absorption and between compressive strength and density respectively. For the same reasons mentioned previously, compressive strength decreased with increased water absorption and decreased density. These relationships are further presented in Equations 6-3 and 6-4.

$$f_{cu} = 89.99e^{-19.61\varphi} \quad (6\text{-}3)$$

$$f_{cu} = 0.006e^{0.004w_c} \quad (6\text{-}4)$$

where f_{cu} is the cube compressive strength (MPa), φ is the water absorption percentage of the CNA and w_c is average 28-day saturated surface dry density (kg/m^3).

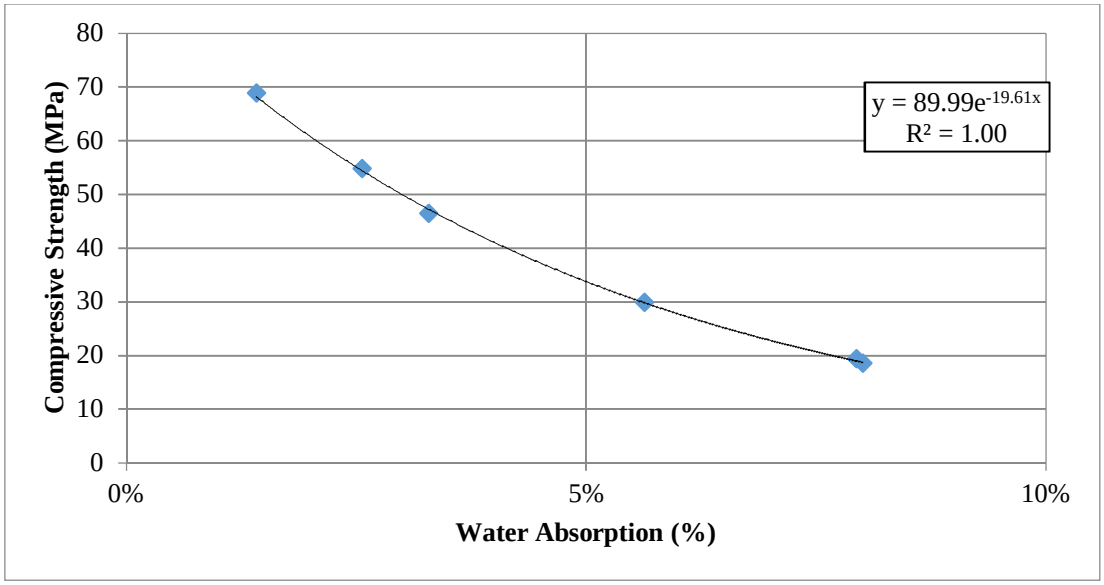

Figure 6-10 Relationship between 28-day compressive strength and average water absorption percent

[Reprint with permission from Monrose et al. (2019b)]

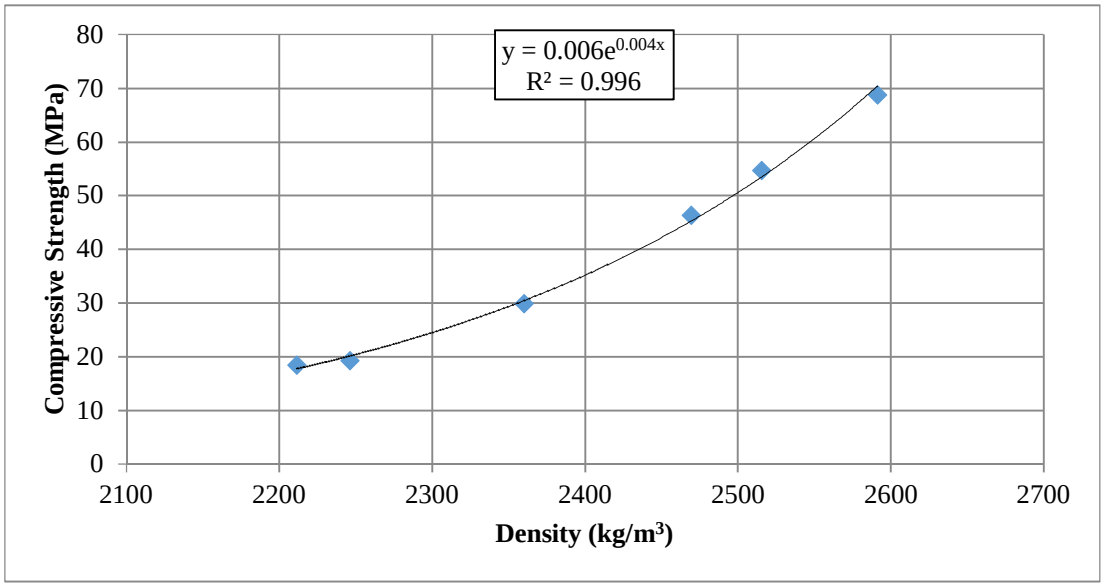

Figure 6-11 Relationship between 28-day compressive strength and density

[Reprint with permission from Monrose et al. (2019b)]

6.4.3 Splitting tensile strength

Tensile loading is usually carried by steel reinforcement in reinforced concrete. However, it is essentially unfeasible to use steel reinforcement in CPPB. It is necessary therefore, for a reliable assessment of the splitting tensile strength of concrete for application as CPPB.

The average 28-day splitting tensile strength results for each mix are shown in Figure 6-12. As with compressive strength values, splitting tensile strengths decreased exponentially with increasing percent CNA. The values ranged from 3.84 MPa (0% CNA mix) to 1.23 MPa (100% CNA mix). Again, this was expected because of the physical properties of the CNA as previously discussed. Equation 6-5 represents the best fit for the results. According to ASTM C330/C330M-17 (ASTM International, 2017a), a 28-day splitting tensile strength of 2.0 MPa is the minimum requirement for structural lightweight aggregate concrete. Natural aggregates replaced with ≤50 wt.%CNA satisfied this minimum requirement.

$$f_{ct} = 3.36e^{-0.01CNA} \quad (6\text{-}5)$$

where f_{ct} is the 28-day splitting tensile strength (MPa) and CNA is the percentage of Carbon-Negative Aggregates added by mass.

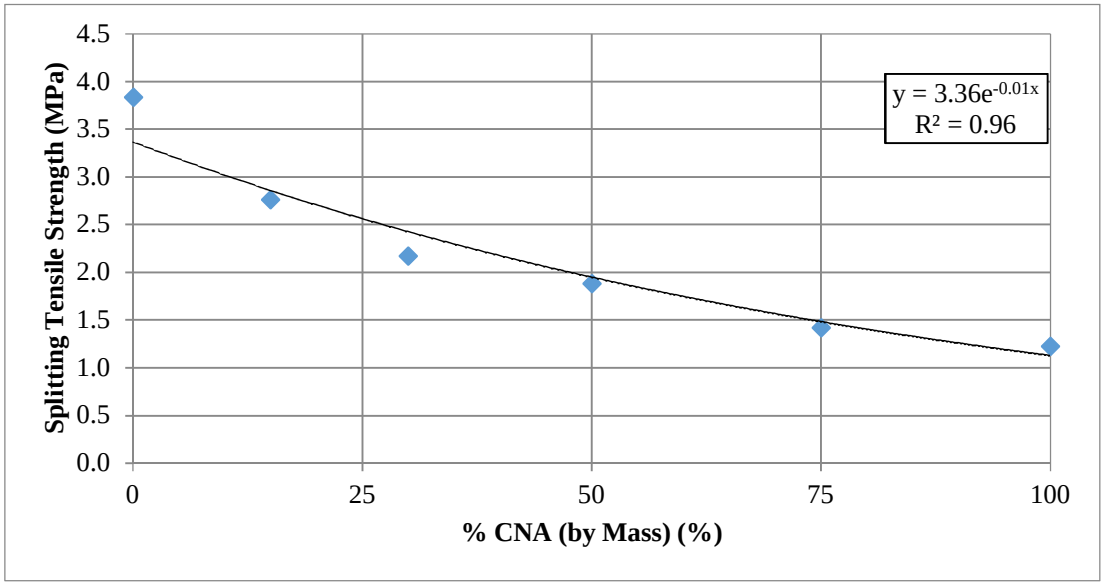

Figure 6-12 Relationship between 28-day splitting tensile strength and %CNA [Reprint with permission from Monrose et al. (2019b)]

Images of some cylinder samples after splitting are shown in Figure 6-13. The predominant mode of failure of all concrete mixes was coarse aggregate failure. Minute cracks (< 2 μm) at the interfacial bond between the CNA and the cementitious paste were observed through

SEM microstructural examination of the fractured surfaces. These cracks were insignificant, thereby confirming good bonding between aggregates and the cementitious paste.

(a) (b) (c) (d) (e) (f)

Figure 6-13 Photos of samples after splitting tensile strength tests (a) 0%CNA, (b) 15%CNA, (c) 30%CNA, (d) 50%CNA, (e) 75%CNA, (f) 100%CNA
[Reprint with permission from Monrose et al. (2019b)]

6.4.4 Relationship between splitting tensile strength and compressive strength

Splitting tensile strength and compressive strength are widely used indices for characterising the mechanical properties of concrete (Gencel et al., 2012). Splitting tensile strength can be estimated from compressive strength using Equation 6-6 (Mehta and Monteiro, 2006, ACI, 2014). An increase in compressive strength results in a general increase in splitting tensile strength.

$$f_{ct} = A f_{cu}^{B} \quad (6\text{-}6)$$

where f_{ct} is the 28-day splitting tensile strength (MPa), f_{cu} is the cube compressive strength (MPa); A and B are adjustable parameters.

Figure 6-14 shows the relationship between 28-day splitting tensile strength and compressive strength of the concrete mixes. Coefficient of determination (R^2) of the relationship was found to be 0.95 which shows satisfactory correlation. Equation 6-7 represents the best fit for the results presented. For comparison, other proposed relationships (Equations 6-8 to 6-11) from the literature are also shown in Figure 6-14. Equation 6-8 was proposed by Lo et al. (2016) for lightweight aggregate concrete containing sintered high-carbon fly ash aggregates with a cubical compressive strength range of 33–55 MPa. Equation 6-9 was proposed by Gesoğlu et al. (2004) for lightweight aggregate concrete containing cold-bonded fly ash with a cubical compressive strength range of 20–47 MPa. Equation 6-10 was

proposed by ACI 318-14 (ACI, 2014) for normal weight concrete with 28-day cylinder compressive strength range of 21–83 MPa. Equation 6-11 was proposed by BS EN 1992 BSI (2004).

By analysing Figure 6-14, it is found out that the equations provided by ACI 318, BS EN 1992, Gesoğlu et al. (2004) and Lo et al. (2016) overestimated the splitting tensile strength by on average 72%, 57%, 41% and 13% respectively.

$$f_{ct} = 0.15 f_{cu}^{0.74} \quad (6\text{-}7)$$

$$f_{ct} = 0.35 f_{cu}^{0.53} \quad (6\text{-}8)$$

$$f_{ct} = 0.27 \sqrt[3]{f_{cu}^{2}} \quad (6\text{-}9)$$

$$f_{ct} = 0.59 f_{cy}^{0.5} \quad (6\text{-}10)$$

$$f_{ct} = 0.30 f_{cu}^{(2/3)} \quad (6\text{-}11)$$

where f_{ct} is the 28-day splitting tensile strength (MPa), f_{cu} and f_{cy} are the cube and cylindrical 28-day compressive strengths (MPa), respectively.

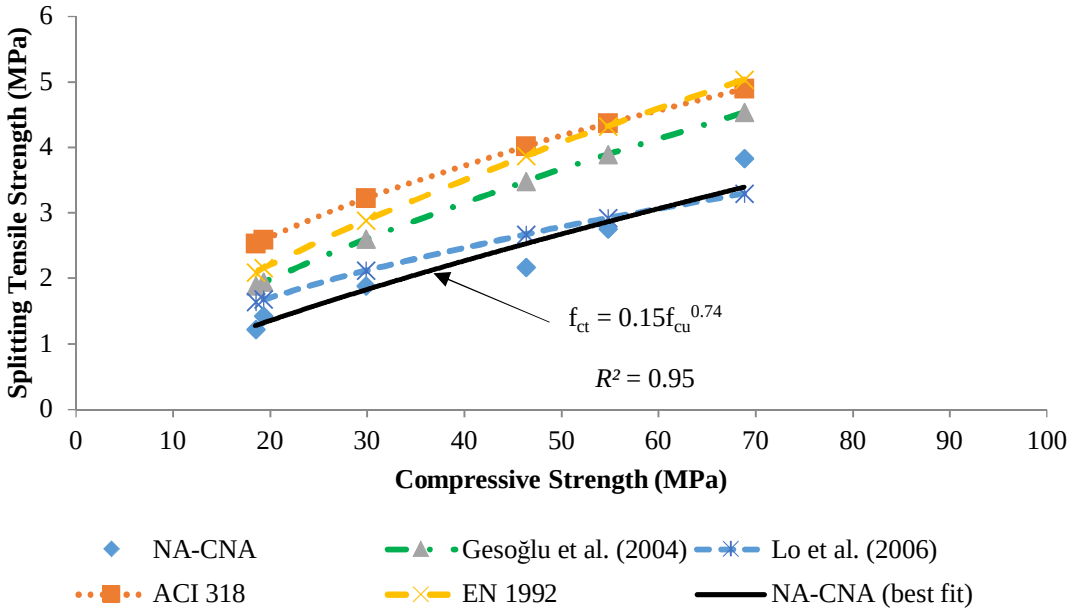

Figure 6-14 Relationship between compressive strength and splitting tensile strength [Reprint with permission from Monrose et al. (2019b)]

6.4.5 SEM observations

Scanning Electron Microscopy (SEM) was used to examine the micro-structure and bonding (ITZ) between the coarse aggregates and the cementitious paste. Bond strength is influenced by the shape of the aggregate, its surface texture and cleanliness. Angular, irregular or rough surface textured aggregates will result in stronger bonds between the aggregate and the paste rather than smooth, rounded aggregates (Dhir and Jackson, 1996). Figures 6-15 to 6-17 show the SEM micrographs for the CNA-paste ITZ whilst Figure 6-18 and Figure 6-19 show the micrographs for the natural aggregate-paste ITZ. As mentioned previously in subsection 6.3.1, two (2) samples were examined at selected points of interest along the bonding zone. The cementitious paste appeared to be homogenous and dense in both samples. Overall, the bonding between the two phases in both samples appeared to be solid. The continuous hydration of the cementitious paste promoted the formation of the cementitious matrix inside the pores of the CNA therefore 'gripping' the aggregate and producing good bonding between the phases (Juan, 2011). Some amount of micro-cracking (< 2 µm) was observed in both samples but appeared to be limited to the ITZ. This separation could have occurred during the preparation of the samples for examination through SEM. This possibility was reported by Kockal and Ozturan (2010).

Further examination of the CNA revealed numerous micro-cracks (< 2 µm) in a mapped pattern over the surface of the CNA as shown in Figure 6-20. This was not surprising given the low strength and pozzolanic nature of the CNA.

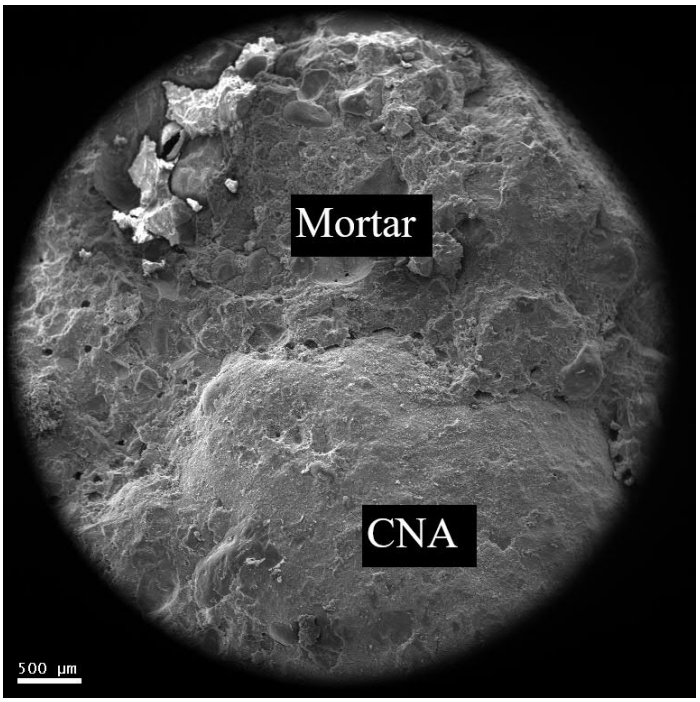

Figure 6-15 SEM micrograph of CNA-cementitious paste interface X 20

[Reprint with permission from Monrose et al. (2019b)]

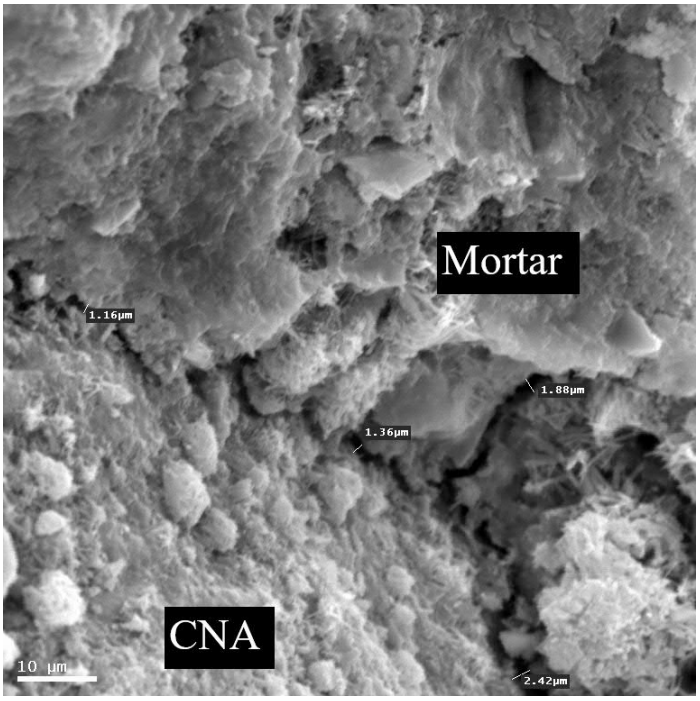

Figure 6-16 SEM micrograph of CNA-cementitious paste interface X 1360

[Reprint with permission from Monrose et al. (2019b)]

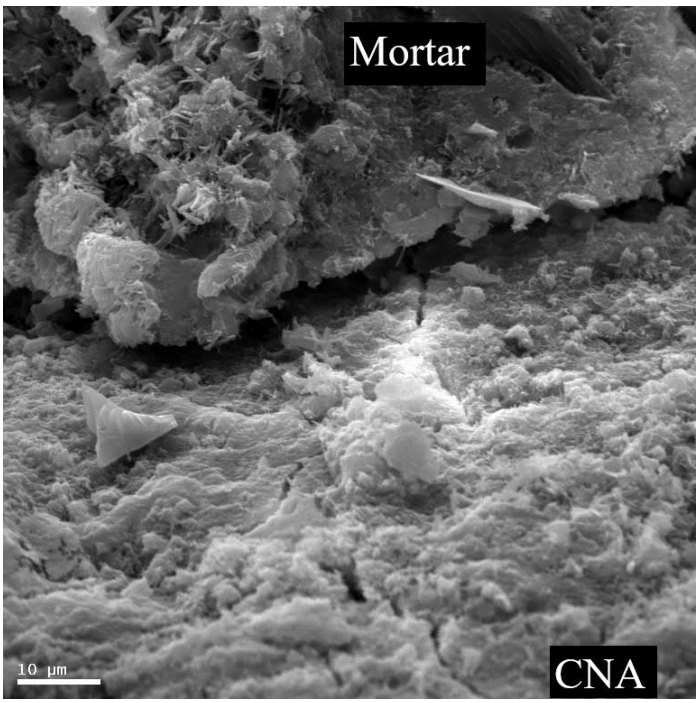

Figure 6-17 SEM micrograph of CNA-cementitious paste interface X 1420

[Reprint with permission from Monrose et al. (2019b)]

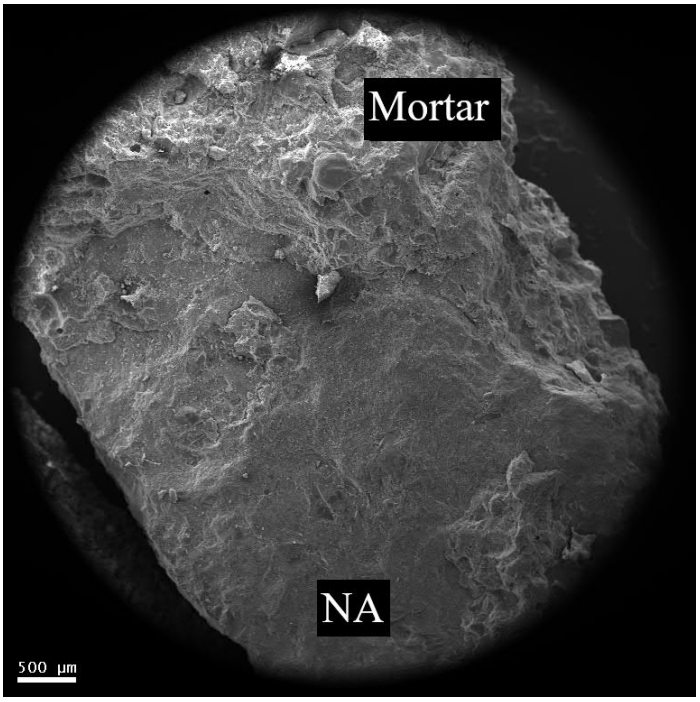

Figure 6-18 SEM micrograph of NA-cementitious paste interface X 20
[Reprint with permission from Monrose et al. (2019b)]

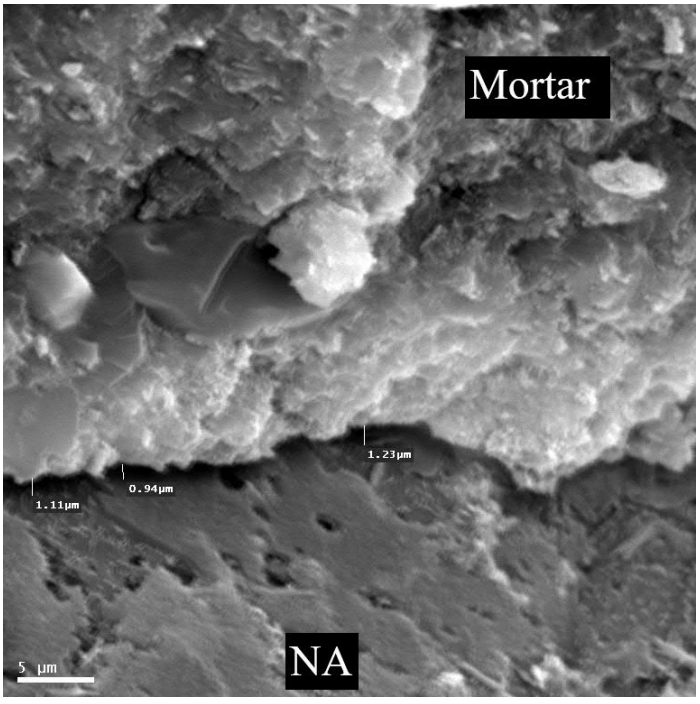

Figure 6-19 SEM micrograph of NA-cementitious paste interface X 2620
[Reprint with permission from Monrose et al. (2019b)]

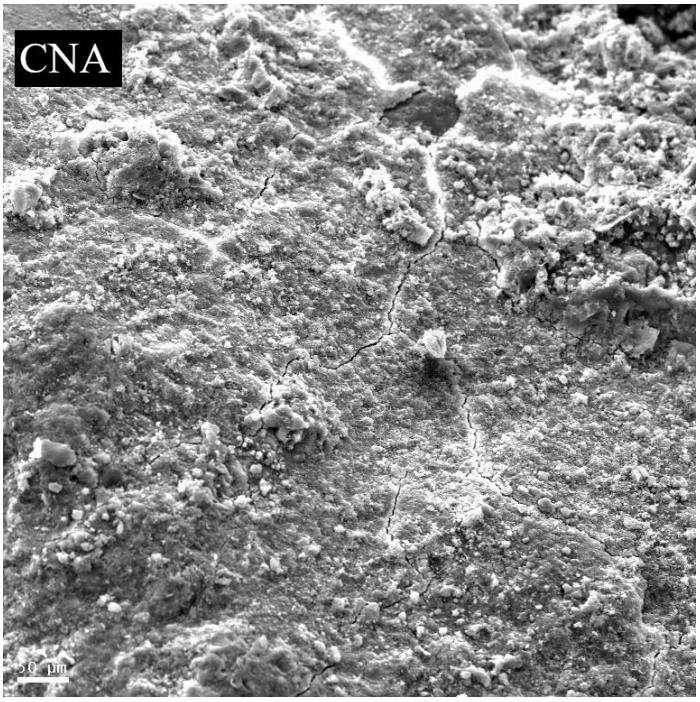

Figure 6-20 SEM micrograph of micro-cracking across CNA surface X 178
[Reprint with permission from Monrose et al. (2019b)]

6.5 Chapter summary

This chapter has examined the effect of CNA on the behaviour of concrete intended for use as novel Concrete Permeable Pavement Blocks (CPPB). Performance indicators targeted compressive strength, splitting tensile strength, density and water absorption. The methodology involved substituting natural aggregates by mass, with CNA at percentages varying from 0 to 100. A scanning electron microscope was used to examine the aggregate-mortar Interfacial Transition Zone (ITZ). Both the compressive and tensile strengths decreased exponentially with the addition of CNA. Average 28-day compressive and splitting tensile strengths ranged from 69 MPa (10000 PSI) to 18 MPa (2600 PSI) and 3.84 MPa (560 PSI) to 1.23 MPa (178 PSI) respectively. Density values decreased linearly with the addition of CNA with average values ranging from 2200 – 2600 kg/m3. Conversely, water absorption increased with increases in CNA with average values ranging from 1.66% to 9.17%. (5) Examination of the split aggregate-mortar ITZ revealed good bonding results for both the CNA and NA. Further examination of the CNA revealed micro-cracks (< 2 µm) over the surface of the CNA. The findings indicated that depending on loading requirements, CNA can replace natural aggregates in CPPB by up to 100%. This chapter answered research question number 5 listed in Chapter 1. The following chapter concludes the research.

CHAPTER 7. CONCLUSIONS, OUTLOOK AND FUTURE RESEARCH

7.1 Conclusions

This research project was undertaken to present novel Permeable Pavement Systems (PPS) as a viable, long-term, sustainable urban drainage option for reduction of flood risk and improvement in urban stormwater runoff quality in SIDS across the Caribbean and to evaluate the performance of recycled/recyclable and low-carbon materials in pavement construction. PPS reduce pollutants from infiltrating stormwater runoff, provide vital reservoir storage for potential reuse of stormwater and improve the hydrologic functions of various locations. The findings presented in this chapter conclude that all research questions listed in Chapter 1 have been answered. Conclusions drawn are organised in accordance with the six (6) research objectives listed in Chapter 1 and repeated hereafter.

1. Perform a comprehensive literature review and survey of PPS, challenges and opportunities of climate change and urban development in SIDS as well as the identification of key factors for consideration for widespread acceptance and utilisation of PPS in SIDS.
2. Assess the physical properties of the natural (basalt, quartzite) and recycled materials (CCA, CNA, C-EPS) and their behaviours in the laboratory.
3. Examine the chemical composition of recycled materials CCA, CNA and C-EPS and how they can be utilised.
4. Compare and evaluate in the laboratory, the performance of four (4) permeable pavement rigs; two containing recycled materials (CCA, C-EPS) and two made up of traditional materials (basalt, quartzite) in the following categories:
    a) Hydrological (lag time, attenuation and retention capacity)
    b) Hydraulic conductivity and long-term clogging
    c) Environmental (pollutant removal efficiencies)
    d) Structural integrity (stiffness and deflection profiles using PFWD testing)
5. Develop and calibrate hydrological rainfall-discharge models for each rig using the Computational Hydraulics International's (CHI) computer software, PCSWMM.
6. Examine the effect of CNA on the compressive and tensile strengths of concrete intended for use as novel Concrete Permeable Pavement Blocks (CPPB).

7.1.1 Objective 1

The answer to research question 1, "What are the key parameters for consideration for widespread acceptance and adoption of PPS in SIDS?" is provided herein. A comprehensive

literature review was undertaken to cover the requirements set out in Objective 1. This review, presented in Chapter 2, provided information about SIDS regarding geography, weather, climate, challenges and opportunities of climate change and urban development. The review also covered various aspects of PPS such as background, types, typical designs and performance (hydrological, pollutant removal, clogging and maintenance) evaluations. Very critical to the review, was the presentation and discussion of numerous key factors which could impact widespread acceptance and utilisation of PPS in SIDS. The review found that unlike most territorial states, the geographically and geologically confined nature of most SIDS present unique parameters for evaluation when designing permeable pavements for SIDS. These parameters include traffic loads, cost, construction aggregate choice(s) and availability, permeability of existing soil at the intended location, depth of water table, potential for groundwater contamination, slope of the pavement, stormwater reuse option, clogging, maintenance and support from policy makers. The review further confirmed a lack of published studies of PPS being an integral part of stormwater management systems across SIDS but found numerous studies of successful applications of permeable pavements in developed areas such as in the USA, UK, Europe and Australia. Moreover, despite the widely reported use of PPS, only a handful of studies have reported on the utilisation and performance of recycled waste materials as sustainable construction materials in PPS.

7.1.2 Objectives 2 and 3

The answers to research question 2, "What are the physical and chemical properties of CCA, CNA and C-EPS?" and question 3, "Are CCA, CNA and C-EPS suitable for use as sub-base materials in permeable pavements?" are provided herein. The physical and chemical properties of the CCA, C-EPS, CNA, basalt and quartzite aggregates were discussed in Chapter 3. All physical tests on the aggregates were performed in the laboratory in accordance with the widely used ASTM or BS standards. The specific gravity of the CCA was as expected, lower than that of basalt and quartzite aggregates but can be considered as high-quality aggregates. The specific gravity of CNA was approximately 40% lower than CCA confirming their lightweight characteristics. The water absorption of the CCA was significantly higher than that of basalt and quartzite aggregates but was within the acceptable range of water absorption values for recycled materials in unbound applications. The water absorption of CNA was at least three (3) times the water absorption of CCA. CCA performed remarkably well (and better than quartzite aggregates) under the L.A abrasion and impact tests with results below 50%. CNA L.A abrasion values were approximately 33% higher than CCA. The pH values of both CCA and CNA indicated that materials were highly alkaline. The compressive strength and permeability of C-EPS was found satisfactory for use in

permeable pavements. However, C-EPS was not recommended for use under vehicular loading because of its low compressive strength (< 1.0 MPa).

Chemical testing of the CNA, CCA and C-EPS was done using an X-ray fluorescence spectrometer (XRF). Chemical testing was not performed on the basalt and quartzite aggregates. The chemical testing found that CNA consisted predominantly of CaO at 49%, SiO_2 at 20% and Cl at 15%. CCA contained mostly CaO and SiO_2 at 29% and 62% respectively whereas C-EPS consisted predominantly of CaO, SiO_2 and C at 52%, 16% and 20% respectively.

The results of the physical and chemical testing undertaken in this research show that both CCA and C-EPS were suitable for use as sub-base materials in PPS. However, C-EPS usage was not recommended for pavements constructed for vehicular traffic because of its low compressive strength (< 1.0 MPa). CNA were found unsuitable as sub-base materials because they lacked strength (66% L.A Abrasion), had high water absorption properties (23.6%) and had the potential to leach excessive amounts of chlorides and other compounds into the environment. CNA was instead used as a bound recycled material in the production of Concrete Permeable Pavement Blocks (CPPB).

7.1.3 Objectives 4

The answer to research question 4, "How do the performances (bearing capacity, permeability, long-term clogging, attenuation and retention capacity, pollutant removal efficiency) of pilot-scale permeable pavement rigs that contain natural aggregates (basalt or quartzite) compare to rigs that contain CCA and C-EPS?" is provided herein. The methodology for the design, construction and testing of the permeable pavement rigs was presented in Chapter 3 and evaluations of the performances of those rigs were presented in Chapter 4. The design of the pavements was carried out in accordance with guidance from literature sources. Performances of the permeable pavement rigs were evaluated in four (4) categories:

7.1.3.1 **Hydrological performance in terms of lag time, attenuation and retention capacity**

Hydrological experiments were conducted to investigate the influence of high intensity and short duration rainfall events on the lag time, attenuation and retention capacity of the permeable pavement rigs. A purpose-built Rainfall Simulation Infiltrometer (RSI), was used to simulate the rainfall events using ordinary tap water. All four (4) rigs behaved similarly in terms of their discharge response to rainfall events. After 53 total rainfall simulation

events, no surface runoff was observed and no statistically significant differences in lag times ($p > 0.05$) were observed between Rigs 1, 2 or 3 which contained quarried basalt, quartzite aggregates and CCA respectively in the sub-base. However, significant differences in lag time ($p < 0.05$) were observed between Rig 4 which contained a monolithic C-EPS filter block and Rigs 1, 2 or 3. In terms of maximum retention (storage) capacity, no significant differences ($p > 0.05$) were found between the four (4) rigs. Lag times averaged 1.5 min for all rigs except Rig 4 which averaged 2.0 min. At least 20% of rainfall by volume was temporarily detained during simulated rainfall events for all rigs. The results showed that under high intensity (> 250 mm/h) and short duration (15 min) simulated rainfall events, the retention capacity of the permeable pavement rigs containing recycled materials (CCA and C-EPS) and natural materials (basalt aggregates and quartzite aggregates) were not significantly different. However, C-EPS increased the retention capacity of the permeable pavements when compared to CCA, quarried basalt and quartzite aggregates.

7.1.3.2 **Water quality performance**

The pollutant removal efficiencies of the four (4) permeable pavement rigs in the laboratory were evaluated using field stormwater runoff collected from various municipalities across Trinidad, W.I. Overall, numerous variations in pollutant removal efficiencies were observed between the rigs.

Significant differences ($p < 0.01$) were found in pH, EC, TDS, DO, PO_4- and SO_4^{2-}, across all rigs. Mean effluent pH values from Rig 1 (7.8 ± 0.1) and Rig 2 (7.9 ± 0.1) were neutral while mean effluent pH values from Rig 3 (12.0 ± 0.1) and Rig 4 (12.3 ± 0.1) were alkaline. EC values increased for all rigs. Rig 1 and Rig 2 had slight increases (33.5% and 17.2% respectively) whereas significant increases were observed from Rig 3 and Rig 4 (908% and 1895% respectively). TDS removal percentages were negative for all rigs. Rig 1 increased TDS by 48%, Rig 2 by 31%, Rig 3 by 212% and Rig 4 by 387%. DO was slightly reduced by 2% from Rigs 1 and 2. Rigs 3 and 4 on the contrary, produced a slight increase in DO by 3% and 5% respectively. Further analysis from Rig 4 found DO values increased by 200% in some samples. DO concentration results from Rig 4 were inconclusive and require further research. In terms of PO_4^{3-}, Rigs 1 and 2 recorded slight increases in PO_4^{3-} of 22% and 9% respectively, while Rigs 3 and 4 had reductions of 18% and 33% respectively. In terms of SO_4^{2-}, Rigs 1 and 2 recorded significant increases in SO_4^{2-} (121% and 66% respectively) while Rig 3 and Rig 4 recorded 33% and 74% reductions in SO_4^{2-} respectively.

With respect to TSS, turbidity, COD, NO_3-N, Zn, Cu, Mn and Fe, no significant differences ($p > 0.05$) were found across all rigs. TSS removal percentages were considerably high for all rigs. Rig 1 had the lowest removal percentages of 52% whilst Rig 4 had the highest, 64%. Rigs 2 and 3 had removal percentages of 53% and 58% respectively. All rigs had positive removal rates for turbidity with Rig 4 recording the highest (57%) while Rig 3 the lowest (10%). Rigs 1 and 2 reduced turbidity by 37% and 31% respectively. COD removal was similar amongst all rigs, ranging from 4.2% (Rig 2) to 7.2% (Rig 1). Rigs 3 and 4 reduced COD by 4.5% and 6.5% respectively. All rigs except Rig 3 had increases in NO_3-N. Rig 1 increased NO_3-N by 27%, Rig 2 by 21% and Rig 4 by 98%. Rig 3 reduced NO_3-N by 20%. For all rigs, there were increases in all metal concentrations except for Rigs 3 and 4 which removed 5% and 10% of Zn respectively and Rig 2 which removed 2% of Fe. Rigs 1, 2 and 3 increased Cu by 16% whilst Rig 4 increased Cu by 6%. Rigs 1 and 2 increased Zn by 7% and 10% respectively. Mn had the largest increases; Rig 1 increased Mn by 38%, Rig 2 by 119%, Rig 3 by 135% and Rig 4 by 71%. Rigs 1, 3 and 4 increased Fe by 1% from Rig 1, 11% and 20% respectively.

Despite the negative removal efficiencies reported, all mean pollutant concentrations were within the Maximum Permissible Levels (MPLs) of water pollutants discharged into the environment according to the Trinidad and Tobago Environmental Management Authority (EMA) and the United States Environmental Protection Agency (US EPA). In this regard, the CCA and C-EPS performed satisfactorily as sub-base materials in the permeable pavement rigs.

7.1.3.3 **Hydraulic conductivity and long-term clogging**

Hydraulic conductivity and long-term clogging patterns were assessed from the simulation of 10 years of accumulated natural sediment. Hydraulic conductivity measurements were made after each simulated year. The results showed an exponential decline in hydraulic conductivity as a function of service life (age) of the permeable pavement rigs. Hydraulic conductivities were reduced by 45%, 44%, 50% and 51% in Rig 1, Rig 2, Rig 3 and Rig 4 respectively. Pearson's correlations, r and regression models were performed to test the hypothesis that the hydraulic conductivity of permeable pavements decreases over time because of clogging. The results of the Pearson's correlation, r, showed that for all rigs, there was a significant ($p < 0.01$) negative and strong correlation between hydraulic conductivity and service life (age) of the pavements. A comparison between linear and exponential regression models confirmed that the exponential regression models simulated a better fit of the observed values. The results were similar for all rigs, confirming that the sub-base

component did not significantly affect the clogging pattern of the permeable pavement rigs. The results confirmed that the hydraulic conductivity of permeable pavements decrease exponentially over time because of clogging. Rapid reduction in hydraulic conductivity occurred during the first few simulated years of accumulation of sediments over the surface joints of the permeable pavement rigs.

7.1.3.4 **Stiffness and deflection**

The as-built load bearing capacity (stiffness and deflection) of the pavement rigs was evaluated through Portable Falling Weight Deflectometer (PFWD) testing in the laboratory. All rigs behaved differently in terms of surface modulus and deflection. Rig 1 (basalt) recorded the lowest mean deflection (493 ± 10.1 μm) and the highest mean surface modulus (53 ± 1.1 MPa) whereas Rig 4 (C-EPS) recorded the highest mean deflection (1095 ± 14.6 μm) and the lowest mean surface modulus (24 ± 0.3 MPa). Rig 3 had mean deflection and surface modulus values of 873 ± 9.8 μm and 30 ± 0.3 MPa respectively whilst Rig 2 had mean deflection and surface modulus values of 681 ± 7.4 μm and 39 ± 0.5 MPa respectively. The results of the as-built PFWD testing have demonstrated that CCA and C-EPS can maintain the structural integrity of permeable pavements when used as sub-base materials. However, due to lower stiffness and higher deflection values obtained from Rig 4 which contained C-EPS it is recommended that Rig 4 be used as pavements only in non-vehicular trafficked surfaces such as building aprons, sidewalks, footpaths, landscapes, pedestrian access and bicycle lanes. To accommodate light vehicular traffic, structural modifications to the pavement structure such as an increase in the thickness of the base layer may be considered and evaluated.

7.1.4 Objective 5

The answer to research question 5, "Is the PCSWMM model able to accurately simulate the outflow from permeable pavements containing CCA and C-EPS in the sub-base?" is provided herein. PCSWMM was used to develop and calibrate rainfall-discharge models of the permeable pavement rigs. The models were calibrated and validated using data obtained from the simulated hydrological performance assessments presented previously in subsection 4.2. High-intensity, short-duration rainfall events (at least 50-year return period) were simulated. Parameter values were estimated based on guidance from literature and from the results obtained from the hydrological performance experiments presented previously. The results found that for all rigs, the drain exponent parameter in the SWMM LID module was the most sensitive LID parameter followed by storage void ratio. Excellent model results according to goodness-of-fit measures NSE, R^2 and RMSE were obtained for the four (4)

rigs during calibration and validation. Additionally, comparison of modelled and observed hydrographs revealed excellent fits for all rigs. PCSWMM was therefore able to accurately model the outflow from all the pavement rigs with similar accuracy.

7.1.5 Objective 6

The answer to research question 6, "What is the effect of CNA on the behaviour of concrete intended for use as solid concrete block pavers in permeable pavements?" is provided herein. The experiment presented in Chapter 6, investigated for the first time, the performance, structurally, when commercially produced lightweight Carbon-Negative Aggregates (CNA), were used in concrete to produce Concrete Permeable Pavement Blocks (CPPB). Natural aggregates were substituted by mass, with CNA at varying percentages ranging from 0 to 100%. Compressive and splitting tensile strengths at 28 days and water absorption tests were evaluated and compared. The results found that depending on structural loading requirements, CNA can replace natural aggregates in CPPB by up to 100%. The high-water absorption percent in CNA necessitates pre-soaking or increasing the water/cement ratio when increasing the mass of CNA in concrete. The 28-day compressive strengths and densities ranged from 18.48 to 68.80 MPa and from 2236 to 2612 kg/m^3, respectively. The 28-day splitting tensile strengths and water absorption percentages ranged from 1.23 to 3.84 MPa and from 1.66 to 9.17%, respectively. Examination of the split aggregate-cementitious paste interfacial transition zone through SEM microstructural studies revealed good bonding results for both the CNA and natural aggregates. Further examination of the CNA revealed micro-cracks (< 2 µm) over the surface of the CNA.

The overall findings of this research project show that Permeable Pavements Systems (PPS) can contribute tremendously to an improvement in the management of urban drainage in SIDS across the Caribbean and that CNA, CCA and C-EPS can be used as suitable replacements for natural aggregates in permeable pavements to produce sustainable, eco-friendly pavements. This can be significant as it presents opportunities for the conservation of rapidly-diminishing natural rocks; significantly reduce the carbon footprint during the production phase of pavements and promote an ecologically-sustainable solution to assist in the management of Municipal Solid Waste (MSW).

7.1.6 Policy implications of the research

To reiterate from Chapter 1, urban stormwater management remains a huge challenge for SIDS authorities which often translates into their inability to mitigate yearly flooding within urban municipalities creating undue distress, lost time and money and frustration.

Traditionally, flooding has been viewed as an externality problem (rainfall and the ensuing runoff) across the Caribbean. Consequently, flood control is not prioritised and is often dealt with reactively. This is evident in Trinidad and Tobago, W.I., for instance, as according to Hassanali (2019), the Government of the Republic of Trinidad and Tobago (GoRTT) spent TT$ 66 million (USD 1.0 million) over a 12-year period on flood prevention and alleviation studies with little to no benefit to the country, as majority of these studies were shelved and unused. Other reactive spending instances include expensive water treatment methods being applied to polluted water sources rather than preventing the pollution and drainage channels being often cleared of solid wastes, rather than the solid waste problem addressed beforehand (Reed, 2004).

SIDS challenges regarding stormwater management are further exacerbated when institutions charged with enforcing polices relating to development and stormwater management, are relaxed in their approach and do little to stop or prevent unplanned or unapproved construction. These unplanned developments contribute immensely to flooding. Again, this is evident in countries such as Trinidad and Tobago and St. Lucia, W.I. by the vast number of unapproved dwellings allowed to be constructed along drainage reserves, flood plains, and hillsides.

The proposed adoption of PPS for incorporation into existing urban stormwater management regimes across Caribbean SIDS will most likely require policy shifts, aggressive education drives and cooperation amongst specific state organisations. Moreover, collaborative efforts amongst key stakeholders such as stormwater management agencies, construction companies, universities, financial organisations and politicians, towards scientific data gathering, installation and maintenance of field test sites and development of guidelines and specifications, will be essential for these successful shifts in policy.

This research encourages Caribbean SIDS governments to implement policies to minimise impervious surfaces by using PPS for lightly-trafficked areas such as sidewalks, building aprons and parking lots in an effort to reduce stormwater runoff. The adoption of PPS promotes a shift away from the reliance on conventional stormwater control measures that focus solely on downstream control, to a more upstream or source control measure. Permeable pavements have been demonstrated to reduce runoff and flood risk in addition to improve stormwater runoff quality. The existing conventional drainage systems in urban areas across Caribbean SIDS, dominated by concrete drains and culverts are mostly restricted in terms of expansion, hence adaptation to climate change and urbanisation is a huge challenge; one which should not be ignored by policy makers.

With regards to the use of recycled materials in the construction of permeable pavements, it may be incumbent on governments to issue market-based policy instruments such as incentives and subsidies towards promoting the use of recycled materials as a form of sustainable and environmental innovation in construction. Most SIDS across the Caribbean have diminishing natural rocks; hence governments should keep a keen interest and encourage the use of recycled materials in construction where appropriate.

The successful implementation, operation and maintenance of PPS in SIDS is heavily dependent on aggressive enforcement of policies that address stormwater management using PPS and SUDS in general. There is an increasing demand for improved stormwater management across Caribbean SIDS. Governments need to be cognizant of the added benefits of adequately managed SUDS such as PPS in addition to the various issues which may be confronted. This knowledge would seek to reduce the need for reactive spending and promote long-term integrated planning instead. There are currently no guidelines developed for PPS specifically targeting SIDS across the Caribbean. Developed nations such as the USA, UK and Australia are far ahead in this regard. This research presents opportunities to development these guidelines for the eventual widespread implementation of PPS across Caribbean SIDS.

7.2 Outlook and future research

This research has presented and discussed findings based on a multi-disciplinary scope regarding permeable pavement for SIDS and the use of recycled materials therein. Listed below are a set of research ideas which provide continuity to this research.

1. To evaluate the performance of PPS containing CCA, C-EPS, CNA or other low-carbon or recycled materials on a field scale setting across Caribbean SIDS. The results of the evaluation s will allow for durability assessments based on short, medium or long-term timelines to be made.
2. To model the hydraulic impact (i.e., impervious vs. pervious) of permeable pavement on a small tropical urban catchment.
3. To evaluate the possible use of stored water from permeable pavements containing CCA, C-EPS or CNA. In this regard, it is further recommended that total metal and leachate testing be conducted.
4. To conduct a detailed life cycle cost analysis of low-carbon permeable pavements taking into consideration the use of recycled/recyclable materials such as CCA, C-EPS and CNA. SIDS usually do not prioritise financial resources to drainage infrastructural projects. As such, additional research into a life cycle cost analysis of

PPS in the Caribbean is recommended. Perhaps innovative ways of reducing the initial costs of PPS can also be researched.

5. Further research is required regarding the performance of PPS installed on expansive clays. PPS installations over fine-grained soils such as expansive clays with little to no infiltration is not ideal but this soil type is found is numerous Caribbean SIDS.
6. To investigate the impact of effluent control (e.g., through valves or raised discharge pipes) to optimise hydraulic performance and storage of water in permeable pavements.
7. To study the hydrological impact of other SUDS in combination with PPS on urban catchments across SIDS.
8. Further research is required regarding the short- and long-term effects of pollutants that remain in the PPS.
9. The nutrient removal capabilities of permeable pavements are not yet fully understood and requires further research as numerous studies have reported varying results.

REFERENCES

AASHTO (1993) *AASHTO Guide for Design of Pavement Structures*, Washington, DC USA: AASHTO.

Abbott, C. L. & Comino-Mateos, L. (2003) In-situ Hydraulic Performance of a Permeable Pavement Sustainable Urban Drainage System. *Water and Environment Journal*. 17. (3), pp. 187–190.

Abdollahian, S., Kazemi, H., Rockaway, T. & Gullapalli, V. (2018) Stormwater quality benefits of permeable pavement systems with deep aggregate layers. *Environments*. 5. (6), pp. 68.

Abouhussien, A. A., Hassan, A. A. A. & Ismail, M. K. (2015) Properties of semi-lightweight self-consolidating concrete containing lightweight slag aggregate. *Construction and Building Materials*. 75 pp. 63–73.

Acevedo Mejia, S. (2016) *Gone with the Wind: Estimating Hurricane and Climate Change Costs in the Caribbean*. Washington, D.C.: IMF. (WP/16/199).

ACI (2013) *308-213R-13 Report on Internally Cured Concrete Using Prewetted Absorptive Lightweight Aggregate*. MI, USA: ACI.

ACI (2014) *Building code requirements for structural concrete (ACI 318-14) and commentary*, MI, USA: American Concrete Institute.

Adachi, K. & Tainosho, Y. (2004) Characterization of heavy metal particles embedded in tire dust. *Environment International*. 30. (8), pp. 1009–1017.

ADB (2014) *The State of Pacific Towns and Cities: Urbanisation in ADB's Pacific Developing Member Countries*. Mandaluyong City, Philippines: ADB.

Agyei, N. M., Strydom, C. A. & Potgieter, J. H. (2002) The removal of phosphate ions from aqueous solution by fly ash, slag, ordinary Portland cement and related blends. *Cement and Concrete Research*. 32. (12), pp. 1889–1897.

Ahn, J., Marcaida, A. K., Lee, Y. & Jung, J. (2018) Development of Test Equipment for Evaluating Hydraulic Conductivity of Permeable Block Pavements. *Sustainability*. 10. (7), pp. 2549.

Akhtar, A. & Sarmah, A. K. (2018) Construction and demolition waste generation and properties of recycled aggregate concrete: A global perspective. *Journal of Cleaner Production*. 186 pp. 262-281.

Alley, E. R. (2007) *Water Quality Control Handbook*, 2nd Ed. New York: McGraw-Hill.

Alshibli, K. A., Abu-Farsakh, M. & Seyman, E. (2005) Laboratory evaluation of the geogauge and light falling weight deflectometer as construction control tools. *Journal of materials in Civil Engineering*. 17. (5), pp. 560-569.

Alsubih, M., Arthur, S., Wright, G. & Allen, D. (2017) Experimental study on the hydrological performance of a permeable pavement. *Urban Water Journal*. 14. (4), pp. 427–434.

Alyaseri, I. & Zhou, J. (2016) Stormwater Volume Reduction in Combined Sewer Using Permeable Pavement: City of St. Louis. *Journal of Environmental Engineering*. 142. (4), pp. 04016002.

Amini, K., Wang, X. & Delatte, N. (2018) Statistical Modeling of Hydraulic and Mechanical Properties of Pervious Concrete Using Nondestructive Tests. *Journal of Materials in Civil Engineering Sustainability*. 30. (6), pp. 04018077.

Andersen, C. T., Foster, I. D. L. & Pratt, C. J. (1999) The role of urban surfaces (permeable pavements) in regulating drainage and evaporation: development of a laboratory simulation experiment. *Hydrological processes*. 13. (4), pp. 597–609.

Andrés-Valeri, V. C., Marchioni, M., Sañudo-Fontaneda, L. A., Giustozzi, F. & Becciu, G. (2016) Laboratory Assessment of the Infiltration Capacity Reduction in Clogged Porous Mixture Surfaces. *Sustainability*. 8. (8), pp. 751.

Antunes, L. N., Thives, L. P. & Ghisi, E. (2016) Potential for Potable Water Savings in Buildings by Using Stormwater Harvested from Porous Pavements. *Water*. 8. (4), pp. 110.

APHA (1998) *Standard Methods for the Examination of Water and Wastewater, 20th Edition*, Washington, DC, USA: American Water Works Association (AWWA), American Public Health Association (APHA), Water Environment Federation (WEF).

Armitage, N. (2011) The challenges of sustainable urban drainage in developing countries. In: *SWITCH Paris Conference*. Paris, January 2011. pp. 132–142.

Arulrajah, A., Piratheepan, J., Disfani, M. M. & Bo, M. W. (2013) Geotechnical and geoenvironmental properties of recycled construction and demolition materials in pavement subbase applications. *Journal of Materials in Civil Engineering*. 25. (8), pp. 1077–1088.

Asaeda, T. & Ca, V. T. (2000) Characteristics of permeable pavement during hot summer weather and impact on the thermal environment. *Building and Environment*. 35. (4), pp. 363-375.

ASTM International (2003) *Standard C33/C33M-16 Standard specification for concrete aggreates*, West Conshohocken, PA USA: ASTM International.

ASTM International (2009a) *C1701/C1701M Standard Test Method for Infiltratin Rate of In Place Pervious Concrete*, West Conshohocken, PA USA: ASTM International.

ASTM International (2009b) *D3385 Standard Test Method for Infiltration Rate of Soils in Field Using Double-Ring Infiltrometer*, West Conshohocken, PA USA: ASTM International.

ASTM International (2011) *Standard E2835-11 Standard Test Method for Measuring Deflections using a Portable Impulse Plate Load Test Device,* West Conshohocken, PA USA: ASTM International.

ASTM International (2013) *Standard C642 Standard Test Method for Density, Absorption, and Voids in Hardened Concrete,* West Conshohocken, PA USA: ASTM International.

ASTM International (2014a) *C131/C131M Standard Specification for Concrete Grid Paving Units,* West Conshohocken, PA USA: ASTM International.

ASTM International (2014b) *C131/C131M Standard Test Method for Resistance to Degradation of Small-Size Coarse Aggregate by Abrasion and Impact in the Los Angeles Machine,* West Conshohocken, PA USA: ASTM International.

ASTM International (2014c) *C136/C136M Standard Test Method for Sieve Analysis of Fine and Coarse Aggregates,* West Conshohocken, PA USA: ASTM International.

ASTM International (2015) *C127 Standard Test Method for Relative Density (Specific Gravity) and Absorption of Coarse Aggregate,* West Conshohocken, PA USA: ASTM International.

ASTM International (2016a) *C33/C33M-16 Standard specification for concrete aggreates,* West Conshohocken, PA USA: ASTM International.

ASTM International (2016b) *C29/C29M Standard Test Method for Bulk Density ("Unit Weight") and Voids in Aggregate,* West Conshohocken, PA USA: ASTM International.

ASTM International (2016c) *D5231-92 Standard Test Method for Determination of the Composition of Unprocessed Municipal Solid Waste,* West Conshohocken, PA USA: ASTM International.

ASTM International (2017a) *C330/C330M Standard Specification for Lightweight Aggregates for Structural Concrete*, West Conshohocken, PA USA: ASTM International.

ASTM International (2017b) *C150/C150M Standard Specification for Portland Cement,* West Conshohocken, PA USA: ASTM International.

ASTM International (2017c) *C496/C496M Standard Test Method for Splitting Tensile Strength of Cylindrical Concrete Specimens,* West Conshohocken, PA USA: ASTM International.

ASTM International (2018a) *C33 Standard Specification for Concrete Aggregates,* West Conshohocken, PA USA: ASTM International.

ASTM International (2018b) *C936/C936M Standard Specification for Solid Concrete Interlocking Paving Units,* West Conshohocken, PA USA: ASTM International.

ASTM International (2018c) *D4439 Standard Terminology for Geosynthetics,* West Conshohocken, PA USA: ASTM International.

AWWA (2011) *Water Quality & Treatment A handbook on Drinking Water,* 6th Ed. New York: McGraw-Hill.

Aziz, H. A., Othman, N., Yusuff, M. S., Basri, D. R. H., Ashaari, F. A. H., Adlan, M. N., Othman, F., Johari, M. & Perwira, M. (2001) Removal of copper from water using limestone filtration technique: determination of mechanism of removal. *Environment International*. 26. (5), pp. 395–399.

Babinard, J., Bennett, C. R., Hatziolos, M. E., Faiz, A. & Somani, A. (2014) Sustainably managing natural resources and the need for construction materials in Pacific island countries: The example of South Tarawa, Kiribati. *Natural Resources Forum*. 38. (1), pp. 58–66.

Babu, D. S., Babu, K. G. & Wee, T. H. (2005) Properties of lightweight expanded polystyrene aggregate concretes containing fly ash. *Cement and Concrete Research*. 35. (6), pp. 1218–1223.

Baker, M. B., Abendeh, R., Abu-Salem, Z. & Khedaywi, T. (2016) Production of sustainable asphalt mixes using recycled polystyrene. *International Journal of Applied Environmental Sciences*. 11. (1), pp. 183-192.

Balades, J. D., Legret, M. & Madiec, H. (1995) Permeable pavements: Pollution management tools. *Water Science and Technology*. 32. (1), pp. 49–56.

Ball, J. E. & Rankin, K. (2010) The hydrological performance of a permeable pavement. *Urban Water Journal*. 7. (2), pp. 79–90.

Barnett, J. & Campbell, J. (2010) *Climate Change and Small Island States. Power, knowledge and the South Pacific,* New York/London: Earthscan.

Bateni, N., Lai, S. H., Putuhena, F. J., Mah, D. Y. S., Mannan, M. A. & Chin, R. J. (2019) Hydrological Performances on the Modified Permeable Pavement with Precast Hollow Cylinder Micro detention Pond Structure. *KSCE Journal of Civil Engineering*. 23. (9), pp. 3951-3960.

Bean, E. Z., Hunt, W. F. & Bidelspach, D. A. (2004) Study on the Surface Infiltration Rate of Permeable Pavements. In: *1st Water and Environment Specialty Conference of the Canadian Society for Civil Engineering*. Saskatoon, Canada, 2–5 June 2004. pp. 1–10.

Bean, E. Z., Hunt, W. F. & Bidelspach, D. A. (2007) Evaluation of Four Permeable Pavement Sites in Eastern North Carolina for Runoff Reduction and Water Quality Impacts. *Journal of Irrigation and Drainage Engineering*. 133. (6), pp. 583–592.

Beecham, S., Pezzaniti, D. & Kandasamy, J. (2012) Stormwater treatment using permeable pavements. *Proceedings of the Institution of Civil Engineers - Water Management*. 165. (3), pp. 161–170.

Behera, M., Bhattacharyya, S. K., Minocha, A. K., Deoliya, R. & Maiti, S. (2014) Recycled aggregate from C&D waste & its use in concrete – A breakthrough towards sustainability in construction sector: A review. *Construction and Building Materials*. 68 pp. 501–516.

Bentarzi, Y., Ghenaim, A., Terfous, A., Wanko, A., Feugeas, F., Poulet, J. B. & Mosé, R. (2016) Hydrodynamic behaviour of a new permeable pavement material under high rainfall conditions. *Urban Water Journal*. 13. (7), pp. 687–696.

Bentarzi, Y., Terfous, A., Ghenaim, A., Wanko, A., Hlawka, F. & Poulet, J. B. (2013) Hydrodynamic characteristics of a new permeable pavement material produced from recycled concrete and organic matter. *Urban Water Journal*. 10. (4), pp. 260–267.

Bhutta, M. A. R., Hasanah, N., Farhayu, N., Hussin, M. W., Tahir, M. b. M. & Mirza, J. (2013) Properties of porous concrete from waste crushed concrete (recycled aggregate). *Construction and Building Materials*. 47 pp. 1243-1248.

Blecken, G.-T., Hunt, W. F., Al-Rubaei, A. M., Viklander, M. & Lord, W. G. (2017) Stormwater control measure (SCM) maintenance considerations to ensure designed functionality. *Urban Water Journal*. 14. (3), pp. 278–290.

Boogaard, F. & Lucke, T. (2019) Long-Term Infiltration Performance Evaluation of Dutch Permeable Pavements Using the Full-Scale Infiltration Method. *Water*. 11. (2), pp. 320.

Boogaard, F., Lucke, T. & Beecham, S. (2014a) Effect of Age of Permeable Pavements on Their Infiltration Function. *CLEAN – Soil Air Water*. 42. (2), pp. 146–152.

Boogaard, F., Lucke, T., van de Giesen, N. & van de Ven, F. (2014b) Evaluating the infiltration performance of eight Dutch permeable pavements using a new full-scale infiltration testing method. *Water*. 6. (7), pp. 2070–2083.

Boomsma, W. & Huurman, M. (2006) Permeable paving systems with storing capacity. In: *8th International Conference on Concrete Block Paving*. San Francisco, CA, USA, 6–8 November 2006. pp. 27–35.

Booth, D. & Leavitt, J. (1999) Field Evaluation of Permeable Pavement Systems for Improved Stormwater Management. *Journal of the American Planning Association*. 65. (3), pp. 314–325.

Borgwardt, S. (2006) Long-term in-situ infiltration performance of permeable concrete block pavement. In: *8th International Conference on Concrete Block Paving*. San Francisco, CA, USA, 6–8 November 2006. pp. 1–12.

Boutet, M., Doré, G., Bilodeau, J.-P. & Pierre, P. (2011) Development of models for the interpretation of the dynamic cone penetrometer data. *International Journal of Pavement Engineering*. 12. (3), pp. 201-214.

Bouvard, D., Chaix, J. M., Dendievel, R., Fazekas, A., Létang, J. M., Peix, G. & Quenard, D. (2007) Characterization and simulation of microstructure and properties of EPS lightweight concrete. *Cement and Concrete Research*. 37. (12), pp. 1666–1673.

Boyd, M. J., Bufill, M. C. & Knee, R. M. (1994) Predicting pervious and impervious storm runoff from urban drainage basins. *Hydrological Sciences Journal*. 39. (4), pp. 321–332.

Brabec, E., Schulte, S. & Richards, P. L. (2002) Impervious surfaces and water quality: a review of current literature and its implications for watershed planning. *Journal of planning literature*. 16. (4), pp. 499–514.

Braswell, A. S., Winston, R. J. & Hunt, W. F. (2018) Hydrologic and water quality performance of permeable pavement with internal water storage over a clay soil in Durham, North Carolina. *Journal of Environmental Management*. 224 pp. 277–287.

Brattebo, B. O. & Booth, D. B. (2003) Long-term stormwater quantity and quality performance of permeable pavement systems. *Water Research*. 37. (18), pp. 4369–4376.

Brown, C., Chu, A., Van Duin, B. & Valeo, C. (2009) Characteristics of sediment removal in two types of permeable pavement. *Water Quality Research Journal of Canada*. 44. (1), pp. 59–70.

Brown, J. & Peake, B. (2006) Sources of heavy metals and polycyclic aromatic hydrocarbons in urban stormwater runoff. *Science of the Total Environment*. 359. (1–3), pp. 145–155.

Brown, R. A. & Borst, M. (2013) Assessment of Clogging Dynamics in Permeable Pavement Systems with Time Domain Reflectometers. *Journal of Environmental Engineering*. 139. (10), pp. 1255–1265.

Brown, R. A. & Borst, M. (2015) Nutrient infiltrate concentrations from three permeable pavement types. *Journal of Environmental Management*. 164 pp. 74–85.

Brunetti, G., Šimůnek, J. & Piro, P. (2016) A comprehensive numerical analysis of the hydraulic behavior of a permeable pavement. *Journal of Hydrology*. 540 pp. 1146–1161.

BSI (1990) *812-112 Testing aggregates. Method for determination of aggregate impact value (AIV)*, London, UK: British Standard Institution BSI.

BSI (2004) *Eurocode 2: Design of concrete structures Part 1-1–General rules and rules for buildings (including NA)*, london, UK: British Standard Institution BSI.

BSI (2009a) *BS 7533-13 Pavements constructed with clay, natural stone or concrete pavers. Guide for the design of permeable pavements constructed with concrete paving blocks and flags, natural stone slabs and setts and clay pavers*, London, UK: British Standard Institution BSI.

BSI (2009b) *BS EN 12390-3 Testing hardened concrete. Compressive strength of test specimens*, London, UK: British Standard Institution BSI.

BSI (2012) *EN 933-3 Tests for geometrical properties of aggregates. Determination of particle shape. Flakiness index*, London, UK: British Standard Institution BSI.

BSI (2018) *1377-3 Methods of test for soils for civil engineering purposes. Chemical and electro-chemical tests*, London, UK: British Standard Institution BSI.

Butler, D. & Davies, J. W. (2011) *Urban Drainage*, 3rd edn. New York, USA: Spon Press.

Cameron, D., Rahman, M. M., Azam, A. M., Gabr, A. G., Andrews, R. & Mitchell, P. W. (2013) The use of recycled aggregates in unbound road pavements. In: *18th International Conference on Soil Mechanics and Geotechnical Engineering*. Paris, France, 2–5 September 2013. France: Presses des Ponts, pp. 3187–3190.

Cashman, A., Nurse, L. & John, C. (2009) Climate change in the Caribbean: the water management implications. *The Journal of Environment and Development*. 19. (1), pp. 41–67.

Castro, D., González-Angullo, N., Rodríguez, J. & Calzada, M. Á. (2007) The influence of paving-block shape on the infiltration capacity of permeable paving. *Land Contamination & Reclamation*. 15. (3), pp. 335–344.

Central Intelligence Agency (2018) *The World Factbook*. Available from: https://www.cia.gov/library/publications/resources/the-world-factbook/fields/2100.html [Accessed 18 January 2018].

Çetin, M. (2015) Consideration of permeable pavement in landscape architecture. *Journal of environmental protection and ecology*. 16. (1), pp. 385–392.

Chang, N., Wang, H. P., Huang, W. L. & Lin, K. S. (1999) The assessment of reuse potential for municipal solid waste and refuse-derived fuel incineration ashes. *Resources, Conservation and Recycling*. 25. (3–4), pp. 255–270.

Chapman, D. & Kimstach, V. (2002) Selection of Water Quality Variables. *In:* Chapman, D. (ed.) *Water Quality Assessments: A guide to the use of Biota, Sediments and Water in Environmental Monitoring.* 2nd ed. Boca Raton, Fl, USA: CRC Press.

Charlesworth, S. M., Beddow, J. & Nnadi, E. O. (2017) The Fate of Pollutants in Porous Asphalt Pavements, Laboratory Experiments to Investigate Their Potential to Impact Environmental Health. *International Journal of Environmental Research and Public Health*. 14. (6), pp. 666.

Charlesworth, S. M. & Warwick, F. (2012) Adapting to and Mitigating Floods Using Sustainable Urban Drainage Systems. *In:* Lamond, J., Proverbs, D., Booth, C.A. & Hammond, F. (eds.) *Flood Hazards: Impacts and Responses for the Built Environment.* Boca Raton, Fla.: CRC Press.

Cheeseman, C. R., Makinde, A. & Bethanis, S. (2005) Properties of lightweight aggregate produced by rapid sintering of incinerator bottom ash. *Resources, Conservation and Recycling*. 43. (2), pp. 147–162.

Chen, B. & Liu, J. (2004) Properties of lightweight expanded polystyrene concrete reinforced with steel fiber. *Cement and Concrete Research*. 34. (7), pp. 1259–1263.

Cheng, M., Coffman, L. S. & Clar, M. L. (2002) Low-Impact development hydrologic analysis. *In:* Field, R & Sullivan, D (eds.) *Wet-Weather Flow in the Urban Watershed: Technology and Management.* Boca Raton, Fla.: CRC Press LLC.

Cheng, S. & Wang, R. (2002) An approach for evaluating the hydrological effects of urbanization and its application. *Hydrological Processes*. 16. (7), pp. 1403–1418.

CHI (2017) *Advanced modeling software for stormwater, wastewater, watershed and water distribution systems*. Available from: https://www.pcswmm.com/ [Accessed 25 July 2017].

Chocat, B., Ashley, R., Marsalek, J., Matos, M. R., Rauch, W., Schilling, W. & Urbonas, B. (2007) Toward the sustainable management of urban storm-water. *Indoor and Built Environment*. 16. (3), pp. 273–285.

Chow, W. T. L. & Roth, M. (2006) Temporal dynamics of the urban heat island of Singapore. *International Journal of Climatology*. 26. (15), pp. 2243–2260.

Chowdhury, R. K., Sharvelle, S. E. & Beecham, S. (2016) Greywater quality changes in a permeable pavement reservoir. *Proceedings of the Institution of Civil Engineers - Water Management*. 169. (4), pp. 190–198.

Cipolla, S. S., Maglionico, M. & Stojkov, I. (2016) Experimental Infiltration Tests on Existing Permeable Pavement Surfaces. *CLEAN – Soil Air Water*. 44. (1), pp. 89–95.

CMAA (2010) *PE01 Permeable Interlocking Concrete Pavements - Design and Construction Guide,* NSW Australia: Concrete Masonry Association of Australia.

CMAA (2016) *Permeable Paving*. Available from: http://www.cmaa.com.au/technical [Accessed 11 November 2016].

Colandini, V., Legret, M., Brosseaud, Y. & Baladès, J. D. (1995) Metallic pollution in clogging materials of urban porous pavements. *Water Science and Technology*. 32. (1), pp. 57–62.

Collins, K. A. (2007). *A field evaluation of four types of permeable pavement with respect to water quality improvement and flood control.* MSc., North Carolina State University.

Collins, K. A., Hunt, W. F. & Hathaway, J. M. (2008) Hydrologic Comparison of Four Types of Permeable Pavement and Standard Asphalt in Eastern North Carolina. *Journal of Hydrologic Engineering*. 13. (12), pp. 1146–1157.

Collins, K. A., Hunt, W. F. & Hathaway, J. M. (2010) Side-by-side comparison of nitrogen species removal for four types of permeable pavement and standard asphalt in eastern North Carolina. *Journal of Hydrologic Engineering*. 15. (6), pp. 512–521.

Cook, D. J. (1983) Expanded polystyrene concrete. *In:* Swamy, R. N. (ed.) *Concrete Technology & Design Vol. 1: New Concrete Materials.* London: Surrey University Press.

Cooley Jr, L. A. (1999) *Permeability of Superpave mixtures: evaluation of field permeameters*. Auburn University, Alabama: National Centre for Asphalt Technology.

Cooper, V. A. (2002). *On automatic calibration of conceptual rainfall runoff models using optimisation techniques.* PhD, McGill University.

Courty, L. G., Wilby, R. L., Hillier, J. K. & Slater, L. J. (2019) Intensity-duration-frequency curves at the global scale. *Environmental Research Letters*. 14. (8), pp. 084045.

Crookes, A. J., Drake, J. A. P. & Green, M. (2017) Hydrologic and Quality Control Performance of Zero-Exfiltration Pervious Concrete Pavement in Ontario. *Journal of Sustainable Water in the Built Environment*. 3. (3), pp. 06017001.

CSO (2010a) *2010 Population and Housing Census Preliminary Report*. Castries, St. Lucia: Government of St. Lucia.

CSO (2010b) *Pocket Digest*. Available from: http://www.planning.gov.tt/sites/default/files/content/mediacentre/documents/Pocket%20Digest.pdf [Accessed 10 May 2016].

Das, B. M. (2010) *Fundamentals of Geotechnical Engineering*, 7th edn. Stamford, CT, USA: Cengage Learning.

David, T. K., Chandrasegaran, R. S. & Nair, S. K. (2018) Modified Pervious Concrete Containing Recycled Asphalt Pavement and Waste Tire Rubber. *IOP Conference Series: Materials Science and Engineering*. 371 pp. 012011.

Davies, J., Pratt, C. & Scott, M. (2002) Laboratory Study of Permeable Pavement Systems to Support Hydraulic Modeling. In: *9th International Conference on Urban Drainage* Portland, Oregon, USA, 8–13 September 2002. pp. 1–7.

Davis, A. P., Shokouhian, M. & Ni, S. (2001) Loading estimates of lead, copper, cadmium, and zinc in urban runoff from specific sources. *Chemosphere*. 44. (5), pp. 997–1009.

Day, G. E., Smith, D. R. & Powers, J. N. (1981) *Runoff and pollution abatement characteristics of concrete grid pavements*, Blacksburg: Virginia Water Resources Centre, Virginia Polytechnic and State University.

Dempewolf, L., Boodram, N., Corbin, C. & Cox, C. (2015) Rainwater Harvesting in the Caribbean- State of Play 2015. In: *24th Annual CWWA Conference and Exhibition*. Florida, USA, 24–28 August 2015. pp. 1–13.

Deng, Y. & Wheatley, A. (2018) Mechanisms of Phosphorus Removal by Recycled Crushed Concrete. *International Journal Environmental Research and Public Health*. 15. (2), pp. 16.

Deo, O., Sumanasooriya, M. & Neithalath, N. (2010) Permeability Reduction in Pervious Concretes due to Clogging: Experiments and Modeling. *Journal of Materials in Civil Engineering*. 22. (7), pp. 741–751.

Dhalla, S. & Zimmer, C. (2010) *Low Impact Development Stormwater Management Planning and Design Guide Chapter 4, Section 4.7, Permeable Pavement*. Toronto, ON, Canada: Toronto and Toronto and Region Conservation Authority.

Dhir, R. K. & Jackson, N. (1996) Concrete. *In:* Jackson, Neil & Dhir, Ravindra K. (eds.) *Civil Engineering Materials.* 5th ed. New York, USA: Palgrave.

Dierkes, C., Kuhlmann, L., Kandasamy, J. & Angelis, G. (2002) Pollution retention capability and maintenance of permeable pavements. In: *9th International Conference on Urban Drainage*. Portland, Oregon, United States, 8–13 September 2002. pp. 1–13.

Dietz, M. E. (2007) Low impact development practices: A review of current research and recommendations for future directions. *Water, Air, & Soil Pollution*. 186. (1), pp. 351–363.

Dietz, M. E. & Clausen, J. C. (2008) Stormwater runoff and export changes with development in a traditional and low impact subdivision. *Journal of Environmental Management*. 87. (4), pp. 560–566.

Diniz, E. V. (1980) *Porous pavement. Phase 1: Design and operational criteria,* Cininnati, Ohio: Municipal Environmental Research Laboratory, Office of Research and Development, U.S. Environmental Protection Agency.

Dongquan, Z., Jining, C., Haozheng, W., Qingyuan, T., Shangbing, C. & Zheng, S. (2009) GIS-based urban rainfall-runoff modeling using an automatic catchment-discretization approach: a case study in Macau. *Environmental Earth Sciences*. 59. (2), pp. 465.

Drake, J., Bradford, A. & Marsalek, J. (2013) Review of environmental performance of permeable pavement systems: state of the knowledge. *Water Quality Research Journal of Canada*. 48. (3), pp. 203–222.

Drake, J., Bradford, A. & Van Seters, T. (2014) Stormwater quality of spring–summer-fall effluent from three partial-infiltration permeable pavement systems and conventional asphalt pavement. *Journal of Environmental Management*. 139 pp. 69–79.

Dreelin, E. A., Fowler, L. & Carroll, C. R. (2006) A test of porous pavement effectiveness on clay soils during natural storm events. *Water Research*. 40. (4), pp. 799–805.

Ekwue, E. (2010) Management of water demand in the Caribbean region: current practices and future needs. *Management*. 32. (1&2), pp. 28–35.

Elliott, A. H. & Trowsdale, S. A. (2007) A review of models for low impact urban stormwater drainage. *Environmental Modelling & Software*. 22. (3), pp. 394–405.

EMA (2001) *Water Pollution Rules,* Port of Spain, Trinidad and Tobago: Environmental Management Authority.

Emerson, C. H., Wadzuk, B. M. & Traver, R. G. (2010) Hydraulic evolution and total suspended solids capture of an infiltration trench. *Hydrological Processes*. 24. (8), pp. 1008–1014.

EN 197-1 (2011) *Cement - Part 1: Composition, specifications and conformity criteria for common cements*, Brussels, Belgium: CEN.

Erlingsson, S., Baltzer, S., Baena, J. & Bjarnason, J. (2009a) Measurement Techniques for Water Flow. *In:* Dawson, A. (ed.) *Water in road structures*. New York: Springer.

Erlingsson, S., Brencic, M. & Dawson, A. (2009b) Water Flow Theory for Saturated and Unsaturated Pavement Material. *In:* Dawson, A. (ed.) *Water in road structures*. New York: Springer.

Fassman, E. A. & Blackbourn, S. (2010) Urban Runoff Mitigation by a Permeable Pavement System over Impermeable Soils. *Journal of Hydrologic Engineering*. 15. (6), pp. 475–485.

Ferguson, B. K. (2005) *Porous Pavements*, Boca Raton, Fl, USA: CRC Press.

Fernández Bertos, M., Simons, S. J. R., Hills, C. D. & Carey, P. J. (2004) A review of accelerated carbonation technology in the treatment of cement-based materials and sequestration of CO2. *Journal of Hazardous Materials*. 112. (3), pp. 193–205.

Field, R., Masters, H. & Singer, M. (1982) An overview of Porous Pavement Research. *Journal of the American Water Resources Association JAWRA* 18. (2), pp. 265–270.

Fleischmann, C. M. (2014). *Evaluating Management Strategies for Urban Stormwater Runof*. PhD, University of Connecticut.

Fleming, P. R., Frost, M. W. & Lambert, J. P. (2007) Review of lightweight deflectometer for routine in situ assessment of pavement material stiffness. *Transportation Research Record: Journal of the Transportation Research Board*. pp. 80–87.

Fletcher, T. D., Shuster, W., Hunt, W. F., Ashley, R., Butler, D., Arthur, S., Trowsdale, S., Barraud, S., Semadeni-Davies, A., Bertrand-Krajewski, J.-L., Mikkelsen, P. S., Rivard, G., Uhl, M., Dagenais, D. & Viklander, M. (2015) SUDS, LID, BMPs, WSUD and more – The evolution and application of terminology surrounding urban drainage. *Urban Water Journal*. 12. (7), pp. 525–542.

Formpave (2016) *Aguaflow permeable paving*, Gloucestershire, UK: Forterra Formpave.

Fry, T. J. (2017). *High Resolution Modeling for Water Quantity and Quality, Understanding the role of Green Infrastructure Best Management Practices in Ultra Urban Environments: Connections, Feedbacks and Interactions*. PhD, Colorado School of Mines.

Garach, L., López, M., Agrela, F., Ordóñez, J., Alegre, J. & Moya, J. A. (2015) Improvement of Bearing Capacity in Recycled Aggregates Suitable for Use as Unbound Road Sub-Base. *Materials*. 8. (12), pp. 8804–8816.

Geiger, W. F. (1990) Appropriate Technology fo Urban Drainage in Developing Countries. In: *Duisberg Symposium*. Duisberg, Germany, 24–28 April 1988. IAHS, pp. 125–134.

Gencel, O., Ozel, C., Koksal, F., Erdogmus, E., Martínez-Barrera, G. & Brostow, W. (2012) Properties of concrete paving blocks made with waste marble. *Journal of Cleaner Production*. 21. (1), pp. 62–70.

Geosyntec Consultants & Wright Water Engineers, I. (2009) *Urban Stormwater BMP Performance Monitoring Manual*. Washington, D.C., USA: US EPA.

Gesoğlu, M., Özturan, T. & Güneyisi, E. (2004) Shrinkage cracking of lightweight concrete made with cold-bonded fly ash aggregates. *Cement and Concrete Research*. 34. (7), pp. 1121–1130.

Ghina, F. (2003) Sustainable Development in Small Island Developing States. *Environment, Development and Sustainability*. 5. (1), pp. 139–165.

Gilbert, J. K. & Clausen, J. C. (2006) Stormwater runoff quality and quantity from asphalt, paver, and crushed stone driveways in Connecticut. *Water Research*. 40. (4), pp. 826–832.

Global Water Partnership (GWP) (2014) *Integrated water resources management in the Caribbean: The Challenges facing Small Island Developing States*. Stockholm, Sweden: GWP.

Göbel, P., Dierkes, C. & Coldewey, W. G. (2007) Storm water runoff concentration matrix for urban areas. *Journal of Contaminant Hydrology*. 91. (1–2), pp. 26–42.

Goldenfum, J. A., Tassi, R., Meller, A., Allasia, D. G. & da Silveira, A. L. (2007) Challenges for the sustainable urban stormwater management in developing countries: from basic education to technical and institutional issues. In: *Novatech 2007 – Sixth International Conference on Sustainable Techniques and Strategies for Urban Water Management*. Lyon, France, 25–28 June 2007. pp.

Goncalves, M., Zischg, J., Rau, S., Sitzmann, M., Rauch, W. & Kleidorfer, M. J. S. (2018) Modeling the effects of introducing low impact development in a tropical city: a case study from Joinville, Brazil. *Sustainability*. 10. (3), pp. 728.

González-Angullo, N., Castro, D., Rodríguez-Hernández, J. & Davies, J. W. (2008) Runoff infiltration to permeable paving in clogged conditions. *Urban Water Journal*. 5. (2), pp. 117–124.

González-Corrochano, B., Alonso-Azcárate, J. & Rodas, M. (2009) Characterization of lightweight aggregates manufactured from washing aggregate sludge and fly ash. *Resources, Conservation and Recycling*. 53. (10), pp. 571–581.

GoRTT (2015) *National Waste Recycling Policy*. Port of Spain, Trinidad: GoRTT.

GoRTT (2018) *Oil and Gas Industry*. Available from: http://www.energy.gov.tt/our-business/oil-and-gas-industry/ [Accessed 24 May 2019].

GoSL & World Bank (2014) *Saint Lucia Joint Rapid Damage and Needs Assessment Flood Event of December 24 – 25, 2013*. Washington, D.C., USA: World Bank Group.

Gössling, S., Peeters, P., Hall, C. M., Ceron, J.-P., Dubois, G. & Scott, D. (2012) Tourism and water use: Supply, demand, and security. An international review. *Tourism Management*. 33. (1), pp. 1-15.

Grontmij A/S 2012. PRIMA 100 LWD User manual. Denmark.

Guan, M., Sillanpää, N. & Koivusalo, H. (2015) Modelling and assessment of hydrological changes in a developing urban catchment. *Hydrological Processes*. 29. (13), pp. 2880–2894.

Gunning, P. J., Hills, C. D. & Carey, P. J. (2009) Production of lightweight aggregate from industrial waste and carbon dioxide. *Waste Management*. 29. (10), pp. 2722–2728.

Gunning, P. J., Hills, C. D. & Carey, P. J. (2010) Accelerated carbonation treatment of industrial wastes. *Waste Management*. 30. (6), pp. 1081–1090.

Gunning, P. J., Hills, C. D., Carey, P. J., Greig, S. & Schilling, M. (2012) Carbonation of MSWI APCr for re-use as a light-weight aggregate. In: *Ash Utilisation 2012 – Ashes in a Sustainable Society*. Stockholm, Sweden, 25–27 January 2012. pp.

Haan, C. T. (2002) *Statistical methods in hydrology,* 2nd ed. Iowa: Iowa State Press.

Hammer, M. J. & Hammer Jr., M. J. (2007) *Water and wastewater technology,* 6th ed. New Jersey: Pearson.

Hassanali, S. (2019) $66m flood-relief studies unused. *Trinidad & Tobago Guardian*, 27 November.

Hein, D. K. (2014) Permeable Pavement Design and Construction Case Studies in North America. In: *2014 Conference and Exhibition of the Transportation Association of Canada*. Montreal, Quebec, Canada, 28 September – 01 October 2014. pp. 1–12.

Hein, D. K., Swan, D. J. & Schaus, L. (2010) Structural and Hydrological Design of Permeable Pavements. In: *2010 Annual Conference of the Transportation Association of Canada*. Halifax, Nova Scotia, 26–29 September 2010. pp.

Hellström, D., Jeppsson, U. & Kärrman, E. (2000) A framework for systems analysis of sustainable urban water management. *Environmental Impact Assessment Review*. 20. (3), pp. 311–321.

Henderson, V. (2012). *Evaluation of the Performance of Pervious Concrete Pavement in the Canadian Climate.* PhD, University of Waterloo.

Henheik, P. (2019) Email to John Monrose, 15 March.

Henze, M., Somlyódy, L., Schilling, W., Tyson, J., Butler, D. & Parkinson, J. (1997a) Sustainable SanitationTowards sustainable urban drainage. *Water Science and Technology*. 35. (9), pp. 53–63.

Henze, M., Somlyódy, L., Schilling, W., Tyson, J., Krebs, P. & Larsen, T. A. (1997b) Guiding the development of urban drainage systems by sustainability criteria. *Water Science and Technology*. 35. (9), pp. 89–98.

Hoang, L. & Fenner, R. A. (2016) System interactions of stormwater management using sustainable urban drainage systems and green infrastructure. *Urban Water Journal*. 13. (7), pp. 739–758.

Hoffmann, O. J.-M., Guzina, B. B. & Drescher, A. (2004) Stiffness estimates using portable deflectometers. *Transportation Research Record: Journal of the Transportation Research Board*. 1869. (1), pp. 59–66.

Horsley Witten Group Inc. (HWG) & Centre for Watershed Protection Inc. (CWP) (2014) *Stormwater Management in Pacific and Caribbean Islands: A Practitioner's Guide to Implementing LID*, Boston, MA: HWG.

Huang, J., He, J., Valeo, C. & Chu, A. (2016) Temporal evolution modeling of hydraulic and water quality performance of permeable pavements. *Journal of Hydrology*. 533 pp. 15–27.

Hunt, B., Stevens, S. & Mayes, D. (2002) Permeable Pavement Use and Research at Two Sites in Eastern North Carolina. In: *9th International Conference on Urban Drainage*. Portland, Oregon, USA, 8–13 September 2002. Global Solutions for Urban Drainage, ASCE, pp. 1–10.

Hunt, W. F. & Collins, K. A. (2008) *Permeable pavement: research update and design implications, in Urban Waterway Series*. Raleigh, North Carolina: North Carolina Cooperative Extension Service. (E08-50327).

Hunte, C. (2019) Citizens should pay for garbage disposal. *Trinidad Express Newspapers*, 12 February.

Huong, H. T. L. & Pathirana, A. (2013) Urbanization and climate change impacts on future urban flooding in Can Tho city, Vietnam. *Hydrology and Earth System Sciences*. 17. (1), pp. 379–394.

HydroSTON (2019a) *Maintenance*. Available from: https://hydroston.com.au/maintenance/ [Accessed 01 December 2019].

HydroSTON (2019b) *Permeable Paving*. Available from: https://hydroston.com.au/ [Accessed 01 December 2019].

IBM 2011. IBM SPSS statistics for Windows, version 20.0. New York, USA: IBM Corp.

ICPI (2006) *Tech Spec, No. 8, Concrete Grid Pavements*. Washington, D.C.: ICPI.

ICPI (2016) *Permeable Pavers*. Available from: https://www.icpi.org/paving-systems/permeable-pavers [Accessed 10 September 2016].

ICPI (2019) *Maintenance*. Available from: https://www.icpi.org/paving-systems/permeable-pavers/maintenance [Accessed 01 December 2019].

Illgen, M., Harting, K., Schmitt, T. G. & Welker, A. (2007) Runoff and infiltration characteristics of pavement structures—Review of an extensive monitoring program. *Water Science and Technology*. 56. (10), pp. 133–140.

Interpave (2018) *Design & Construction of Concrete Block Permeable Pavements*, 7th Ed. Leicester, UK: Interpave.

Inyang, H. I. (2003) Framework for Recycling of Wastes in Construction. *Journal of Environmental Engineering*. 129. (10), pp. 887–898.

Ioannidou, V. & Arthur, S. (2018) Hydrological Response of a Permeable Pavement Laboratory Rig for Stormwater Management. *Proceedings*. 2. (11), pp. 607.

IPCC (2007) *Climate Change 2007: Impacts, Adaptation and Vulnerability. Contribution of Working Group II to the Fourth Assessment Report of the Intergovernmental Panel on Climate Change*, Cambridge, UK: Cambridge University Press.

IPCC 2008. Climate Change and Water. Technical Paper of the Intergovernmental Panel on Climate Change. *In:* Bates, B., Kundzewicz, Z. W., Wu, S. & Palutikof, J. P. (eds.). Geneva: IPCC Secretariat.

IPCC, I. P. o. C. C. (2006) Volume 5: Wastes; Chapter 2 Waste Generation, Composition and Management Data. *IPCC Guidelines for National Greenhouse Gas Inventories*. Hayama, Japan: Institute for Global Environmental Strategies (IGES).

James, W. & Shahin, R. (1998) A Laboratory Examination of Pollutants Leached from Four Different Pavements by Acid Rain. *Journal of Water Management Modeling*. 200. (17), pp. 321–349.

Jamshidi, A., Kurumisawa, K., Nawa, T. & Igarashi, T. (2016) Performance of pavements incorporating waste glass: The current state of the art. *Renewable and Sustainable Energy Reviews*. 64. (Supplement C), pp. 211–236.

Jamshidi, A., Kurumisawa, K., White, G., Nishizawa, T., Igarashi, T., Nawa, T. & Mao, J. (2019) State-of-the-art of interlocking concrete block pavement technology in Japan as a post-modern pavement. *Construction and Building Materials*. 200 pp. 713–755.

Jang, J. G., Ahn, Y. B., Souri, H. & Lee, H. K. (2015) A novel eco-friendly porous concrete fabricated with coal ash and geopolymeric binder: Heavy metal leaching characteristics and compressive strength. *Construction and Building Materials*. 79 pp. 173-181.

Jato-Espino, D., Charlesworth, S. M., Bayon, J. R. & Warwick, F. (2016a) Rainfall–Runoff Simulations to Assess the Potential of SuDS for Mitigating Flooding in Highly Urbanised Catchments. *International Journal of Environmental Research and Public Health*. 13. (1), pp. 149.

Jato-Espino, D., Sillanpää, N., Charlesworth, S. & Andrés-Doménech, I. J. W. (2016b) Coupling GIS with stormwater modelling for the location prioritization and hydrological simulation of permeable pavements in urban catchments. *Water*. 8. (10), pp. 451.

Jayakaran, A. D., Knappenberger, T., Stark, J. D. & Hinman, C. J. W. (2019) Remediation of Stormwater Pollutants by Porous Asphalt Pavement. *Water*. 11. (3), pp. 520.

Jiajun, Y., Shuguang, H., Fazhou, W., Yufei, Z. & Zhichao, L. (2006) Effect of pre-wetted light-weight aggregate on internal relative humidity and autogenous shrinkage of concrete. *Journal of Wuhan University of Technology-Mater. Sci. Ed.* 21. (1), pp. 134–137.

Jindal, A. & Ransinchung, G. D. (2018) Behavioural study of pavement quality concrete containing construction, industrial and agricultural wastes. *International Journal of Pavement Research and Technology*. 11. (5), pp. 488-501.

Joint Steering Committee for Water Sensitive Cities (JSCWSC) (2009) *Evaluating Options for Water Sensitive Urban Design–A National Guide*, Brisbane, Australia: JSCWSC.

Juan, K. Y. (2011). *Cracking Mode and Shear Strength of Lightweight Concrete Beams*. PhD, National University of Singapore.

Juranwan-Richards, S. (2016) Email to John Monrose, 10 May.

Kan, A. & Demirboğa, R. (2009) A novel material for lightweight concrete production. *Cement and Concrete Composites*. 31. (7), pp. 489–495.

Kawalec, J., Kwiecien, S., Pilipenko, A. & Rybak, J. (2017) Application of Crushed Concrete in Geotechnical Engineering – Selected Issues. *IOP Conference Series: Earth and Environmental Science*. 95 pp. 022057.

Kaya, A. & Kar, F. (2016) Properties of concrete containing waste expanded polystyrene and natural resin. *Construction and Building Materials*. 105 pp. 572–578.

Kayhanian, M., Weiss, P. T., Gulliver, J. S. & Khazanovich, L. (2015) *The Application of Permeable Pavement with Emphasis on Successful Design, Water Quality Benefits, and Identification of Knowledge and Data Gaps: A summary report from the National Centre for Sustainable Transportation*. Davis, CA, USA: National Centre for Sustainable Transportation.

Kaza, S., Yao, L., Bhada-Tata, P. & Van Woerden, F. (2018) *What a Waste 2.0: A Global Snapshot of Solid Waste Management to 2050*, Washington, DC, USA: World Bank.

Kazemi, F. & Hill, K. (2015) Effect of permeable pavement basecourse aggregates on stormwater quality for irrigation reuse. *Ecological Engineering*. 77 pp. 189–195.

Kelman, I. & West, J. J. (2009) Climate change and small island developing states: a critical review. *Ecological and Environmental Anthropology*. 5. (1), pp. 1–16.

Kevern, J. T., Schaefer, V. R. & Wang, K. (2009) Temperature Behavior of Pervious Concrete Systems. *Transportation Research Record: Journal of the Transportation Research Board*. 2098. (1), pp. 94-101.

Khankhaje, E., Rafieizonooz, M., Salim, M. R., Mirza, J., Salmiati & Hussin, M. W. (2017) Comparing the effects of oil palm kernel shell and cockle shell on properties of pervious concrete pavement. *International Journal of Pavement Research and Technology*. 10. (5), pp. 383–392.

Kim, J. R., Kang, H. B., Kim, D., Park, D. S. & Kim, W. J. (2007) Evaluation of In Situ Modulus of Compacted Subgrades Using Portable Falling Weight Deflectometer and Plate-Bearing Load Test. *Journal of Materials in Civil Engineering*. 19. (6), pp. 492–499.

Kinnaman, T. C. (2010) Solid Waste Management in the Caribbean. *Journal of Eastern Caribbean Studies*. 35. (2), pp. 38–60.

Kockal, N. U. & Ozturan, T. (2010) Effects of lightweight fly ash aggregate properties on the behavior of lightweight concretes. *Journal of Hazardous Materials*. 179. (1), pp. 954–965.

Kockal, N. U. & Ozturan, T. (2011) Durability of lightweight concretes with lightweight fly ash aggregates. *Construction and Building Materials*. 25. (3), pp. 1430–1438.

Kottegoda, N. T. & Rosso, R. (2008) *Applied Statistics for Civil and Environmental Engineers*, 2nd Ed. Chichester, West Sussex, UK: Blackwell Publishing Ltd.

Kourtis, I. M., Kopsiaftis, G., V., B. & Tsihrintzis, V. A. (2017) Calibration and validation of SWMM model in two urban catchments in Athens, Greece. In: *15th International Conference on Environmental Science and Technology*. Rhodes, Greece, 31 August – 02 September 2017. pp. 1– 5.

Kourtis, I. M., Tsihrintzis, V. A. & Baltas, E. (2018) Simulation of Low Impact Development (LID) Practices and Comparison with Conventional Drainage Solutions. *Proceedings*. 2. (11), pp. 640.

Kumar, K. (2014) Review on Permeable Pavement Systems. In: *11th Transportation Planning and Implementation Methodologies for Developing Countries*. Bombay, 10–12 December 2014. pp. 1–20.

Kumar, K., Kozak, J., Hundal, L., Cox, A., Zhang, H. & Granato, T. (2016) In-situ infiltration performance of different permeable pavements in a employee used parking lot–A four-year study. *Journal of Environmental Management*. 167 pp. 8–14.

Kwiatkowski, M., Welker, A. L., Traver, R. G., Vanacore, M. & Ladd, T. (2007) Evaluation of an Infiltration Best Management Practice Utilising Pervious Concrete. *Journal of the American Water Resources Association JAWRA*. 43. (5), pp. 1208–1222.

LADPW (2002) *Development planning for storm water management*, Los Angeles, CA: Los Angeles County.

Lalla, J. R. F. & Mwasha, A. (2014) Investigating the Compressive Strengths of Guanapo Recycled Aggregate Concrete as Compared to that of its Waste Material. *West Indian Journal of Engineering*. 36. (2), pp. 12–19.

Larsen, T. A. & Gujer, W. (1997) The concept of sustainable urban water management. *Water Science and Technology*. 35. (9), pp. 3–10.

Lee, J. G., Borst, M., Brown, R. A., Rossman, L. & Simon, M. A. (2015) Modeling the Hydrologic Processes of a Permeable Pavement System. *Journal of Hydrologic Engineering*. 20. (5), pp. 04014070.

Legates, D. R. & McCabe, G. J. (1999) Evaluating the use of "goodness-of-fit" measures in hydrologic and hydroclimatic model validation. *Water resources research*. 35. (1), pp. 233–241.

Legret, M. & Colandini, V. (1999) Effects of a porous pavement with reservoir structure on runoff water: water quality and fate of heavy metals. *Water Science and Technology*. 39. (2), pp. 111–117.

Leming, M. L., Malcom, R. H. & Tennis, P., D. (2007) *Hydrologic Design of Pervious Concrete*, Skokie, IL: Portland Cement Association.

Li, H., Harvey, J. & Jones, D. (2013a) Cooling Effect of Permeable Asphalt Pavement under Dry and Wet Conditions. *Transportation Research Record Journal of the Transportation Research Board*. 2372. (1), pp. 97-107.

Li, H., Harvey, J. T., Holland, T. J. & Kayhanian, M. (2013b) The use of reflective and permeable pavements as a potential practice for heat island mitigation and stormwater management. *Environmental Research Letters*. 8. (1), pp. 14.

Li, H., Kayhanian, M. & Harvey, J. T. (2013c) Comparative field permeability measurement of permeable pavements using ASTM C1701 and NCAT permeameter methods. *Journal of Environmental Management*. 118 pp. 144–152.

Li, H., Li, Z., Zhang, X., Li, Z., Liu, D., Li, T. & Zhang, Z. (2017) The effect of different surface materials on runoff quality in permeable pavement systems. *Environmental Science and Pollution Research*. 24. (26), pp. 21103–21110.

Li, X., Bertos, M. F., Hills, C. D., Carey, P. J. & Simon, S. (2007) Accelerated carbonation of municipal solid waste incineration fly ashes. *Waste Management*. 27. (9), pp. 1200–1206.

Lim, H. S. & Lu, X. X. (2016) Sustainable urban stormwater management in the tropics: An evaluation of Singapore's ABC Waters Program. *Journal of Hydrology*. 538 pp. 842–862.

Lin, W., Ryu, S. & Cho, Y.-H. (2016) Performance of Permeable Block Pavements in Accelerated Pavement Test and Rainfall Simulation. *Journal of Performance of Constructed Facilities*. 30. (1), pp. 04014186.

Lin, W., Ryu, S. & Cho, Y. (2014) A case study of flow characteristics of permeable pavements by time and space model. *Canadian Journal of Civil Engineering*. 41. (7), pp. 660–666.

Liu, J. & Borst, M. (2018) Performances of metal concentrations from three permeable pavement infiltrates. *Water Research*. 136 pp. 41–53.

Lo, T. Y., Cui, H., Memon, S. A. & Noguchi, T. (2016) Manufacturing of sintered lightweight aggregate using high-carbon fly ash and its effect on the mechanical properties and microstructure of concrete. *Journal of Cleaner Production*. 112 pp. 753–762.

Lockrey, S., Nguyen, H., Crossin, E. & Verghese, K. (2016) Recycling the construction and demolition waste in Vietnam: opportunities and challenges in practice. *Journal of Cleaner Production*. 133 pp. 757-766.

Lu, G., Liu, P., Wang, Y., Faßbender, S., Wang, D. & Oeser, M. (2019) Development of a sustainable pervious pavement material using recycled ceramic aggregate and bio-based polyurethane binder. *Journal of Cleaner Production*. 220 pp. 1052–1060.

Lucke, T. & Beecham, S. (2011a) Field investigation of clogging in a permeable pavement system. *Building Research & Information*. 39. (6), pp. 603–615.

Lucke, T. & Beecham, S. (2011b) An investigation into long term infiltration rates for permeable pavements on sloping subcatchments. In: *12th International Conference on Urban Drainage*. Porto Alegre, Brazil, 11–16 September 2011. pp. 1–8.

Lucke, T., Boogaard, F. & Van de Ven, F. (2014) Evaluation of a new experimental test procedure to more accurately determine the surface infiltration rate of permeable pavement systems. *Urban, Planning and Transport Research*. 2. (1), pp. 22–35.

Lucke, T., White, R., Nichols, P. & Borgwardt, S. (2015) A Simple Field Test to Evaluate the Maintenance Requirements of Permeable Interlocking Concrete Pavements. *Water*. 7. (6), pp. 2542–2554.

Lumbroso, D. M., Boyce, S., Bast, H. & Walmsley, N. (2011) The challenges of developing rainfall intensity-duration-frequency curves and national flood hazard maps for the Caribbean. *Journal of Flood Risk Management*. 4 pp. 42–52.

Lyman Ott, R. & Longnecker, M. (2010) *An Introduction to Statistical Methods and Data Analysis*, 6th Ed. Belmont, California, USA: Brooks/Cole, Cengage Learning.

Mac Berthouex, P. & Brown, L. C. (2002) *Statistics for Environmental Engineers*, 2nd Ed. Boca Raton, Florida, USA: Lewis Publishers.

Mai, Y., Zhang, M., Chen, W., Chen, X., Huang, G. & Li, D. (2018) Experimental study on the effects of LID measures on the control of rainfall runoff. *Urban Water Journal*. 15. (9), pp. 827–836.

Mallick, R. B. & El-Korchi, T. (2017) *Pavement Engineering - Principles and Practice,* 3rd Ed. Boca Raton, FL, USA: CRC Press.

Martinho, F. C. G., Picado-Santos, L. G. & Capitão, S. D. (2018) Feasibility Assessment of the Use of Recycled Aggregates for Asphalt Mixtures. *Sustainability*. 10. (6), pp. 1737.

Marzolf, N. C., Cañeque, F. C., Klein, J. & Loy, D. (2015) *A Unique Approach for Sustainable Energy in Trinidad and Tobago*. Washington, D.C., USA: IDB.

McCuen, R. H. (2003) *Modeling Hydrologic Change: Statistical Methods,* Boca Raton, FL: CRC press.

Mehta, K. P. & Monteiro, P. J. M. (2006) *Concrete: Microstrructure, Properties, and Materials,* 3rd Ed. New York, USA: McGraw-Hill.

Miron, L. E. R. D. & Magaña, M. E. L. (2017) Influence of Sulfur Ions on Concrete Resistance to Microbiologically Induced Concrete Corrosion. *In:* Miron, L. E. R. D. & Koleva, D. A. (eds.) *Concrete Durability.* New York: Springer International Publishing.

Mohee, R., Mauthoor, S., Bundhoo, Z. M. A., Somaroo, G., Soobhany, N. & Gunasee, S. (2015) Current status of solid waste management in small island developing states: A review. *Waste Management*. 43. (Supplement C), pp. 539–549.

Monrose, J. & Tota-Maharaj, K. (2018) Technological Review of Permeable Pavement Systems for Applications in Small Island Developing States. *CLEAN – Soil, Air, Water*. 46. (9), pp. 1700168.

Monrose, J., Tota-Maharaj, K. & Mwasha, A. (2019a) Assessment of the physical characteristics and stormwater effluent quality of permeable pavement systems containing recycled materials. *Road Materials and Pavement Design*. pp. 1-33.

Monrose, J., Tota-Maharaj, K., Mwasha, A. & Hills, C. (2019b) Effect of carbon-negative aggregates on the strength properties of concrete for permeable pavements. *International Journal of Pavement Engineering*. pp. 1-9.

Mooney, M. A. & Miller, P. K. (2009) Analysis of Lightweight Deflectometer Test Based on In Situ Stress and Strain Response. *Journal of Geotechnical and Geoenvironmental Engineering*. 135. (2), pp. 199-208.

Moriasi, D. N., Arnold, J. G., Van Liew, M. W., Bingner, R. L., Harmel, R. D. & Veith, T. L. (2007) Model evaluation guidelines for systematic quantification of accuracy in watershed simulations. *Transactions of the ASABE*. 50. (3), pp. 885–900.

Mullaney, J. & Lucke, T. (2013) Practical review of pervious pavement designs. *CLEAN – Soil Air Water*. 42. (2), pp. 111–124.

Murugan, R. B., Natarajan, C. & Chen, S.-E. (2016) Material development for a sustainable precast concrete block pavement. *Journal of Traffic and Transportation Engineering (English Edition)*. 3. (5), pp. 483-491.

Mwasha, A. (2009) Natural and Recycled Guanapo Quarzite Aggregates for Ready Mix Concrete. *The Journal of the Association of Professional Engineers of Trinidad and Tobago*. 38. (1), pp. 50–56.

Mwasha, A., Armstrong-Richardson, A. & Wilson, W. (2013) Management of Polystyrene Wastes Using a Supercritical Solvent - Propanone. *The Journal of Association of Professional Engineers of Trinidad and Tobago*. 41. (1), pp. 23–28.

Myers, B., Beecham, S. & Leeuwen, J. A. v. (2011) Water quality with storage in permeable pavement basecourse. *Proceedings of the Institution of Civil Engineers - Water Management*. 164. (7), pp. 361–372.

Myers, B. R., Beecham, S., Van Leeuwen, J. & Keegan, A. (2009) Depletion of E. coli in permeable pavement mineral aggregate storage and reuse systems. *Water Science and Technology*. 60. (12), pp. 3091–3099.

Nash, J. E. & Sutcliffe, J. V. (1970) River flow forecasting through conceptual models part I — A discussion of principles. *Journal of Hydrology*. 10. (3), pp. 282–290.

Newman, A. P., Pratt, C. J., Coupe, S. J. & Cresswell, N. (2002) Oil bio-degradation in permeable pavements by microbial communities. *Water Science and Technology*. 45. (7), pp. 51–56.

Newman, A. P., Puehmeier, T., Kwok, V., Lam, M., Coupe, S. J., Shuttleworth, A. & Pratt, C. J. (2004) Protecting groundwater with oil-retaining pervious pavements: historical perspectives, limitations and recent developments. *Quarterly Journal of Engineering Geology and Hydrogeology*. 37. (4), pp. 283–291.

Ngugi, H. N., Kaluli, J. W. & Abiero-Gariy, Z. (2017) Use of expanded polystyrene technology and materials recycling for building construction in Kenya. *American Journal of Engineering Technology Management*. 2. (5), pp. 41-50.

Nichols, P. W. B., Lucke, T. & Dierkes, C. (2014) Comparing two methods of determining infiltration rates of permeable interlocking concrete pavers. *Water*. 6. (8), pp. 2353–2366.

Nichols, P. W. B., White, R. & Lucke, T. (2015) Do sediment type and test durations affect results of laboratory-based, accelerated testing studies of permeable pavement clogging? *Science of the Total Environment*. 511 pp. 786–791.

Nicols, P. W. B. & Lucke, T. (2017) A Detailed Analysis of Sediment Particle Sizes and Clogging in Permeable Pavements. *CLEAN – Soil Air Water*. 45. (4), pp. 170078.

Nipper, J. (2016). *Measurement and Modeling of Stormwater from Small Suburban Watersheds in Vermont*. PhD, The University of Vermont.

Nishigaki, M. (2000) Producing permeable blocks and pavement bricks from molten slag. *Waste Management*. 20. (2–3), pp. 185–192.

Nnadi, E. O., Coupe, S. J., Sañudo-Fontaneda, L. A. & Rodriguez-Hernandez, J. (2014) An evaluation of enhanced geotextile layer in permeable pavement to improve stormwater infiltration and attenuation. *International Journal of Pavement Engineering*. 15. (10), pp. 925–932.

Nnadi, E. O., Newman, A. P., Coupe, S. J. & Mbanaso, F. U. (2015) Stormwater harvesting for irrigation purposes: An investigation of chemical quality of water recycled in pervious pavement system. *Journal of Environmental Management*. 147 pp. 246–256.

NRCS (1986) *Urban Hydrology for Small Watersheds: TR-55*, Washington, D.C.: Natural Resources Conservation Service.

NRMCA (2004) *CIP 38 - Pervious Concrete*. Available from: http://www.nrmca.org/GreenConcrete/CIP%2038p.pdf [Accessed 18 January 2018].

Nurse, L. A., McLean, R. F., Agard, L. P., Briguglio, L. P., Duvat-Magnan, V., Pelesikoti, N., Tompkins, E. & Webb, A. (2014) Small islands. *In:* Barros, V.R., Field, C.B., Dokken, D.J., Mastrandrea, M.D., Mach, K.J., Bilir, T.E., Chatterjee, M., Ebi, K.L., Estrada, Y.O., Genova, R.C., Girma, B., Kissel, E.S., Levy, A.N., MacCracken, S., Mastrandrea, P.R. & White, L.L. (eds.) *Climate Change 2014: Impacts, Adaptation, and Vulnerability. Part B: Regional Aspects. Contribution of Working Group II to the Fifth Assessment Report of the Intergovernmental Panel on Climate Change*. Cambridge, United Kingdom and New York, NY, USA: Cambridge University Press.

Orlov, V., Martynov, S. & Kunytskiy, S. (2016) Energy saving in water treatment technologies with polystyrene foam filters. *Journal of Water and Land Development*. 31. (1), pp. 119.

Osuagwu, J. C., Nwakwasi, N. L. & Nwachukwu, A. N. (2018) Iron removal in waste water using expanded polystyrene as an artificial media. *Nigerian Journal of Technology*. 37. (3), pp. 841-845.

Pagotto, C., Legret, M. & Le Cloirec, P. (2000) Comparison of the hydraulic behaviour and the quality of highway runoff water according to the type of pavement. *Water Research*. 34. (18), pp. 4446–4454.

Pakzad, P., Osmond, P. & Corkery, L. (2017) Developing Key Sustainability Indicators for Assessing Green Infrastructure Performance. *Procedia Engineering*. 180 pp. 146–156.

Park, D., Sandoval, N., Lin, W., Kim, H. & Cho, Y. (2014) A case study: Evaluation of water storage capacity in permeable block pavement. *KSCE Journal of Civil Engineering*. 18. (2), pp. 514–520.

Parkinson, J. (2002) Urban drainage in developing countries – challenges and opportunities. *Waterlines*. 20. (4), pp. 2–5.

Pazwash, H. (2011) *Urban Storm Water Management*, Boca Raton, Fl, USA: CRC Press.

Pelling, M. & Uitto, J. I. (2001) Small island developing states: natural disaster vulnerability and global change. *Environmental Hazards*. 3. (2), pp. 49–62.

Penn, A. B. (2012) *The Virgin Islands Climate Change Adaptation Policy: Achieving Low-Carbon, Climate-Resilient Development*. The Virgin Islands: Government of the Virgin Islands, Ministry of Natural Resources and Labour, Conservation and Fisheries Department,.

Pezzaniti, D., Beecham, S. & Kandasamy, J. (2009) Influence of clogging on the effective life of permeable pavements. *Water Management*. 162. (3), pp. 211–220.

Phillips, W. & Thorne, E. (2013) *Municipal solid waste management in the Caribbean - A benefit-cost analysis*: Economic Commission for Latin America and the Caribbean, ECLAC.

Pilgrim, D. H. & Cordey, I. (1992) Flood runoff. *In:* Maidment, D. R. (ed.) *Handbook of hydrology.* New York: McGraw-Hill.

Pilon, B. S., Tyner, J. S., Yoder, D. C. & Buchanan, J. R. (2019) The Effect of Pervious Concrete on Water Quality Parameters: A Case Study. *Water*. 11. (2), pp. 263.

Pitt, R., Clark, S. & Field, R. (1999) Groundwater contamination potential from stormwater infiltration practices. *Urban Water*. 1. (3), pp. 217–236.

Poleto, C. & Tassi, R. (2012) Sustainable Urban Drainage Systems. *In:* Javaid, M. S. (ed.) *Drainage Systems.* InTech.

Poon, C. & Chan, D. (2006) Feasible use of recycled concrete aggregates and crushed clay brick as unbound road sub-base. *Construction and Building Materials*. 20. (8), pp. 578–585.

Pratt, C. J. (1990) Permeable pavments for stormwater quality enhancement. In: Torno, H.C. *Engineering Foundation Conference*. Davos Platz, Switzerland, 22–27 October 1989. ASCE, pp. 131–155.

Pratt, C. J. (1997) Design guidelines for porous/permeable pavements. In: Rowney, Charles *Engineering Foundation Conference: Sustaining Water Resources in the 21st Century*. Malmö, Sweden, 7–12 September 1997. ASCE, pp. 196–211.

Pratt, C. J. (1999) Use of permeable, reservoir pavement constructions for stormwater treatment and storage for re-use. *Water Science and Technology*. 39. (5), pp. 145–151.

Pratt, C. J., Mantle, J. D. G. & Schofield, P. A. (1995) UK research into the performance of permeable pavement, reservoir structures in controlling stormwater discharge quantity and quality. *Water Science and Technology*. 32. (1), pp. 63–69.

Pratt, C. J., Newman, A. P. & Bond, P. C. (1999) Mineral oil bio-degradation within a permeable pavement: Long term observations. *Water Science and Technology*. 39. (2), pp. 103–109.

Pratt, C. J., Wilson, S. & Cooper, P. (2002) *Source control using constructed pervious surfaces, C582*, Westminster, London: CIRIA.

Qin, Y. (2015) A review on the development of cool pavements to mitigate urban heat island effect. *Renewable and Sustainable Energy Reviews*. 52 pp. 445-459.

Radfar, A. & Rockaway, T. D. (2016a) Captured Runoff Prediction Model by Permeable Pavements Using Artificial Neural Networks. *Journal of Infrastructure Systems*. 22. (3), pp. 04016007.

Radfar, A. & Rockaway, T. D. (2016b) Clogging Prediction of Permeable Pavement. *Journal of Irrigation and Drainage Engineering*. 142. (4), pp. 04015069.

Rafiei, K., Kavussi, A. & Yasrobi, S. (2012) Construction Quality Control of Unbound Layers Based on Stiffness Modulus Criteria. *Journal of Civil Engineering and Management*. 18. (1), pp. 5-13.

Rahman, M. A., Imteaz, M., Arulrajah, A. & Disfani, M. M. (2014) Suitability of recycled construction and demolition aggregates as alternative pipe backfilling materials. *Journal of Cleaner Production*. 66 pp. 75–84.

Rahman, M. A., Imteaz, M. A., Arulrajah, A., M. Disfani, M. & Horpibulsuk, S. (2015a) Engineering and Environmental Assessment of Recycled Construction and Demolition Materials Used with Geotextile for Permeable Pavements. *Journal of Environmental Engineering*. 141. (9), pp. 04015019.

Rahman, M. A., Imteaz, M. A., Arulrajah, A., Piratheepan, J. & Disfani, M. M. (2015b) Recycled construction and demolition materials in permeable pavement systems: geotechnical and hydraulic characteristics. *Journal of Cleaner Production*. 90 pp. 183–194.

Rama, M. & Shanthi, V. M. (2018) Experimental Study on Sedimentation Removal of Pervious Concrete. *Archives of Civil Engineering*. 64. (1), pp. 181–195.

Rand, T., Haukohl, J. & Marxen, U. (2000) *Municipal Solid Waste Incineration: A Decision Maker's Guide*. Washington, D.C., USA: The World Bank.

Rao, A., Jha, K. N. & Misra, S. (2007) Use of aggregates from recycled construction and demolition waste in concrete. *Resources, Conservation and Recycling*. 50. (1), pp. 71–81.

Razzaghmanesh, M. & Beecham, S. (2018) A review of permeable pavement clogging investigations and recommended maintenance regimes. *Water*. 10. (337), pp. 9.

Razzaghmanesh, M. & Borst, M. (2019) Long-term effects of three types of permeable pavements on nutrient infiltrate concentrations. *Science of The Total Environment*. 670 pp. 893–901.

Reddy, K. R., Xie, T. & Dastgheibi, S. (2014) Removal of heavy metals from urban stormwater runoff using different filter materials. *Journal of Environmental Chemical Engineering*. 2. (1), pp. 282–292.

Reed, B. (2004) *Sustainable urban drainage in low-income countries - a scoping study*. Leicestershire, UK: WEDC, Loughborough University.

Renou, S., Givaudan, J. G., Poulain, S., Dirassouyan, F. & Moulin, P. (2008) Landfill leachate treatment: Review and opportunity. *Journal of Hazardous Materials*. 150. (3), pp. 468–493.

Rizvi, R., Tighe, S., Henderson, V. & Norris, J. (2010) Evaluating the use of recycled concrete aggregate in pervious concrete pavement. *Transportation Research Record: Journal of the Transportation Research Board*. (2164), pp. 132–140.

Rizwan, A. M., Dennis, L. Y. C. & Chunho, L. (2008) A review on the generation, determination and mitigation of Urban Heat Island. *Journal of Environmental Sciences*. 20. (1), pp. 120–128.

Robinson, D. A., Jones, S. B., Wraith, J. M., Or, D. & Friedman, S. P. (2003) A review of advances in dielectric and electrical conductivity measurement in soils using time domain reflectometry. *Vadose Zone Journal*. 2. (4), pp. 444–475.

Rocheta, V. L. S., Isidoro, J. M. G. P. & de Lima, J. L. M. P. (2017) Infiltration of Portuguese cobblestone pavements – An exploratory assessment using a double-ring infiltrometer. *Urban Water Journal*. 14. (3), pp. 291–297.

Rodriguez-Hernandez, J., Andrés-Valeri, V. C., Ascorbe-Salcedo, A. & Castro-Fresno, D. (2016) Laboratory Study on the Stormwater Retention and Runoff Attenuation Capacity of Four Permeable Pavements. *Journal of Environmental Engineering*. 142. (2), pp. 04015068.

Rodríguez-Rojas, M. I., Huertas-Fernández, F., Moreno, B., Martínez, G. & Grindlay, A. L. (2018) A study of the application of permeable pavements as a sustainable technique for the mitigation of soil sealing in cities: A case study in the south of Spain. *Journal of Environmental Management*. 205 pp. 151–162.

Rosa, D. J., Clausen, J. C. & Dietz, M. E. (2015) Calibration and Verification of SWMM for Low Impact Development. *Journal of the American Water Resources Association (JAWRA)*. 51. (3), pp. 746–757.

Rossman, L. A. (2010) Modeling low impact development alternatives with SWMM. *Journal of Water Management Modeling*. pp. 167–182.

Rossman, L. A. (2015) *Storm Water Management Model User's Manual Version 5.1*, Cincinnati, OH USA: U.S. Environmental Protection Agency.

Rossman, L. A. (2016) *Storm Water Management Model Reference Manual Volume III – Water Quality*. Cincinnati, OH USA:

Rossman, L. A. & Huber, W. C. (2016a) *Storm Water Management Model Reference Manual Volume I – Hydrology (Revised)*. Cincinnati, OH USA:

Rossman, L. A. & Huber, W. C. (2016b) *Storm Water Management Model Reference Manual Volume II – Hydraulics*. Cincinnati, OH USA:

Roy, A. H., Wenger, S. J., Fletcher, T. D., Walsh, C. J., Ladson, A. R., Shuster, W. D., Thurston, H. W. & Brown, R. R. (2008) Impediments and Solutions to Sustainable, Watershed-Scale Urban Stormwater Management: Lessons from Australia and the United States. *Environmental Management*. 42. (2), pp. 344–359.

Rushton, B. T. (2001) Low-impact parking lot design reduces runoff and pollutant loads. *Journal of Water Resources Planning and Management*. 127. (3), pp. 172–179.

Sabnis, G. M. & Obla, K. H. (2009) Pervious Concrete for Sustainable Development. *In:* Sabnis, G. M. (ed.) *Green Building with Concrete: Sustainable Design and Construction.* Boca Raton, Florida: CRC Press.

Sansalone, J., Kuang, X. & Ranieri, V. (2008) Permeable Pavement as a Hydraulic and Filtration Interface for Urban Drainage. *Journal of Irrigation and Drainage Engineering*. 134. (5), pp. 666–674.

Sansalone, J., Kuang, X., Ying, G. & Ranieri, V. (2012) Filtration and clogging of permeable pavement loaded by urban drainage. *Water Research*. 46. (20), pp. 6763-6774.

Sañudo-Fontaneda, L. A. (2014). *The analysis of rainwater infiltration into permeable pavements, with concrete blocks and porous mixtures, for the source control of flooding.* PhD, University of Cantabria.

Sañudo-Fontaneda, L. A., Charlesworth, S. M., Castro-Fresno, D., Andres-Valeri, V. C. A. & Rodriguez-Hernandez, J. (2014) Water quality and quantity assessment of pervious pavements performance in experimental car park areas. *Water Science and Technology*. 69. (7), pp. 1526–1533.

Sawyer, C. N., McCarty, P. L. & Parkin, G. F. (2003) *Chemistry for Environmental Engineering and Science,* 5th Ed. New York: McGraw-Hill.

Scholz, M. (2013) Water quality improvement performance of geotextiles within permeable pavement systems: A critical review. *Water*. 5. (2), pp. 462–479.

Scholz, M., Charlesworth, S. M. & Coupe, S. J. (2014) Drainage Benefits of Porous, Permeable and Pervious Paving. *In:* Booth, C.A. & Charlesworth, S. M. (eds.) *Water Resources in the Built Environment: Management Issues and Solutions.* Chichester, UK. : John Wiley & Sons, Ltd.

Scholz, M. & Grabowiecki, P. (2007) Review of permeable pavement systems. *Building and Environment*. 42. (11), pp. 3830–3836.

Schöntag, J. M., Pizzolatti, B. S., Jangada, V. H., de Souza, F. H. & Sens, M. L. (2015) Water quality produced by polystyrene granules as a media filter on rapid filters. *Journal of Water Process Engineering*. 5. (Supplement C), pp. 118–126.

Scrivener, K. L., Crumbie, A. K. & Laugesen, P. (2004) The Interfacial Transition Zone (ITZ) Between Cement Paste and Aggregate in Concrete. *Interface Science*. 12. (4), pp. 411–421.

Sehgal, K., Drake, J., Seters, T. & Vander Linden, W. J. W. (2018) Improving restorative maintenance practices for mature permeable interlocking concrete pavements. *Water*. 10. (11), pp. 1588.

Selvakumar, A. & O'Connor, T. P. (2018) Organism Detection in Permeable Pavement Parking Lot Infiltrates at the Edison Environmental Centre, New Jersey. *Water Environment Research*. 90. (1), pp. 21–29.

Senseney, C. T., Grasmick, J. & Mooney, M. A. (2014) Sensitivity of lightweight deflectometer deflections to layer stiffness via finite element analysis. *Canadian Geotechnical Journal*. 52. (7), pp. 961-970.

Shackel, B. (2010) The design, construction and evaluation of permeable pavements in Australia. In: *24th ARRB Conference-Building on 50 Years of Road and Transports Research*. Melbourne, Australia, 13 – 15 October 2010. pp. 1–14.

Sharma, A. K., Gray, S., Diaper, C., Liston, P. & Howe, C. (2008) Assessing integrated water management options for urban developments–Canberra case study. *Urban Water Journal*. 5. (2), pp. 147–159.

Sharma, D. (2008) Sustainable Drainage System (SuDs) for Stormwater Management: A Technological and Policy Intervention to Combat Diffuse Pollution. In: *11th International Conference on Urban Drainage*. Edinburgh, Scotland, UK, 31 August – 05 September 2008. pp. 1–10.

Shrivastava, G. (2016) A Road Collapse at Pont Cassé, Dominica: Hydrologic and Hydraulic Aspects. *The West Indian Journal of Engineering*. 38. (2), pp. 59–63.

Shuster, W. D., Bonta, J., Thurston, H. W., Warnemuende, E. & Smith, D. R. (2005) Impacts of impervious surface on watershed hydrology: a review. *Urban Water Journal*. 2. (4), pp. 263–275.

Simon, A., Javier, X. L., Alistair, R. G., John, A. C., Badin, R. G. & Colin, D. W. (2016) Interactions between sea-level rise and wave exposure on reef island dynamics in the Solomon Islands. *Environmental Research Letters*. 11. (5), pp. 054011.

Siriwardene, N. R., Deletic, A. & Fletcher, T. D. (2007) Clogging of stormwater gravel infiltration systems and filters: Insights from a laboratory study. *Water research*. 41. (7), pp. 1433–1440.

SLSWMA (2002) *Waste Characterization Study - St. Lucia*. Castries, St. Lucia: SLSWMA.

SLSWMA (2008) *Waste Characterization Study - St. Lucia*. Castries, St. Lucia: SLSWMA.

SLSWMA (2015) *Saint Lucia Solid Waste Management Authority Annual Report 2014-2015*. Castries, St. Lucia: SLSWMA.

Smith, D. R. (2011) *Permeable Interlocking Concrete Pavement (PICP) - Selection Design Construction Maintenance*, 4th Ed. Herndon, VA: Interlocking Pavement Concrete Institute (ICPI).

Sokolović, R. S., Sokolović, S. & Govedarica, D. (2009) Performance of expanded polystyrene particles in deep bed filtration. *Separation and Purification Technology*. 68. (2), pp. 267–272.

Sounthararajah, D. P., Loganathan, P., Kandasamy, J. & Vigneswaran, S. (2017) Removing heavy metals using permeable pavement system with a titanate nano-fibrous adsorbent column as a post treatment. *Chemosphere*. 168 pp. 467–473.

Stamp, D. H. & Mooney, M. A. (2013) Influence of lightweight deflectometer characteristics on deflection measurement. *Geotechnical Testing Journal*. 36. (2), pp. 216–226.

Stander, E. K., Rowe, A. A., Borst, M. & O'Connor, T. P. (2013) Novel Use of Time Domain Reflectometry in Infiltration-Based Low Impact Development Practices. *Journal of Irrigation and Drainage Engineering*. 139. (8), pp. 625–634.

Steinert, B. C., Humphrey, D. N. & Kestler, M. A. (2005) *Portable Falling Weight Deflectometer Study*. University of Connecticut, Storrs, CT: New England Transportation Consortium.

Stewart, R. & Hytiris, N. (2008) The role of Sustainable Urban Drainage Systems in reducing the flood risk associated with infrastructure A93 Craighall Gorge to Middle Mause Farm-Road Realignment, Perth, Scotland–Case Study. In: *11th International Conference on Urban Drainage*. Edinburgh, Scotland, UK, 31 August – 05 September 2008. pp. 1–15.

Suleiman, M. T., Gopalakrishnan, K. & Kevern, J. T. (2011) Structural Response of Pervious Concrete Pavement Systems Using Falling Weight Deflectometer Testing and Analysis. *Journal of Transportation Engineering*. 137. (12), pp. 907–917.

SWMCOL (2010) *Trinidad Solid Waste Management Program, Waste Characterization and Centroid Study, Final Report*. Port of Spain, Trinidad: SWMCOL.

SWMCOL (2016) *Trinidad and Tobago's Waste Generation Per Capita*. Available from: http://www.swmcol.co.tt/ [Accessed 10 May 2016].

Takebayashi, H. & Moriyama, M. (2009) Study on the urban heat island mitigation effect achieved by converting to grass-covered parking. *Solar Energy*. 83. (8), pp. 1211-1223.

Tatsuoka, F., Tomita, Y.-I., Iguchi, Y. & Hirakawa, D. (2013) Strength and stiffness of compacted crushed concrete aggregate. *Soils and Foundations*. 53. (6), pp. 835–852.

Tavares, L. M. & Kazmierczak, C. S. (2016) The influence of recycled concrete aggregates in pervious concrete. *Revista IBRACON de Estruturas e Materiais*. 9. (1), pp. 75–89.

Tennis, P. D., Leming, M. L. & Akers, D. J. (2004) *Pervious concrete pavements*, Skokie, IL: Portland Cement Association.

Thelen, E., Grover, W. C., Hoiberg, A. J. & Haigh, T. I. (1972) *Investigation of porous pavements for urban runoff control*, Washington, D.C.: US EPA.

Thomas, A., Haselbach, L., Poor, C. & Freimund, M. (2015) Long-Term Metal Retention Performance of Media Filter Drains for Stormwater Management. *Sustainability*. 7. (4), pp. 3721–3733.

Thomas, S. (2013) The "Future is Urban" Challenge of Sustainable Urban Development in the Caribbean: The Search for Sustainable Urban Forms In: *49th ISOCARP Congress*. Brisbane, Australia, 1–4 October 2013. pp. 1–12.

Tirado, C., Gamez-Rios, K. Y., Fathi, A., Mazari, M. & Nazarian, S. (2017) Simulation of Lightweight Deflectometer Measurements Considering Nonlinear Behavior of Geomaterials. *Transportation Research Record*. 2641. (1), pp. 58-65.

Topp, G. C., Davis, J. L. & Annan, A. P. (1980) Electromagnetic determination of soil water content: Measurements in coaxial transmission lines. *Water Resources Research*. 16. (3), pp. 574–582.

Toronto and Region Conservation (2008) *Performance Evaluation of Permeable Pavement and a Bioretention Swale - Seneca College, King City, Ontario* Ontario, Canada:

Tota-Maharaj, K. (2010). *Geothermal paving systems for urban runoff treatment and renewable energy efficiency.* PhD, The University of Edinburgh.

Tota-Maharaj, K., Grabowiecki, P., Akintunde, B. & Coupe, S. J. (2012) The performance and effectiveness of geotextiles within permeable pavements for treating concentrated stormwater. In: *Sixteenth International Water Technology Conference, IWTC 16*. Istanbul, Turkey 7–10 May 2012. pp. 1–13.

Tota-Maharaj, K. & Scholz, M. (2010) Efficiency of permeable pavement systems for the removal of urban runoff pollutants under varying environmental conditions. *Environmental Progress & Sustainable Energy*. 29. (3), pp. 358–369.

Treasure, A. S.-O. (2003) Comparison of municipal waste characterization and generation rates in selected caribbean territories and their implications. In: *12th Annual Caribbean Water and Wastewater Association Conference and Exhibition*. Paradise Island, Bahamas, 28 September – 03 October 2003. pp. 1–10.

Treidel, H., Martin-Bordes, J. L. & Gurdak, J. J. (2012) *Climate change effects on groundwater resources: a global synthesis of findings and recommendations*, AK Leiden, The Netherlands: CRC Press/Balkema.

Trinidad & Tobago Guardian (2015) Minister: $321m to manage waste disposal, 15 August.

Turco, M., Kodešová, R., Brunetti, G., Nikodem, A., Fér, M. & Piro, P. (2017) Unsaturated hydraulic behaviour of a permeable pavement: Laboratory investigation and numerical analysis by using the HYDRUS-2D model. *Journal of hydrology*. 554 pp. 780–791.

Tyner, J. S., Wright, W. C. & Dobbs, P. A. (2009) Increasing exfiltration from pervious concrete and temperature monitoring. *Journal of Environmental Management*. 90. (8), pp. 2636–2641.

UN-DESA (2010) *Trends in Sustainable Development: Small Island Developing States (SIDS)*. New York, USA: UN-DESA.

UN-DESA (2015) *World Urbanization Prospects: The 2014 Revision*. New York, USA: UN-DESA.

UN-DESA (2018) *Small Island Developing States*. Available from: https://sustainabledevelopment.un.org/topics/sids/list [Accessed 18 January 2018].

UN-FCCC (2007) *Climate Change: Impacts, Vulnerabilities and Adaptation in Developing Countries*. New York, USA: UN-FCCC.

UN-Habitat (2015) *Urbanization and Climate Change in Small Island Developing States*. Nairobi: UN-Habitat.

UN-OHRLLS (2009) *The impact of climate change on the development prospects of the least developed countries and small island developing states*. New York, USA: UN-OHRLLS.

UN-OHRLLS (2011) *Small Island Developing States: Small Island Big(ger) Stakes*. New York, USA: UN-OHRLLS.

UN (1992) *United Nations Framework Convention on Climate Change*. New York, USA: UN.

UN (1994) *Report on the Global Conference on the Sustainable Development of Small Island Developing States*. New York, USA: UN.

UNEP (1999) *Waste Management in Small Island Developing States*. Available from: http://islands.unep.ch/d99-6a2.htm [Accessed 10 March 2017].

UNEP (2012) *Integrated Water Resources Management Planning Approach for Small Island Developing States*, Nairobi, Kenya: UNEP.

UNEP, UN-DESA & FAO (2012) *SIDS-FOCUSED Green Economy: An Analysis of Challenges and Opportunities*. New York, USA: UN.

US EPA (2008) *Reducing Urban Heat Islands: Compendium of Strategies–Cool Pavements*. Washington, D. C., USA: US EPA.

US EPA (2012) *Guidelines for Water Reuse*, Washington, D.C.: CDM Smith Inc.

US EPA (2018) *Rule Chapter: 62-302 Surface Water Quality Standards*, Washington, DC, USA: US EPA.

USDA & NRCS (2009) Hydrologic Soil Groups. *In:* USDA & NRCS (eds.) *Part 630 Hydrology National Engineering Handbook.*

Vadas, T. M., Smith, M. & Luan, H. (2017) Leaching and retention of dissolved metals in particulate loaded pervious concrete columns. *Journal of Environmental Management*. 190 pp. 1–8.

Van Heystraeten, G. & Moraux, C. (1990) Ten years' experience of porous asphalt in Belgium. *Transportation Research Record: Journal of the Transportation Research Board*. (1265), pp. 1.

Vancura, M., Macdonald, K. & Khazanovich, L. (2011) Structural Analysis of Pervious Concrete Pavement. *Transportation Research Record: Journal of the Transportation Research Board*. 2226. (1), pp. 13–20.

Vaze, J., Jordan, P., Beecham, R., Frost, A. & Summerell, G. (2012) *Guidelines for rainfall-runoff modelling: Towards best practice model application,* Australia: eWater Cooperative Research Centre.

Walsh, S. P., Rowe, A. & Guo, Q. (2014) Laboratory Scale Study to Quantify the Effect of Sediment Accumulation on the Hydraulic Conductivity of Pervious Concrete. *Journal of Irrigation and Drainage Engineering*. 140. (6), pp. 04014014.

Wang, K.-H. & Altunkaynak, A. (2012) Comparative Case Study of Rainfall-Runoff Modeling between SWMM and Fuzzy Logic Approach. *Journal of Hydrologic Engineering*. 17. (2), pp. 283-291.

Wang, X., Chen, J., Kong, Y. & Shi, X. (2014) Sequestration of phosphorus from wastewater by cement-based or alternative cemetitious materials. *Water Research*. 62 pp. 88–96.

Weiss, P. T., Kayhanian, M., Gulliver, J. S. & Khazanovich, L. (2019) Permeable pavement in northern North American urban areas: research review and knowledge gaps. *International Journal of Pavement Engineering*. 20. (2), pp. 143–162.

White, D., Thompson, M. & Vennapusa, P. (2007) *Field Validation of Intelligent Compaction Monitoring Technology for Unbound Materials.* St Paul, MN, USA: Minnesota Department of Transportation.

Willems, P., Arnbjerg-Nielsen, K., Olsson, J. & Nguyen, V. T. V. (2012) Climate change impact assessment on urban rainfall extremes and urban drainage: Methods and shortcomings. *Atmospheric Research*. 103 pp. 106–118.

Wilson, S., Newman, A. P., Puehmeier, T. & Shuttleworth, A. (2003) Performance of an oil interceptor incorporated into a pervious pavement. *Engineering Sustainability*. 156. (1), pp. 51–58.

Winston, R. J., Al-Rubaei, A. M., Blecken, G. T., Viklander, M. & Hunt, W. F. (2016) Maintenance measures for preservation and recovery of permeable pavement surface

infiltration rate – The effects of street sweeping, vacuum cleaning, high pressure washing, and milling. *Journal of Environmental Management*. 169 pp. 132–144.

Woods Ballard, B., Kellagher, R., Martin, P., Jefferies, C., Bray, R. & Shaffer, P. (2007) *The SuDS Manual, C697,* London, UK: CIRIA.

Woods Ballard, B., Wilson, S., Udale-Clarke, H., Illman, S., Scott, T., Ashley, R. & Kellagher, R. (2015) *The SuDS Manual, C753,* London, UK: CIRIA.

World Bank (2018) *Average precipitation in depth (mm per year)*. Available from: https://data.worldbank.org/indicator/ag.lnd.prcp.mm [Accessed 18 January 2018].

World Commission on Environment and Development (1987) *Our Common Future,* New York, USA: Oxford University Press.

Xu, Y., Jiang, L., Xu, J. & Li, Y. (2012) Mechanical properties of expanded polystyrene lightweight aggregate concrete and brick. *Construction and Building Materials*. 27. (1), pp. 32–38.

Yao, X., Wang, W., Liu, M., Yao, Y. & Wu, S. (2019) Synergistic use of industrial solid waste mixtures to prepare ready-to-use lightweight porous concrete. *Journal of Cleaner Production*. 211 pp. 1034-1043.

Yener, M. K. (2006). *Semi-Distributed Hydroloic Modeling Studies in Yuvacik Basin.* MSc., Middle East Technical University.

Yong, C. F., Deletic, A., Fletcher, T. D. & Grace, M. R. (2008) The clogging behaviour and treatment efficiency of a range of porous pavements. In: *11th International Conference on Urban Drainage*. Edinburgh, Scotland, UK, 31 August – 05 September 2008. pp. 1–10.

Yong, C. F., McCarthy, D. T. & Deletic, A. (2013) Predicting physical clogging of porous and permeable pavements. *Journal of Hydrology*. 481 pp. 48–55.

Zanders, J. M. (2005) Road sediment: characterization and implications for the performance of vegetated strips for treating road run-off. *Science of the Total Environment*. 339. (1–3), pp. 41–47.

Zhang, G. (2009). *Development of a Multi-objective Optimization Framework for Implementing Low Impact Development Scenarios in an Urbanising Watershed.* PhD, The Pennsylvania State University.

Zhang, S. & Guo, Y. (2014) SWMM Simulation of the Storm Water Volume Control Performance of Permeable Pavement Systems. *Journal of Hydrologic Engineering*. 20. (8), pp. 06014010.

Zhang, Z., Li, Z., Zhang, X., Liu, D., Li, Z. & Li, H. (2018) Systematically Investigated the Influences of Permeable Pavement Materials on the Water Quality of Runoff: Batch and Column Experiments. *Water, Air, & Soil Pollution*. 229. (5), pp. 155.

Zhou, Q. (2014) A review of sustainable urban drainage systems considering the climate change and urbanization impacts. *Water*. 6. (4), pp. 976–992.

Zhou, Q., Mikkelsen, P. S., Halsnæs, K. & Arnbjerg-Nielsen, K. (2012) Framework for economic pluvial flood risk assessment considering climate change effects and adaptation benefits. *Journal of Hydrology*. 414–415 pp. 539–549.

APPENDIX A PHYSICAL PROPERTIES OF AGGREGATES

Table A-1 Determination of specific gravity and water absorption values of basalt aggregates

Aggregate size (mm)		25.4	19.0	12.5	9.5	Average
Aggregate size (in)		1	3/4	1/2	3/8	
Mass of Saturated Surface Dry (SSD) sample in air (g):	A	2119.5	2114.4	2113.1	2200.9	
Wire basket + SSD in Water (g):	B	1346.2	1342.6	1341.8	1399.4	
Mass of oven dry sample (g):	C	2097.5	2091.2	2086.2	2170.4	
Bulk Specific Gravity (G_{sb}):	C/(A-B)	2.712	2.710	2.705	2.708	2.709
Bulk SSD Specific Gravity (G_{sb}SSD):	A/(A-B)	2.741	2.740	2.740	2.746	2.742
Apparent Specific Gravity (G_{sa}):	C/(C-B)	2.792	2.793	2.803	2.815	2.801
Percent Absorption (%):	**([A-C]/C) *100**	**1.0**	**1.1**	**1.3**	**1.4**	**1.2**

Table A-2 Determination of unit weight, voids and porosity values of basalt aggregates

Mould Calibration

Mass of mould in air (kg):	2.53
Mass of mould + water (kg):	5.22
Temperature of water (°C):	29
Unit weight of water (kg/m^3):	995.83
Volume of mould (m^3):	0.0027

Sample Description	Mass of Sample + mould (kg)				Bulk Density (kg/m^3)	Voids	Porosity (%)	SSD Bulk Density (kg/m^3)
	1	2	3	Average				
25.4 mm (1")	6.71	6.68	6.71	6.70	1544.444	0.428	30.0	1559.888
19 mm (3/4")	6.69	6.67	6.64	6.67	1533.333	0.432	30.2	1550.200
12.5 mm (1/2")	6.59	6.65	6.66	6.63	1518.519	0.436	30.4	1538.260
9.5 mm (3/8")	6.62	6.63	6.55	6.60	1507.407	0.441	30.6	1528.511
ASTM No. 5	6.70	6.70	6.67	6.69	1540.741	0.429	30.0	1559.230
ASTM No. 57	6.72	6.78	6.73	6.74	1559.259	0.422	29.7	1577.970
ASTM No. 8	6.66	6.65	6.67	6.66	1529.630	0.433	30.2	1547.986

Table A-3 Determination of Los Angeles (L.A) Abrasion value of basalt aggregates

Sieve Size		Weight for each Grading (g)			
Passing	Retained on	A	B	C	D
37.5 mm (1.5")	25.4 mm (1")	1250 ± 25			
25.4 mm (1")	19 mm (3/4")	1250 ± 25			
19 mm (3/4")	12.5 mm (1/2")	1250 ± 25	2500 ± 10		
12.5 mm (1/2")	9.5 mm (3/8")	1250 ± 25	2500 ± 10		
9.5 mm (3/8")	6.4 mm (1/4")			2500 ± 10	
6.4 mm (1/4")	No. 4			2500 ± 10	
No. 4	No. 8				5000 ± 10
Total Weight		5000 ± 10	5000 ± 10	5000 ± 10	5000 ± 10
No. of spheres		12	11	8	6
Revolutions		500	500	500	500

Grading of sample:	A
Weight of sample (g):	5001.0
Weight retained on No. 12 sieve after test (g):	4097.9
Weight pass No. 12 sieve after test (g):	903.1
Percent Wear (%):	**18**

Table A-4 Determination of flakiness index value of basalt aggregates

Sieve Sizes	Equivalent (mm)	Weight Retained (g)	Weight passing (g)	Total Weight	Flakiness index (%)
3"	75	0.0	0.0	0.00	
2"	50	0.0	0.0	0.00	
1 1/2"	37.5	0.0	0.0	0.00	
1"	25	322.8	0.0	322.80	0
3/4"	19	1252.6	0.8	1253.40	0
1/2"	12.5	969.4	9.9	979.30	1
3/8"	9.5	334.9	5.0	339.90	1
1/4"	6.35	535.0	8.2	543.20	2
Total		**3414.7**	**23.9**	**3438.6**	**1**

Table A-5 Determination of impact value of basalt aggregates

Test No.	1	2
Weight of Sample, A (g):	315.6	318.8
Weight retained on No.7 sieve after test (g):	262	270.4
Weight passing No.7 sieve after test, B (g):	53.6	48.4
Impact Value (B/A × 100) (%):	17	15
Average Impact Value (%):	**16**	

Table A-6 Determination of specific gravity and water absorption values of quartzite aggregates

Aggregate size (mm)		25.4	19.0	12.5	9.5	Average
Aggregate size (in)		1	3/4	1/2	3/8	
Mass of Saturated Surface Dry (SSD) sample in air (g):	A	2119.5	2114.4	2113.1	2200.9	
Wire basket + SSD in Water (g):	B	1346.2	1342.6	1341.8	1399.4	
Mass of oven dry sample (g):	C	2097.5	2091.2	2086.2	2170.4	
Bulk Specific Gravity (G_{sb}):	C/(A-B)	2.564	2.572	2.578	2.585	2.575
Bulk SSD Specific Gravity (G_{sb}SSD):	A/(A-B)	2.585	2.591	2.597	2.606	2.595
Apparent Specific Gravity (G_{sa}):	C/(C-B)	2.620	2.622	2.628	2.639	2.627
Percent Absorption (%):	**([A-C]/C) *100**	**0.8**	**0.7**	**0.7**	**0.8**	**0.8**

Table A-7 Determination of unit weight, voids and porosity values of quartzite aggregates

Mould Calibration

Mass of mould in air (kg):	2.53
Mass of mould + water (kg):	5.22
Temperature of water (°C):	29
Unit weight of water (kg/m^3):	995.83
Volume of mould (m^3):	0.0027

Sample Description	Mass of Sample + mould (kg)				Bulk Density (kg/m^3)	Voids	Porosity (%)	SSD Bulk Density (kg/m^3)
	1	2	3	Average				
25.4 mm (1")	6.40	6.34	6.29	6.34	1411.111	0.447	30.9	1422.400
19 mm (3/4")	6.46	6.45	6.46	6.46	1455.556	0.432	30.2	1465.745
12.5 mm (1/2")	6.55	6.59	6.61	6.58	1500.000	0.416	29.4	1510.500
9.5 mm (3/8)"	6.60	6.67	6.58	6.62	1514.815	0.412	29.2	1526.934
ASTM No. 5	6.60	6.58	6.58	6.59	1503.704	0.414	29.3	1515.734

Table A-8 Determination of Los Angeles (L.A) Abrasion value of quartzite aggregates

Sieve Size		Weight for each Grading (g)			
Passing	Retained on	A	B	C	D
37.5 mm (1.5")	25.4 mm (1")	1250 ± 25			
25.4 mm (1")	19 mm (3/4")	1250 ± 25			
19 mm (3/4")	12.5 mm (1/2")	1250 ± 25	2500 ± 10		
12.5 mm (1/2")	9.5 mm (3/8")	1250 ± 25	2500 ± 10		
9.5 mm (3/8")	6.4 mm (1/4")			2500 ± 10	
6.4 mm (1/4")	No. 4			2500 ± 10	
No. 4	No. 8				5000 ± 10
Total Weight		5000 ± 10	5000 ± 10	5000 ± 10	5000 ± 10
No. of spheres		12	11	8	6
Revolutions		500	500	500	500

Grading of sample:	A
Weight of sample (g):	5002.6
Weight retained on No. 12 sieve after test (g):	2366.2
Weight pass No. 12 sieve after test (g):	2636.4
Percent Wear (%):	**53**

Table A-9 Determination of flakiness index value of quartzite aggregates

Sieve Sizes	Equivalent (mm)	Weight Retained (g)	Weight passing (g)	Total Weight	Flakiness index (%)
3"	75	0.0	0.0	0.00	
2"	50	0.0	0.0	0.00	
1 1/2"	37.5	0.0	0.0	0.00	
1"	25	421.1	39.4	460.50	9
3/4"	19	708.1	26.5	734.60	4
1/2"	12.5	639.5	5.4	644.90	1
3/8"	9.5	435.8	2.1	437.90	0
1/4"	6.35	24.1	0.4	24.50	2
Total		**2228.6**	**73.8**	**2302.4**	**3**

Table A-10 Determination of impact value of quartzite aggregates

Test No.	1	2
Weight of Sample, A (g):	322.3	322.7
Weight retained on No.7 sieve after test (g):	194	206.6
Weight passing No.7 sieve after test, B (g):	128.3	116.1
Impact Value (B/A×100) (%):	40	36
Average Impact Value (%):	**38**	

Table A-11 Determination of specific gravity and water absorption values of CCA

Aggregate size (mm)		25.4	19.0	12.5	9.5	Average
Aggregate size (in)		1	3/4	1/2	3/8	
Mass of Saturated Surface Dry (SSD) sample in air (g):	A	2119.0	2077.3	2006.8	2022.6	
Wire basket + SSD in Water (g):	B	1232.8	1211.6	1175.0	1182.7	
Mass of oven dry sample (g):	C	1967.0	1909.5	1903.1	1901.6	
Bulk Specific Gravity (G_{sb}):	C/(A-B)	2.220	2.206	2.288	2.264	2.245
Bulk SSD Specific Gravity (G_{sb}SSD):	A/(A-B)	2.391	2.400	2.413	2.408	2.403
Apparent Specific Gravity (G_{sa}):	C/(C-B)	2.679	2.736	2.614	2.645	2.669
Percent Absorption (%):	**([A-C]/C) *100**	**7.7**	**8.8**	**5.4**	**6.4**	**7.1**

Table A-12 Determination of unit weight, voids and porosity values of CCA

Mould Calibration

Mass of mould in air (kg):	2.53
Mass of mould + water (kg):	5.22
Temperature of water (°C):	29
Unit weight of water (kg/m^3):	995.83
Volume of mould (m^3):	0.0027

Sample Description	Mass of Sample + mould (kg)				Bulk Density (kg/m^3)	Voids	Porosity (%)	SSD Bulk Density (kg/m^3)
	1	2	3	Average				
25.4 mm (1")	5.85	5.89	5.87	5.87	1237.037	0.440	30.6	1332.289
19 mm (3/4")	5.93	5.94	5.94	5.94	1262.963	0.425	29.8	1374.104
12.5 mm (1/2")	5.91	5.93	5.93	5.92	1255.556	0.449	31.0	1323.356
ASTM No. 5	5.90	5.92	5.92	5.91	1251.852	0.440	30.6	1340.733

Table A-13 Determination of Los Angeles (L.A) Abrasion value of CCA

Sieve Size		Weight for each Grading (g)			
Passing	Retained on	A	B	C	D
37.5 mm (1.5")	25.4 mm (1")	1250 ± 25			
25.4 mm (1")	19 mm (3/4")	1250 ± 25			
19 mm (3/4")	12.5 mm (1/2")	1250 ± 25	2500 ± 10		
12.5 mm (1/2")	9.5 mm (3/8")	1250 ± 25	2500 ± 10		
9.5 mm (3/8")	6.4 mm (1/4")			2500 ± 10	
6.4 mm (1/4")	No. 4			2500 ± 10	
No. 4	No. 8				5000 ± 10
Total Weight		5000 ± 10	5000 ± 10	5000 ± 10	5000 ± 10
No. of spheres		12	11	8	6
Revolutions		500	500	500	500

Grading of sample:	A
Weight of sample (g):	5000.3
Weight retained on No. 12 sieve after test (g):	2799.8
Weight pass No. 12 sieve after test (g):	2200.5
Percent Wear (%):	**44**

Table A-14 Determination of impact value of CCA

Test No.	1	2
Weight of Sample, A (g):	243.94	247.02
Weight retained on No.7 sieve after test (g):	141.36	146.69
Weight passing No.7 sieve after test, B (g):	102.58	100.33
Impact Value (B/A×100) (%):	42	41
Average Impact Value (%):	**42**	

Table A-15 Determination of specific gravity and water absorption values of CNA

Aggregate size (mm)		9.5
Aggregate size (in)		3/8
Mass of Saturated Surface Dry (SSD) sample in air (g):	A	2002.5
Wire basket + SSD in Water (g):	B	990.9
Mass of oven dry sample (g):	C	1620.8
Bulk Specific Gravity (G_{sb}):	C/(A-B)	1.602
Bulk SSD Specific Gravity (G_{sb}SSD):	A/(A-B)	1.980
Apparent Specific Gravity (G_{sa}):	C/(C-B)	2.573
Percent Absorption (% Abs):	**((A-C)/C) *100**	**23.6**

Table A-16 Determination of unit weight, voids and porosity values of CNA

Mould Calibration

Mass of mould in air (kg):	2.53
Mass of mould + water (kg):	5.22
Temperature of water (°C):	29
Unit weight of water (kg/m^3):	995.83
Volume of mould (m^3):	0.0027

Sample Description	Mass of Sample + mould (kg)				Bulk Density (kg/m^3)	Voids	Porosity (%)	SSD Bulk Density (kg/m^3)
	1	2	3	Average				
9.5 mm (3/8")	5.66	5.65	5.66	5.66	1159.259	0.273	21.4	1432.844

Table A-17 Determination of Los Angeles (L.A) Abrasion value of CNA

Sieve Size		Weight for each Grading (g)			
Passing	Retained on	A	B	C	D
37.5 mm (1.5")	25.4 mm (1")	1250 ± 25			
25.4 mm (1")	19 mm (3/4")	1250 ± 25			
19 mm (3/4")	12.5 mm (1/2")	1250 ± 25	2500 ± 10		
12.5 mm (1/2")	9.5 mm (3/8")	1250 ± 25	2500 ± 10		
9.5 mm (3/8")	6.4 mm (1/4")			2500 ± 10	
6.4 mm (1/4")	No. 4			2500 ± 10	
No. 4	No. 8				5000 ± 10
Total Weight		5000 ± 10	5000 ± 10	5000 ± 10	5000 ± 10
No. of spheres		12	11	8	6
Revolutions		500	500	500	500

Grading of sample:	A
Weight of sample (g):	5000.0
Weight retained on No. 12 sieve after test (g):	1704.2
Weight pass No. 12 sieve after test (g):	3295.8
Percent Wear (%):	**66**

APPENDIX B OXIDES ANALYSIS REPORT OF RECYCLED MATERIALS

CARIRI
Caribbean Industrial Research Institute
Mailing Address: Tunapuna Post Office, Trinidad and Tobago
Telephone: (868) 299-0210 Telefax: (868) 662-7177
www.cariri.com E-Mail: mail@cariri.com

SERVICE PROJECT REPORT

CLIENT:	UNIVERSITY OF THE WEST INDIES – DEPARTMENT OF CIVIL AND ENVIRONMENTAL ENGINEEERING
ADDRESS:	St. Augustine Campus, St. Augustine
PROJECT TITLE:	Oxide / XRD Analysis of a three aggregate samples
PROJECT CODE:	EC03815174/17
REPORT NO:	1203/17
DATE:	July 17, 2017

1. INTRODUCTION

The client submitted three aggregate samples on June 23, 2017 for oxide and compound analysis. The samples were assigned CARIRI identification numbers as follows:

Table 1
Sample Identification

Item No.	Client ID	CARIRI ID
1)	Sample 1 Carbon (UWI)	M170705
2)	Sample 2 EPB (UWI)	M170706
3)	Sample 3 (UWI)	M170707

2. APPROACH

2.1 XRF Analysis - Oxide analysis was carried out using a Bruker-Axs X-Ray Spectrometer model SRS 3400. A standard-less method with an accuracy of ± 10% was used for measuring concentration.

An ELTRA CS2000 Carbon/Sulphur Determinator was used to determine the percentage of Carbon and Sulphur present.

2.2 Oxides Calculation - Oxides calculation was conducted using the mathematical model that is part of the analyser software. It is based on simple oxide forms. The oxides forms used for the calculation are not necessarily present in the sample. More complex forms of the oxides may be present.

2.3 XRD Analysis - Compound identification was carried out using a Bruker-Axs X-Ray Diffractometer (XRD) Model D8 Advance.

3. RESULTS

3.1 Oxide analysis

The results of the elemental analysis are presented in Table 2.

Table 2
Elemental analysis results

Sample ID / Element	Percentage composition by weight (% W/W)		
	M170705	**M170706**	**M170707**
CaO	48.69	52.04	28.72
SiO_2	19.65	16.14	62.12
Cl	14.58	0.08	Below LLD
Na_2O	3.87	Below LLD	Below LLD
C	2.75	20.09	1.20
Al_2O_3	2.64	3.58	3.66
K_2O	2.34	0.12	0.39
Fe_2O_3	1.74	4.68	2.45
S	0.89	0.80	0.31
ZnO	0.79	Below LLD	Below LLD
P_2O_5	0.73	0.20	0.19
MgO	0.66	1.47	0.63
TiO_2	0.38	0.30	0.17
PbO	0.13	Below LLD	Below LLD
MnO	0.07	0.08	0.03
SrO	0.04	0.21	0.10
Cr_2O_3	0.04	0.05	0.02
ZrO_2	0.01	0.01	0.01
WO_3	Below LLD	0.13	Below LLD

LLD – Lower Limit of Detection

3.2 Compound analysis

The results of the compound analysis are presented in Tables 3, 4 and 5.

Table 3
Compound analysis of sample M170705

Compound Name	Compound Formula
Quartz, syn	SiO_2
Calcite, syn	$CaCO_3$
1,3-Diphenylurea carbanilide	$C_{13}H_{12}N_2O$
Halite, syn	NaCl
Zinc Oxide	ZnO
Stishovite, syn	SiO_2
Calcium Sulfate	$CaSO_4$
Calcium Hydroxide	$Ca(OH)_2$
Calcium Silicate Oxide	$Ca_3(SiO_4)O$
Magnetite	$Fe2.932O_4$
Calcium Silicate	$Ca_2(SiO_4)$
Aluminum Oxide	$Al2.667O_4$
Sodium Sulfate	$Na_2S_2O_7$
Calcium Oxide Hydrate	$CaO_2(H_2O)_8$

The main compounds detected in the sample were Quartz, syn and Calcite, syn.

Table 4
Compound analysis of sample M170706

Compound Name	Compound Formula
Calcite	$Ca(CO_3)$
Vaterite	$CaCO_3$
Quartz alpha, syn	SiO_2
Calcium Sulfate	$CaSO_4$
Grossular	$Ca_3Al_2(SiO_4)_3$
Silicon Oxide Zeolite Y, dealuminated	SiO_2
Iron Oxide Hydroxide	FeO(OH)
Aluminum Oxide	Al_2O_3
Iron Oxide	Fe_3O_4
Stishovite, syn	SiO_2
Magnetite	$Fe2.894O_4$
Boehmite, syn	AlO(OH)

The main compounds detected in the sample were Calcite and Vaterite.

Table 5
Compound analysis of sample M170707

Compound Name	Compound Formula
Quartz, syn	SiO_2
Calcite, syn	$CaCO_3$
Hydrogen Sulfide	H_2S
Portlandite, syn	$Ca(OH)_2$
Silicon Oxide Zeolite ZSM-11 (dehydrated) - artificial	SiO_2
Aluminum Oxide	Al_2O_3
Iron Oxide	Fe_2O_3

The main compound detected in the sample was Quartz, syn.

The Diffractograms are shown in Appendices 1.

Approved by:

[redacted]

Senior Materials Engineer
Industrial Materials Unit

1. This report relates solely to the specific sample of the product which has been tested or analysed by CARIRI as the basis for preparing the report. The report shall be used solely for informing the Client of the results of the test or analysis of that specific sample. It shall not be used for purposes of certification of similar or other products produced by the same manufacturer or the Client or for any other purpose.
2. The report is confidential to the Client and shall not be disclosed by the Client to any person other than professional advisers and responsible officers and employees of the Client who require such disclosure where necessary for the proper performance of their duties and who will individually comply with all obligations of confidentiality imposed on the Client by this provision. Without limiting the generality of the foregoing the report shall not be used or referred to in any advertisement or the marketing of the product.

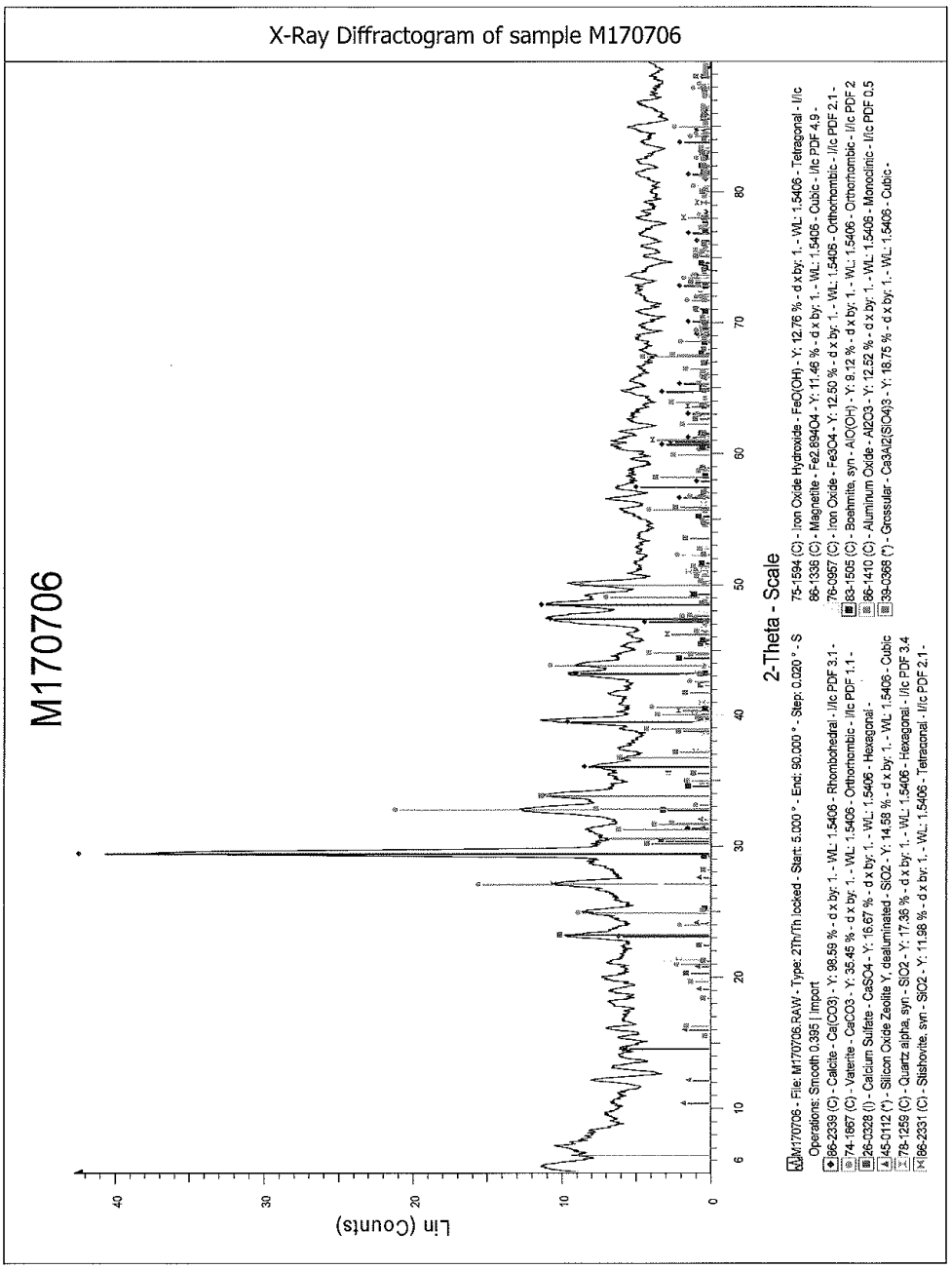

1. This report relates solely to the specific sample of the product which has been tested or analysed by CARIRI as the basis for preparing the report. The report shall be used solely for informing the Client of the results of the test or analysis of that specific sample. It shall not be used for purposes of certification of similar or other products produced by the same manufacturer or the Client or for any other purpose.
2. The report is confidential to the Client and shall not be disclosed by the Client to any person other than professional advisers and responsible officers and employees of the Client who require such disclosure where necessary for the proper performance of their duties and who will individually comply with all obligations of confidentiality imposed on the Client by this provision. Without limiting the generality of the foregoing the report shall not be used or referred to in any advertisement or the marketing of the product.

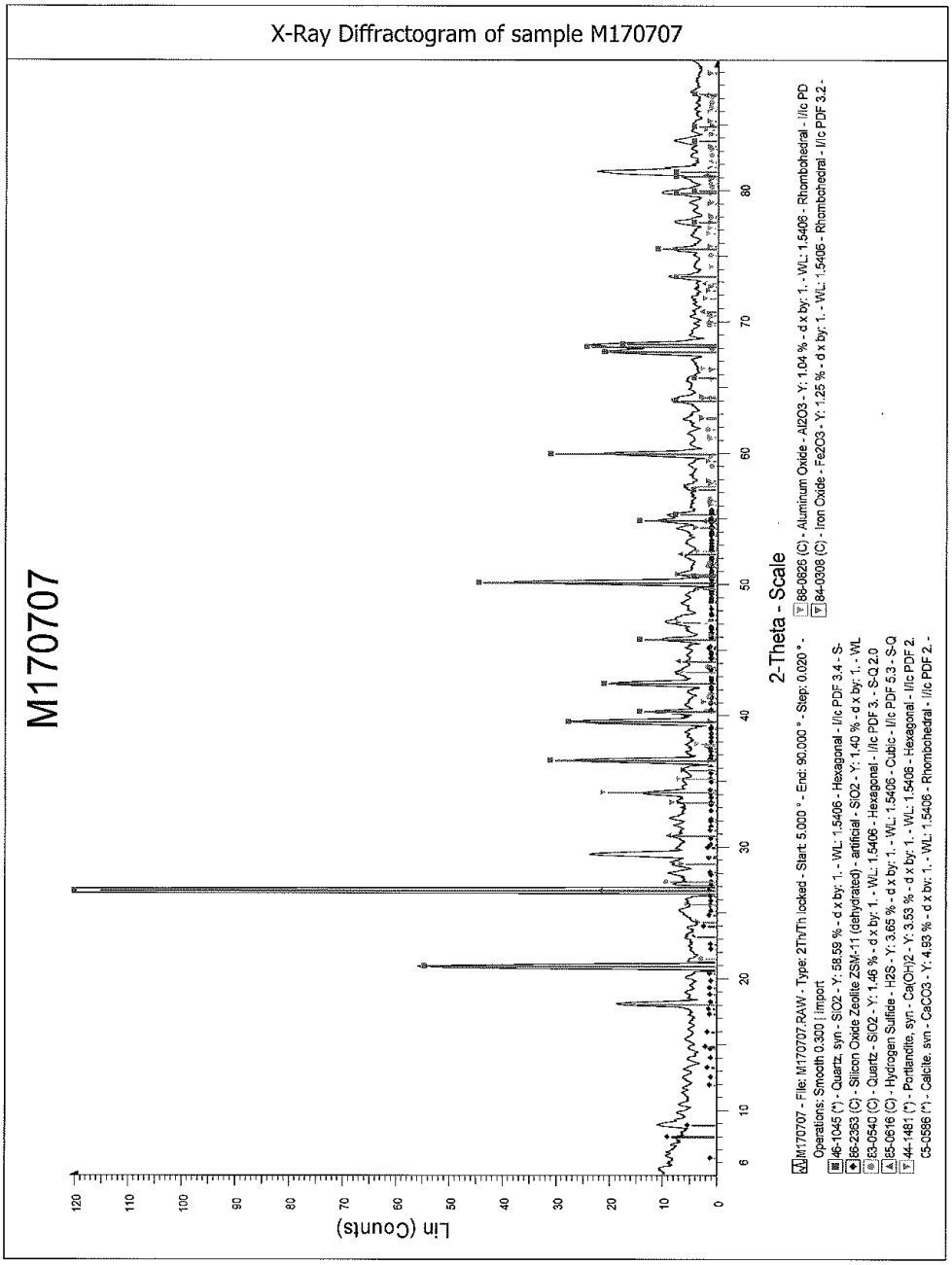

1. This report relates solely to the specific sample of the product which has been tested or analysed by CARIRI as the basis for preparing the report. The report shall be used solely for informing the Client of the results of the test or analysis of that specific sample. It shall not be used for purposes of certification of similar or other products produced by the same manufacturer or the Client or for any other purpose.
2. The report is confidential to the Client and shall not be disclosed by the Client to any person other than professional advisers and responsible officers and employees of the Client who require such disclosure where necessary for the proper performance of their duties and who will individually comply with all obligations of confidentiality imposed on the Client by this provision. Without limiting the generality of the foregoing the report shall not be used or referred to in any advertisement or the marketing of the product.

APPENDIX C HYDROLOGICAL ANALYSIS

Table C-1 Analysis of rainfall-discharge events for Rig 1

Event No.	Date	Inflow (Rainfall)					Outflow (Discharge)								Storage during rainfall	
		Volume		Total Duration (min)	Average intensity		Lag time (min)	Volume during rainfall		Total Duration (min)	Total Volume		Peak Flow			
		(L)	(mm)		(L/min)	(mm/h)		(L)	(mm)		(L)	(mm)	(L/min)	(m^3/s)	Vol. (mm)	Vol. (%)
1	14-Dec-16	79.04	418.22	15	4.94	1566	1	66.54	352.086	29	77.67	388.368	77.67	1.29E-03	66.13	16%
2	19-Dec-16	17.16	90.79	15	1.05	333	1	13.67	72.335	29	15.84	79.208	15.84	2.64E-04	18.46	20%
3	20-Jan-17	15.68	82.96	15	0.93	294	1	12.55	66.382	29	14.36	71.796	14.36	2.39E-04	16.58	20%
4	31-Jan-17	15.46	81.78	15	0.95	300	2	12.14	64.231	28	14.14	70.702	14.14	2.36E-04	17.55	21%
5	2-Feb-17	16.30	86.22	15	1.00	316	2	12.82	67.814	28	14.96	74.794	14.96	2.49E-04	18.41	21%
6	4-Feb-17	29.76	157.46	15	1.84	584	1	24.56	129.954	29	28.46	142.301	28.46	4.74E-04	27.51	17%
7	10-Feb-17	23.81	125.97	15	1.46	462	1	19.80	104.778	29	22.53	112.641	22.53	3.75E-04	21.19	17%
8	17-Feb-17	25.75	136.22	15	1.55	492	1	21.74	115.020	29	24.45	122.266	24.45	4.08E-04	21.20	16%
9	1-Mar-17	25.34	134.07	15	1.59	504	1	20.14	106.536	29	24.00	119.999	24.00	4.00E-04	27.53	21%
10	20-Apr-17	11.92	63.06	15	0.72	229	2	9.09	48.090	23	10.81	54.054	10.81	1.80E-04	14.97	24%
11	26-Apr-17	11.52	60.95	15	0.71	226	2	8.47	44.804	23	10.24	51.186	10.24	1.71E-04	16.15	26%
12	2-May-17	11.64	61.58	15	0.72	227	2	8.99	47.588	23	10.71	53.570	10.71	1.79E-04	13.99	23%
13	8-May-17	13.80	73.02	15	0.85	271	2	10.56	55.879	23	12.53	62.670	12.53	2.09E-04	17.14	23%
14	9-May-17	13.50	71.43	15	0.83	262	2	10.22	54.064	23	12.15	60.769	12.15	2.03E-04	17.36	24%

Table C-2 Analysis of rainfall-discharge events for Rig 2

Event No.	Date	Inflow (Rainfall)					Outflow (Discharge)								Storage during rainfall	
		Volume		Total Duration (min)	Average intensity		Lag time (min)	Volume during rainfall		Total Duration (min)	Total Volume		Peak Flow			
		(L)	(mm)		(L/min)	(mm/h)		(L)	(mm)		(L)	(mm)	(L/min)	(m^3/s)	Vol. (mm)	Vol. (%)
1	19-Dec-16	18.31	96.87	15	1.12	356	1	14.91	78.878	29	17.31	91.587	16.92	2.82E-04	17.99	19%
2	3-Jan-17	16.88	89.31	15	1.03	327	1	13.73	72.634	29	15.92	84.233	15.57	2.59E-04	16.68	19%
3	20-Jan-17	14.59	77.21	16	0.81	256	1	11.69	61.849	29	13.66	72.294	13.36	2.23E-04	15.36	20%
4	31-Jan-17	10.51	55.59	15	0.65	207	2	8.37	44.263	28	10.09	53.392	9.87	1.64E-04	11.32	20%
5	2-Feb-17	17.37	91.90	15	1.06	334	1	14.27	75.505	29	16.45	87.013	16.08	2.68E-04	16.40	18%
6	4-Feb-17	23.81	126.00	15	1.46	461	1	19.99	105.763	29	22.99	121.638	22.48	3.75E-04	20.24	16%
7	10-Feb-17	22.99	121.64	15	1.40	444	1	19.62	103.789	29	22.58	119.458	22.07	3.68E-04	17.85	15%
8	17-Feb-17	24.73	130.87	15	1.51	478	1	20.82	110.180	29	24.00	126.976	23.46	3.91E-04	20.69	16%
9	1-Mar-17	12.88	68.12	15	0.77	244	2	9.17	48.505	28	12.15	64.286	11.88	1.98E-04	19.62	29%
10	20-Apr-17	12.83	67.86	15	0.79	251	2	9.69	51.265	23	11.78	62.315	11.51	1.92E-04	16.60	24%
11	26-Apr-17	12.40	65.62	15	0.76	242	2	9.59	50.729	23	11.53	60.984	11.27	1.88E-04	14.89	23%
12	2-May-17	12.00	63.49	15	0.75	237	2	9.21	48.740	23	11.14	58.944	10.89	1.82E-04	14.75	23%
13	8-May-17	13.34	70.56	16	0.77	245	2	10.46	55.362	23	12.38	65.497	12.10	2.02E-04	15.19	22%
14	9-May-17	14.18	75.02	15	0.88	278	2	11.44	60.509	23	13.19	69.812	12.90	2.15E-04	14.51	19%

Table C-3 Analysis of rainfall-discharge events for Rig 3

Event No.	Date	Inflow (Rainfall)					Outflow (Discharge)								Storage during rainfall	
		Volume		Total Duration (min)	Average intensity		Lag time (min)	Volume during rainfall		Total Duration (min)	Total Volume		Peak Flow			
		(L)	(mm)		(L/min)	(mm/h)		(L)	(mm)		(L)	(mm)	(L/min)	(m^3/s)	Vol. (mm)	Vol. (%)
1	15-Dec-16	42.23	223.43	15	2.58	816	1	33.31	176.238	29	41.18	217.889	40.46	6.74E-04	47.19	21%
2	19-Dec-16	18.51	97.95	15	1.14	362	1	15.16	80.199	29	17.50	92.577	17.19	2.86E-04	17.75	18%
3	3-Jan-17	17.24	91.21	15	1.15	364	1	13.87	73.403	29	15.90	84.127	1.19	1.99E-05	17.80	20%
4	20-Jan-17	16.10	85.19	15	1.02	323	1	12.79	67.656	29	15.04	79.579	14.78	2.46E-04	17.53	21%
5	31-Jan-17	20.33	107.57	15	1.23	389	1	16.74	88.594	29	19.38	102.516	19.04	3.17E-04	18.97	18%
6	4-Feb-17	22.63	119.75	15	1.39	440	1	19.00	100.506	29	22.01	116.439	21.62	3.60E-04	19.25	16%
7	10-Feb-17	24.67	130.54	15	1.49	473	1	20.22	106.959	29	23.74	125.582	23.32	3.89E-04	23.58	18%
8	16-Feb-17	20.38	107.85	15	1.22	387	1	16.73	88.522	29	19.56	103.505	19.22	3.20E-04	19.33	18%
9	17-Feb-17	24.25	128.31	15	1.49	471	1	19.81	104.820	29	23.13	122.394	22.73	3.79E-04	23.49	18%
10	20-Apr-17	11.70	61.90	15	0.72	227	2	8.91	47.145	23	10.88	57.587	10.69	1.78E-04	14.76	24%
11	26-Apr-17	16.30	86.22	15	1.00	316	1	13.25	70.115	24	15.35	81.228	15.01	2.50E-04	16.11	19%
12	2-May-17	12.31	65.14	15	0.75	239	2	9.15	48.396	23	11.16	59.032	10.91	1.82E-04	16.75	26%
13	8-May-17	14.52	76.84	15	0.88	279	2	11.33	59.937	23	13.65	72.196	13.34	2.22E-04	16.90	22%
14	9-May-17	14.94	79.02	15	0.93	294	2	11.64	61.567	23	14.05	74.344	13.74	2.29E-04	17.45	22%

Table C-4 Analysis of rainfall-discharge events for Rig 4

Event No.	Date	Inflow (Rainfall)					Outflow (Discharge)								Storage during rainfall	
		Volume		Total Duration (min)	Average intensity		Lag time (min)	Volume during rainfall		Total Duration (min)	Total Volume		Peak Flow			
		(L)	(mm)		(L/min)	(mm/h)		(L)	(mm)		(L)	(mm)	(L/min)	(m^3/s)	Vol. (mm)	Vol. (%)
1	16-Dec-16	51.49	272.44	15	3.18	1007	1	44.56	235.778	29	51.09	270.328	49.90	8.32E-04	36.67	13%
2	19-Dec-16	19.36	102.43	15	1.20	380	2	15.12	79.984	28	18.22	96.410	17.80	2.97E-04	22.45	22%
3	3-Jan-17	15.60	82.56	15	0.95	302	2	12.33	65.226	28	14.73	77.913	14.38	2.40E-04	17.33	21%
4	20-Jan-17	13.71	72.53	15	0.82	261	2	10.46	55.359	28	13.07	69.135	12.76	2.13E-04	17.17	24%
5	31-Jan-17	22.65	119.86	15	1.37	433	2	16.72	88.460	28	20.46	108.233	19.98	3.33E-04	31.40	26%
6	2-Feb-17	13.44	71.12	15	0.83	264	2	10.35	54.760	28	13.16	69.638	12.85	2.14E-04	16.36	23%
7	10-Feb-17	25.85	136.78	15	1.60	507	2	20.05	106.109	28	24.48	129.542	23.91	3.99E-04	30.67	22%
8	16-Feb-17	21.62	114.39	15	1.32	417	2	16.65	88.070	28	20.69	109.487	20.21	3.37E-04	26.32	23%
9	17-Feb-17	20.21	106.93	15	1.23	391	2	15.62	82.640	28	18.81	99.505	18.36	3.06E-04	24.29	23%
10	1-Mar-17	25.47	134.78	15	1.49	473	2	20.46	108.269	28	24.66	130.492	24.08	4.01E-04	26.51	20%
11	26-Apr-17	17.30	91.51	15	1.08	344	3	11.78	62.323	27	17.35	91.799	16.94	2.82E-04	29.19	32%

APPENDIX D HYETOGRAPHS AND HYDROGRAPHS DATA

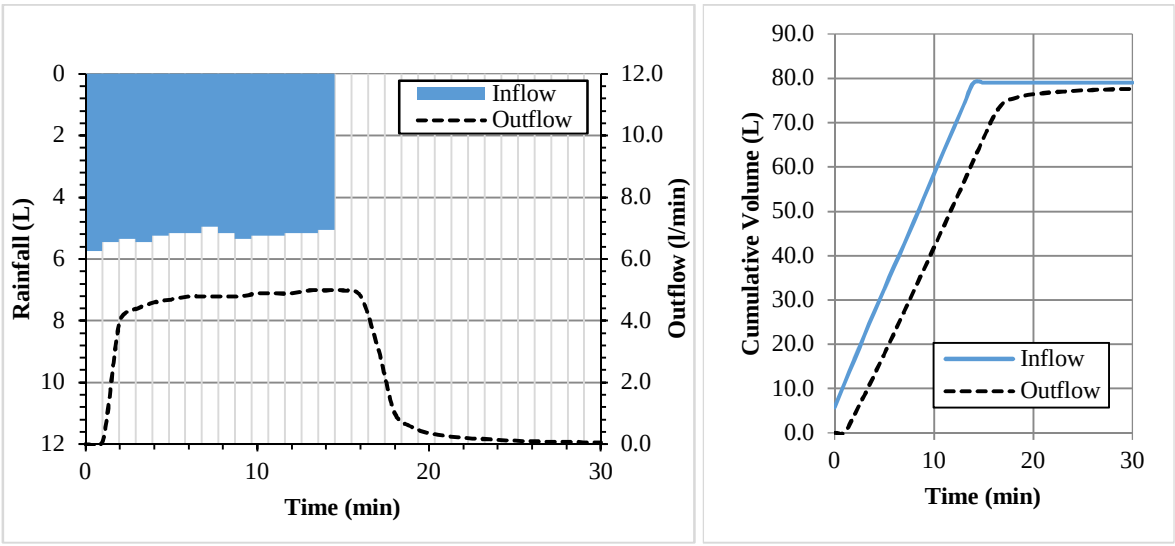

Figure D-1 Rig 1 rainfall event 1–inflow hyetograph, discharge hydrograph and cumulative hydrographs

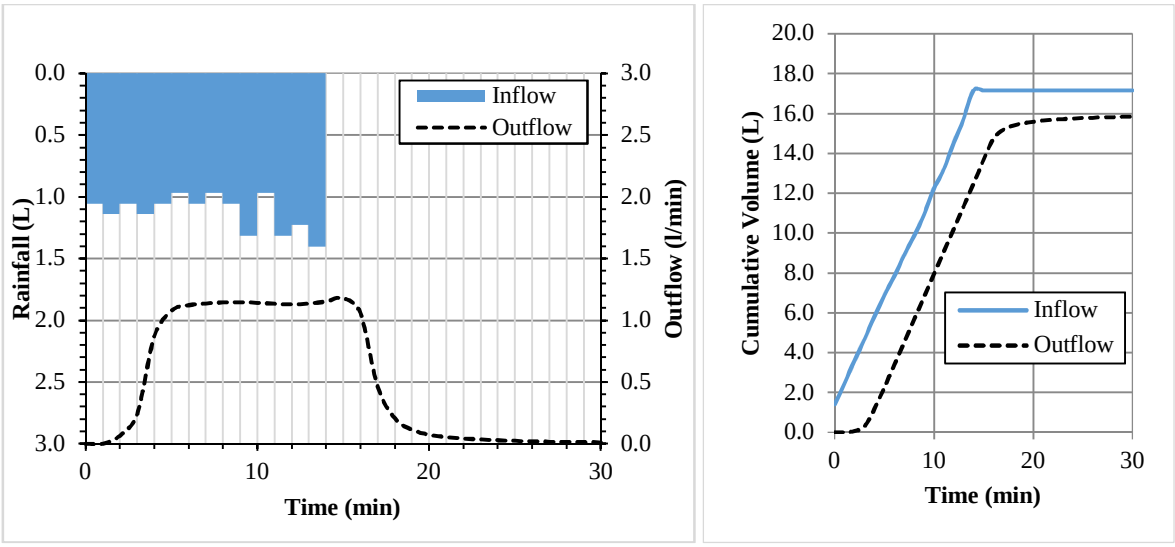

Figure D-2 Rig 1 rainfall event 2–inflow hyetograph, discharge hydrograph and cumulative hydrographs

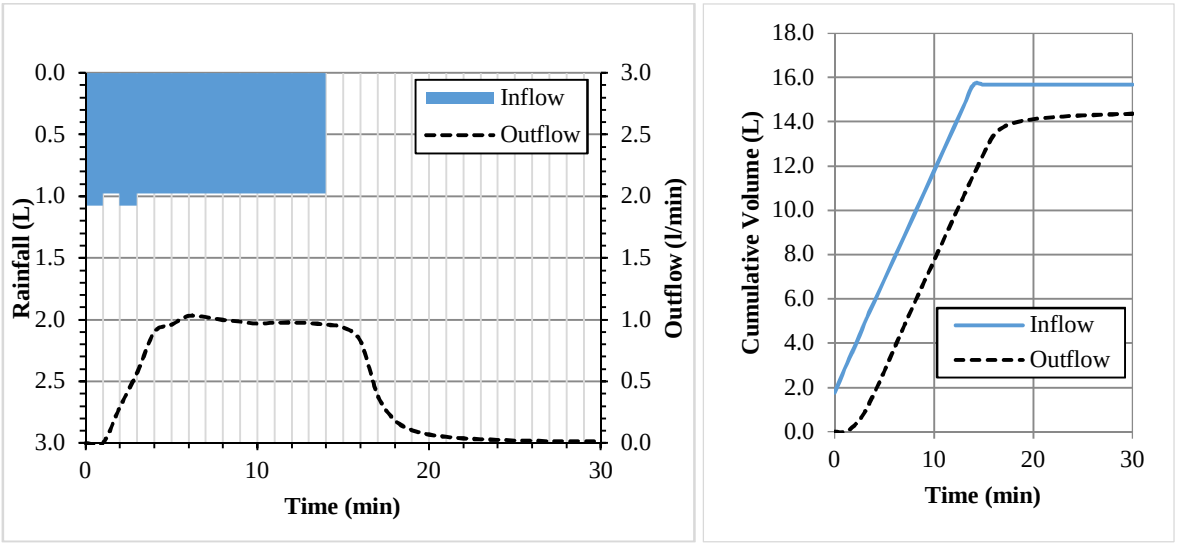

Figure D-3 Rig 1 rainfall event 3–inflow hyetograph, discharge hydrograph and cumulative hydrographs

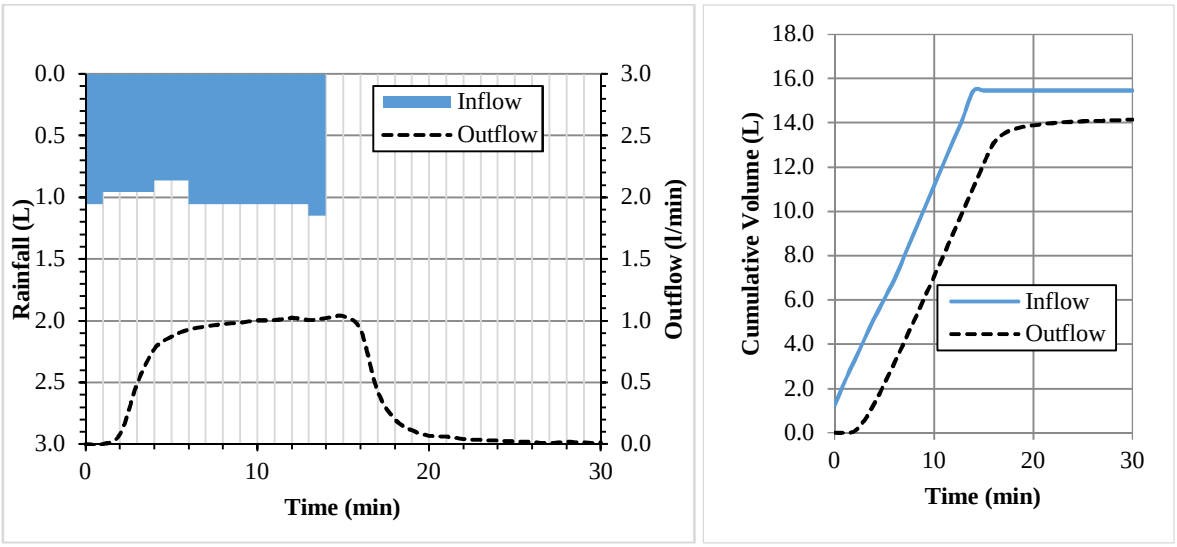

Figure D-4 Rig 1 rainfall event 4–inflow hyetograph, discharge hydrograph and cumulative hydrographs

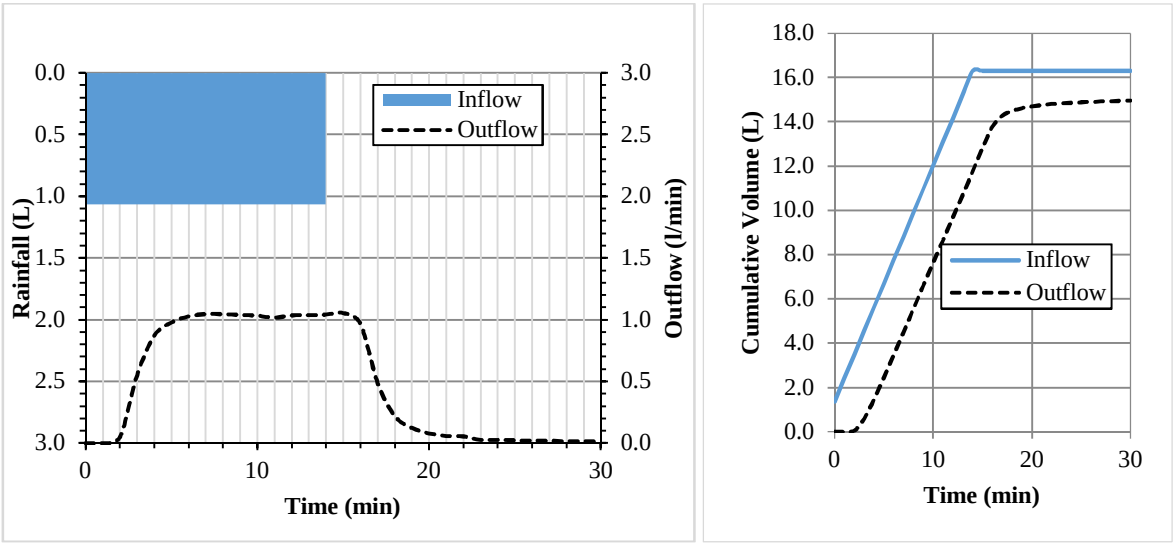

Figure D-5 Rig 1 rainfall event 5–inflow hyetograph, discharge hydrograph and cumulative hydrographs

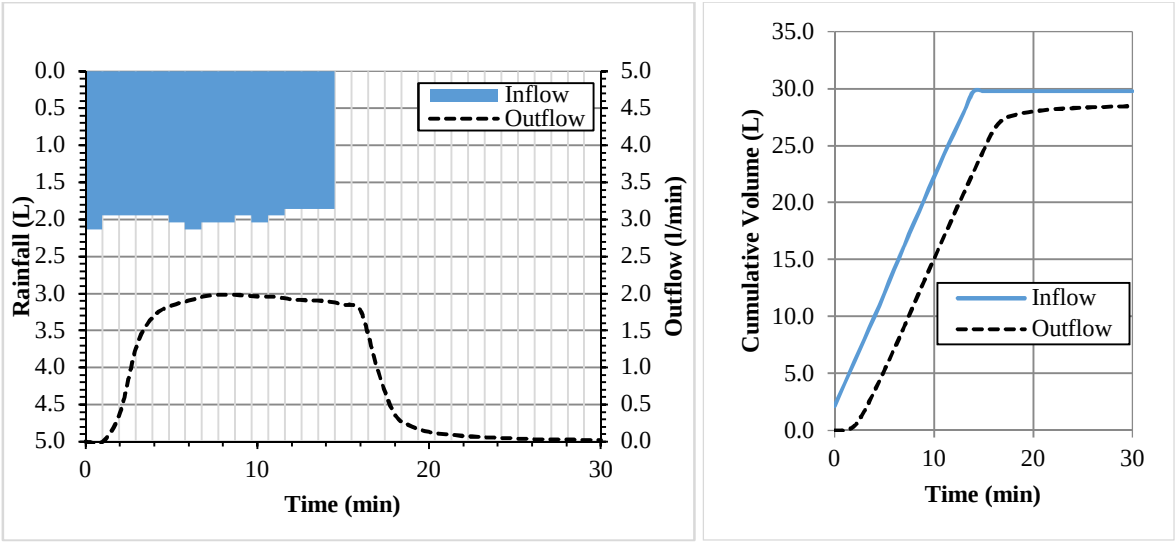

Figure D-6 Rig 1 rainfall event 6–inflow hyetograph, discharge hydrograph and cumulative hydrographs

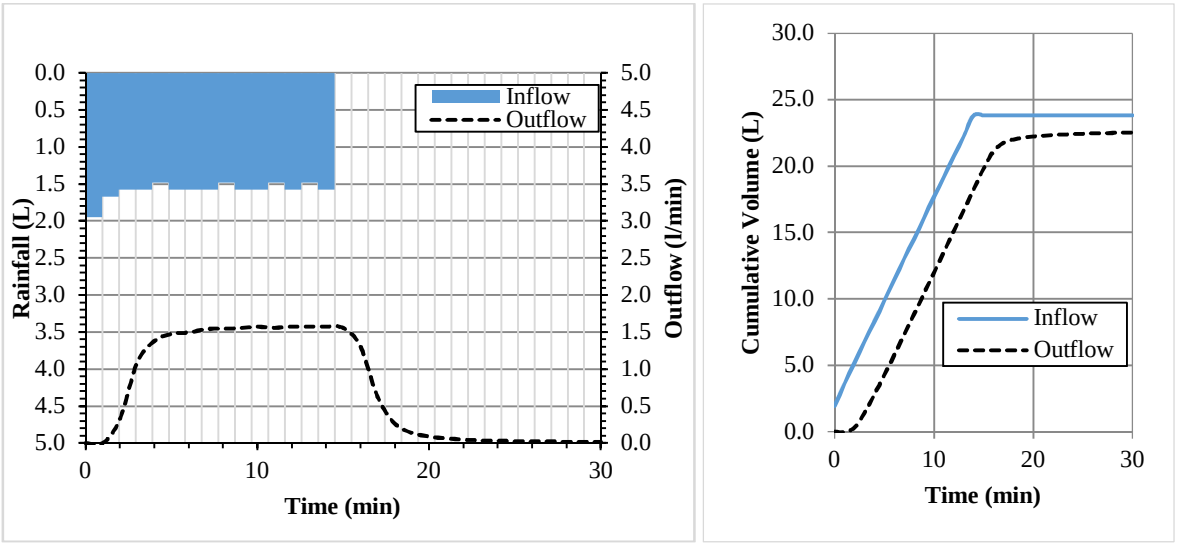

Figure D-7 Rig 1 rainfall event 7–inflow hyetograph, discharge hydrograph and cumulative hydrographs

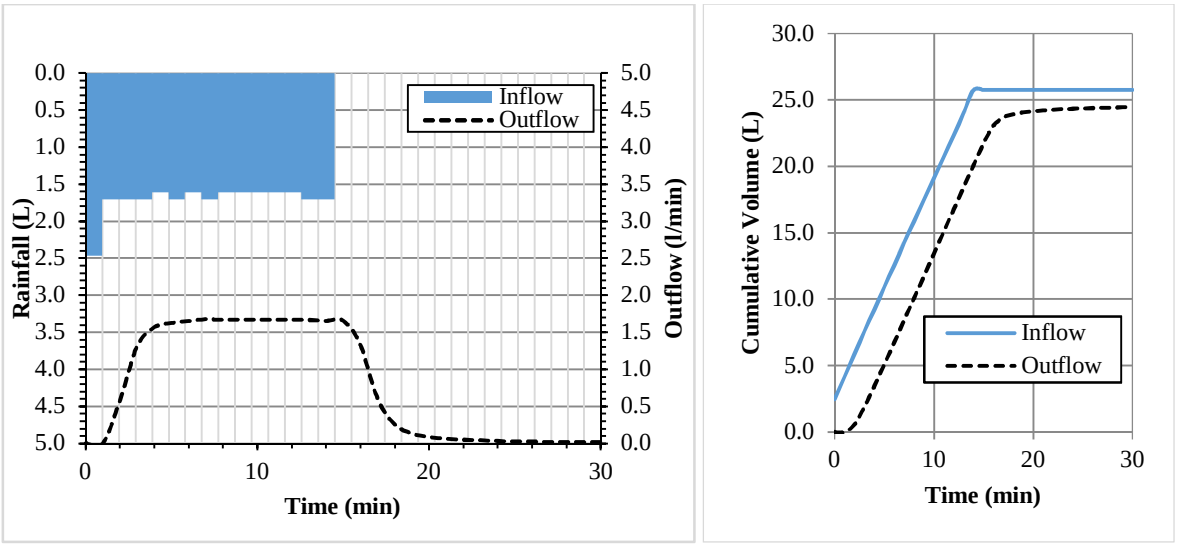

Figure D-8 Rig 1 rainfall event 8–inflow hyetograph, discharge hydrograph and cumulative hydrographs

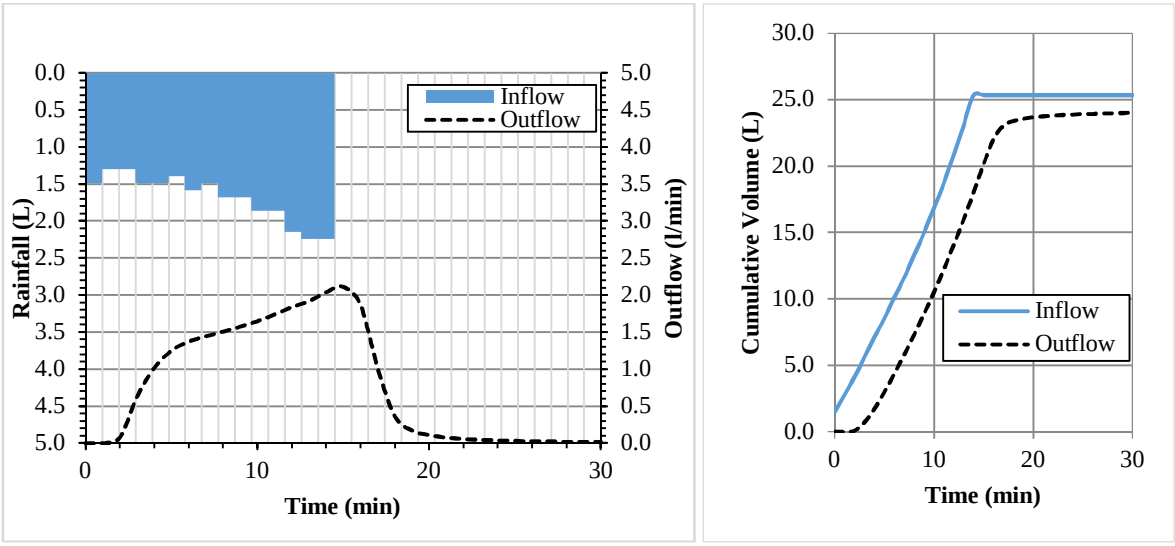

Figure D-9 Rig 1 rainfall event 9–inflow hyetograph, discharge hydrograph and cumulative hydrographs

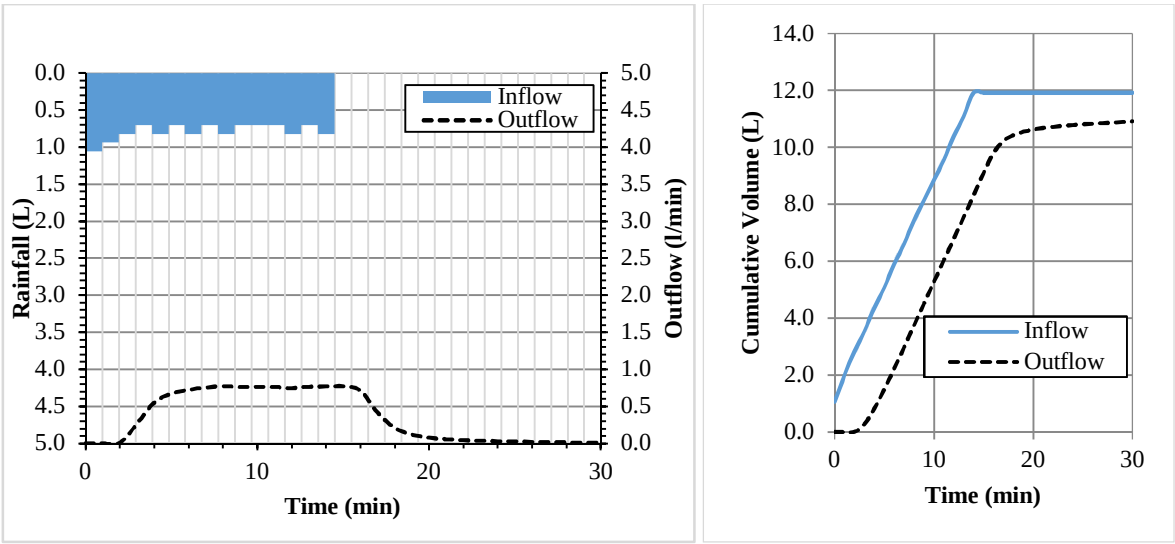

Figure D-10 Rig 1 rainfall event 10–inflow hyetograph, discharge hydrograph and cumulative hydrographs

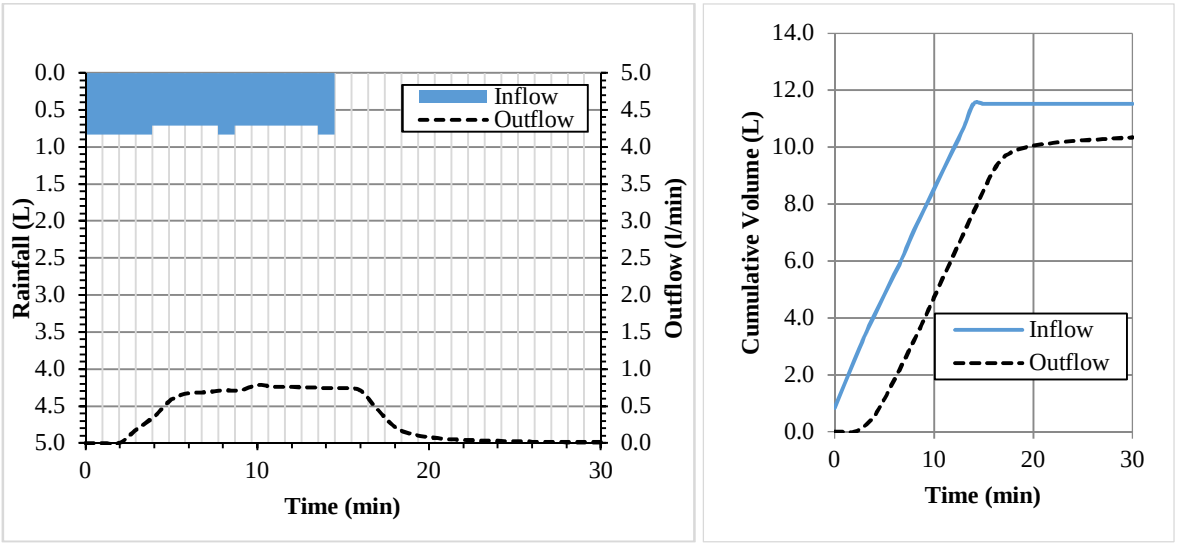

Figure D-11 Rig 1 rainfall event 11–inflow hyetograph, discharge hydrograph and cumulative hydrographs

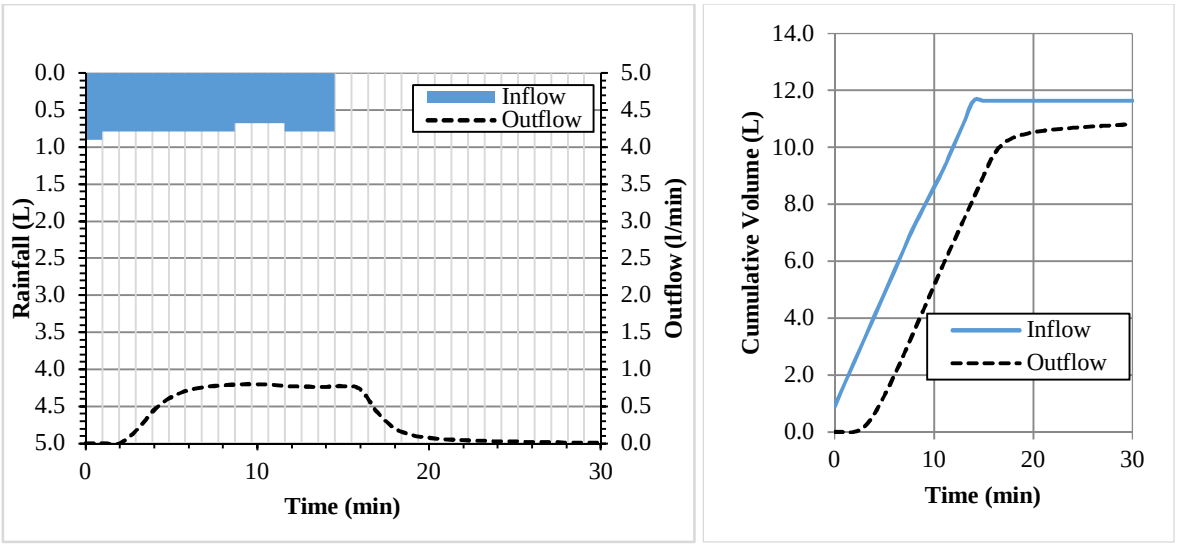

Figure D-12 Rig 1 rainfall event 12–inflow hyetograph, discharge hydrograph and cumulative hydrographs

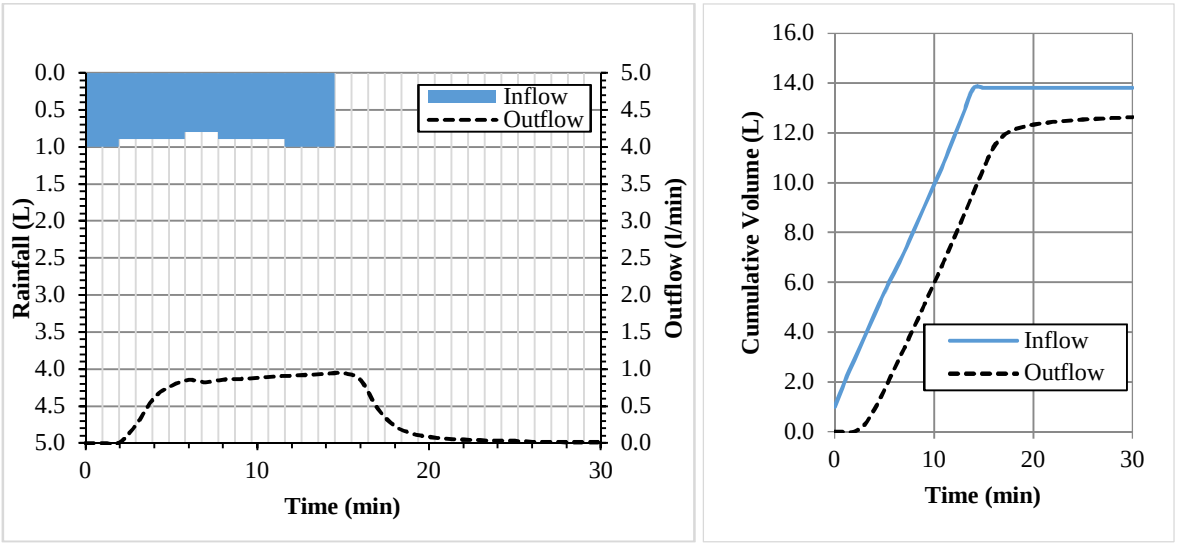

Figure D-13 Rig 1 rainfall event 13–inflow hyetograph, discharge hydrograph and cumulative hydrographs

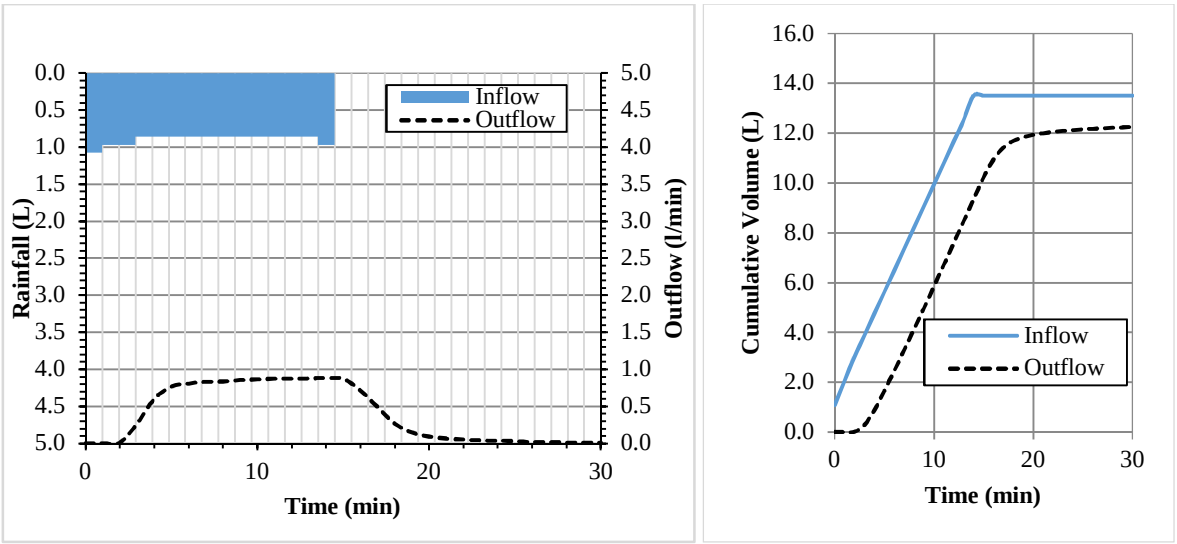

Figure D-14 Rig 1 rainfall event 14–inflow hyetograph, discharge hydrograph and cumulative hydrographs

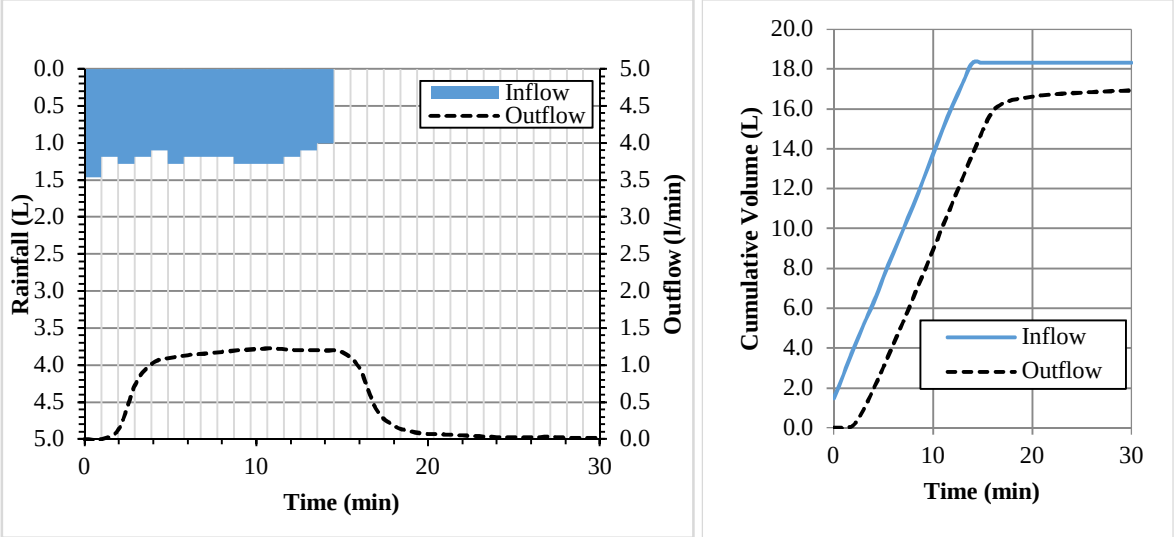

Figure D-15 Rig 2 rainfall event 1–inflow hyetograph, discharge hydrograph and cumulative hydrographs

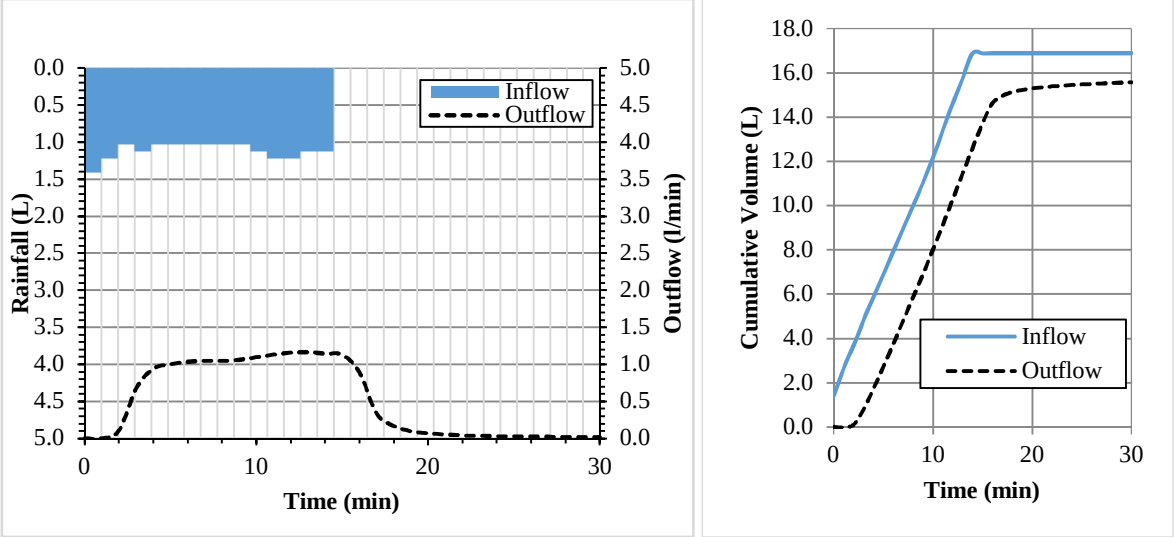

Figure D-16 Rig 2 rainfall event 2–inflow hyetograph, discharge hydrograph and cumulative hydrographs

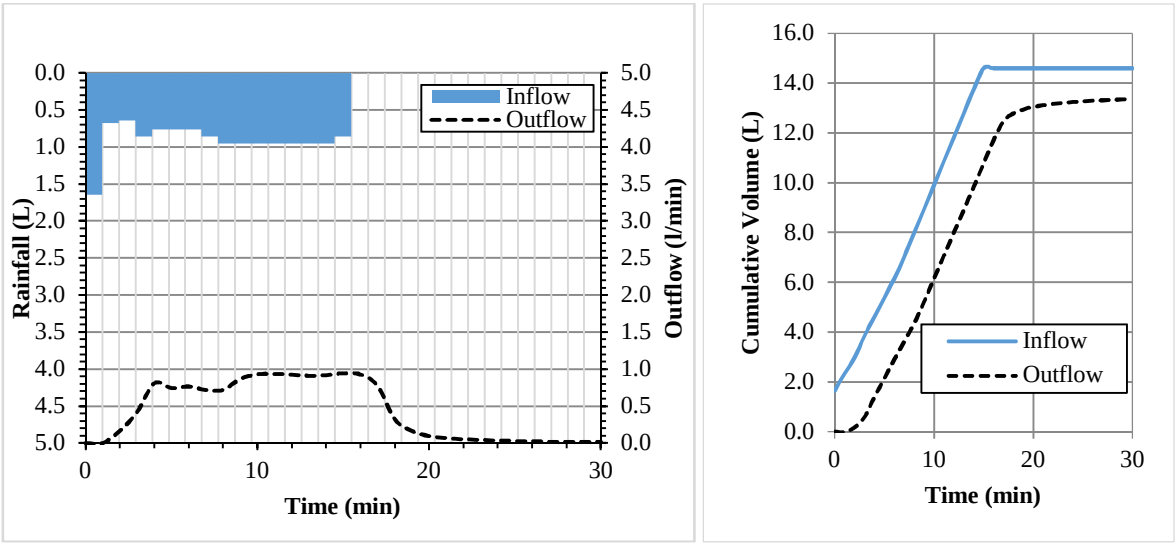

Figure D-17 Rig 2 rainfall event 3–inflow hyetograph, discharge hydrograph and cumulative hydrographs

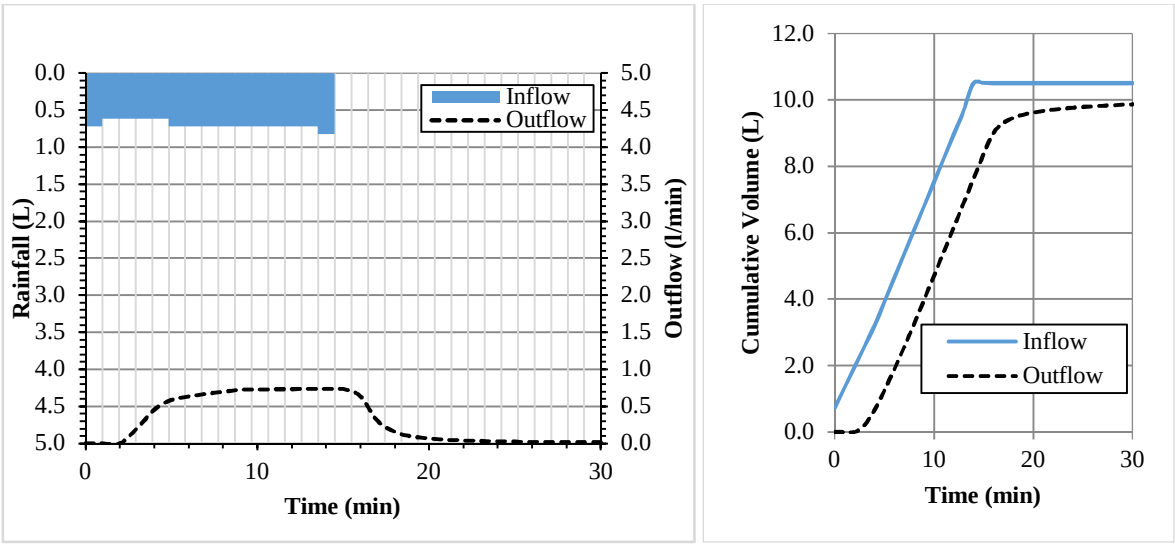

Figure D-18 Rig 2 rainfall event 4–inflow hyetograph, discharge hydrograph and cumulative hydrographs

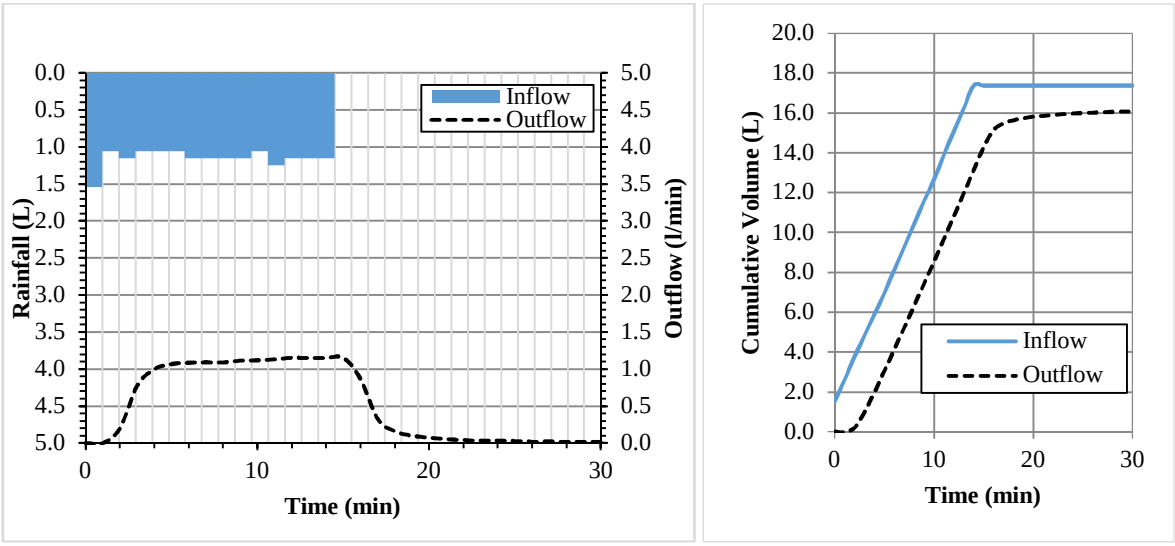

Figure D-19 Rig 2 rainfall event 5–inflow hyetograph, discharge hydrograph and cumulative hydrographs

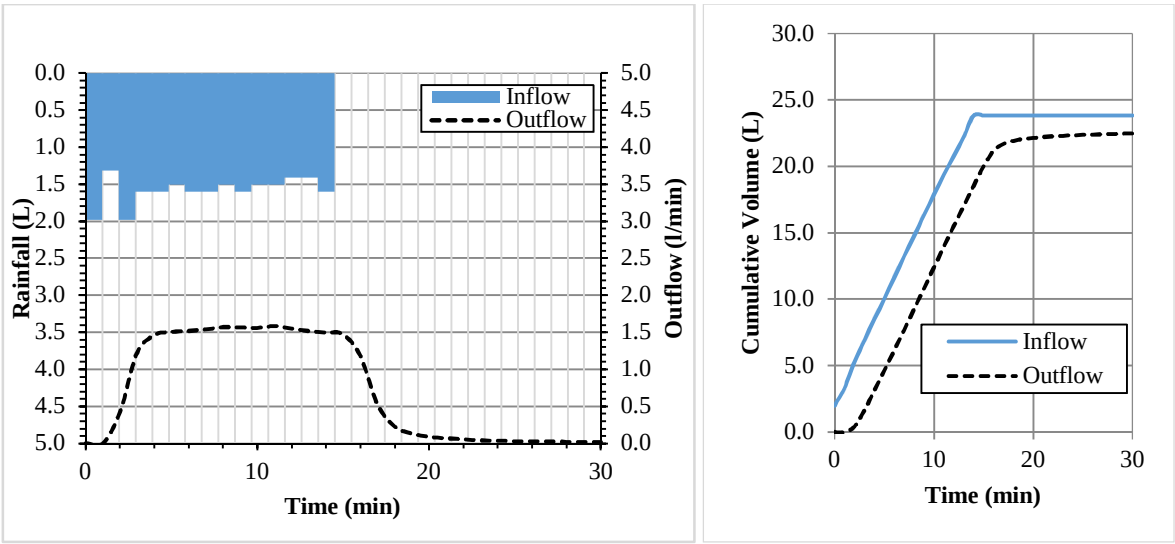

Figure D-20 Rig 2 rainfall event 6–inflow hyetograph, discharge hydrograph and cumulative hydrographs

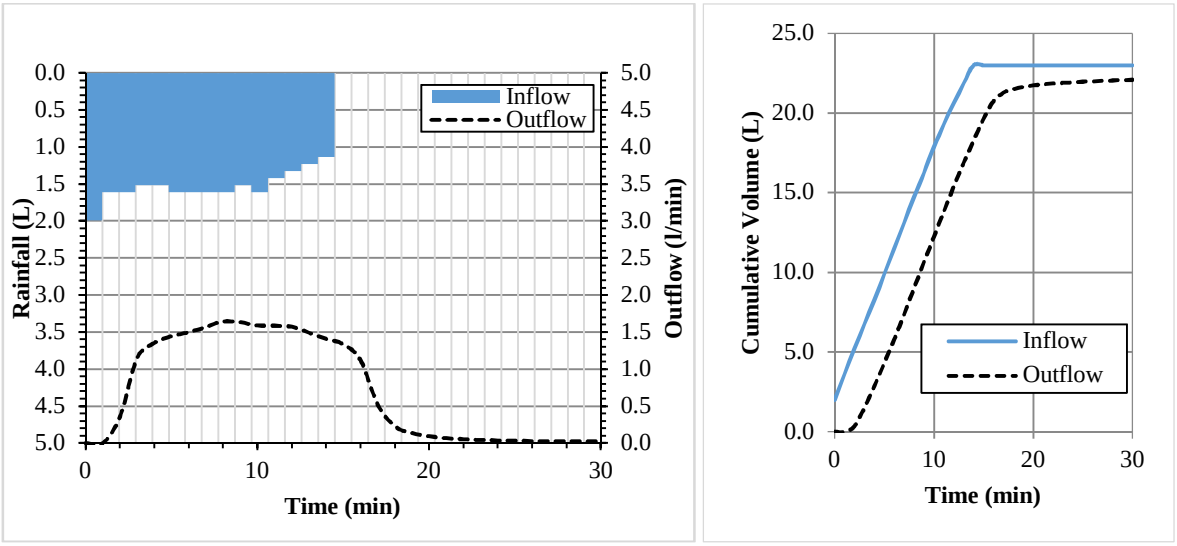

Figure D-21 Rig 2 rainfall event 7–inflow hyetograph, discharge hydrograph and cumulative hydrographs

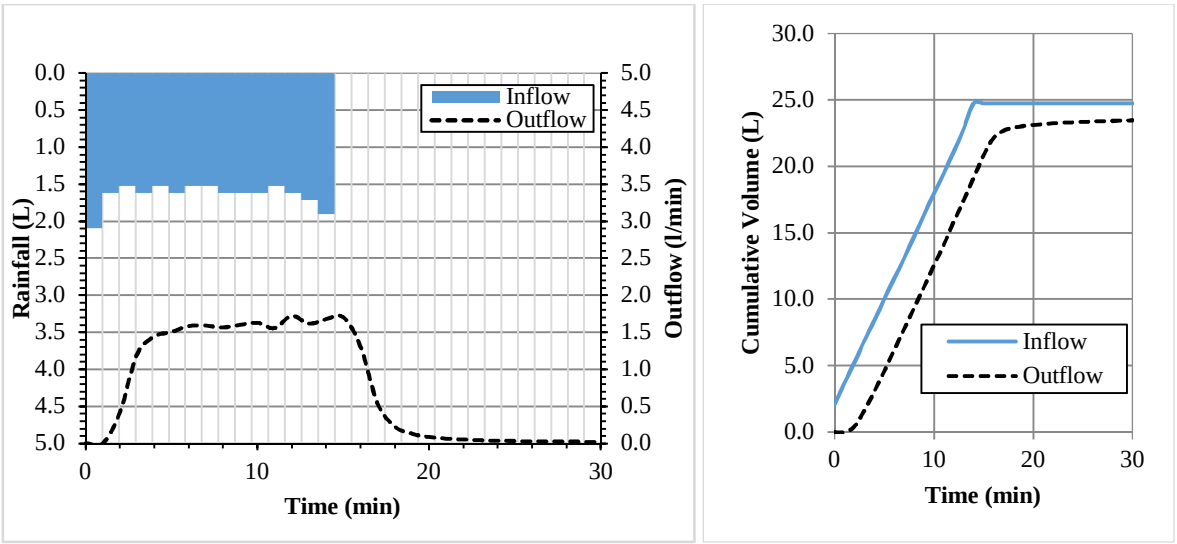

Figure D-22 Rig 2 rainfall event 8–inflow hyetograph, discharge hydrograph and cumulative hydrographs

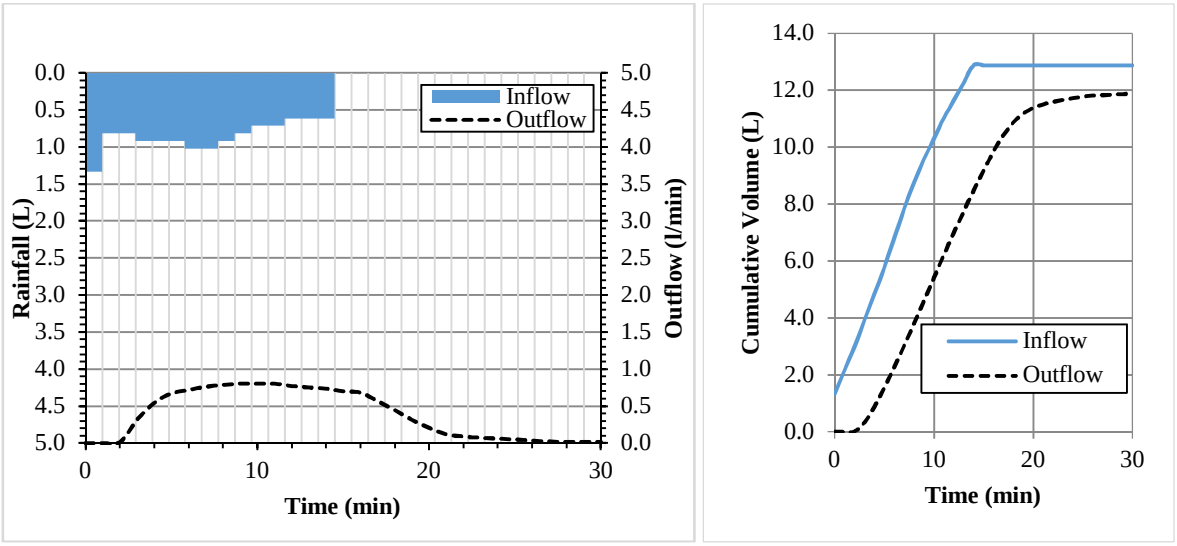

Figure D-23 Rig 2 rainfall event 9–inflow hyetograph, discharge hydrograph and cumulative hydrographs

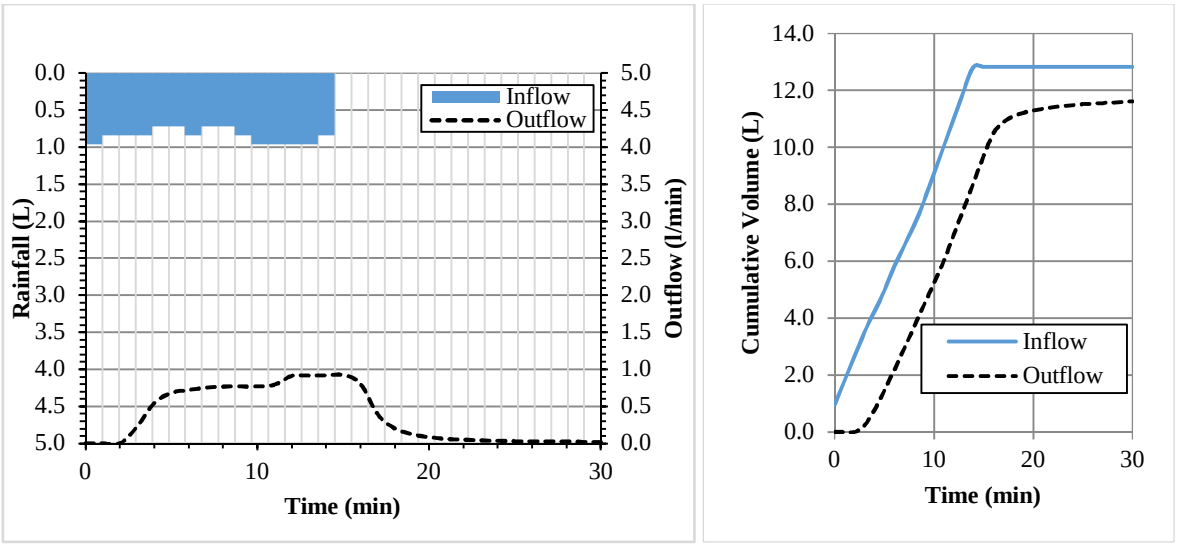

Figure D-24 Rig 2 rainfall event 10–inflow hyetograph, discharge hydrograph and cumulative hydrographs

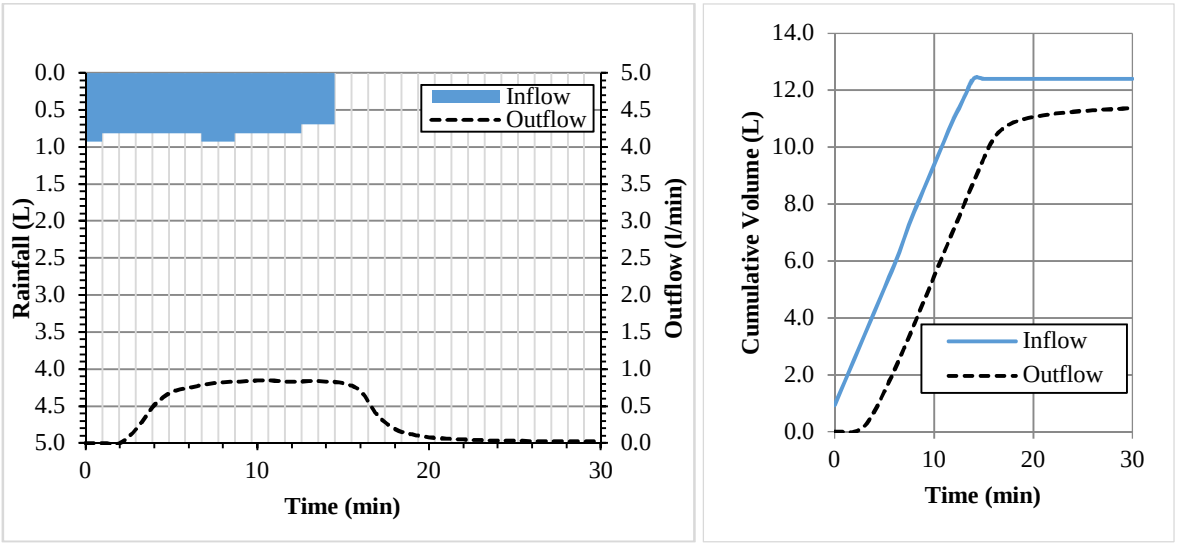

Figure D-25 Rig 2 rainfall event 11–inflow hyetograph, discharge hydrograph and cumulative hydrographs

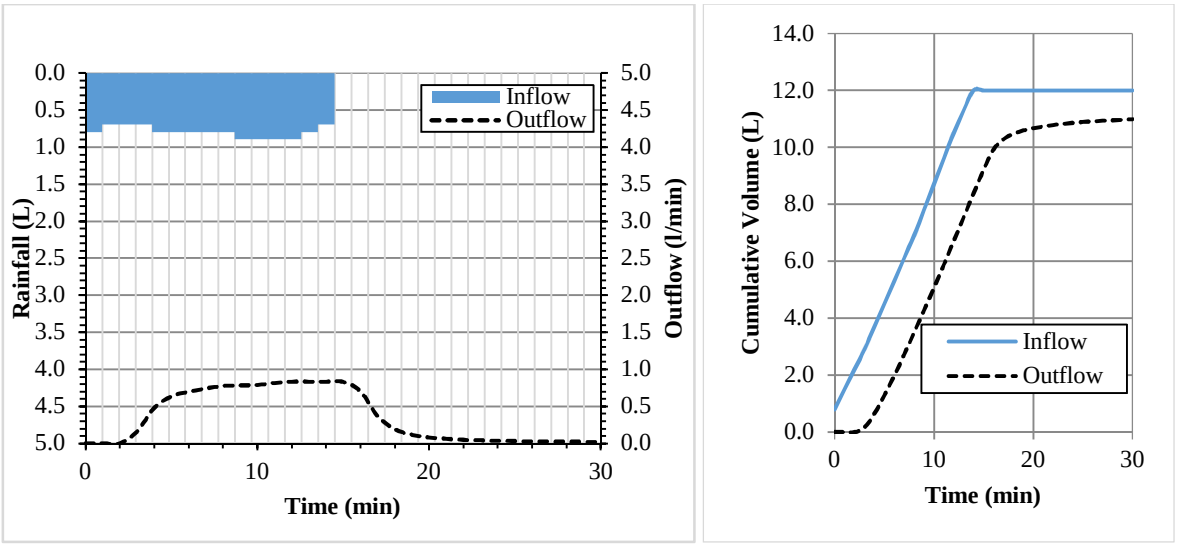

Figure D-26 Rig 2 rainfall event 12–inflow hyetograph, discharge hydrograph and cumulative hydrographs

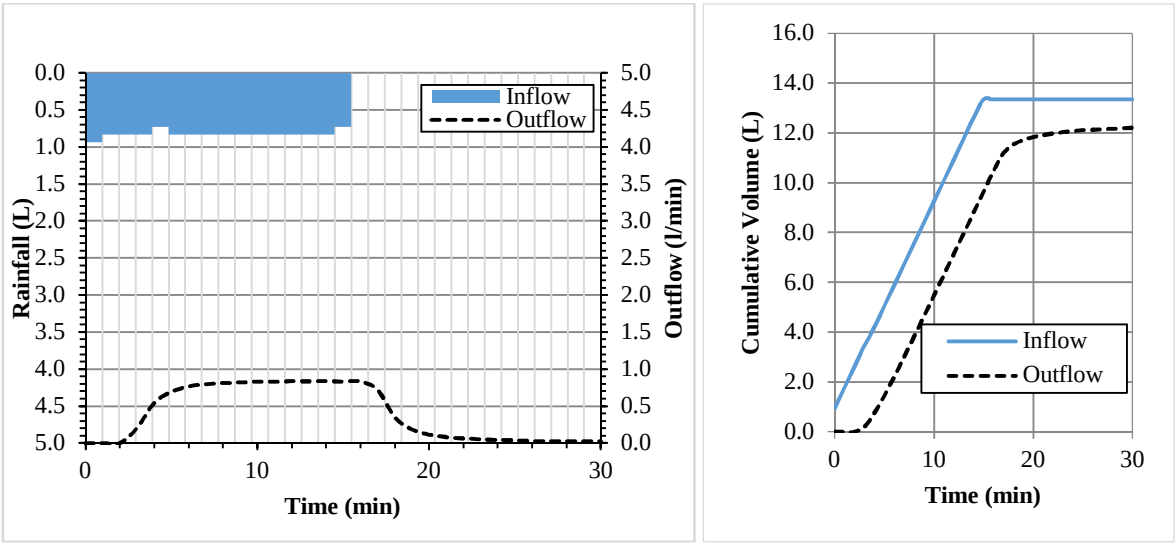

Figure D-27 Rig 2 rainfall event 13–inflow hyetograph, discharge hydrograph and cumulative hydrographs

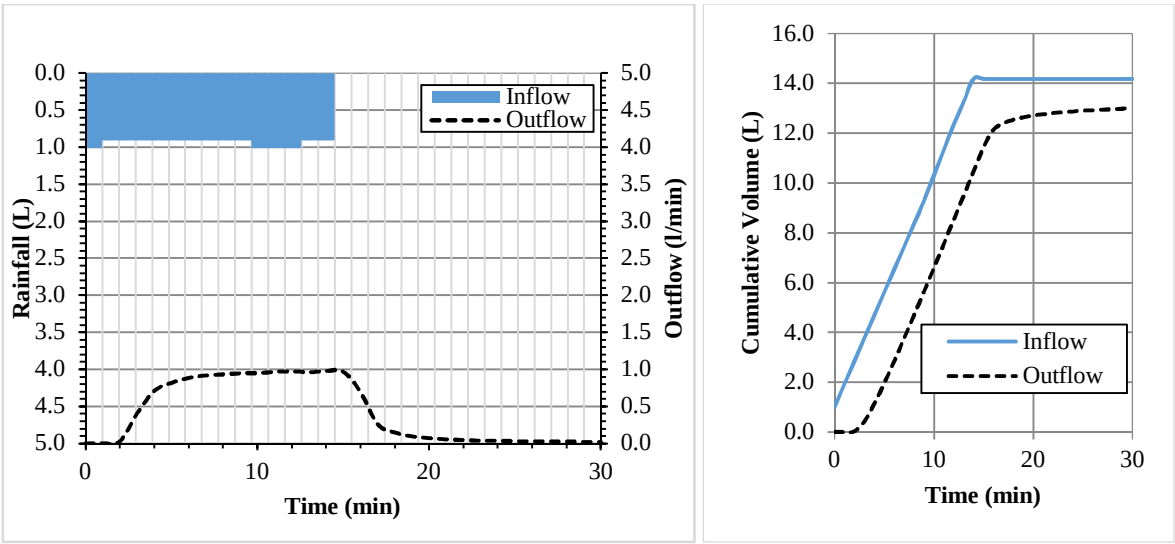

Figure D-28 Rig 2 rainfall event 14–inflow hyetograph, discharge hydrograph and cumulative hydrographs

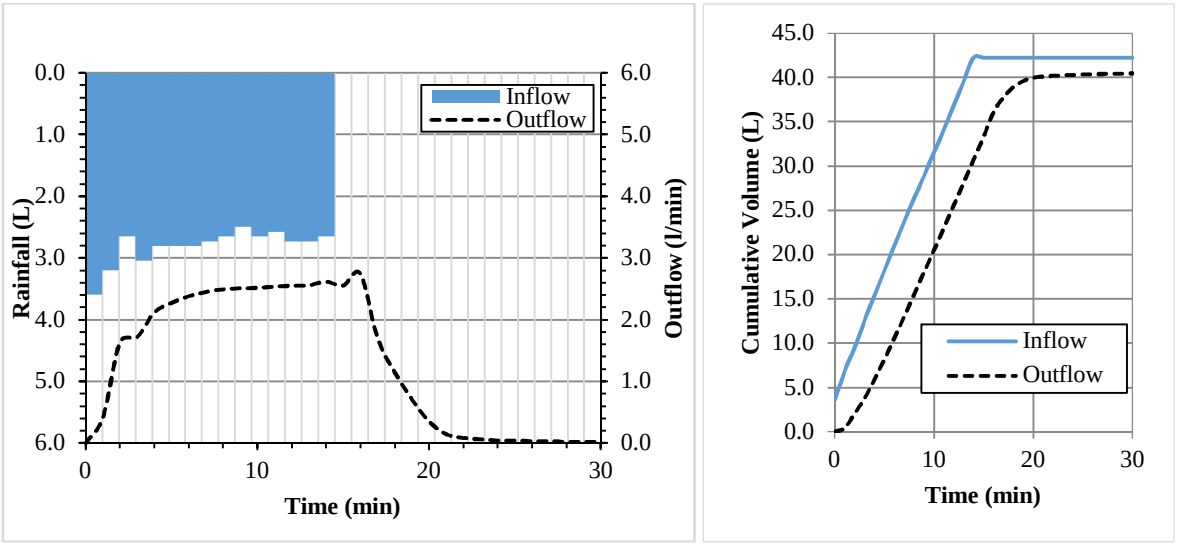

Figure D-29 Rig 3 rainfall event 1–inflow hyetograph, discharge hydrograph and cumulative hydrographs

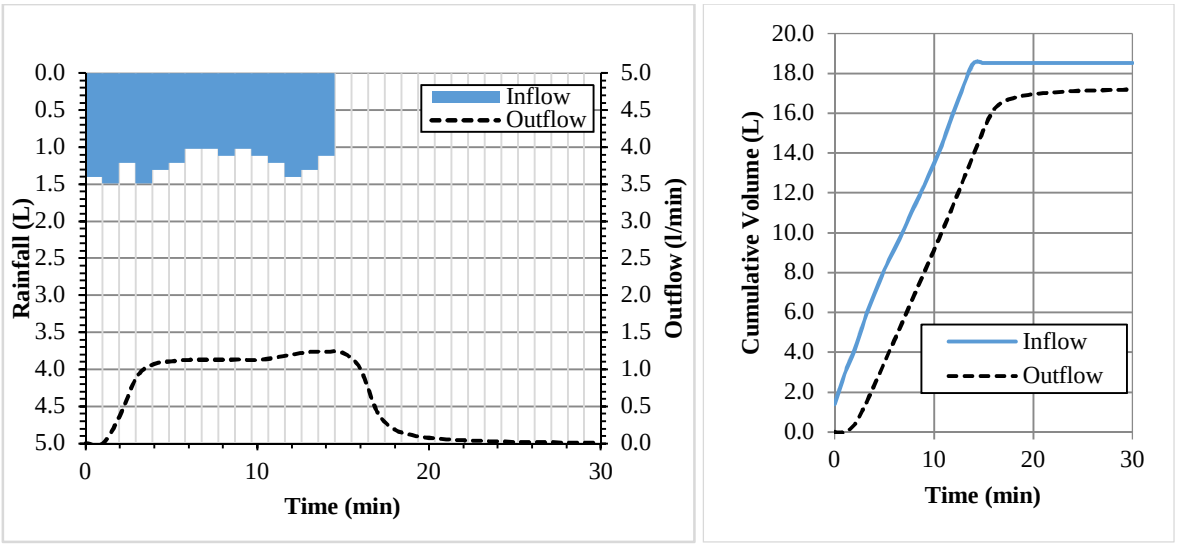

Figure D-30 Rig 3 rainfall event 2–inflow hyetograph, discharge hydrograph and cumulative hydrographs

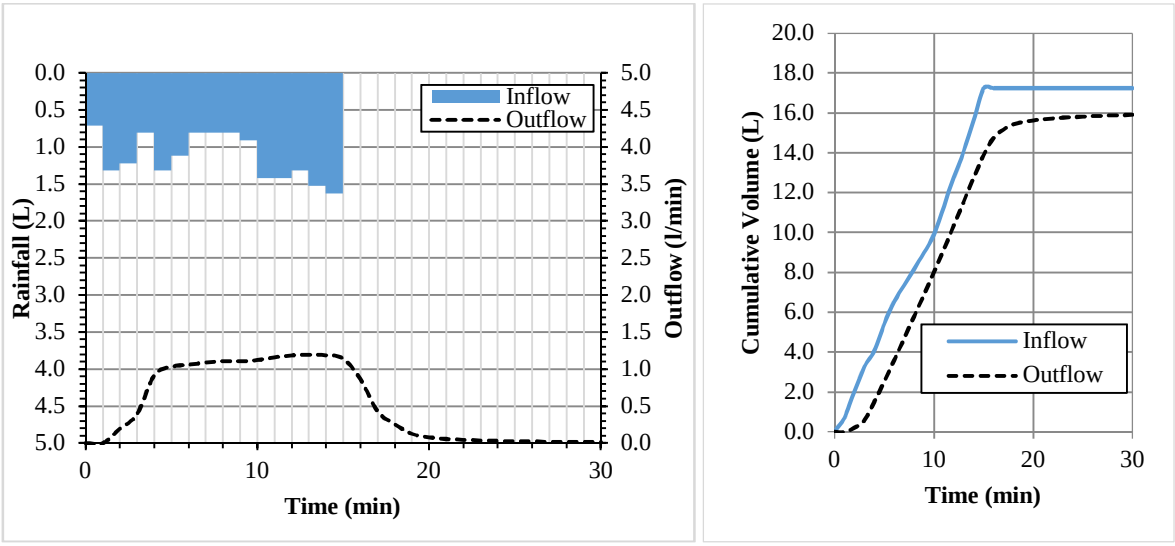

Figure D-31 Rig 3 rainfall event 3–inflow hyetograph, discharge hydrograph and cumulative hydrographs

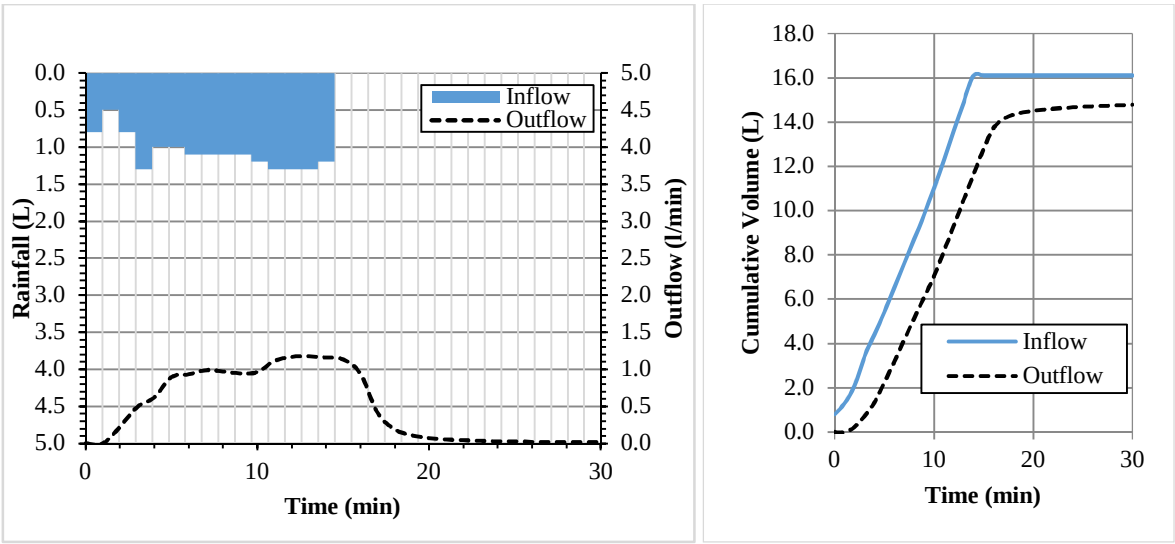

Figure D-32 Rig 3 rainfall event 4–inflow hyetograph, discharge hydrograph and cumulative hydrographs

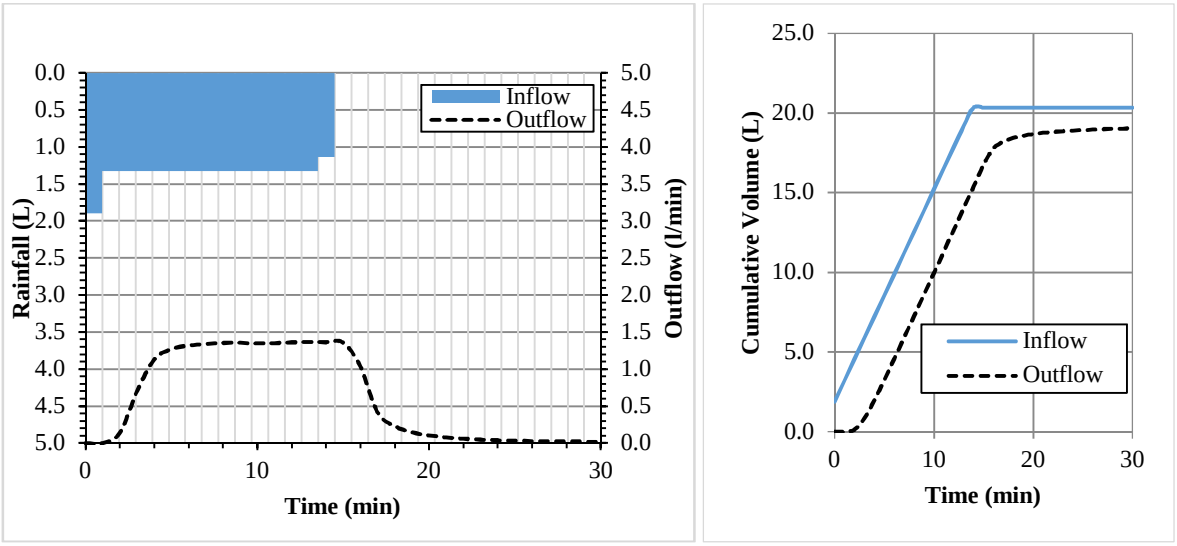

Figure D-33 Rig 3 rainfall event 5–inflow hyetograph, discharge hydrograph and cumulative hydrographs

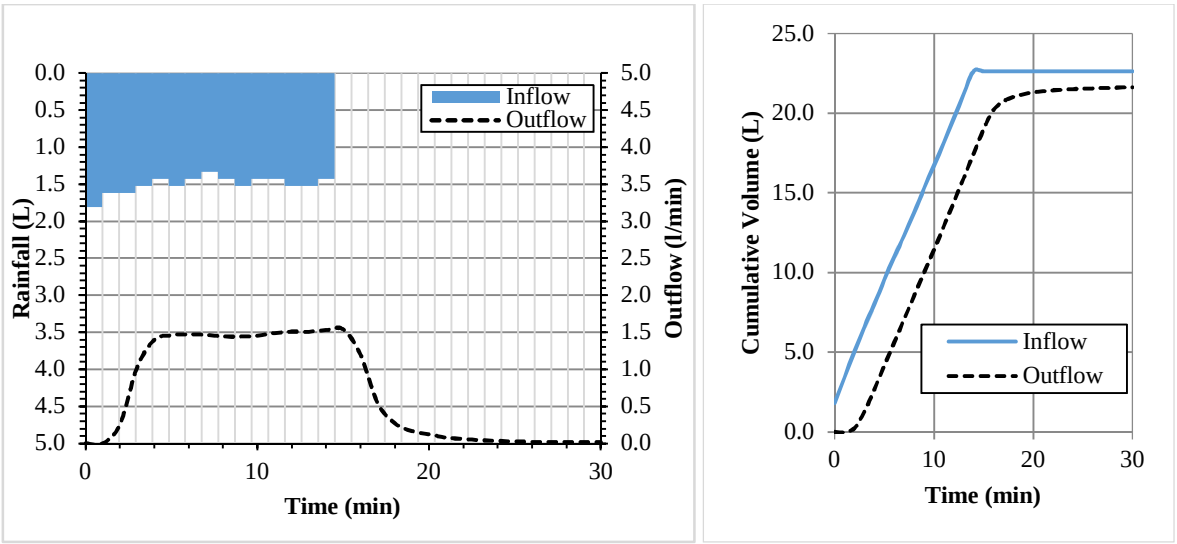

Figure D-34 Rig 3 rainfall event 6–inflow hyetograph, discharge hydrograph and cumulative hydrographs

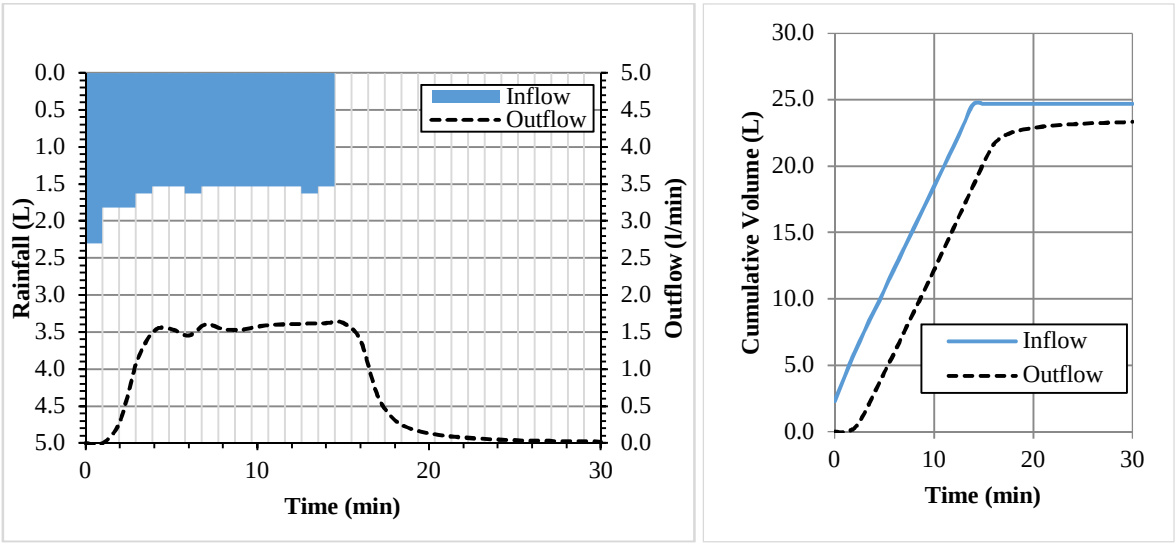

Figure D-35 Rig 3 rainfall event 7–inflow hyetograph, discharge hydrograph and cumulative hydrographs

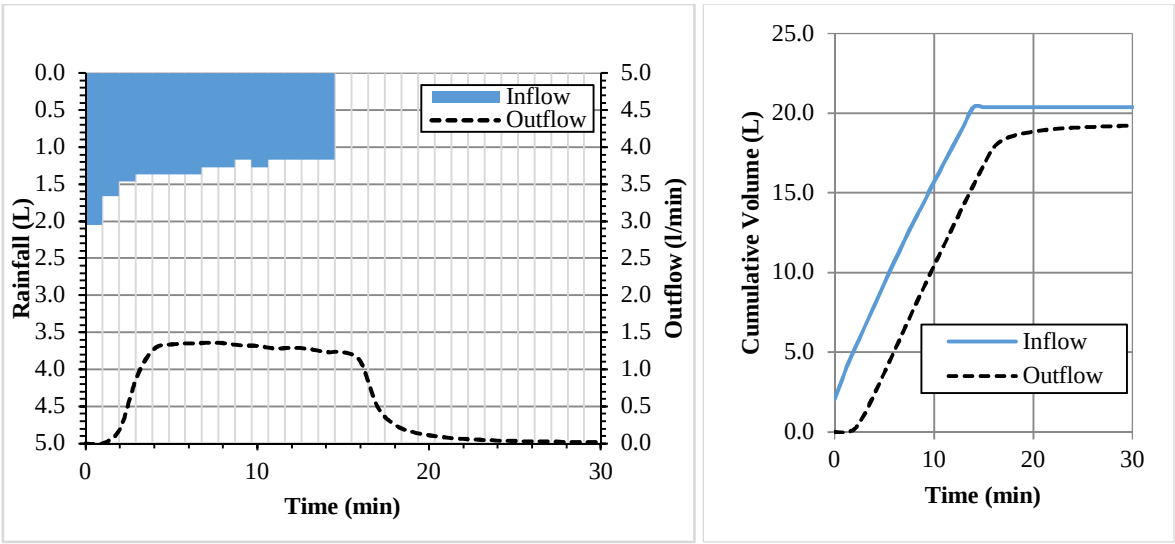

Figure D-36 Rig 3 rainfall event 8–inflow hyetograph, discharge hydrograph and cumulative hydrographs

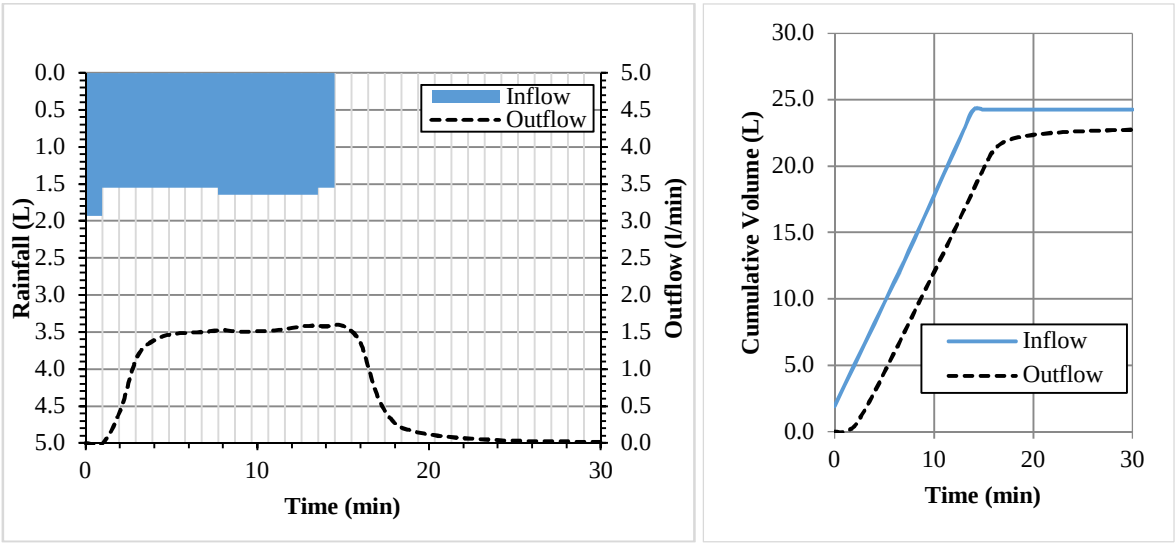

Figure D-37 Rig 3 rainfall event 9–inflow hyetograph, discharge hydrograph and cumulative hydrographs

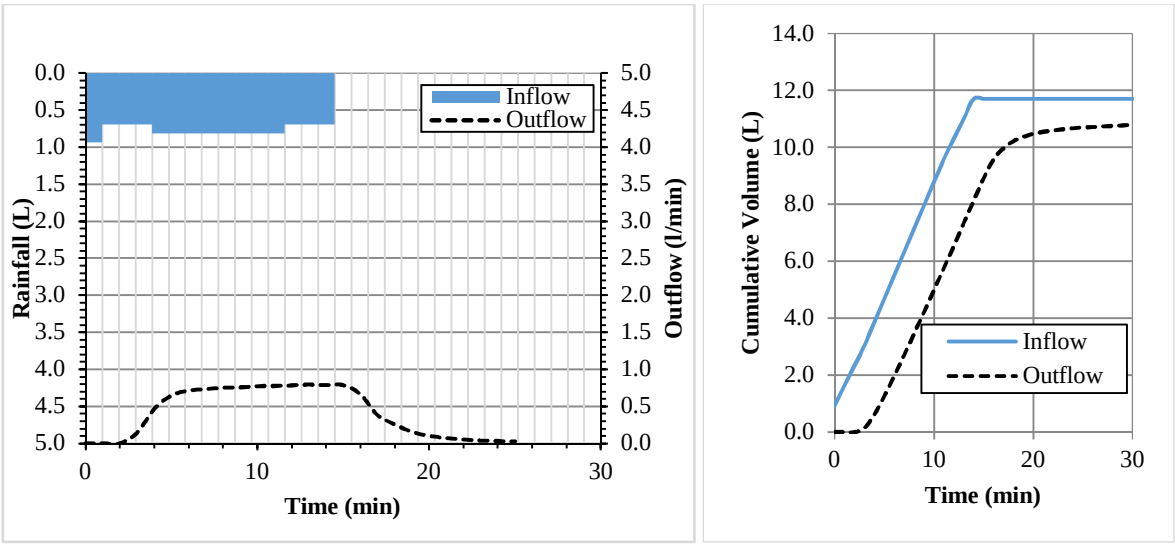

Figure D-38 Rig 3 rainfall event 10–inflow hyetograph, discharge hydrograph and cumulative hydrographs

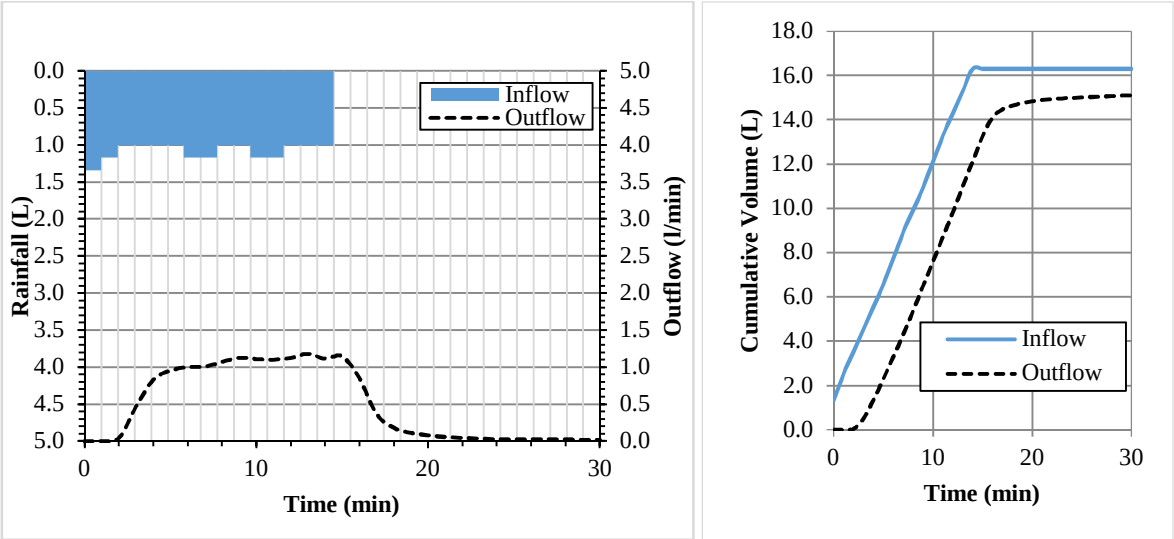

Figure D-39 Rig 3 rainfall event 11–inflow hyetograph, discharge hydrograph and cumulative hydrographs

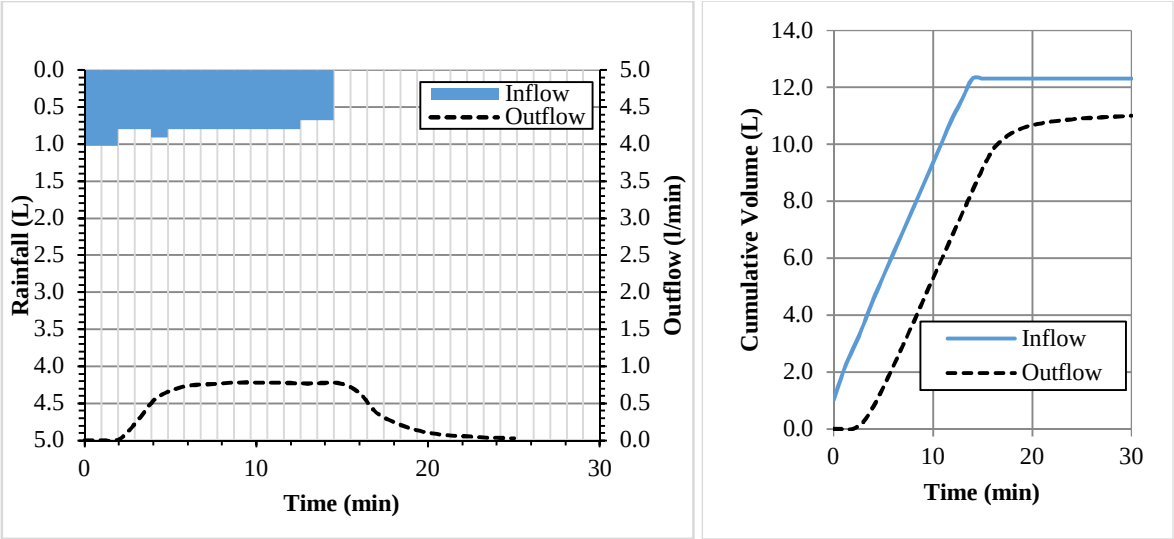

Figure D-40 Rig 3 rainfall event 12–inflow hyetograph, discharge hydrograph and cumulative hydrographs

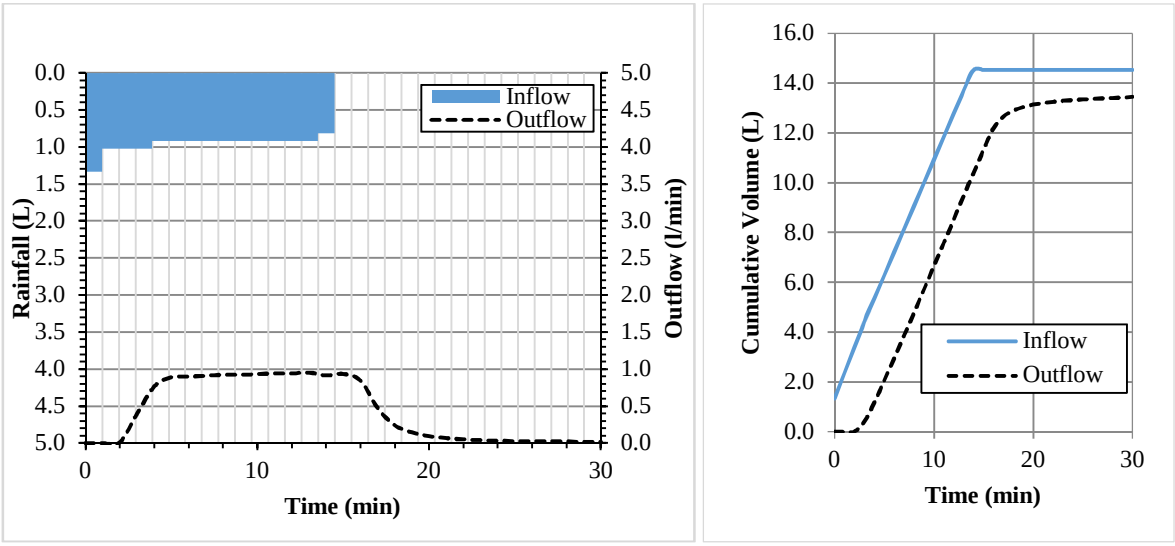

Figure D-41 Rig 3 rainfall event 13–inflow hyetograph, discharge hydrograph and cumulative hydrographs

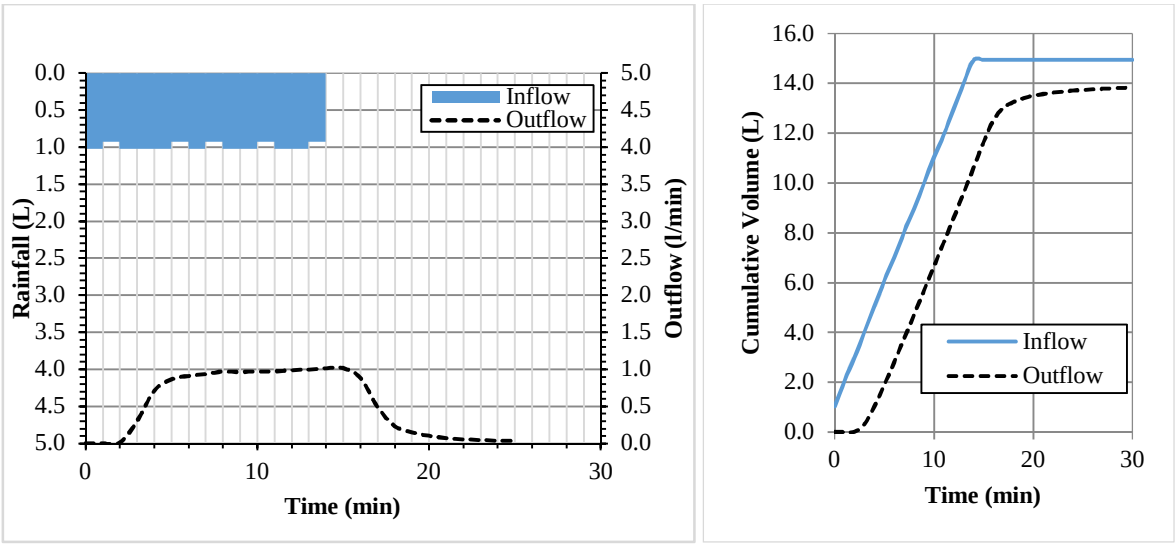

Figure D-42 Rig 3 rainfall event 14–inflow hyetograph, discharge hydrograph and cumulative hydrographs

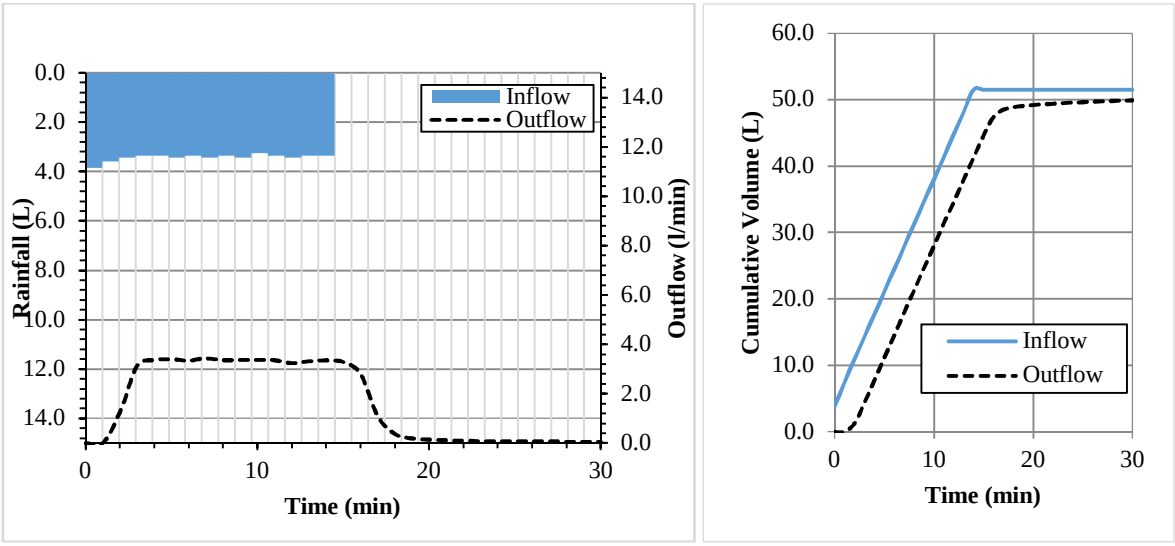

Figure D-43 Rig 4 rainfall event 1–inflow hyetograph, discharge hydrograph and cumulative hydrographs

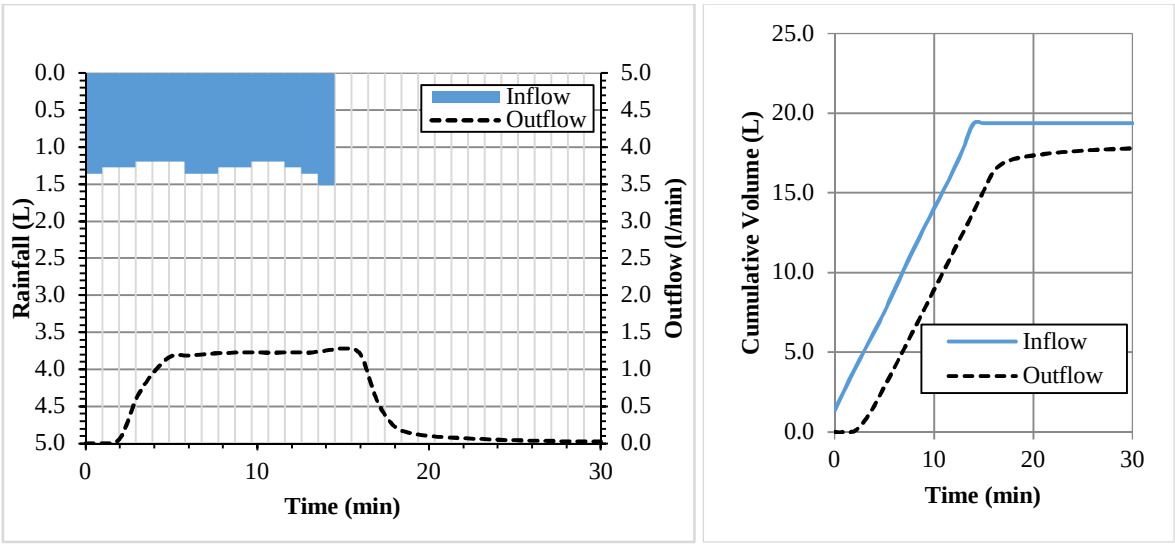

Figure D-44 Rig 4 rainfall event 2–inflow hyetograph, discharge hydrograph and cumulative hydrographs

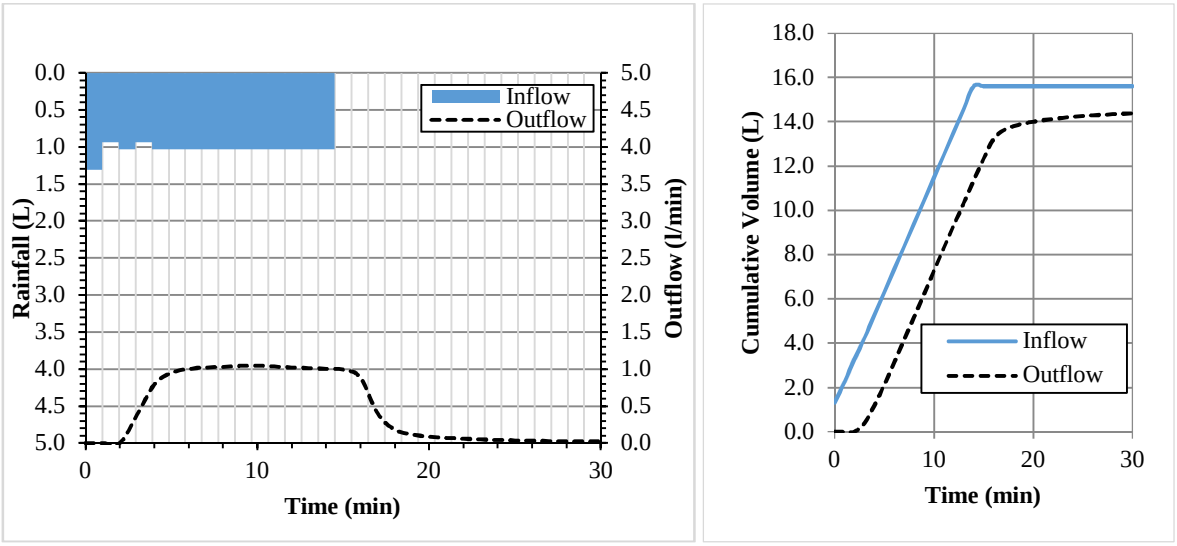

Figure D-45 Rig 4 rainfall event 3–inflow hyetograph, discharge hydrograph and cumulative hydrographs

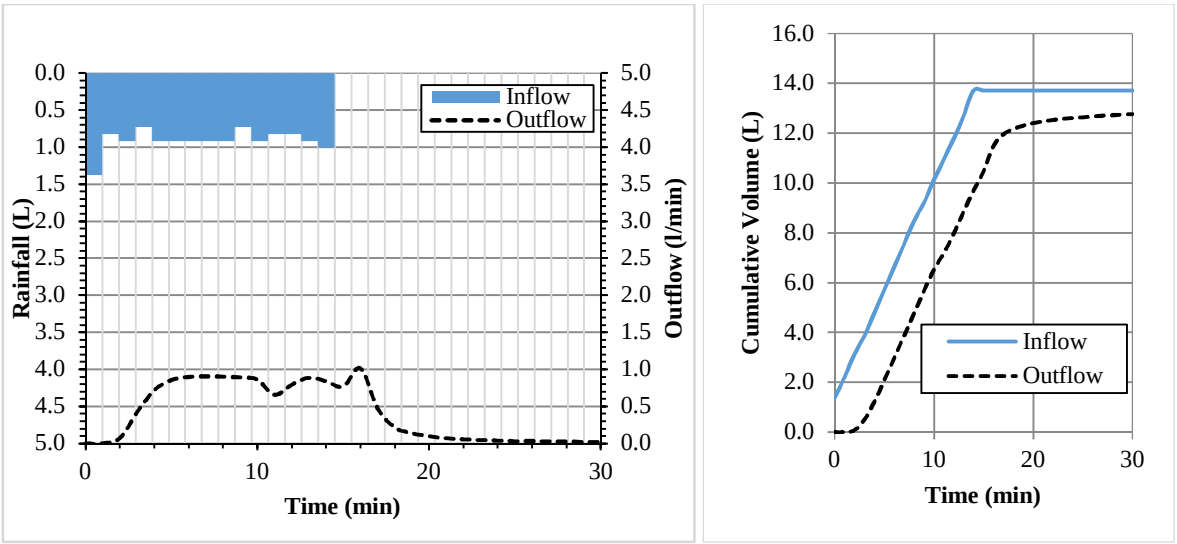

Figure D-46 Rig 4 rainfall event 4–inflow hyetograph, discharge hydrograph and cumulative hydrographs

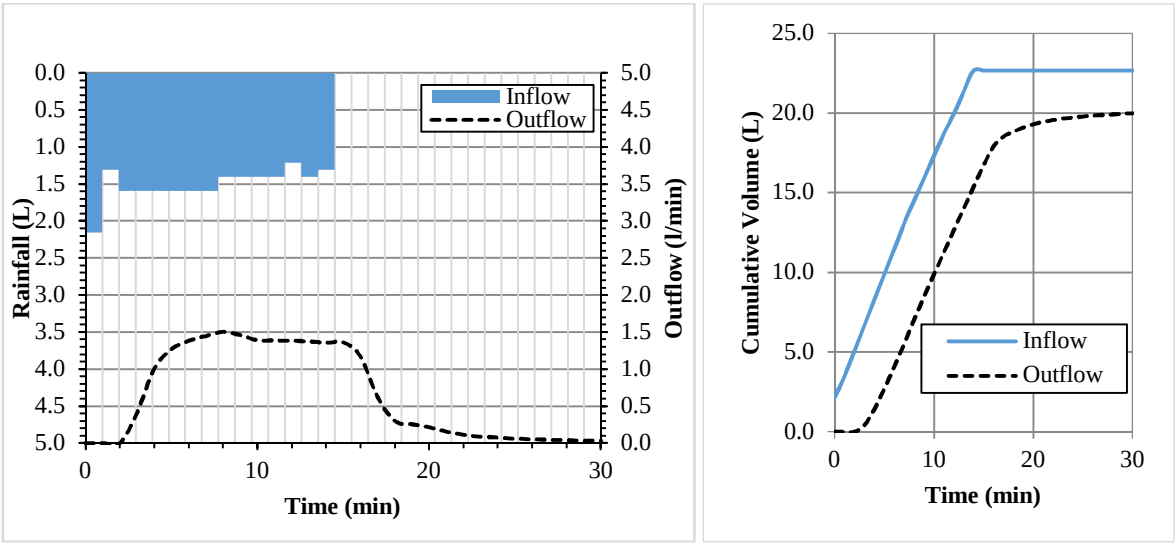

Figure D-47 Rig 4 rainfall event 5–inflow hyetograph, discharge hydrograph and cumulative hydrographs

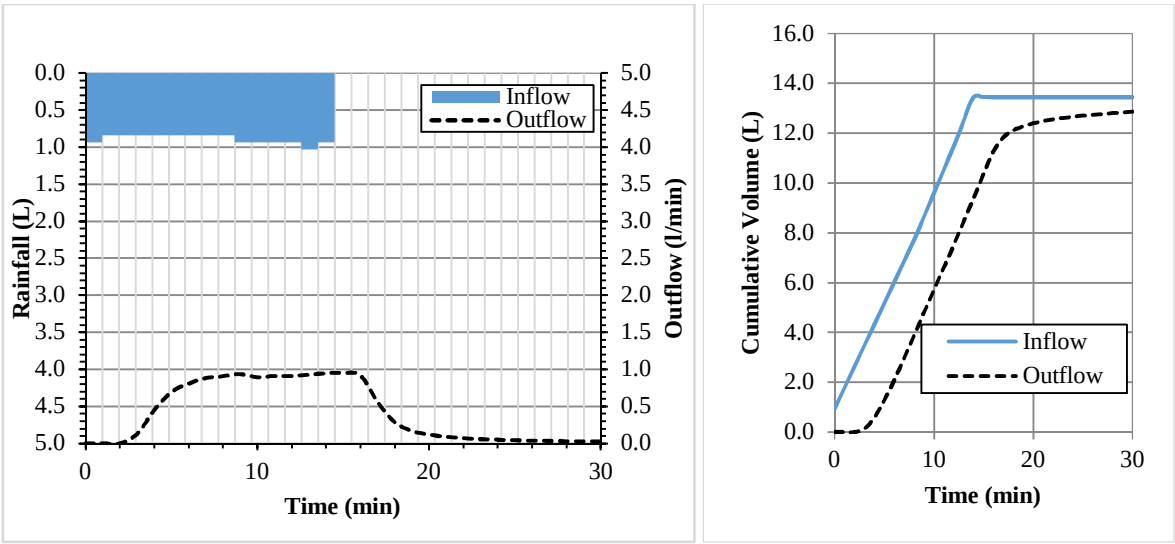

Figure D-48 Rig 4 rainfall event 6–inflow hyetograph, discharge hydrograph and cumulative hydrographs

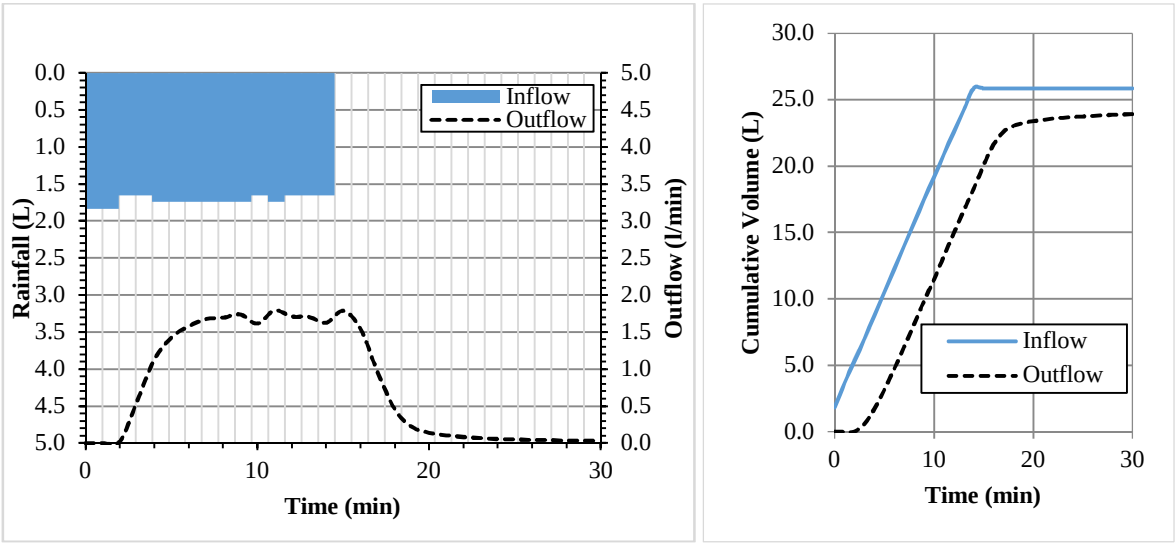

Figure D-49 Rig 4 rainfall event 7–inflow hyetograph, discharge hydrograph and cumulative hydrographs

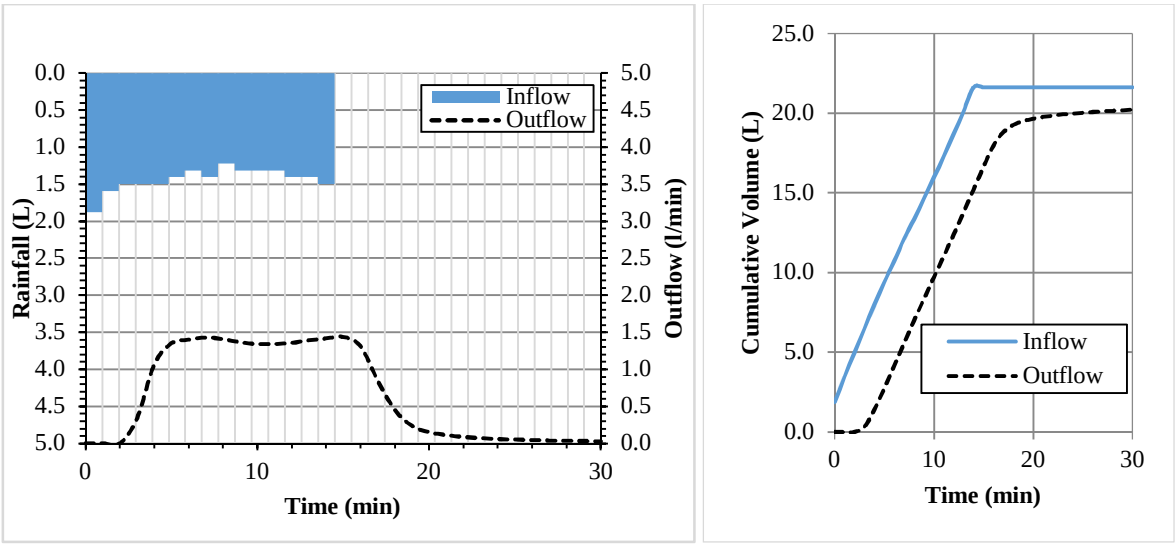

Figure D-50 Rig 4 rainfall event 8–inflow hyetograph, discharge hydrograph and cumulative hydrographs

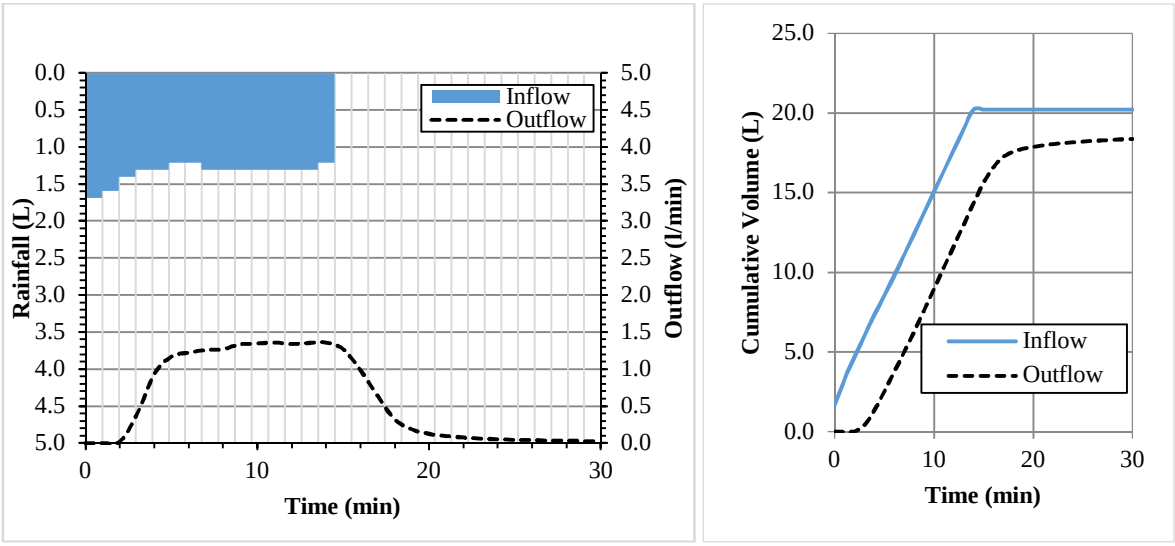

Figure D-51 Rig 4 rainfall event 9–inflow hyetograph, discharge hydrograph and cumulative hydrographs

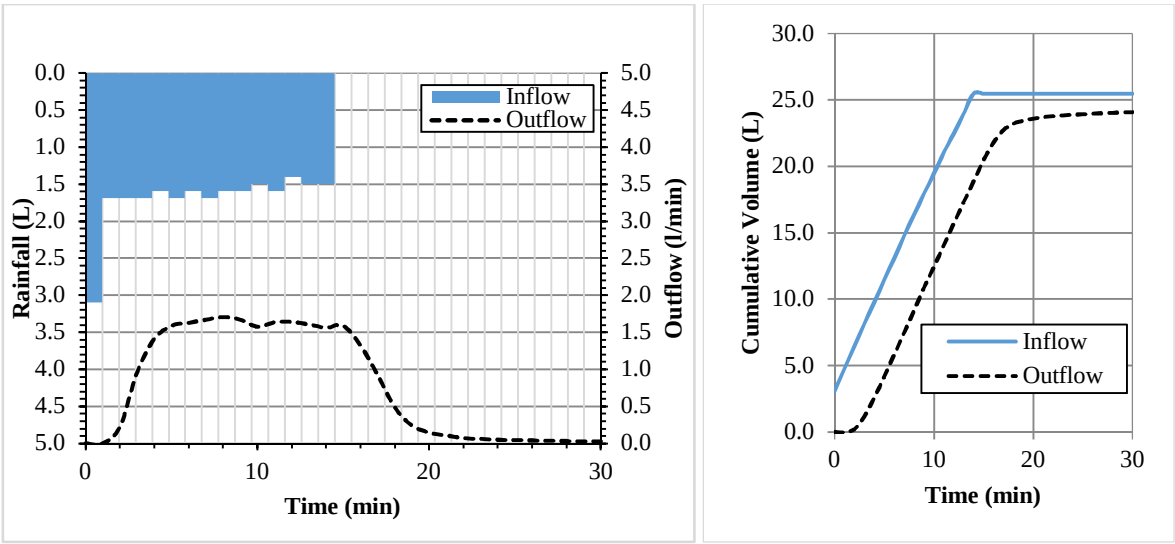

Figure D-52 Rig 4 rainfall event 10–inflow hyetograph, discharge hydrograph and cumulative hydrographs

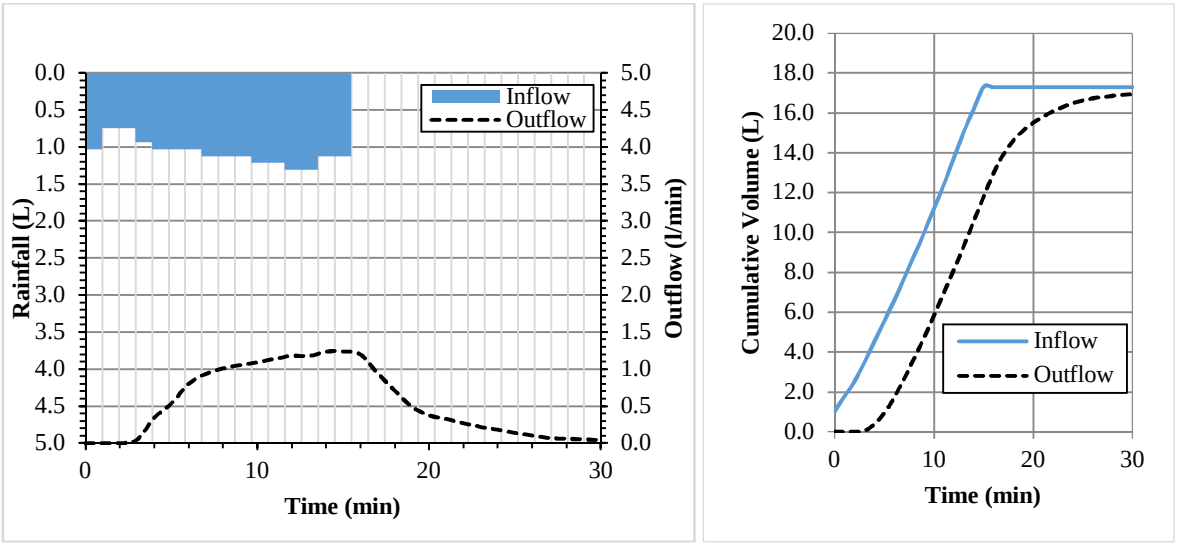

Figure D-53 Rig 4 rainfall event 11–inflow hyetograph, discharge hydrograph and cumulative hydrographs

APPENDIX E WATER QUALITY DATA

Table E-1 Effluent concentrations from December 2016 to August 2018 (n = 30)

Parameter	Rig No.	Range	$\overline{x}$	$\sigma_{\bar{x}}$	σ	MPL	
						EMA[a]	US EPA[b]
pH	1	6.8–9.36	7.80	0.60	0.12	6-9	6-8.5
	2	6.92–9.77	7.93	0.67	0.13		
	3	11.19–12.72	11.96	0.49	0.10		
	4	11.38–13.24	12.34	0.54	0.12		
COD (mg/L)	1	38–109	64.30	17.14	3.43	250	-
	2	37.9–119	67.12	21.43	4.29		
	3	40.9–104	66.10	16.78	3.36		
	4	49.7–98	68.27	14.81	3.23		
DO (mg/L)	1	6.21–7.77	7.02	0.42	0.11	> 4	> 4
	2	6.07–7.67	6.99	0.47	0.13		
	3	6.1–7.9	7.37	0.57	0.15		
	4	7.08–7.94	7.53	0.27	0.07		
NO_3-N (mg/L)	1	0–5.9	1.45	1.19	0.24	-	-
	2	0–5.8	1.46	1.30	0.26		
	3	0–5.1	1.14	1.34	0.27		
	4	0–5.7	2.08	1.58	0.34		
PO_4^{3-} (mg/L)	1	1.2–4.1	2.14	0.79	0.16	5	-
	2	0.8–3.9	1.90	0.83	0.17		
	3	0.4–3.7	1.50	0.86	0.17		
	4	0.1–3.7	1.33	0.81	0.17		
SO_4^{2-} (mg/L)	1	6–72	26.64	17.48	3.50	< 200	-
	2	4–75	23.48	20.53	4.11		
	3	0–39	11.92	12.06	2.41		
	4	0–19	4.73	6.65	1.42		
Turbidity (NTU)	1	2–122	33.08	34.68	7.08	5	≤ 29
	2	2–126	35.46	35.27	7.20		
	3	4–144	45.29	41.05	8.38		
	4	0–89	28.95	28.43	6.20		
TDS (mg/L)	1	62–416	238.36	99.69	21.25	-	≤ 1000
	2	58–436	217.45	97.79	20.85		
	3	122–782	428.68	168.05	35.83		
	4	258–1018	622.42	215.21	49.37		
TSS (mg/L)	1	8–222	64.48	63.82	13.93	50	-
	2	10–230	64.14	66.57	14.53		
	3	5–196	60.10	60.08	13.11		
	4	4–152	46.50	40.02	9.43		
EC (µS/cm)	1	84.9–401	196.68	81.82	16.36	-	≤ 1275
	2	68.5–455	184.43	93.96	18.79		

	3	391–1923	1197.52	351.79	70.36		
	4	1280–3510	2543.82	520.89	111.05		
Cu (mg/L)	1	0–0.24	0.04	0.06	0.01	0.5	0.5
	2	0–0.26	0.05	0.07	0.01		
	3	0–0.27	0.04	0.07	0.01		
	4	0–0.30	0.04	0.07	0.02		
Zn (mg/L)	1	0.05–0.22	0.11	0.05	0.01	2	1
	2	0.05–0.23	0.11	0.05	0.01		
	3	0.05–0.18	0.10	0.05	0.01		
	4	0.04–0.18	0.11	0.05	0.01		
Mn (mg/L)	1	0–0.61	0.14	0.19	0.04	-	-
	2	0–0.65	0.16	0.20	0.04		
	3	0–0.65	0.17	0.21	0.04		
	4	0–0.65	0.13	0.18	0.04		
Fe (mg/L)	1	0.08–1.17	0.38	0.22	0.04	3.5	1
	2	0.06–1.48	0.39	0.29	0.06		
	3	0.08–0.7	0.39	0.18	0.04		
	4	0.20–0.71	0.39	0.15	0.03		

[a]EMA for inland surface water (EMA, 2001)

[b]US EPA for Class IV Agricultural water supplies (US EPA, 2018)

APPENDIX F FLOW COMPARISON HYDROGRAPHS DURING CALIBRATION AND VALIDATION

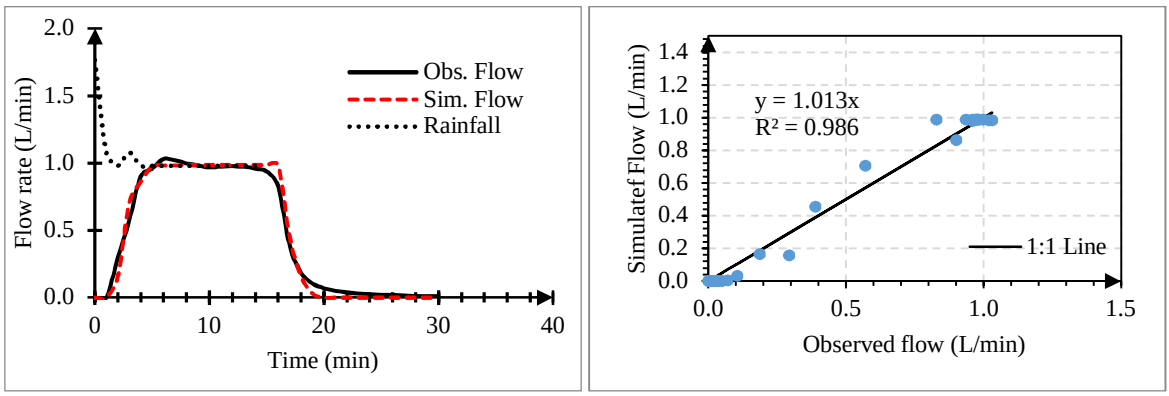

Figure F-1 Rig 1 Hydrographs and scatter graph for Calibration event 1

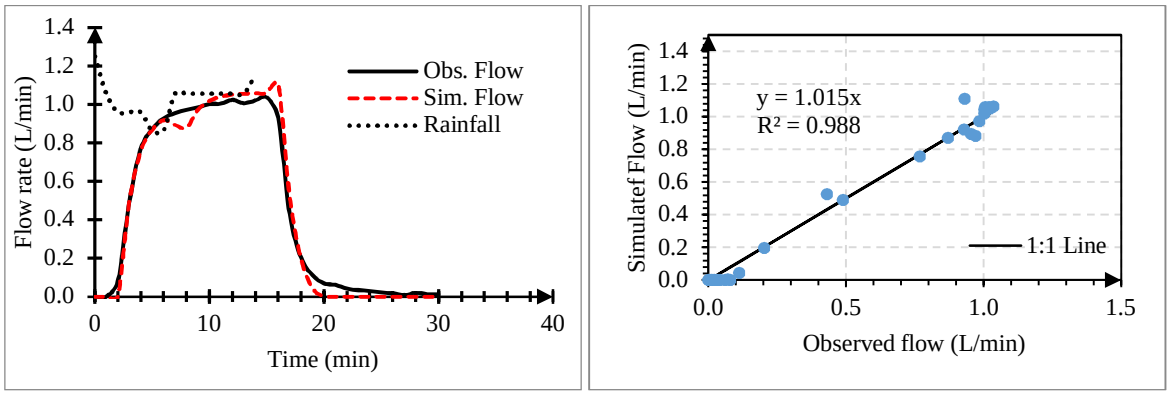

Figure F-2 Rig 1 Hydrographs and scatter graph for Calibration event 2

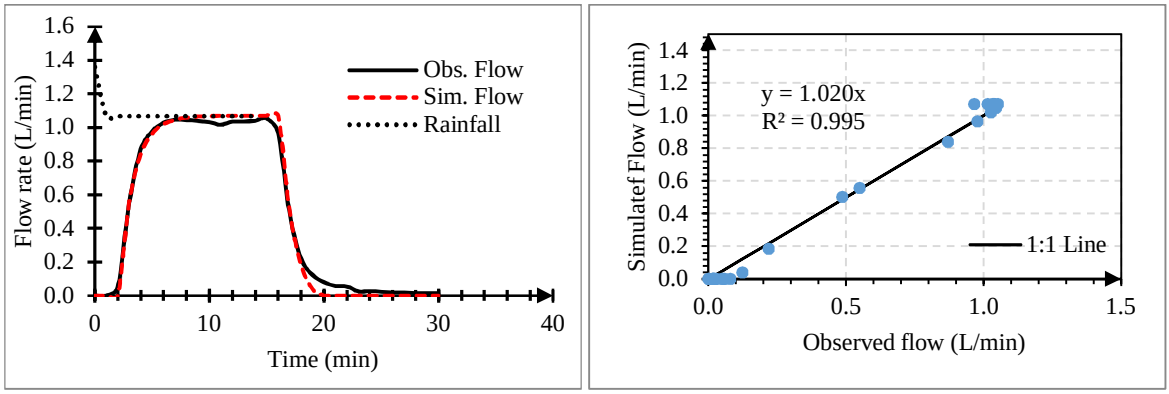

Figure F-3 Rig 1 Hydrographs and scatter graph for Calibration event 3

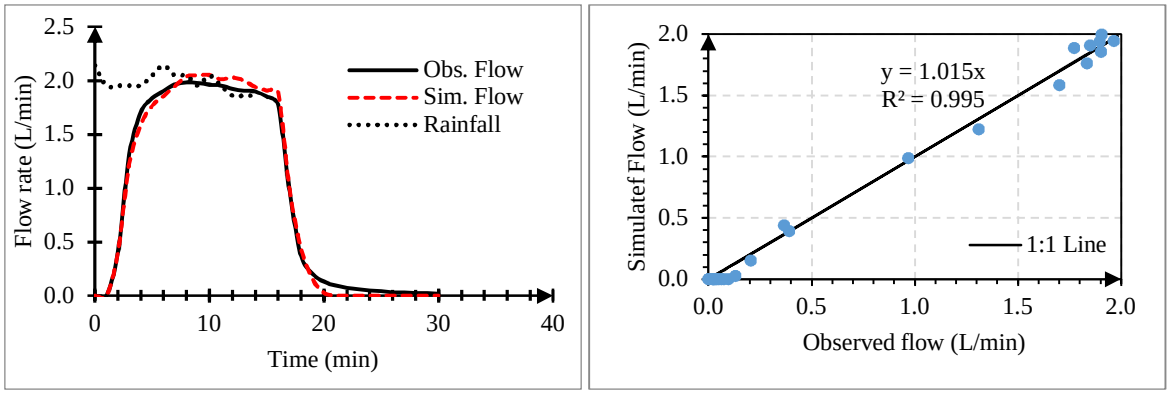

Figure F-4 Rig 1 Hydrographs and scatter graph for Calibration event 4

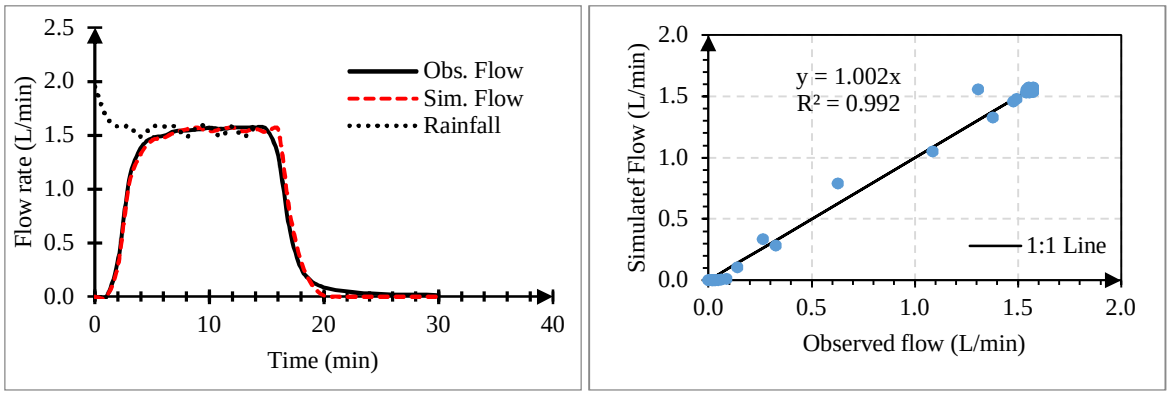

Figure F-5 Rig 1 Hydrographs and scatter graph for Calibration event 5

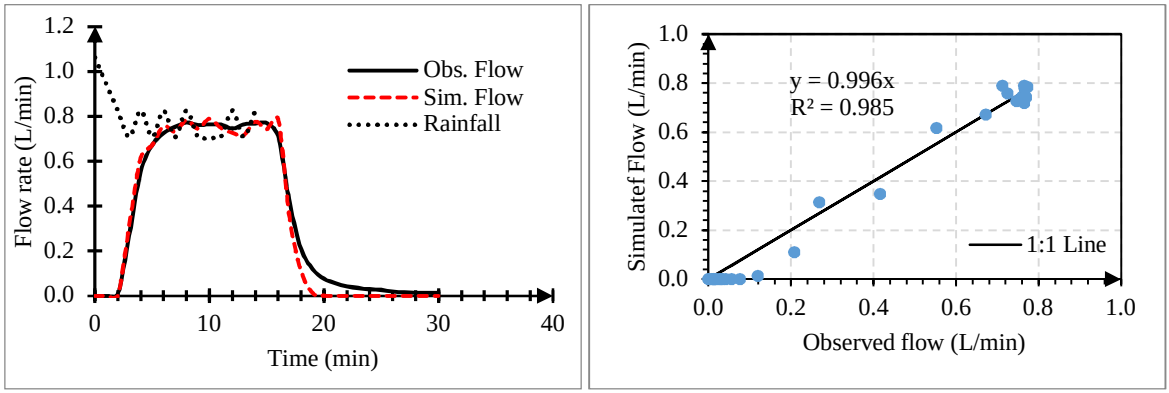

Figure F-6 Rig 1 Hydrographs and scatter graph for Calibration event 6

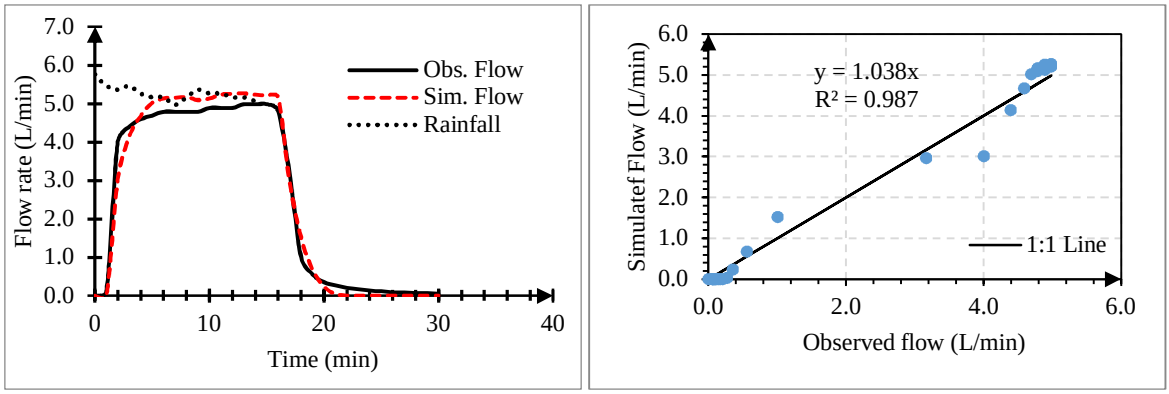

Figure F-7 Rig 1 Hydrographs and scatter graph for Validation event 1

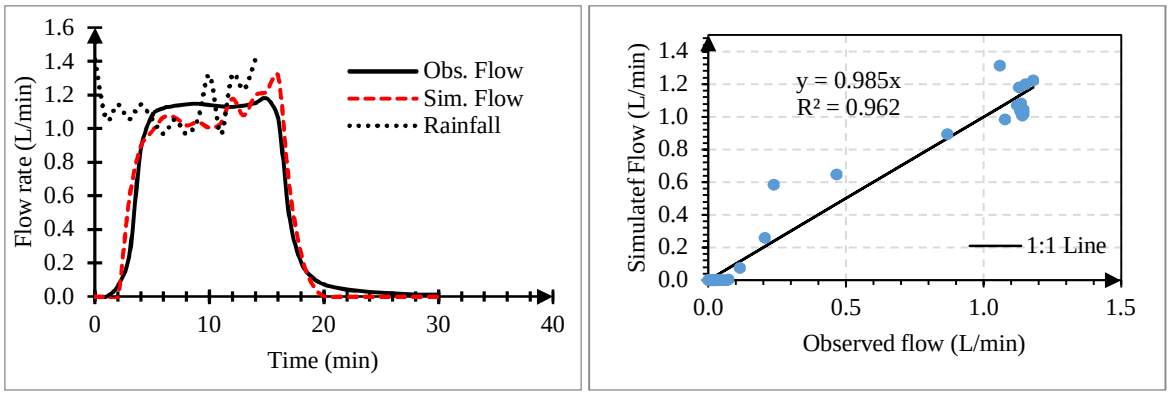

Figure F-8 Rig 1 Hydrographs and scatter graph for Validation event 2

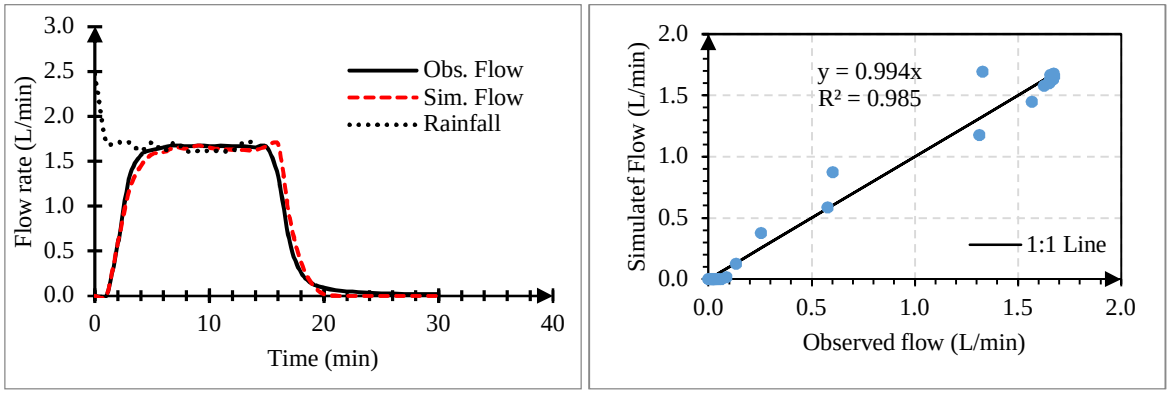

Figure F-9 Rig 1 Hydrographs and scatter graph for Validation event 3

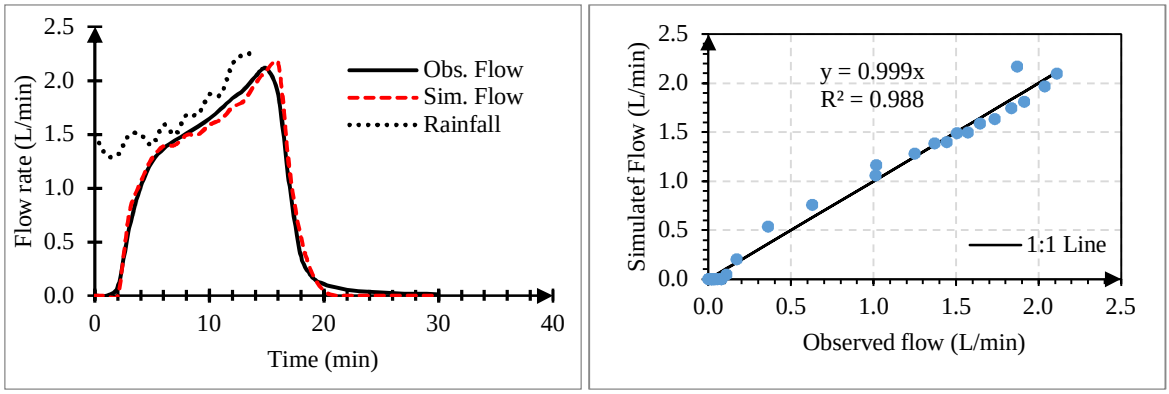

Figure F-10 Rig 1 Hydrographs and scatter graph for Validation event 4

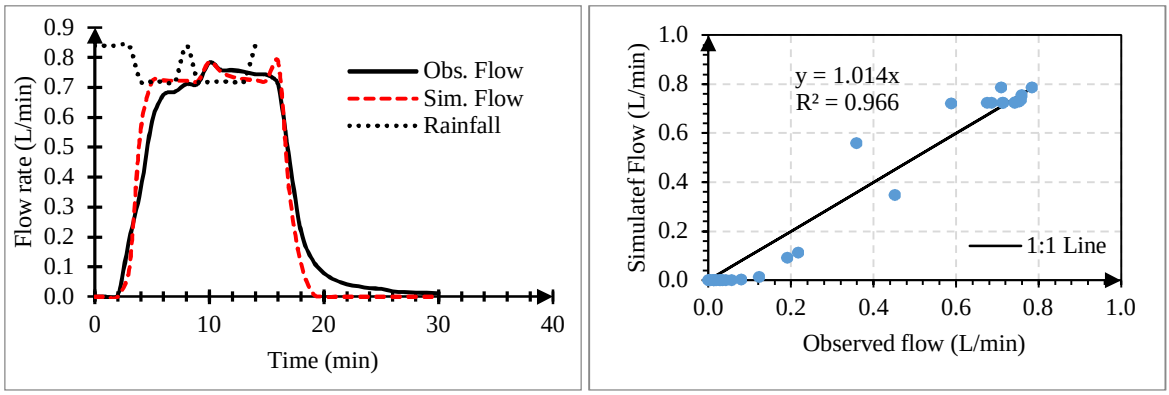

Figure F-11 Rig 1 Hydrographs and scatter graph for Validation event 5

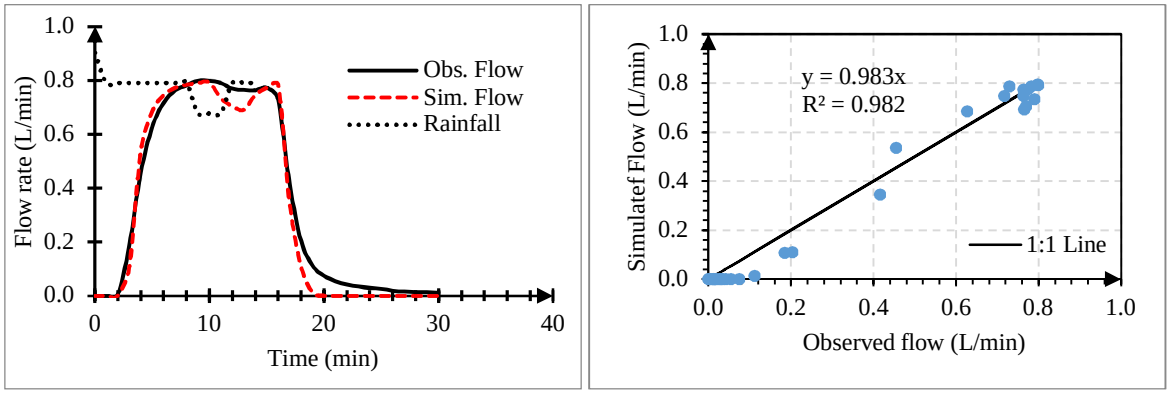

Figure F-12 Rig 1 Hydrographs and scatter graph for Validation event 6

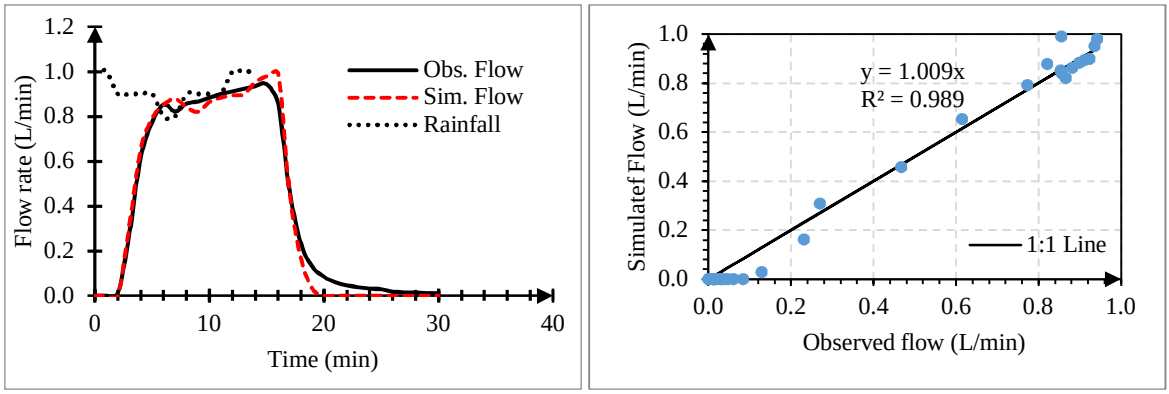

Figure F-13 Rig 1 Hydrographs and scatter graph for Validation event 7

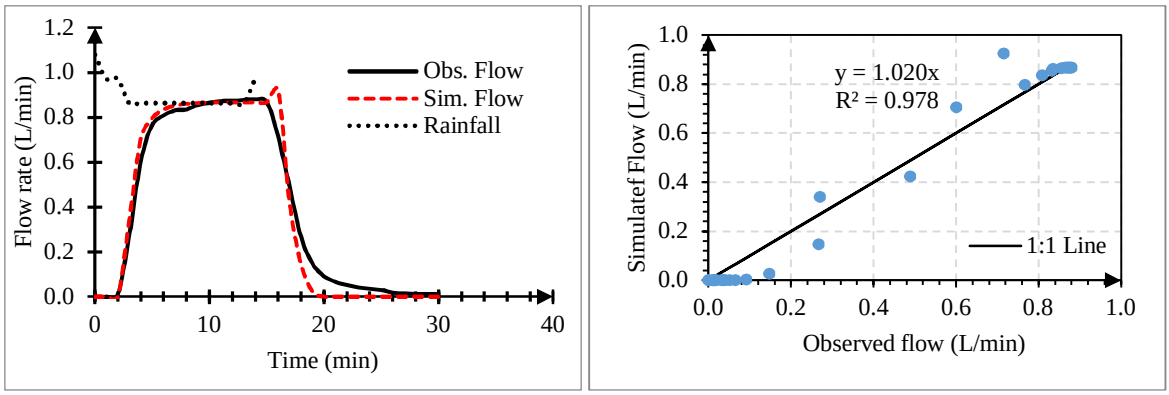

Figure F-14 Rig 1 Hydrographs and scatter graph for Validation event 8

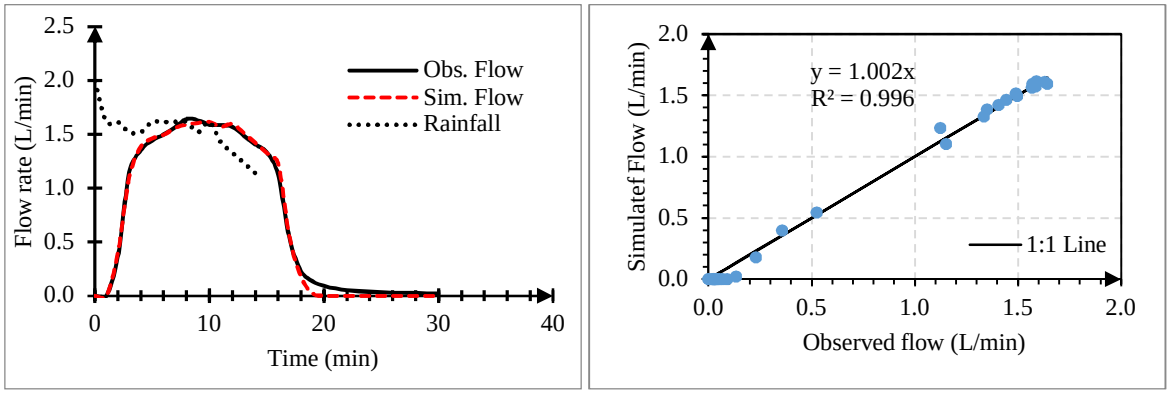

Figure F-15 Rig 2 Hydrographs and scatter graphs for Calibration event 1

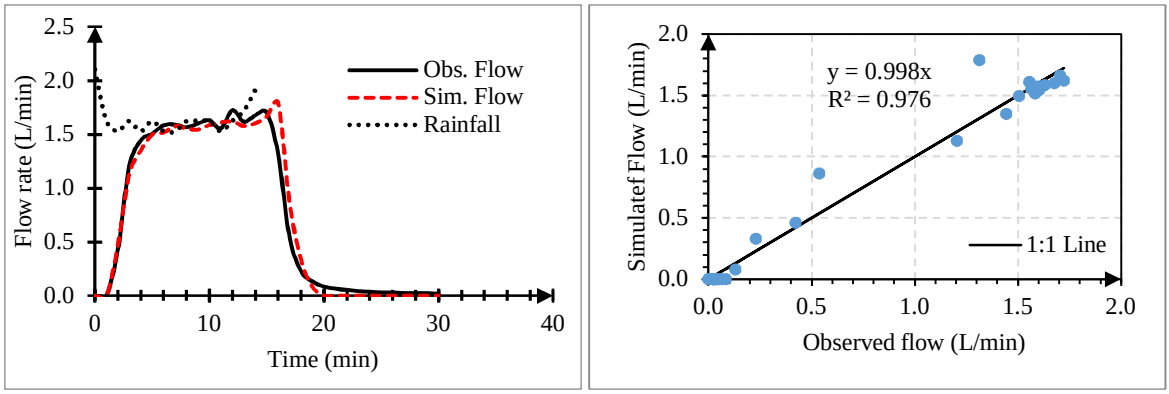

Figure F-16 Rig 2 Hydrographs and scatter graphs for Calibration event 2

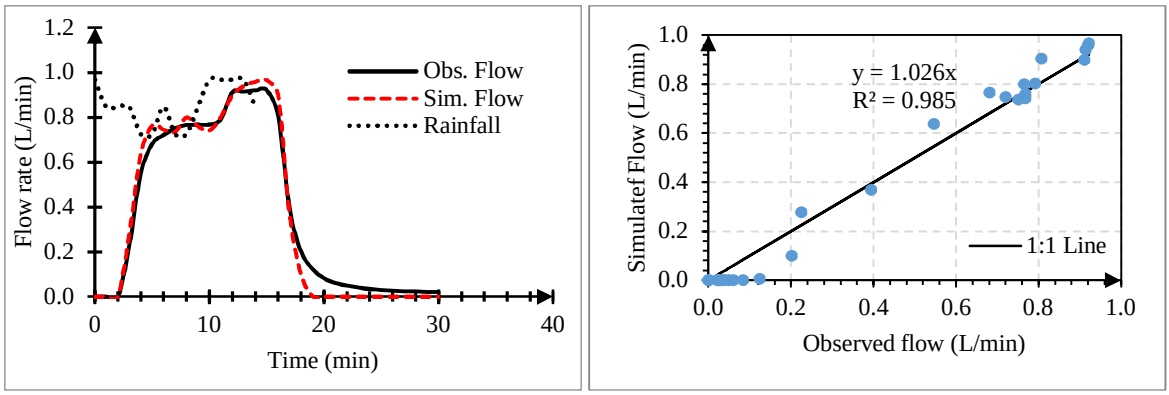

Figure F-17 Rig 2 Hydrographs and scatter graphs for Calibration event 3

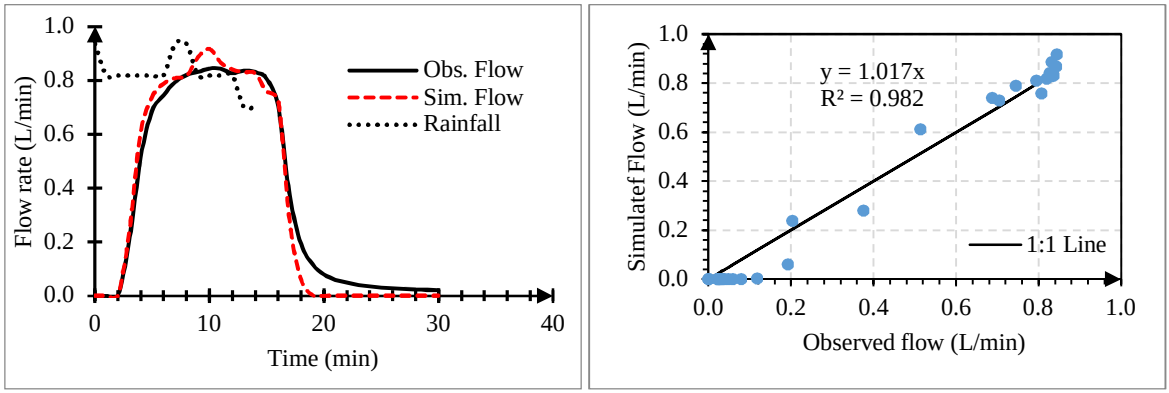

Figure F-18 Rig 2 Hydrographs and scatter graphs for Calibration event 4

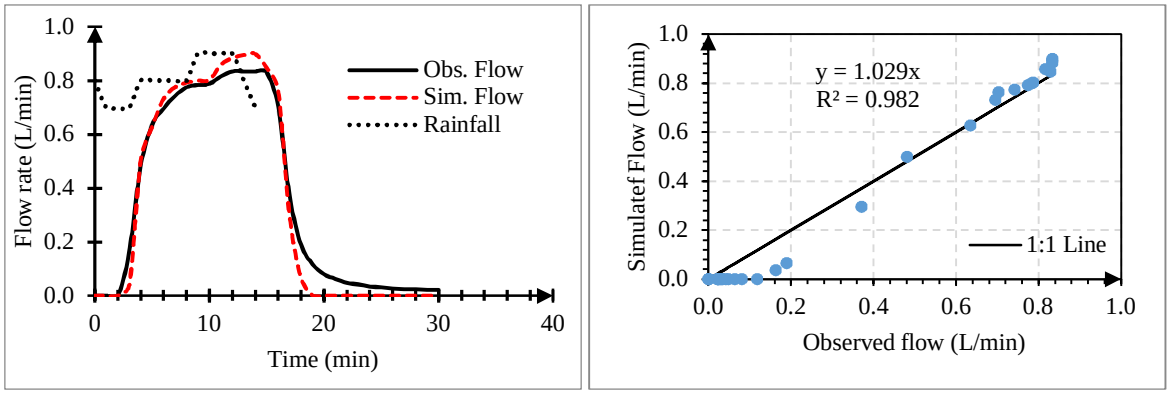

Figure F-19 Rig 2 Hydrographs and scatter graphs for Calibration event 5

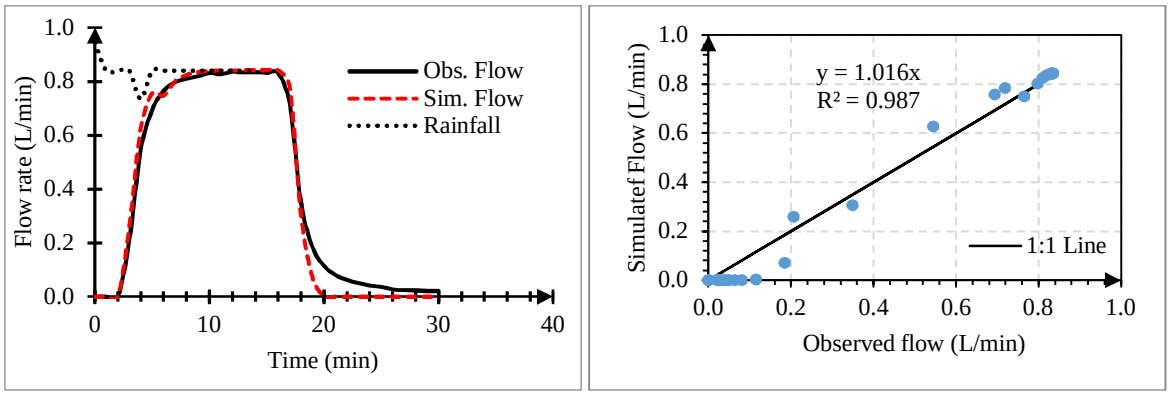

Figure F-20 Rig 2 Hydrographs and scatter graphs for Calibration event 6

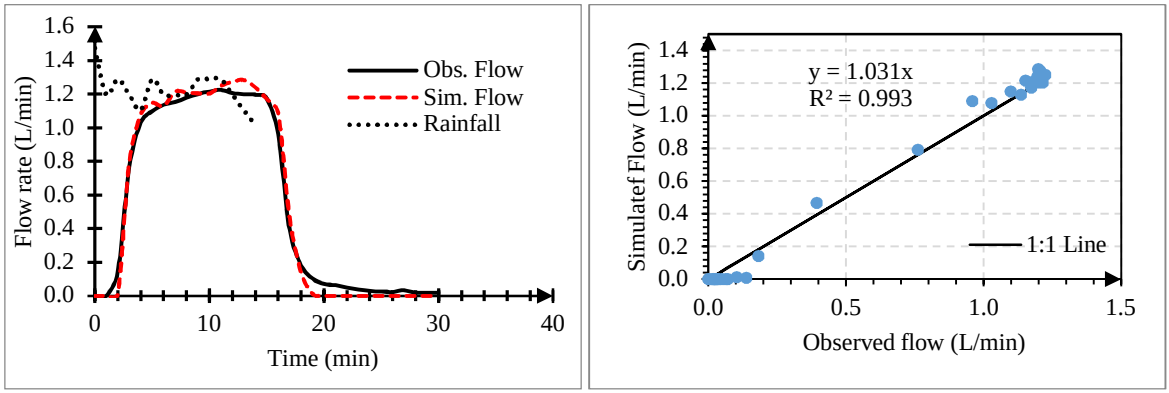

Figure F-21 Rig 2 Hydrographs and scatter graph for Validation event 1

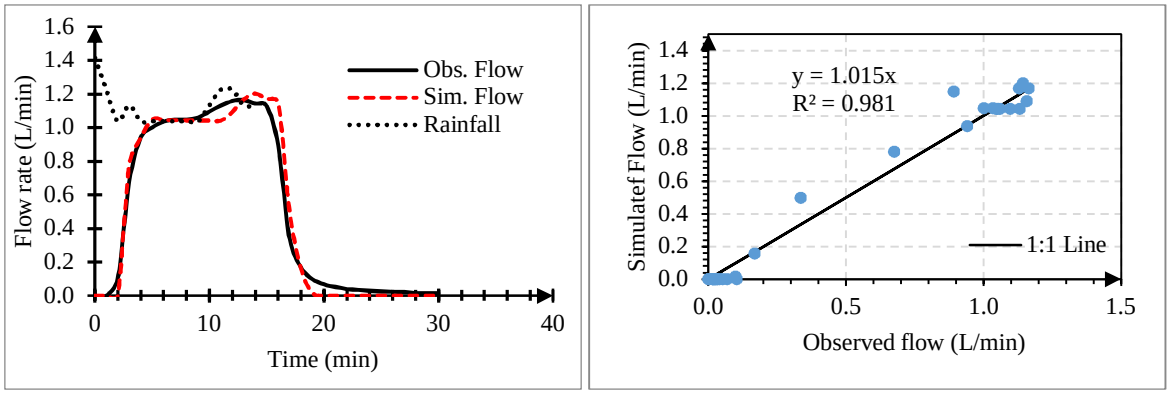

Figure F-22 Rig 2 Hydrographs and scatter graph for Validation event 2

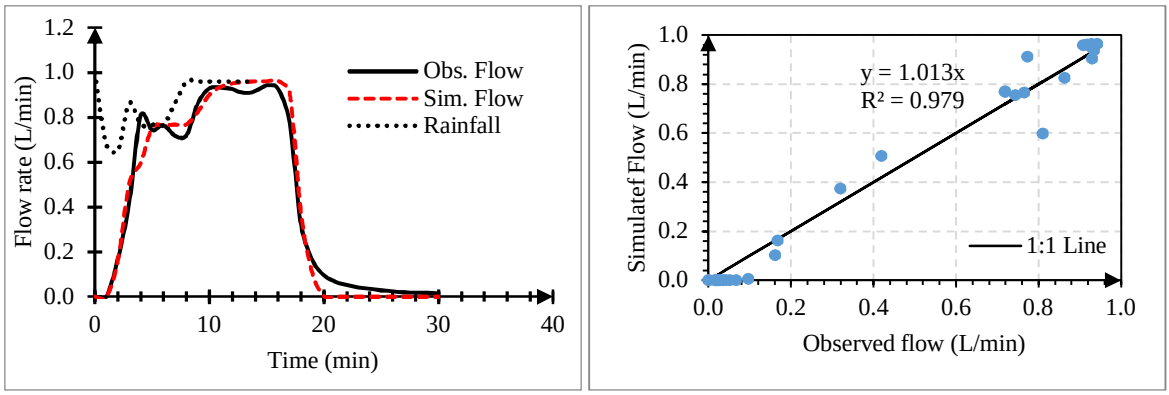

Figure F-23 Rig 2 Hydrographs and scatter graph for Validation event 3

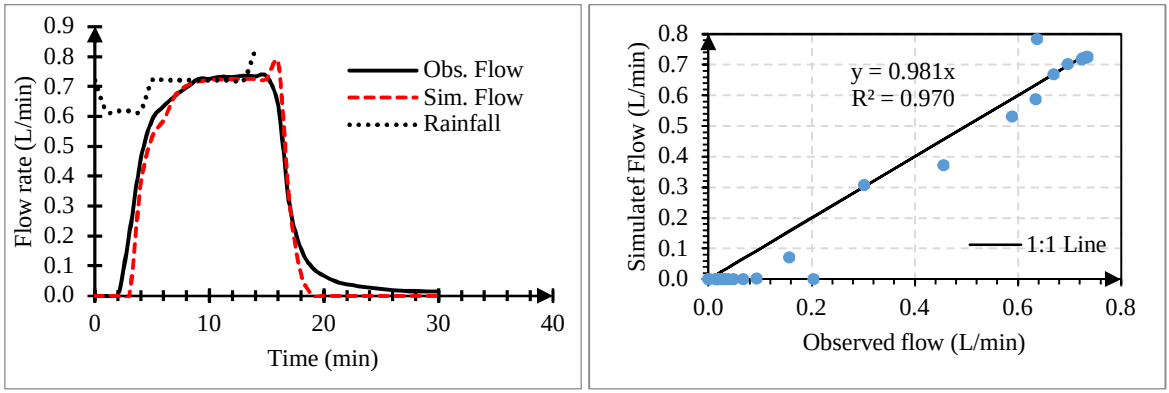

Figure F-24 Rig 2 Hydrographs and scatter graph for Validation event 4

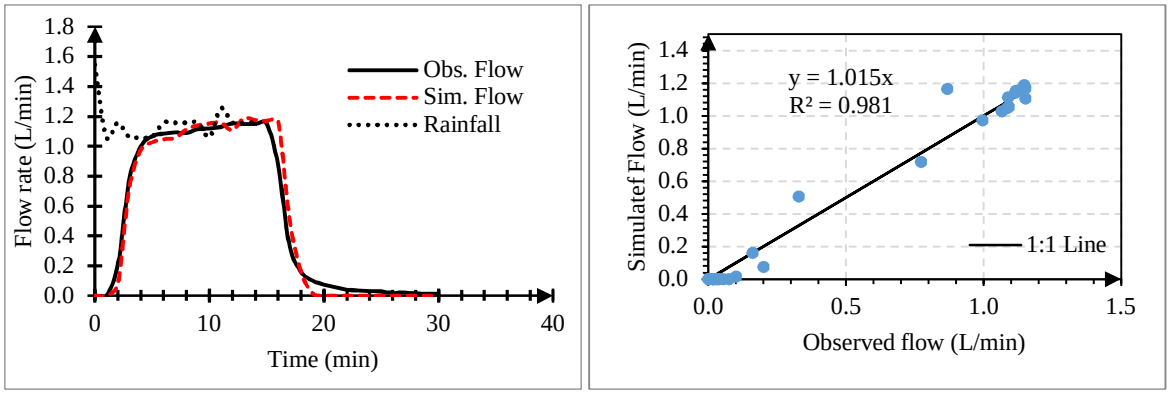

Figure F-25 Rig 2 Hydrographs and scatter graph for Validation event 5

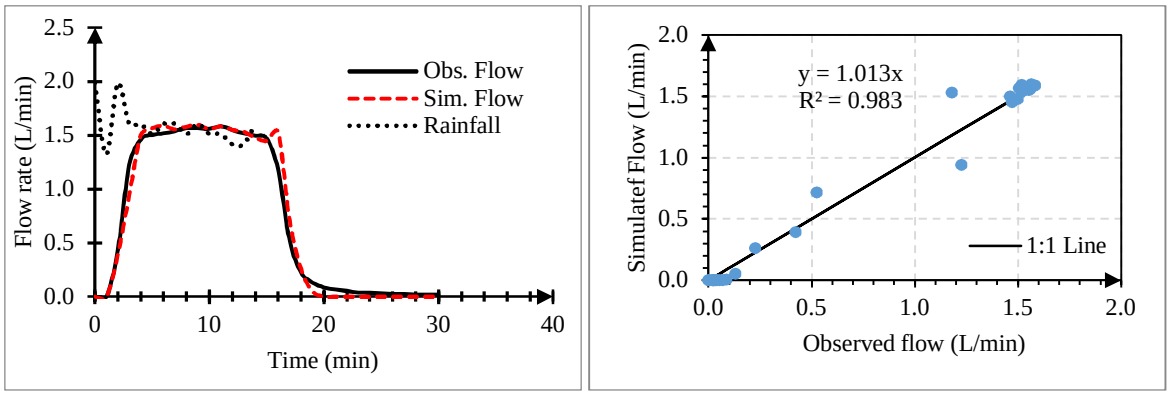

Figure F-26 Rig 2 Hydrographs and scatter graph for Validation event 6

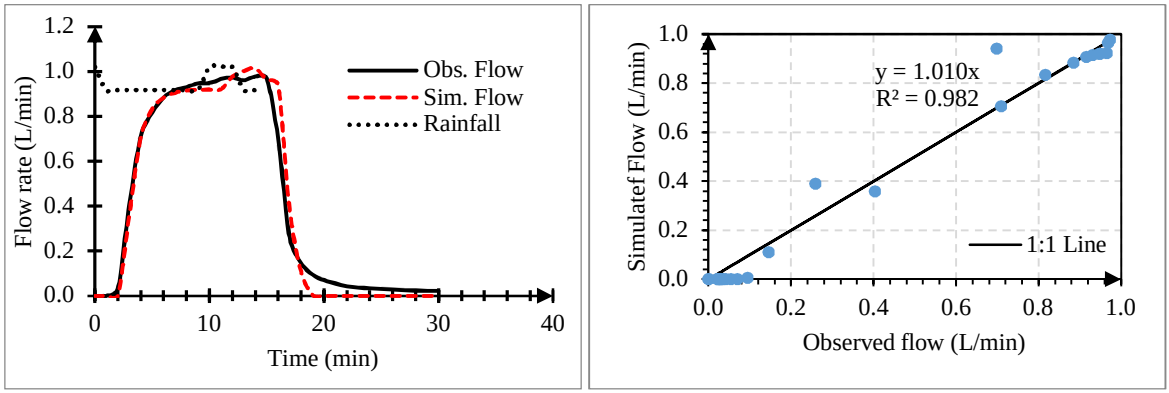

Figure F-27 Rig 2 Hydrographs and scatter graph for Validation event 7

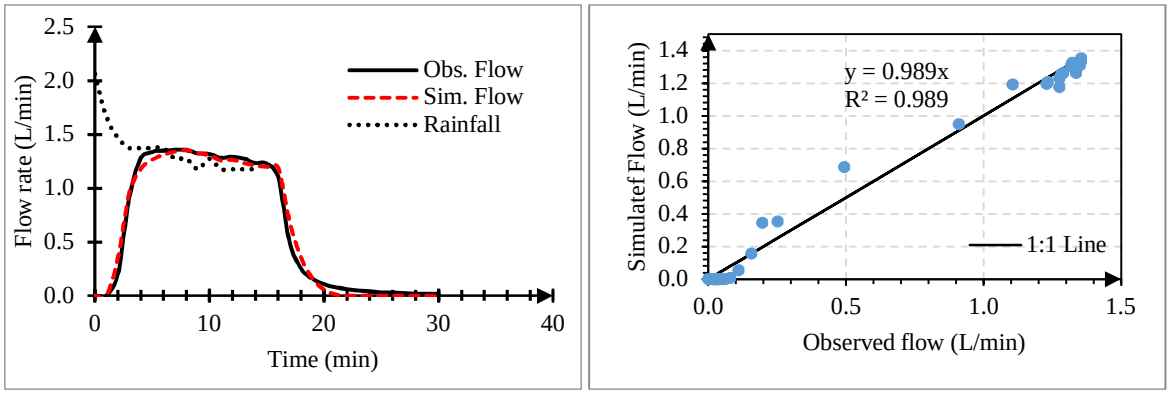

Figure F-28 Rig 3 Hydrographs and scatter graphs for Calibration event 1

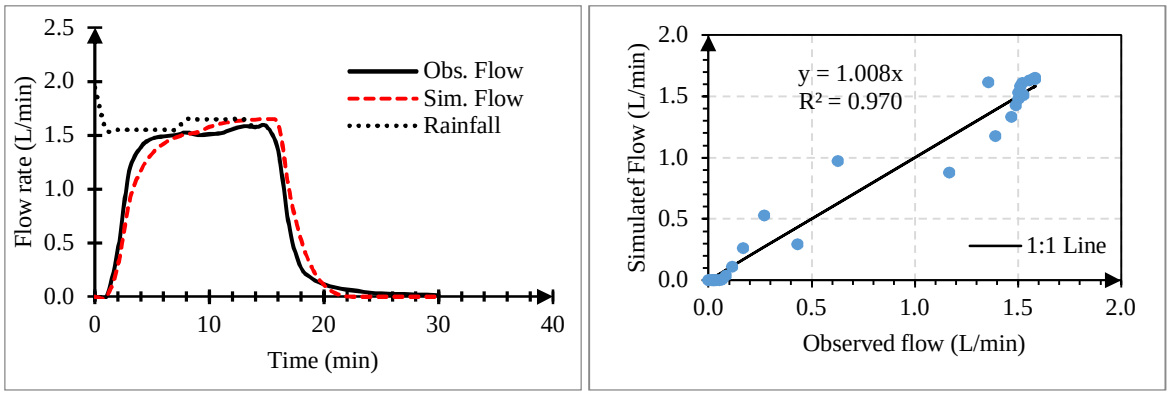

Figure F-29 Rig 3 Hydrographs and scatter graphs for Calibration event 2

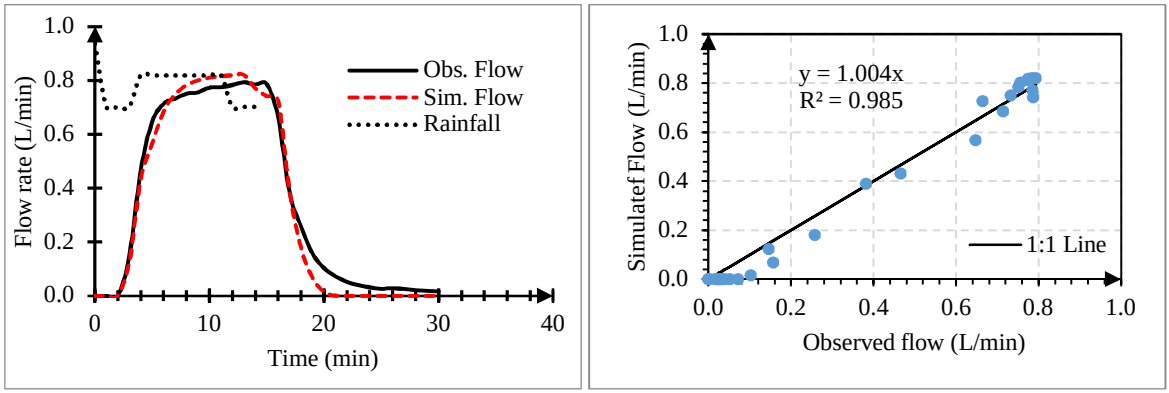

Figure F-30 Rig 3 Hydrographs and scatter graphs for Calibration event 3

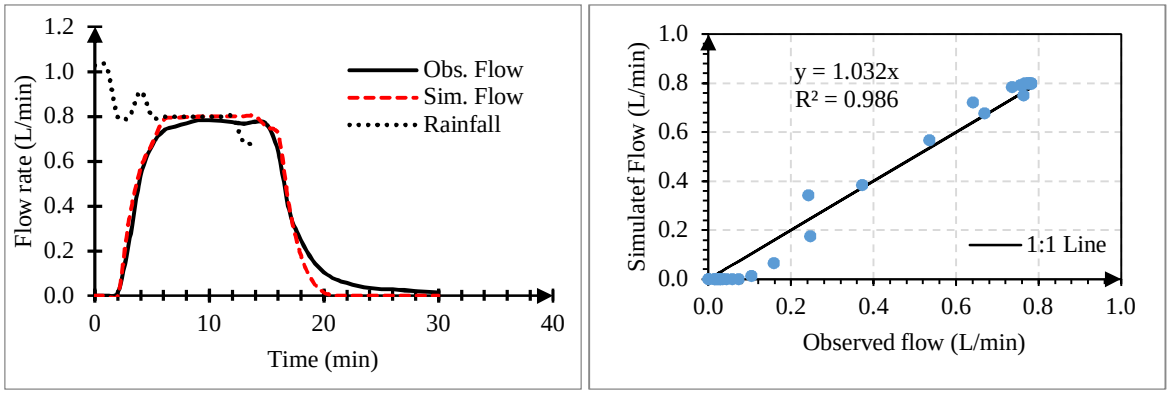

Figure F-31 Rig 3 Hydrographs and scatter graphs for Calibration event 4

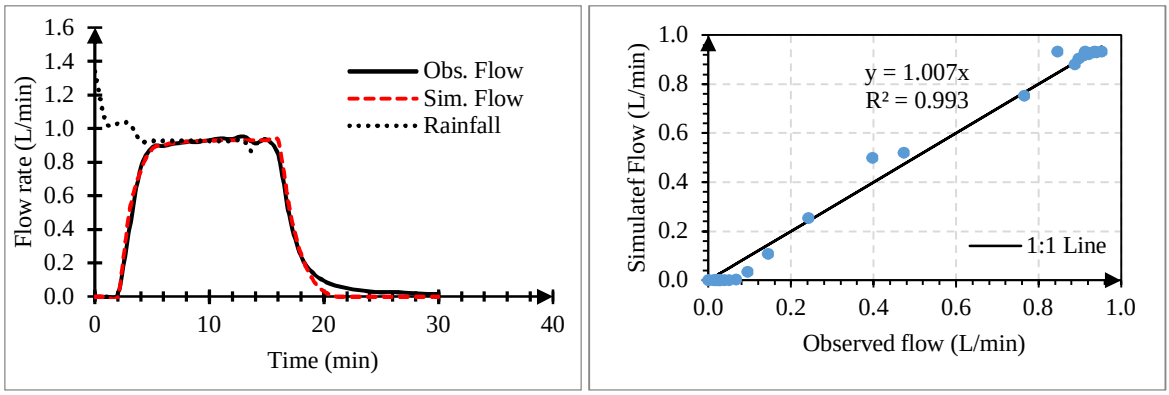

Figure F-32 Rig 3 Hydrographs and scatter graphs for Calibration event 5

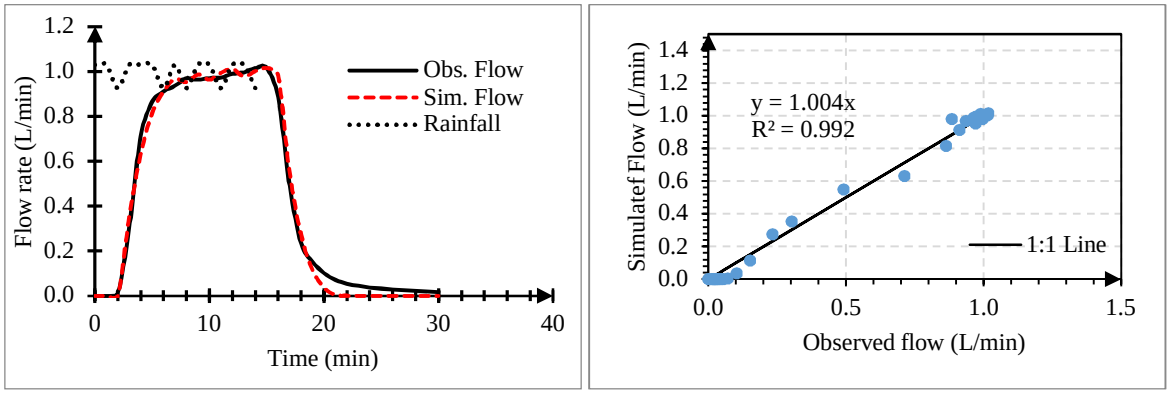

Figure F-33 Rig 3 Hydrographs and scatter graphs for Calibration event 6

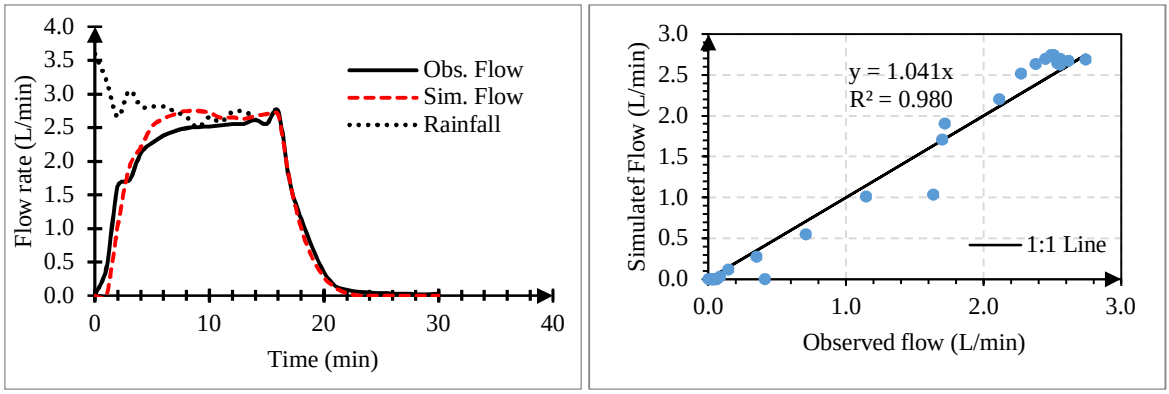

Figure F-34 Rig 3 Hydrographs and scatter graph for Validation event 1

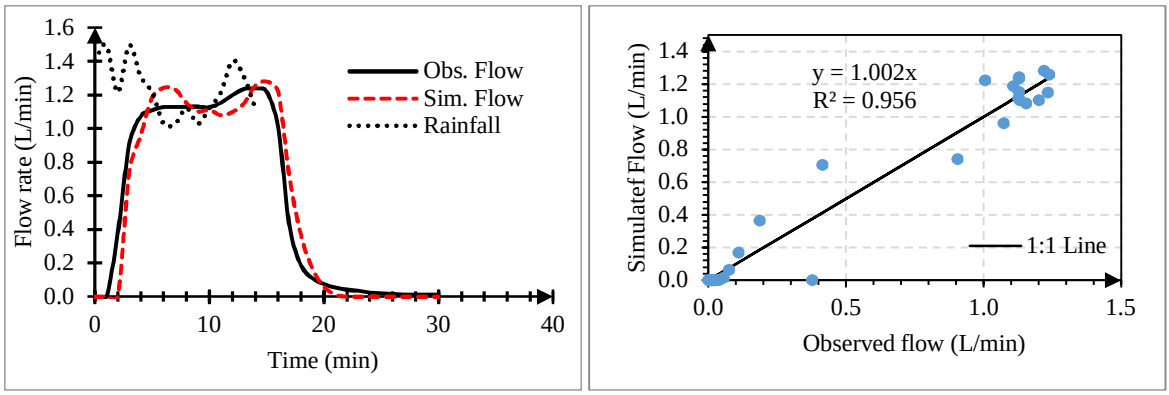

Figure F-35 Rig 3 Hydrographs and scatter graph for Validation event 2

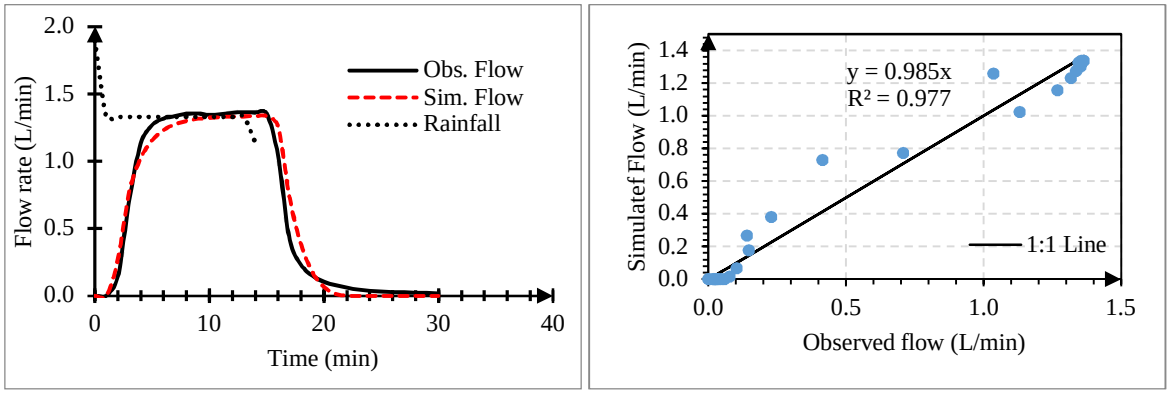

Figure F-36 Rig 3 Hydrographs and scatter graph for Validation event 3

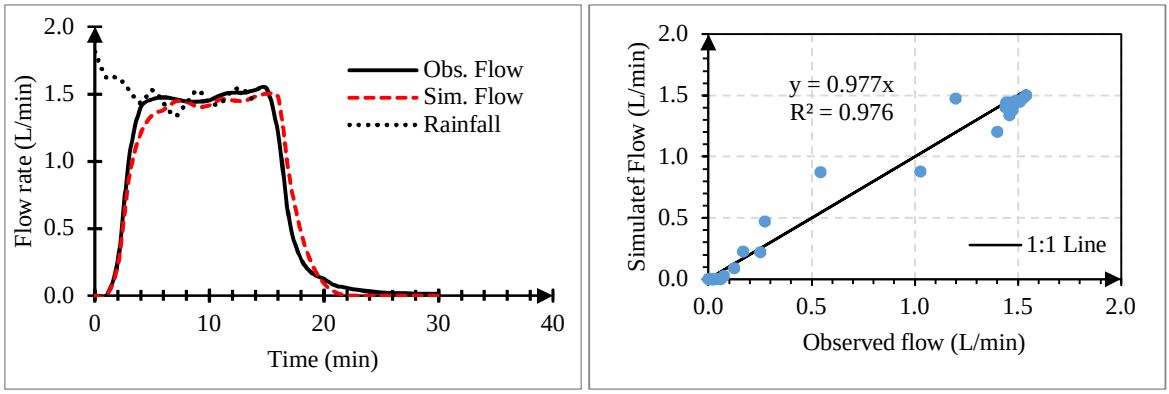

Figure F-37 Rig 3 Hydrographs and scatter graph for Validation event 4

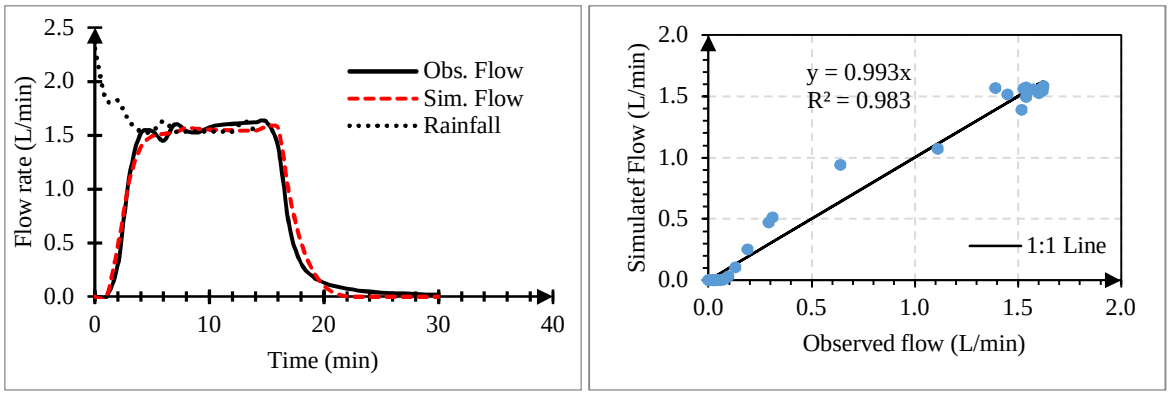

Figure F-38 Rig 3 Hydrographs and scatter graph for Validation event 5

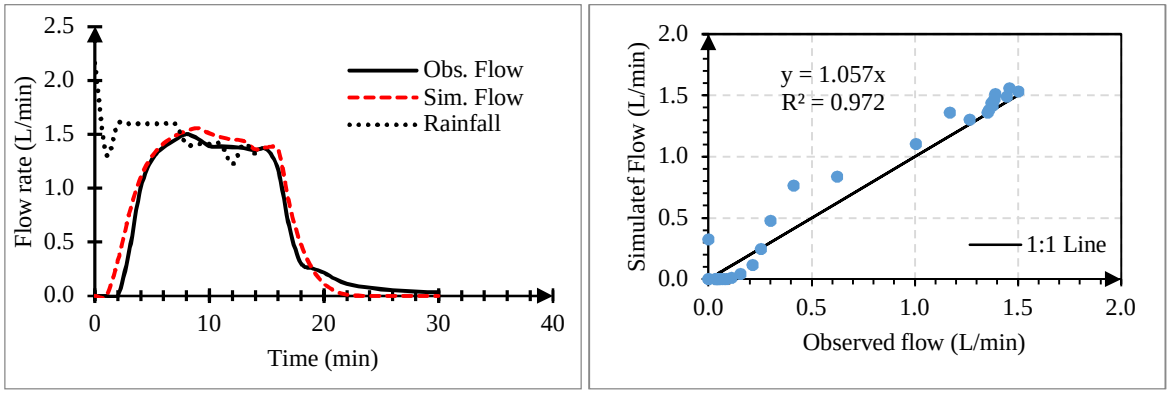

Figure F-39 Rig 4 Hydrographs and scatter graphs for Calibration event 1

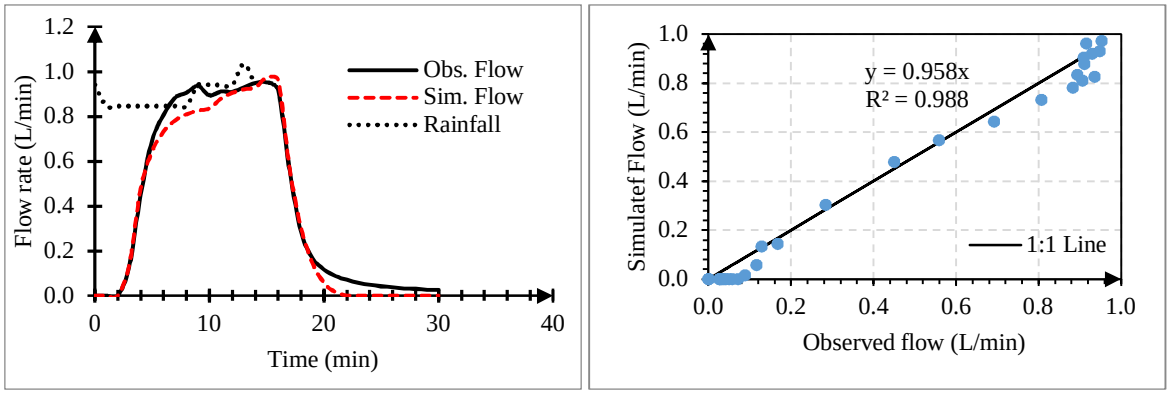

Figure F-40 Rig 4 Hydrographs and scatter graphs for Calibration event 2

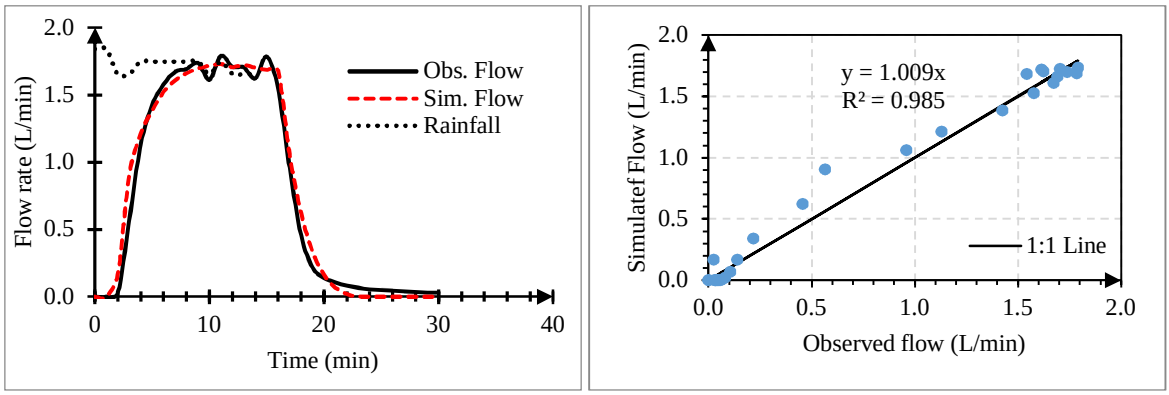

Figure F-41 Rig 4 Hydrographs and scatter graphs for Calibration event 3

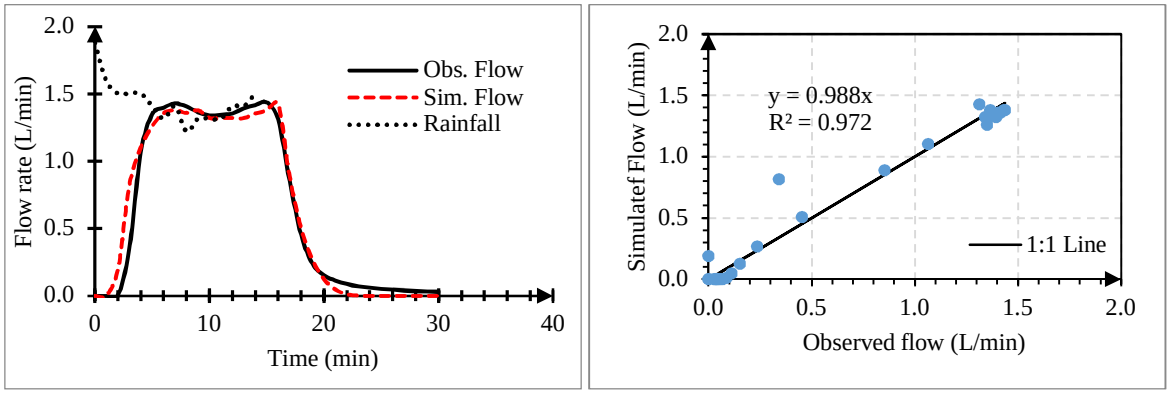

Figure F-42 Rig 4 Hydrographs and scatter graphs for Calibration event 4

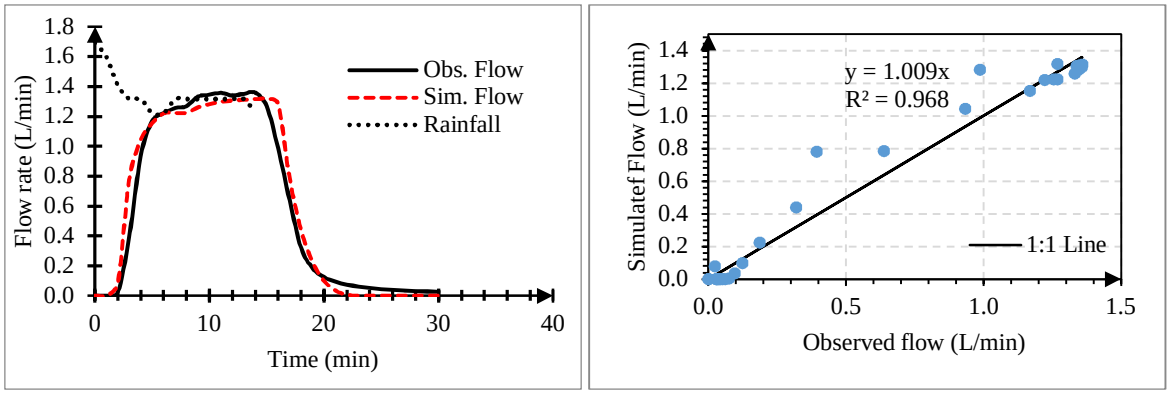

Figure F-43 Rig 4 Hydrographs and scatter graphs for Calibration event 5

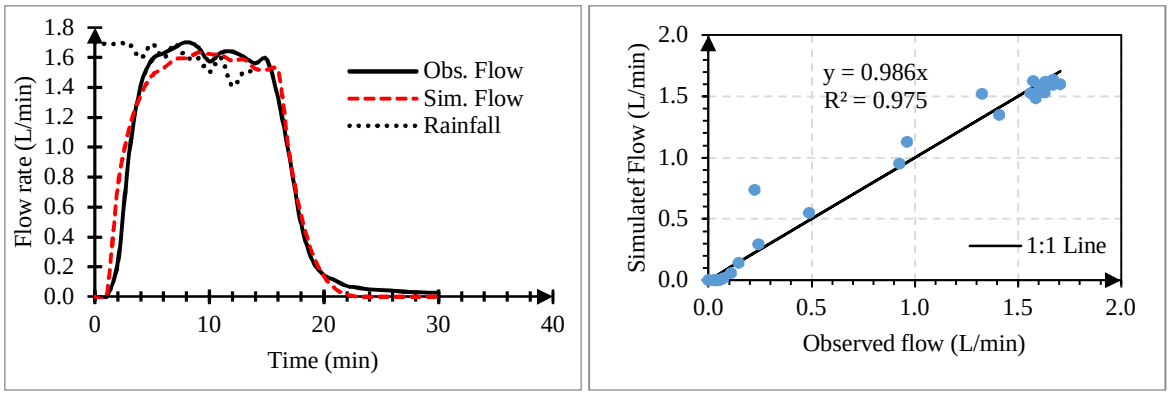

Figure F-44 Rig 4 Hydrographs and scatter graphs for Calibration event 6

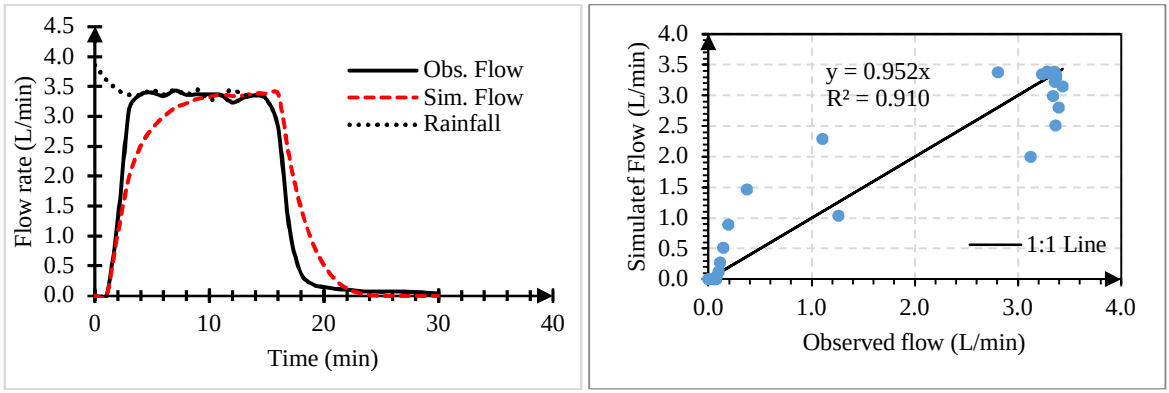

Figure F-45 Rig 4 Hydrographs and scatter graph for Validation event 1

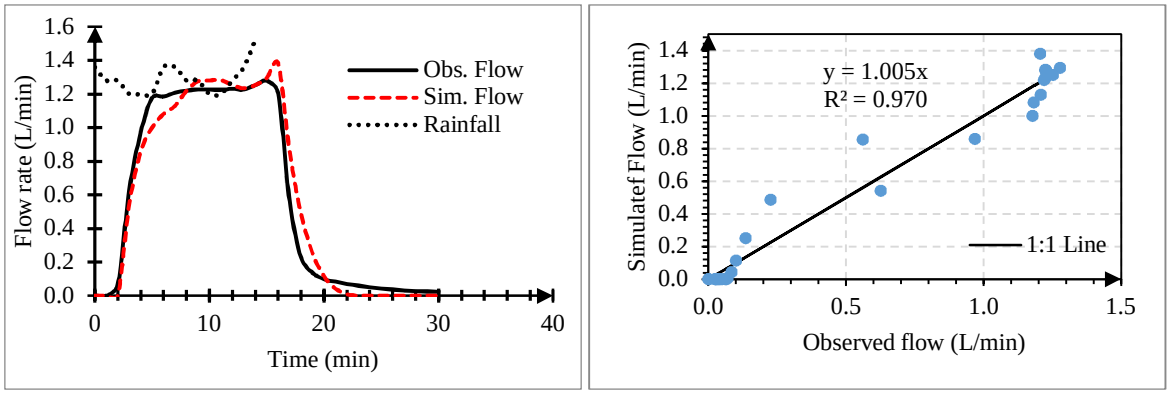

Figure F-46 Rig 4 Hydrographs and scatter graph for Validation event 2

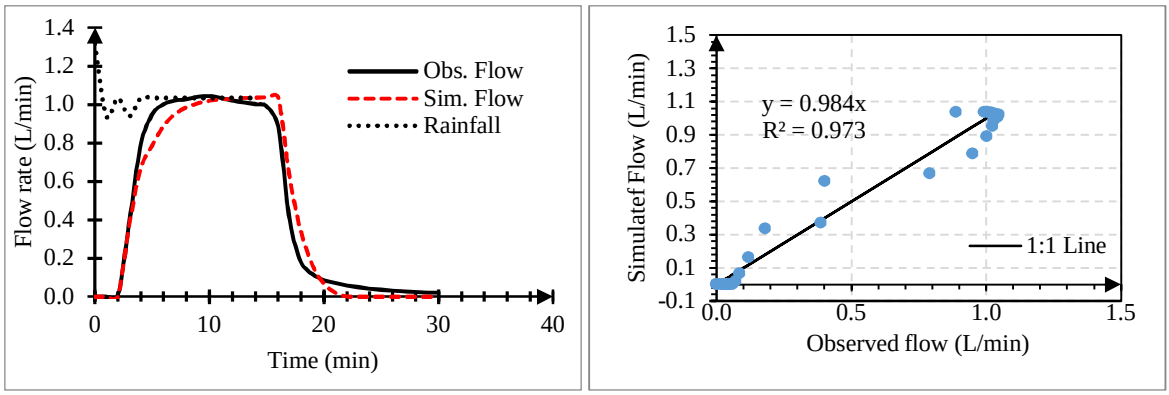

Figure F-47 Rig 4 Hydrographs and scatter graph for Validation event 3

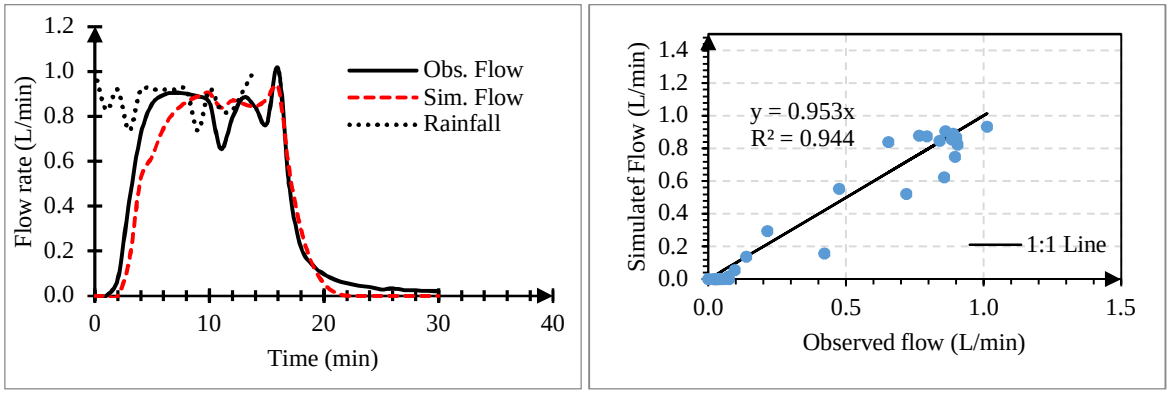

Figure F-48 Rig 4 Hydrographs and scatter graph for Validation event 4

APPENDIX G PCSWMM EVENT MODEL SENSITIVITY ANALYSIS

Table G-1 Rainfall simulation event model sensitivity analysis results for Rig 1

Parameter	Input/ Output	Parameter Change										
		-50%	-40%	-30%	-20%	-10%	0%	10%	20%	30%	40%	50%
Storage Void ratio	Input	0.25	0.30	0.35	0.40	0.45	0.50	0.55	0.60	0.65	0.70	0.75
	NSE	0.903	0.94	0.963	0.974	0.985	0.99	0.99	0.986	0.98	0.971	0.961
	R^2	0.909	0.947	0.971	0.982	0.992	0.995	0.993	0.989	0.982	0.973	0.964
	RMSE	0.009	0.007	0.006	0.005	0.004	0.003	0.003	0.004	0.005	0.005	0.006
Drain exponent	Input	0.43	0.51	0.60	0.68	0.77	0.85	0.94	1.02	1.11	1.19	1.28
	NSE	-10.50	-3.350	0.144	0.799	0.970	0.990	0.965	0.934	0.909	0.845	0.339
	R^2	0.051	0.248	0.609	0.845	0.970	0.995	0.974	0.943	0.916	0.850	0.341
	RMSE	0.039	0.034	0.022	0.012	0.005	0.003	0.006	0.008	0.008	0.012	0.046
Drain coefficient	Input	10.00	12.00	14.00	16.00	18.00	20.00	22.00	24.00	26.00	28.00	30.00
	NSE	0.803	0.910	0.960	0.982	0.990	0.990	0.985	0.976	0.966	0.953	0.939
	R^2	0.850	0.920	0.960	0.982	0.993	0.995	0.992	0.984	0.975	0.962	0.949
	RMSE	0.012	0.008	0.006	0.004	0.003	0.003	0.004	0.005	0.006	0.007	0.007
Drain offset height	Input	12.50	15.00	17.50	20.00	22.50	25.00	27.50	30.00	32.50	35.00	37.50
	NSE	0.969	0.979	0.985	0.988	0.988	0.99	0.989	0.985	0.979	0.968	0.954
	R^2	0.974	0.983	0.989	0.993	0.993	0.995	0.994	0.99	0.984	0.974	0.961
	RMSE	0.005	0.005	0.004	0.004	0.004	0.003	0.004	0.004	0.005	0.005	0.005

Table G-2 Rainfall simulation event model sensitivity analysis results using AS coefficients for Rig 1

Parameter	Input/ Output	Parameter Change										
		-50%	-40%	-30%	-20%	-10%	0%	10%	20%	30%	40%	50%
Storage Void ratio	Input	0.25	0.30	0.35	0.40	0.45	0.50	0.55	0.60	0.65	0.70	0.75
	NSE	0.348	0.250	0.180	0.160	0.100	0.000	0.000	0.040	0.067	0.095	0.116
	R^2	0.344	0.240	0.160	0.130	0.060	0.000	0.040	0.060	0.087	0.110	0.124
	RMSE	0.022	0.021	0.019	0.021	0.021	0.000	0.004	0.007	0.008	0.009	0.009
Drain exponent	Input	0.43	0.51	0.60	0.68	0.77	0.85	0.94	1.02	1.11	1.19	1.28
	NSE	27.04	12.765	3.318	1.124	0.235	0.000	0.294	0.329	0.318	0.426	1.532
	R^2	2.220	2.197	1.514	0.882	0.294	0.000	0.247	0.306	0.310	0.426	1.539
	RMSE	0.083	0.090	0.074	0.051	0.024	0.000	0.034	0.025	0.019	0.025	0.101
Drain coefficient	Input	10	12	14	16	18	20	22	24	26	28	30
	NSE	0.019	0.010	0.005	0.002	0.000	0.000	0.003	0.004	0.004	0.005	0.005
	R^2	0.015	0.009	0.006	0.003	0.001	0.000	0.002	0.003	0.003	0.004	0.005
	RMSE	0.001	0.001	0.000	0.000	0.000	0.000	0.001	0.001	0.000	0.000	0.000
Drain offset height	Input	12.50	15.00	17.50	20.00	22.50	25.00	27.50	30.00	32.50	35.00	37.50
	NSE	0.002	0.001	0.001	0.000	0.001	0.000	0.000	0.001	0.001	0.002	0.003
	R^2	0.002	0.001	0.001	0.000	0.001	0.000	0.000	0.001	0.001	0.002	0.003
	RMSE	0.000	0.000	0.000	0.000	0.000	0.000	0.000	0.000	0.000	0.000	0.000

Table G-3 Rainfall simulation event model sensitivity analysis results for Rig 2

Parameter	Input/ Output	Parameter Change										
		-50%	-40%	-30%	-20%	-10%	0%	10%	20%	30%	40%	50%
Storage Void ratio	Input	0.20	0.24	0.28	0.32	0.36	0.40	0.44	0.48	0.52	0.56	0.60
	NSE	0.909	0.934	0.956	0.971	0.978	0.98	0.977	0.972	0.967	0.96	0.952
	R^2	0.914	0.94	0.962	0.977	0.983	0.984	0.981	0.974	0.969	0.961	0.953
	RMSE	0.009	0.008	0.007	0.006	0.005	0.005	0.005	0.005	0.006	0.006	0.007
Drain exponent	Input	0.43	0.51	0.60	0.68	0.77	0.85	0.94	1.02	1.11	1.19	1.28
	NSE	-12.50	-3.630	0.170	0.784	0.954	0.980	0.957	0.942	0.882	0.372	0.490
	R^2	0.024	0.218	0.587	0.825	0.954	0.984	0.966	0.950	0.889	0.375	0.352
	RMSE	0.043	0.037	0.024	0.013	0.006	0.005	0.007	0.008	0.011	0.047	0.049
Drain coefficient	Input	10.00	12.00	14.00	16.00	18.00	20.00	22.00	24.00	26.00	28.00	30.00
	NSE	0.810	0.902	0.947	0.969	0.978	0.980	0.977	0.971	0.962	0.956	0.955
	R^2	0.843	0.909	0.947	0.969	0.980	0.984	0.982	0.978	0.969	0.964	0.963
	RMSE	0.013	0.009	0.007	0.005	0.005	0.005	0.005	0.006	0.007	0.007	0.007
Drain offset height	Input	12.50	15.00	17.50	20.00	22.50	25.00	27.50	30.00	32.50	35.00	37.50
	NSE	0.957	0.966	0.973	0.977	0.98	0.98	0.977	0.974	0.972	0.969	0.963
	R^2	0.961	0.97	0.976	0.981	0.983	0.984	0.981	0.978	0.977	0.973	0.968
	RMSE	0.006	0.006	0.005	0.005	0.005	0.005	0.005	0.005	0.005	0.006	0.006

Table G-4 Rainfall simulation event model sensitivity analysis results using AS coefficients for Rig 2

Parameter	Input/ Output	Parameter Change										
		-50%	-40%	-30%	-20%	-10%	0%	10%	20%	30%	40%	50%
Storage Void ratio	Input	0.20	0.24	0.28	0.32	0.36	0.50	0.44	0.48	0.52	0.56	0.60
	NSE	0.355	0.287	0.200	0.113	0.050	0.000	0.075	0.100	0.108	0.125	0.140
	R^2	0.350	0.275	0.183	0.088	0.025	0.000	0.075	0.125	0.125	0.144	0.155
	RMSE	0.021	0.023	0.021	0.015	0.003	0.000	0.000	0.006	0.009	0.010	0.011
Drain exponent	Input	0.43	0.51	0.60	0.68	0.77	0.85	0.94	1.02	1.11	1.19	1.28
	NSE	31.718	13.559	3.176	1.153	0.306	0.000	0.271	0.224	0.384	1.788	1.153
	R^2	2.259	2.253	1.557	0.935	0.353	0.000	0.212	0.200	0.373	1.791	1.487
	RMSE	0.090	0.096	0.077	0.052	0.020	0.000	0.028	0.017	0.024	0.124	0.104
Drain coefficient	Input	10	12	14	16	18	20	22	24	26	28	30
	NSE	0.017	0.010	0.006	0.003	0.001	0.000	0.002	0.002	0.003	0.003	0.003
	R^2	0.014	0.009	0.006	0.004	0.002	0.000	0.001	0.002	0.003	0.003	0.002
	RMSE	0.001	0.001	0.000	0.000	0.000	0.000	0.000	0.000	0.000	0.000	0.000
Drain offset height	Input	12.5	15.0	17.5	20.0	22.5	25.0	27.5	30.0	32.5	35.0	37.5
	NSE	0.002	0.001	0.001	0.001	0.000	0.000	0.001	0.001	0.001	0.001	0.001
	R^2	0.002	0.001	0.001	0.001	0.000	0.000	0.001	0.001	0.001	0.001	0.001
	RMSE	0.000	0.000	0.000	0.000	0.000	0.000	0.000	0.000	0.000	0.000	0.000

Table G-5 Rainfall simulation event model sensitivity analysis results for Rig 3

Parameter	Input/ Output	Parameter Change										
		-50%	-40%	-30%	-20%	-10%	0%	10%	20%	30%	40%	50%
Storage Void ratio	Input	0.23	0.27	0.32	0.36	0.41	0.45	0.50	0.54	0.59	0.63	0.68
	NSE	0.907	0.935	0.965	0.98	0.99	0.992	0.989	0.983	0.974	0.964	0.95
	R^2	0.913	0.942	0.971	0.985	0.993	0.994	0.991	0.985	0.976	0.967	0.954
	RMSE	0.008	0.007	0.006	0.004	0.003	0.003	0.003	0.004	0.005	0.005	0.006
Drain exponent	Input	0.43	0.51	0.60	0.68	0.77	0.85	0.94	1.02	1.11	1.19	1.28
	NSE	-13.70	-5.040	-0.474	0.675	0.951	0.992	0.972	0.936	0.905	0.873	0.559
	R^2	0.047	0.190	0.537	0.797	0.955	0.994	0.980	0.945	0.913	0.879	0.562
	RMSE	0.036	0.033	0.024	0.014	0.006	0.003	0.005	0.008	0.009	0.011	0.027
Drain coefficient	Input	8.00	9.60	11.20	12.80	14.40	16.00	17.60	19.20	20.80	22.40	24.00
	NSE	0.716	0.870	0.940	0.974	0.988	0.992	0.989	0.983	0.975	0.964	0.953
	R^2	0.819	0.899	0.947	0.974	0.989	0.994	0.994	0.989	0.982	0.972	0.961
	RMSE	0.013	0.009	0.006	0.004	0.003	0.003	0.003	0.004	0.005	0.006	0.007
Drain offset height	Input	12.50	15.00	17.50	20.00	22.50	25.00	27.50	30.00	32.50	35.00	37.50
	NSE	0.972	0.979	0.982	0.987	0.99	0.992	0.99	0.987	0.98	0.97	0.963
	R^2	0.975	0.981	0.984	0.989	0.993	0.994	0.993	0.991	0.985	0.976	0.97
	RMSE	0.004	0.004	0.004	0.003	0.003	0.003	0.003	0.004	0.004	0.004	0.005

Table G-6 Rainfall simulation event model sensitivity analysis results using AS coefficients for Rig 3

Parameter	Input/ Output	Parameter Change										
		-50%	-40%	-30%	-20%	-10%	0%	10%	20%	30%	40%	50%
Storage Void ratio	Input	0.23	0.27	0.32	0.36	0.41	0.50	0.50	0.54	0.59	0.63	0.68
	NSE	0.378	0.317	0.200	0.133	0.044	0.000	0.067	0.100	0.133	0.156	0.187
	R^2	0.360	0.289	0.170	0.100	0.022	0.000	0.067	0.100	0.133	0.150	0.178
	RMSE	0.024	0.023	0.020	0.016	0.004	0.000	0.007	0.009	0.012	0.012	0.013
Drain exponent	Input	0.43	0.51	0.60	0.68	0.77	0.85	0.94	1.02	1.11	1.19	1.28
	NSE	34.57	17.74	5.749	1.865	0.482	0.000	0.235	0.329	0.341	0.350	1.019
	R^2	2.228	2.365	1.792	1.159	0.459	0.000	0.165	0.288	0.318	0.338	1.016
	RMSE	0.077	0.087	0.083	0.066	0.035	0.000	0.030	0.028	0.025	0.024	0.056
Drain coefficient	Input	8.00	9.60	11.20	12.80	14.40	20.00	17.60	19.20	20.80	22.40	24.00
	NSE	0.035	0.019	0.011	0.006	0.003	0.000	0.002	0.003	0.004	0.004	0.005
	R^2	0.022	0.015	0.010	0.006	0.003	0.000	0.000	0.002	0.003	0.003	0.004
	RMSE	0.001	0.001	0.001	0.000	0.000	0.000	0.000	0.000	0.000	0.000	0.000
Drain offset height	Input	12.50	15.00	17.50	20.00	22.50	25.00	27.50	30.00	32.50	35.00	37.50
	NSE	0.002	0.001	0.001	0.001	0.001	0.000	0.001	0.001	0.002	0.002	0.002
	R^2	0.002	0.001	0.001	0.001	0.000	0.000	0.000	0.001	0.001	0.002	0.002
	RMSE	0.000	0.000	0.000	0.000	0.000	0.000	0.000	0.000	0.000	0.000	0.000

Table G-7 Rainfall simulation event model sensitivity analysis results for Rig 4

Parameter	Input/ Output	Parameter Change										
		-50%	-40%	-30%	-20%	-10%	0%	10%	20%	30%	40%	50%
Storage Void ratio	Input	0.25	0.30	0.35	0.40	0.45	0.50	0.55	0.60	0.65	0.70	0.75
	NSE	0.899	0.936	0.959	0.974	0.982	0.985	0.985	0.982	0.976	0.97	0.961
	R^2	0.903	0.939	0.962	0.976	0.983	0.986	0.985	0.982	0.978	0.972	0.965
	RMSE	0.014	0.012	0.009	0.007	0.006	0.006	0.006	0.007	0.008	0.008	0.009
Drain exponent	Input	0.43	0.51	0.60	0.68	0.77	0.85	0.94	1.02	1.11	1.19	1.28
	NSE	-32.60	-11.900	-2.720	0.235	0.904	0.985	0.951	0.887	0.815	0.717	0.294
	R^2	0.014	0.078	0.363	0.703	0.928	0.986	0.955	0.891	0.817	0.718	0.294
	RMSE	0.064	0.060	0.050	0.032	0.014	0.006	0.011	0.015	0.017	0.021	0.078
Drain coefficient	Input	8.00	9.60	11.20	12.80	14.40	16.00	17.60	19.20	20.80	22.40	24.00
	NSE	0.600	0.818	0.916	0.961	0.980	0.985	0.982	0.975	0.964	0.951	0.937
	R^2	0.802	0.886	0.938	0.967	0.981	0.986	0.984	0.977	0.967	0.954	0.941
	RMSE	0.026	0.018	0.013	0.009	0.007	0.006	0.005	0.007	0.009	0.010	0.012
Drain offset height	Input	12.50	15.00	17.50	20.00	22.50	25.00	27.50	30.00	32.50	35.00	37.50
	NSE	0.963	0.969	0.974	0.979	0.983	0.985	0.987	0.988	0.99	0.991	0.991
	R^2	0.966	0.972	0.976	0.98	0.984	0.986	0.987	0.988	0.99	0.991	0.991
	RMSE	0.008	0.007	0.007	0.006	0.006	0.006	0.006	0.006	0.006	0.005	0.005

Table G-8 Rainfall simulation event model sensitivity analysis results using AS for Rig 4

Parameter	Input/ Output	Parameter Change										
		-50%	-40%	-30%	-20%	-10%	0%	10%	20%	30%	40%	50%
Storage Void ratio	Input	0.25	0.30	0.35	0.40	0.45	0.50	0.55	0.60	0.65	0.70	0.75
	NSE	0.344	0.245	0.173	0.110	0.060	0.000	0.000	0.030	0.060	0.075	0.096
	R^2	0.332	0.235	0.160	0.100	0.060	0.000	0.020	0.040	0.053	0.070	0.084
	RMSE	0.034	0.028	0.021	0.008	0.001	0.000	0.006	0.009	0.012	0.013	0.014
Drain exponent	Input	0.43	0.51	0.60	0.68	0.77	0.85	0.94	1.02	1.11	1.19	1.28
	NSE	79.02	37.897	14.529	4.412	0.953	0.000	0.400	0.576	0.667	0.788	1.626
	R^2	2.288	2.672	2.443	1.665	0.682	0.000	0.365	0.559	0.663	0.788	1.628
	RMSE	0.136	0.160	0.174	0.156	0.093	0.000	0.055	0.052	0.044	0.044	0.170
Drain coefficient	Input	8.00	9.60	11.20	12.80	14.40	20.00	17.60	19.20	20.80	22.40	24.00
	NSE	0.048	0.026	0.014	0.008	0.003	0.000	0.002	0.003	0.004	0.005	0.006
	R^2	0.023	0.016	0.010	0.006	0.003	0.000	0.001	0.003	0.004	0.005	0.006
	RMSE	0.002	0.002	0.001	0.001	0.001	0.000	0.000	0.000	0.001	0.001	0.001
Drain offset height	Input	12.50	15.00	17.50	20.00	22.50	25.00	27.50	30.00	32.50	35.00	37.50
	NSE	0.002	0.002	0.001	0.001	0.001	0.000	0.001	0.001	0.001	0.001	0.000
	R^2	0.002	0.001	0.001	0.001	0.001	0.000	0.000	0.000	0.001	0.001	0.000
	RMSE	0.000	0.000	0.000	0.000	0.000	0.000	0.000	0.000	0.000	0.000	0.000